HIROYUKI YAMAMOTO

BIOMECHANICS OF WOOD – TOWARD UTILIZATION OF FOREST BIOMASS IN THE 21st CENTURY

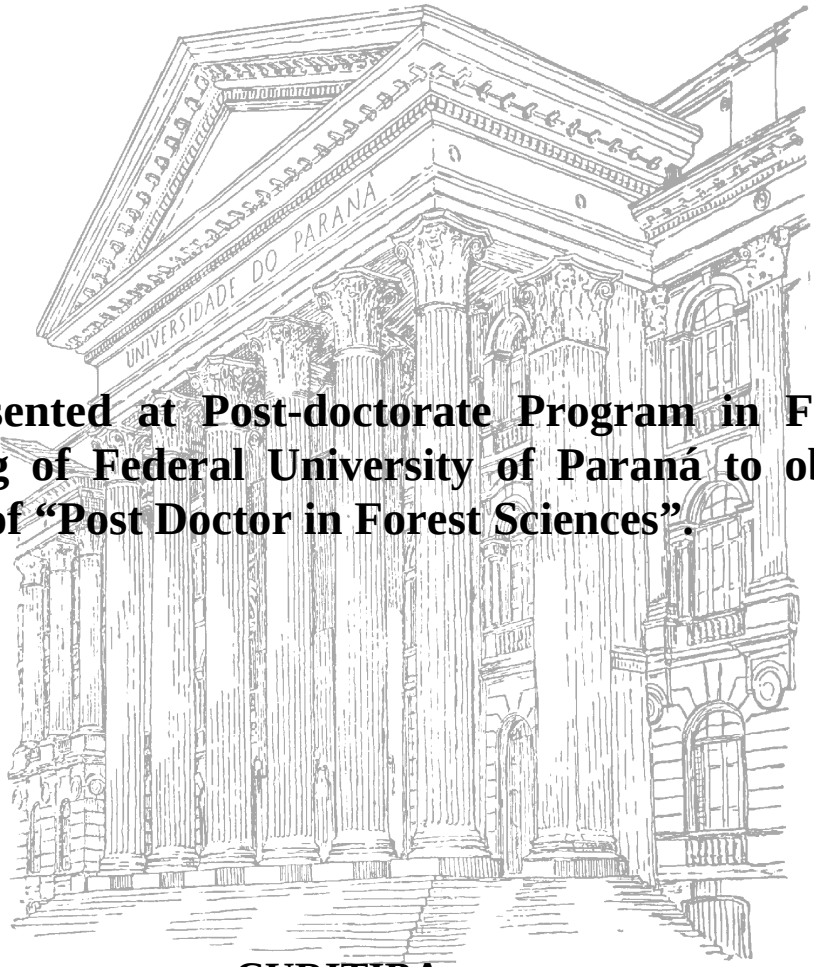

Thesis presented at Post-doctorate Program in Forest Engineering of Federal University of Paraná to obtain the degree of "Post Doctor in Forest Sciences".

CURITIBA

March 2005

HIROYUKI YAMAMOTO

BIOMECHANICS OF WOOD – TOWARD UTILIZATION OF FOREST BIOMASS IN THE 21st CENTURY

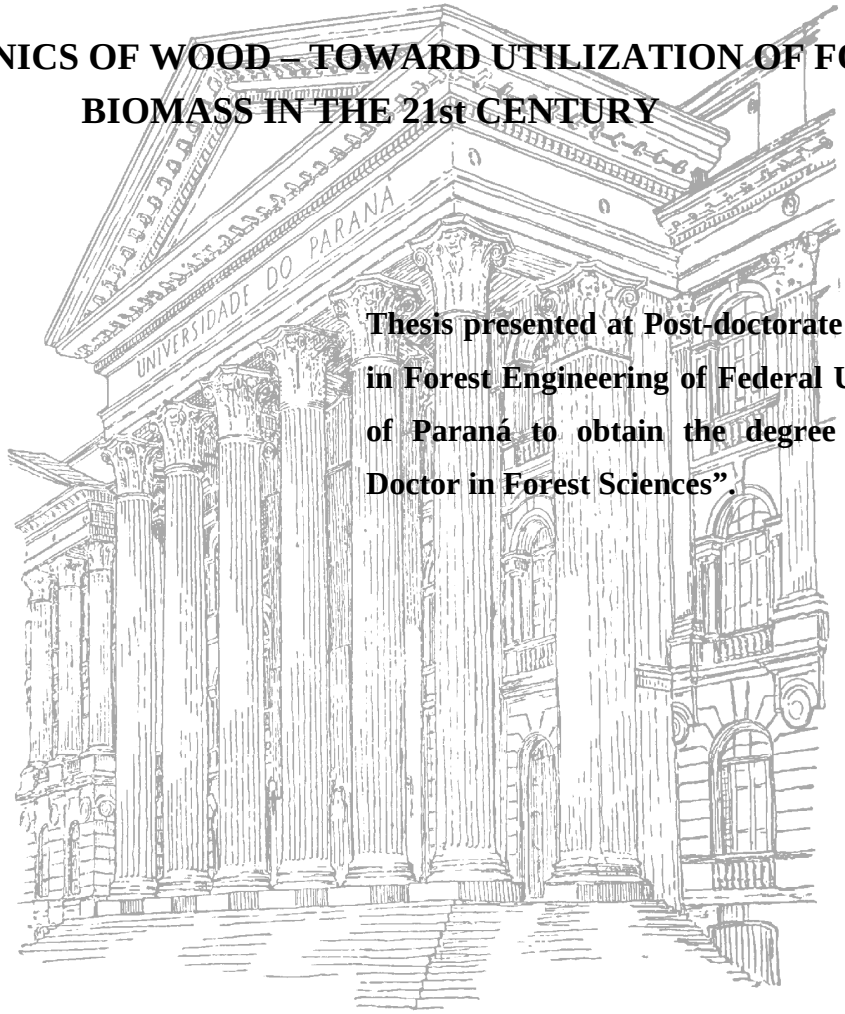

Thesis presented at Post-doctorate Program in Forest Engineering of Federal University of Paraná to obtain the degree of "Post Doctor in Forest Sciences".

CURITIBA

April 2005

Acknowledgements

I am indebted to many scientists and their scientific instructions for completing this dissertation, especially for Professor Dr. Setsuo IWAKIRI, Professor Dr. Jorge de MATOS, and Senior Professor Dr. Roberto T. HOSOKAWA in Faculty of Forest Engineering, Federal University of Parana, Brazil. They gave me a great opportunity to carry out Post-doctorate Program in Forest Engineering, opened the door to my study in Brazil. They long-sufferingly encouraged me to continue my Post-doctorate program in UFPR.
I am also indebted to Mr. Ricardo M. PAIM, Msc, and Mr. LUIZ O. de Andrade in Rigesa Ltd for their cooperation to prepared Chopper treated samples.

I am deeply grateful to Professor Dr. Ken-ichi HIRASHIMA, Graduate School of Engineering, Yamanashi University, Japan, for his keen advices and suggestions especially for completing theoretical treatise in this dissertation.

I also thank Professor Dr. Joseph GRIL, Laboratoire de Mecanique et Genie Civil, Universite Montpellier 2, France for his helpful advices and his deep friendship.

I am also thankful to Professor Dr. Fabio M. YAMAJI, Saô Paulo State University at Itapeva, and his wife Akiko for their kind and warm cooperation in my private life in Brazil. They were always with me, and heartening me during my stay in Curitiba.

I also appreciate my wife Masayo, my daughter Chihaya, my son Goh for their tolerant understandings for my frequent absence in our home. They have been my inspiration and my strength during my scientific activity, and for ever.

Finally, I would like to express my deepest gratitude to Late Professor Takashi OKUYAMA. OKUYAMA-sensei had been always with me, and gave me his hearty guidance in my scientific research since my school days. Without his warm and affectionate cooperation, I could not complete any works, including this dissertation, in my past career. My beautiful memories with OKUYAMA-sensei are unlikely to go away unless the earth would evanish.

List of Tables

List of Figures

List of symbols

1. Quantities generally used in this paper

l, t, r: coordinate signs representing the longitudinal, the tangential, and the radial directions in the cylindrical coordinate systems.

x, y, z: coordinate signs representing x, y, and z in the Cartesian coordinate system.

r: coordinate variable in the radial directions in the cylindrical coordinate systems, or radial distance from the central axis.

x, *y*, *z*: coordinate variable in the Cartesian coordinate system.

L, T. R: Signs representing the longitudinal, the tangential, and the radial directions in the wood at the macroscopic level.

t; time or moisture content.

T; moisture content at the fiber saturation point (FSP).

τ: $\equiv t/T$. the moisture content normalized by the moisture content at FSP.

2. Symbols concerned in the micromechanical properties of the wall layer element (see Section 2-1, Chapter 2)

σ ; stress field in a body.

ε ; compatible strain field in a body.

C^I ; elastic constant of the inhomogeneity.

C^M; elastic constant of the matrix substance.

ε^I, ε^M; eigen-strains of thermal (or humid) expansions in the inhomogeneity and the matrix, respectively.

ε^{I*} ; eigen-strain of the inhomogeneity in the equivalent inclusion problem (1).

ε^T ; $\equiv\varepsilon^I-\varepsilon^M$.

ε^{T*} ; $\equiv\varepsilon^{I*}-\varepsilon^M$. This is an equivalent transformation strain in the equivalent inclusion problem (1).

S ; Eshelby's tensor

ε^* ; eigen-strain of the equivalent inclusion in the equivalent inclusion method (2).

$[\sigma^F]$; mean stress generated in a rod-like polysaccharide fibril as the ellipsoidal inclusion with

infinitely long axis.

$[\sigma^M]$; mean stress generated in the matrix substance which is embedding the numerous rod-like polysaccharide fibrils.

σ^f ; $\equiv\phi[\sigma^F]$, where ϕ is volumetric fraction of the polysaccharide framework in the cell wall layer. According to the "the reinforced-matrix hypothesis", σ^f is regarded as the stress field in the polysaccharide framework bundle in the cell wall layer.

σ^m ; $\equiv(1-\phi[\sigma^M]$. According to the "the reinforced-matrix hypothesis", σ^m is regarded as the stress field in the matrix skeleton in the cell wall layer.

C^F ; elastic constant of a rod-like polysaccharide fibril.

C^M ; elastic constant of the matrix substance.

C^f ; $\equiv\phi\cdot C^F$. This is regarded as the elastic constant of the polysaccharide framework as the bundle.

C^m ; $\equiv(1-\phi\cdot C^M$. This is regarded as the elastic constant of the matrix as the skeleton.

3. Symbols concerned in the properties of the macroscopic xylem

F, *V*, *R, P*; area compositions of the domains of the wood fiber, the vessel, the ray parenchyma and the axial parenchyma in the cross-section of the macroscopic wood, respectively.

s: area ratio of the lignified layer in the cross-section of the wood fiber domain.

g: area ratio of the gelatinous layer in the cross-section of the wood fiber domain.

N_n : Frequency of the normal wood fiber per unit area in the wood fiber domain.

N_g : Frequency of the gelatinous fiber per unit area in the wood fiber domain.

f : $= N_n+N_g$.

ϕ : relative frequency of the gelatinous fiber in the wood fiber domain ($=N_g/f$).

E_L^X, E_L ; Longitudinal Young's modulus of the wood at the macroscopic level.

E_L^F, E_L^V, E_L^R ; Longitudinal Young's moduli of the domains of the wood fiber, the vessel, and the ray in the sandwiched model of the macroscopic wood, respectively (see Fig.2-1(b)).

α_L, α_L^X ; Longitudinal drying shrinkage of the wood at the macroscopic level.

α_L^F, α_L^V, α_L^R; Longitudinal drying shrinkage of the each domain in the sandwiched model of the macroscopic wood.

ε_L, ε_L^X ; Longitudinal growth strain or released strain of the growth stress in the surface of the

xylem at the macroscopic level.

ε_T ; Tangential growth strain or released strain of the growth stress in the surface of the xylem at the macroscopic level.

ε_L^F, ε_L^V, ε_L^R; Longitudinal growth strain of the each domain in the sandwiched model of the macroscopic xylem.

4. Symbols concerned in the mechanical behaviors of deforming wood fiber

ε_l, ε_t, ε_r; Respectively, longitudinal, the tangential, and the radial normal strains induced at every point of the wood fiber model under the *l*tr-cylindrical coordinate system.

σ_l, σ_t, σ_r; Respectively, longitudinal, the tangential, and the radial normal stresses induced at every point of the wood fiber model under the *l*tr-cylindrical coordinate system.

ε_L, ε_T : strains of the dimensional changes of the wood fiber in the direction along the fiber axis and the diameter, respectively. Or, the growth strains of the wood fiber in the direction along the axis and the diameter, respectively. Sometimes, we use the signs "α" and "β" for representing the strains of the longitudinal and the diametral deformation of the wood fiber, respectively (see Section 2-2), or the strains of the longitudinal and the diametral swelling of the wood fiber, respectively (see Section 4-1).

E; Young's modulus of the polysaccharide framework bundle in each layer of the secondary wall in the direction parallel to the molecular chains of the cellulose. Accurately to say, the value of *E* should be distinguished in respective layers. *E* is subdivided into E_1 , E_2, and E_3 in the S1, the S2, and the G layers, respectively.

S; Shear modulus (×2) of the matrix skeletons in each layer of the secondary wall. In the same way as *E*, *S* takes respective value in each layer. *S* is denoted by S_1, S_2, and S_3 in the S1, the S2, and the G layers, respectively.

S_0; Shear modulus (×2) of the CML.

M; $=S_2/S_1$. *N*; $=S_3/S_2$.

r_{in}; the inner radius of each layer. r_{in} is denoted by r_1, r_2, r_3, and r_4 in the CML, the S1, the S2, and the G layers, respectively

r_{out}; the outer radius of each layer. r_{out} is denoted by r_0 ($=r_1+h$), r_1, r_2, and r_3 in the CML, the

S1, the S2, and the G-layers, respectively.

h; thickness of the CML layer.

$\rho_0 = r_0 / r_1$,, $\rho_1 = r_1 / r_2$,, $\rho_2 = r_2 / r_3$,, $\rho_3 = r_3 / r_4$

θ; the microfibril angle (MFA).

ε^m; internal expansive strain in the matrix skeleton of each layer. ε^m is denoted by ε_1^m, ε_2^m, and ε_3^m in the S1, the S2, and the G layers, respectively. Those strains are generated by a certain biomechanical change occurring in respective layers.

ε^f; internal expansive strains in the polysaccharide framework bundle of each layer. ε^f is denoted by ε_1^f, ε_2^f, and ε_3^f in the S1, the S2, and the G layers, respectively. Those strains are generated in the direction parallel to the cellulose molecular chains.

P_{in}; boundary pressure acting to the inner surface of each layer. P_{in} is denoted as P_1, P_2, P_3, and P_4 in the CML, the S1, the S2, and the G layers, respectively.

P_{out}; boundary pressure acting to the outer surface of each layer. P_{out} is denoted as P_0, P_1, P_2, and P_3 in the CML, the S1, the S2, and the G layers, respectively.

L_0, L_1, L_2, L_3 ; the tensile or compressive loads induced in the CML, the S1, the S2, and the G layers, respectively.

G ; $=E/S$. G is denoted as G_1, G_2, and G_3 in the S1, the S2, and the G layers, respectively.

Q ; $= S_0 \cdot h/(r_1 \cdot E_1)$. Sometimes, we use the sign, F $(=S_0 \cdot h/r_1)$, then, $Q=F/E_1$.

ε_T^{ri} ; $= \varepsilon_T(r)|_{r=ri}$. Tangential normal strain induced at $r = r_i$ (i = 0, 1, 2, 3, 4).

5. Symbols concerning the biomechanical motion of the tree shoot.

r_0 ; Radius of the elongation zone.

Δl ; Length of the elongation zone.

Δr ; Thickness of the thickening zone.

N ; Number of the growth step.

ρ ; The specific weight of the stem.

E ; Elastic modulus (Young's modulus) of the stem in the axial direction.

θ_C ; Preferred angle of the elongation zone, if the elongation zone always appears with a certain directional angle.

$(m_i^{(k)}, n_i^{(k)})$; xy-coordinates of the i-th node just after completion of the k-th growth step.

$l_i^{(k-1)}$; The length of the i-th member just after completion of the (k–1)-th growth step. For simplification, we often denote $l_i^{(k-1)}$ as l_i.

$\Delta p_i^{(k)}$; The increment of the load acting on the i-th node, which is caused by the weight growth during the k-th growth step.

$\theta_i^{(k-1)}$; The directional angle of the i-th member just after completion of the (k−1)-th growth step. For simplification, we often denote $\theta_i^{(k-1)}$ as θ_i.

$\Delta h_i^{(k)}$; The weight of the new foliage at the i-th node during the k-th growth step.

$h_{k+1}^{(k)}$; The weight of the new foliage at the shoot apex during the k-th growth step.

$\Delta \Omega_i^{(k)}$; The weight of the thickening zone in the i-th member during the k-th growth step.

$\Delta \Lambda_i^{(k)}$; $= \Delta \Omega_i^{(k)} \cdot \theta_i^{(k-1)}$

$\Delta \omega_i^{(k)}$; $= \Delta \Lambda_i^{(k)} / l_i^{(k-1)}$

$\Delta M_i^{o(k)}$; The increment of the nodal moment at the i-th node during the k-th growth step. Positive bending moment makes the element concave upward.

$\Delta M_i^{s(k)}$; Recovery moment generated in the thickening zone in the i-th member during the k-th growth step.

Abbreviation

MFA: microfibril angle in the middle layer of the secondary wall.

TW: tension wood.

CW: compression wood.

NW: normal wood.

OW: opposite wood.

CML: compound middle lamella.

S1: the outer layer of the secondary wall.

S2: the middle layer of the secondary wall.

S3: the innermost layer of the secondary wall

G: gelatinous layer

G-fiber: gelatinous fiber

CMF: cellulose microfibril

MT: matrix

FSP : fiber saturation point.

To my teacher

Late Professor Dr. Takashi OKUYAMA (1943~2004)

Contents

Curriculum Vitae

Hiroyuki YAMAMOTO

Associate Professor of Forest Products Science

Labo. Bio-materials Physics, Graduate School of Bio-agricultural Sciences, Nagoya University

Chikusa, Nagoya 464-8601, Japan

August 1961 Born in Aichi-prefecture, JAPAN

(Academic degree)

1986 B.Sc. in Agriculture (Forest products Science), Nagoya University

1988 M.Sc. in Agriculture (Forest products Science), Nagoya University

1993 Ph.D. in Agriculture (Forest products Science), Nagoya University

2004 Ph.D. in Engineering (Civil Engineering), Yamanashi University

2005 Pós-Doutor (Forest engineering), Dederal University of Paraná

2005 Japan Wood Research Society Prize

(Academic job)

1988 Research Associate, School of Agricultural Sciences, Nagoya University

1995 Associate Professor, School of Agricultural Sciences, Nagoya University

1999~ Associate Professor, Graduate School of Bio-agricultural Sciences, Nagoya University

2002~2005 Pós-Doutorado fellow in Federal University of Paraná, Brazil

Chapter 1

GENELAL BACKGROUND

1-1 Necessity for modeling the structural hierarchy of wood

Wood is a biological material that is formed during the tree secondary growth. Differently from non-biological materials, e.g. stone, metal, synthesized polymer, etc., the wood shows very complicated and hierarchical structure from the constituent macromolecules to the macroscopic xylem. We often find a precisely designed structure in each hierarchical order, which is one of the most outstanding properties of the biological materials. Material properties of the wood at the macroscopic level are evolved when such the structural hierarchy takes shape. Therefore, it is indispensable to clarify the various qualities of wood in relation to the structural hierarchy of the wood not only for maximizing the mechanical performance of the structural member in the building or furniture but also for developing the novel engineering materials.

Studies to analyze the mechanical properties of wood from the viewpoint of its morphological properties were started with recognizing the wood as a heterogeneous and anisotropic material. Many scientists have attended to formulating and designing the mechanical behaviors of the timber or the wood-based material with a development of the general theory of anisotropic elasticity. Those efforts came to fruition as various new technologies, e.g. innovations in the material testing methods, invention and prevalence of various engineered woods and novel constructions, etc. In those investigations, scientists considered the wood as a macroscopic continuum body, that is, a three dimensional orthotropic body or a polar anisotropic material. However, they had no cognizance of the fact that the wood is the biomaterial with hierarchical structure.

From 1950s to 1960s, the techniques for the microscopic observation were rapidly improved, which enabled the plant anatomists to reveal the fine composite structure of the wood cell wall. As the result, they concluded that each layer in the wood cell wall consists of “the two-phase structure”, comprising the bundle of rigid polysaccharide microfibrils and the embedding matrix of lignin-hemicellulose compounds. At the same time, micromechanical method for analyzing the mechanical properties of the composite materials at the microscopic level were developed, which led the material scientists to analyze the mechanical interaction between the inclusions (e.g. rigid polysaccharide microfibrils) and the matrix (embedding compounds of hemicellulose and lignin). Under those efforts, trials to clarify the origins of

mechanical properties peculiar to the wood were started on the basis of the idea of “the two-phase structure”. Those trials brought important and novel knowledge on both research fields of the wood mechanics and cell wall anatomy. Moreover, some of the obtained results were applied to the technique of the wood modification, e.g. the bentwood, surface consolidation, dimensional stabilization, etc. Thus, it can be said that the idea of “the two-phase structure” successfully filled up a gap which once existed between the situation to develop the novel engineering materials and that to investigate the fine structure of the wood cell wall, and its formation.

Investigation based on the structural hierarchy is not necessarily confined to understanding the mechanical properties of the wood as an assembly of behavior of each constituent in the cell wall. In many cases, it is still difficult to measure the internal property and structure of each constituent material directly as it exists in the composite material. If we could formulate the generation mechanism of the mechanical properties of the wood theoretically on the basis of the concept of the structural hierarchy of the wood, it is anticipated to compare the predicted behaviors of the wood with the observed ones. Through such comparisons, it is expected to extract the information on the interfacial structure between the cell wall constituents in addition to the property and fine structure in each cell wall constituent as it exists in the cell wall. In other words, it is considered that the modeling of the fine composite structure of the biomaterial often plays as if it were a virtual micro-testing instrument or a nondestructive microscope.

1-2 Necessity for affirmative use of the forest resources

Let our eyes turn to the present affairs in the earth and the human society. Fossil fuel and metal resources have been almost exhausted while modern society based on the consumer economy becomes overripe after the Industrial Revolution. Moreover, irreversible destruction of the forest environment has been progressing in the tropical countries, and the atmospheric carbon dioxide is still increasing with mass consumption of the fossil fuel. Those are the most crucial problems that the human society has ever experienced before (Hosokawa et al. 2002). If we leave those problems off as they are, it would be the ruin of the modern civilization in the near future. Then, our urgent countermeasure is to find substitutes for the fossil and metal resources, and to mitigate the increasing atmospheric carbon dioxide as soon as possible.

Under those situations, some people believe that “the forest biomass” can solve the above-mentioned crises because the forest products are sustainable resources based on the repetition of afforestation and harvesting. Another reason is that the forest biomass plays an

important part as a massive storage of the fixed carbon dioxide. However, it may be rather belated to device a countermeasure. Large-scale exploitation of the forest resource has been executed since the Industrial Revolution, causing an irreversible destruction especially in the tropical forest region. As the result, many of commercial species were almost exhausted, which provokes serious undersupply of the useful species in the world timber market. Even if we would take a policy to protect the forest by prohibiting any deforestation in the natural forest from now on, it may take several hundred years or more to recover the fallen forest environment as it were.

As one of the countermeasures to avoid the above crises, some scientists recommend the afforestation of the fast-growing species and its utilization as the industrial materials. In fact, the plantation activity of the fast-growing species recently becomes very popular in the tropical and subtropical countries. The growing rate of the fast-growing species often becomes several times faster or more than that of the commercial species in the temperate zone, therefore, it is anticipated that the plantation of the fast-growing species plays an important part not only in mitigating the increasing atmospheric carbon dioxide rapidly but also in supplying the forest products to the world market. Some people agree that whether or not we can sustain the modern civilization in the future depends largely on the success of the afforestation of the fast-growing species.

The plantation program can be executed under a fundamental premise that the products from the plantation are purchased as the economical-valued materials, such as construction, furniture, pulp and paper, and so forth. A part of the profits is reinvested in the plantation activity. Plantation of the fast-growing species is no exception to that premise. On the useful species, which has been used in the usual wood industry, people have accumulated abundant knowledge on the material properties and processing conditions. On the other hand, there is very little information on the material properties of the fast-growing species, because many of those species are very new materials in the modern wood industry, and people have never had a chance to use them except as the fuel or charcoal. Moreover, not a few people believe that those species cannot be used besides fuel or charcoal because they often contain the reaction woods, the juvenile woods, and other low-grade woods. However, if we succeed in turning those materials to advantage as the industrial material by developing the novel processing techniques, we can increase the demand for those materials in the world market, which encourages the plantation activity of those species from the economical point of view.

Scientists also point out the importance of the silvicultural management even in the natural forest, because an appropriate management, e.g. thinning of old trees, and removal of windfall trees, can keep the ability of carbon fixation in the forest at a higher level. Many of

obtained resources from the natural forest are lesser-known or lesser-used species that we have never used in the wood industry. Also in this case, what is important is to transform those products into the commercial-valued materials by developing the appropriate techniques, which gives an economical necessity to the silvicultural activity in the natural forest.

From the above discussions, we recognize that affirmative use of the lesser-used species, including the fast-growing species, saves the global crises that humankind is now confronted. For this purpose, we must urgently develop advanced techniques to utilize those lesser-used resources as the industrial materials.

1-3 Wood biomechanics – aim and scope of the present paper

Now is the time to establish a fundamental theory that makes us possible to develop advanced techniques to utilize the forest biomass including lesser-used resources. One of the best ways is to find a general principle that describes the origins of material properties of various wood species in relation to its higher-ordered structure. The author tries to find it from the biomechanical properties and its structural hierarchy of the wood cell wall.

The territory of “biomechanics” covers the research field whose goal is to clarify the origins of various biological phenomena on the basis of the mechanical viewpoint, and to apply obtained fruits to the human welfare. The subject of biomechanics hitherto has been focusing largely on the animal behaviors, because its fruits are practically useful in the field of medical sciences. However, from the above-mentioned reason, people are getting more alive than they once were to the importance of the wood biomechanics. The author of the present dissertation has been exploring the general theory to explain the origins of some biomechanical properties of wood especially in relation to its hierarchical structure, hoping that obtained fruits would be used for developing the novel functions of the forest products in the future.

In this dissertation, the author discusses the origin of the biomechanical properties of wood focusing on the following four topics that will be practically important when we use the forest products as the industrial materials.

The first topic is concerned with the general theory of the elastic behavior of the single wood fiber having multi-layered cell wall (= a homogenized model of the clear wood specimen). In this topic, with reference to the theory of micromechanics, mechanical properties of the single wood fiber is mathematically formulated.

The second topic is the biomechanical problems concerned in maturing xylem. This includes (1) the generation mechanism of the abnormal growth stress in the reaction wood

xylem, and (2) its role in controlling the negative-gravitropic behavior and the pattern formation of the growing tree shoot. In (1), the growth strain of maturing wood fiber is simulated by the formula derived in the first topic, and in (2), time-dependent evolution of the growing shoot is simulated on the basis of the structural mechanics. Future scopes of this topic are to develop the technique for detecting the reaction wood tissue formation and reducing the residual stress distributed inside the logs, and to predict and design the vegetation landscapes of the forest or the plantation.

The third topic is concerning the biomechanics of sawn wood. The simulation using the formula derived in the first topic plays an important role also in this topic. Aim of this topic is to understand the hygromechanical behaviors peculiar to the sawn wood in relation to its hierarchical structure. Especially in this paper, we focus on the hygroexpansive behavior and moisture-dependent elasticity of softwood. Future scope of this topic is to develop the technique for turning the low-grade materials, such as the reaction wood, the juvenile wood, and the naughty species, to advantage as the industrial material that can be used for wood-based materials or construction members.

The last fourth topic is on the biomechanics of tension wood properties. Tension wood formation is an indispensable tropism for inclined arboreal dicot shoot to evolve the negative-gravitropic response, while it often causes uncomfortable problems in the wood industry. Some researchers point out that the fast-growing species often contains the tension wood tissue. The time will come when we confront the processing problems caused by the tension wood in the fast-growing species, because we expect that plantation of the fast-growing species becomes very popular in the near future. Some researchers believe that the characteristic properties of the tension wood can be attributable to the appearance of gelatinous layer consisting of the pure cellulose crystal. Then, in this topic, we discuss the role of the gelatinous layer on the abnormal properties of the tension wood, i.e. high tensile growth stress, high axial shrinkage, and large axial Young's modulus. The protagonist in this topic is the simulation using the formula derived in the first topic. In the same way as the other topics, future scope in this topic is to develop the technique for turning the materials containing the tension wood to advantage for building or furniture materials.

References in Chapter 1

Hosokawa, R.T., Yamamoto, H., Rochadelli, R., Klock, U., Reicher, F., Bochicchio, R.: Reforestation: the dynamics of safe, efficient CO_2 storages, *Nagoya University Forest Science*, **21**, 9-18 (2002).

Chapter 2

MICROMECHANICS ON THE MULTI-LAYERED STRUCTURE OF THE WOOD CELL WALL

2-1 Reinforced-matrix theory

2-1-1 Model of the hierarchical structure of the wood from the macroscopic xylem to the single wood fiber

Wood consists of numerous fibrous elements. Those elements can be divided into two groups according to their morphological aspects, i.e. axial and radial elements. Most part of the softwood xylem consists of the axial elements, that is, numerous axial tracheids, and some parenchymae. The ray tissue is also differentiated in the softwood xylem, however its volume fraction is quite smaller than that of the axial elements. In the hardwood xylem, the vessel element is well developed, and the ray tissue generally becomes quite complicated as well as the axial parenchyma. Nonetheless, the wood fiber (i.e. libriform fiber, fiber-tracheid, and tracheid) often occupies the most part of the xylem.

Every xylem fiber (i.e. tracheid in softwood and hardwood, libriform wood fiber in hardwood, and fiber-tracheid in hardwood) shows very high aspect ratios, and it is arranged in the direction parallel to a common orientation in xylem, that is, the fiber direction. From this fact, it can be easily understood that the fiber properties largely influences the physical properties of the macroscopic wood especially in its longitudinal direction.

Among the longitudinal properties of the wood, the longitudinal Young's modulus and strength become very important material indicators when we use the wood as engineering materials, and those indicators are generally desired to take higher values as possible. The shrinkage coefficients and the growth stress levels are also both very important indicators, which are desired to be smaller as possible in the light of the wood industry. Those indicators or properties are macroscopic reflections of the properties or behaviors of each xylem fiber having a stiff and thick lignified cell wall. In this section, we intend to discuss such xylem characteristics from the viewpoint of the classical rule of mixture.

First, let us notice a homogeneous block of the wood as shown in Fig.2-1(a). Next, we transmute this block into a three-layered sandwich panel. It is assumed that a layer constituting the sandwich panel corresponds to each tissue in the wood as the parallel

composite consisting of xylem fiber, vessel element, and ray tissue (see Fig.2-1(b)).

If we apply the simple law of mixture to the three layered sandwich panel, the longitudinal Young's modulus of the panel (E_L) can be formulated as the following formula :

$$E_L = \frac{1}{F+V+R}\left(F \cdot E_L^F + V \cdot E_L^V + R \cdot E_L^R\right), \tag{2-1}$$

where E_L^F, E_L^V, and E_L^R are Young's modulus of respective tissues, and F, V, R stand for the area composition of domain of each tissue in the crosscut surface, e.g., wood fiber, vessel, and ray tissue, respectively. And, we assume $F+V+R=1$. Considering $E_L^V/E_L^F<<1$, and $E_L^R/E_L^F<<1$, we obtain

$$E_L^F = E_L/F \quad . \tag{2-1'}$$

In this approximation, we regarded $E_L^R \approx 0$ since the ray tissues are thin-walled tubes which are sparsely distributed inside the wood. In a certain hardwood species, the amount of the axial parenchyma becomes larger as compared with that of the other tissue. In such a case, we cannot ignore the effect of the axial parenchyma on the mechanical properties of the macroscopic wood. However, in the present analysis, we exclude such species as nontarget cases.

The longitudinal shrinkage of the parallel composite panel (α_L) can be formulated as the following formula :

$$\alpha_L = \frac{F \cdot E_L^F \cdot \alpha_L^F + V \cdot E_L^V \cdot \alpha_L^V + R \cdot E_L^R \cdot \alpha_L^R}{F \cdot E_L^F + V \cdot E_L^V + R \cdot E_L^R}, \tag{2-2}$$

where α_L^F, α_L^V, and α_L^R stand for the longitudinal shrinkage in respective tissues. E_L^F, E_L^V, and E_L^R are respective Young's moduli. Assuming $E_L^V/E_L^F<<1$, $E_L^R/E_L^F<<1$, and $F+V+R=1$, we obtain

$$\alpha_L^F = \alpha_L. \tag{2-2'}$$

The wood fiber, the vessel element, the ray parenchyma, and the axial parenchyma in the differentiating xylem tend to deform during their secondary wall maturation. Thus, the growth strain is generated in the maturing xylem. The longitudinal growth strain of the xylem at the macroscopic level (ε_L) can be expressed as the following formula:

$$\varepsilon_L = \frac{F \cdot E_L^F \cdot \varepsilon_L^F + V \cdot E_L^V \cdot \varepsilon_L^V + R \cdot E_L^R \cdot \varepsilon_L^R}{F \cdot E_L^F + V \cdot E_L^V + R \cdot E_L^R}, \tag{2-3}$$

where ε_L^F, ε_L^V, and ε_L^R are the longitudinal growth strain in respective tissues. Assuming $E_L^V/E_L^F<<1$, $E_L^R/E_L^F<<1$ and $F+V+R=1$, we obtain

$$\varepsilon_L^F = \varepsilon_L. \qquad (2\text{-}3')$$

Thus, it is concluded that the longitudinal shrinkage and the growth strain generated in a single wood fiber almost coincide with those generated in a macroscopic wood as a homogeneous aggregation of numerous wood fiber. In other words, we can formulate the hierarchical property in the mechanical behaviors of the wood from the single fiber to the macroscopic xylem on the bases of eqs.(2-1'), (2-2'), and (2-3').

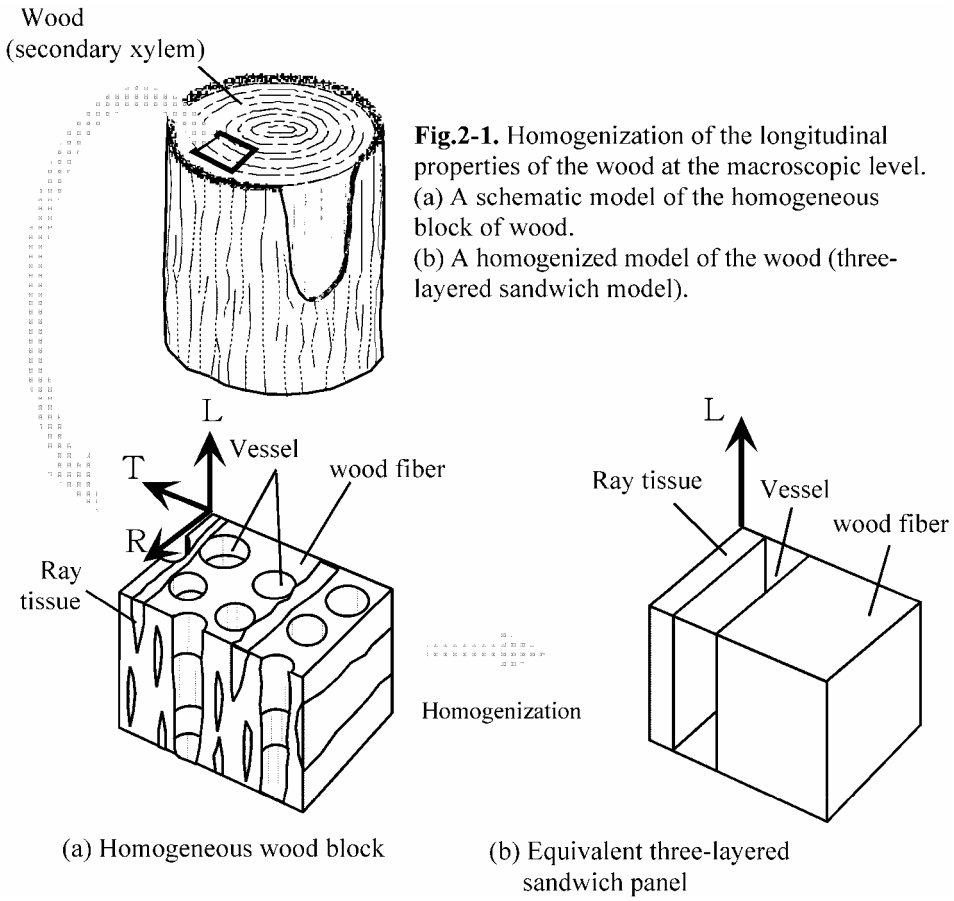

Fig.2-1. Homogenization of the longitudinal properties of the wood at the macroscopic level. (a) A schematic model of the homogeneous block of wood. (b) A homogenized model of the wood (three-layered sandwich model).

2-1-2 Model of the hierarchical structure of the wood from the cell wall constituents to the single wood fiber

A single wood fiber consists of the thick secondary wall (S), and the compound middle lamella (CML). Every wood fiber is glued to each other through the CML (Fig.2-2). The S is divided into three sub layers, i.e., outermost (S1), the middle (S2), and the innermost layers (S3). The S2 is the thickest among those three layers, which occupies the volume of 80~90 percent in the whole cell wall. In a case of the tension wood, the gelatinous layer (G) is formed as the innermost layer in the tension wood fiber. Some researchers consider that

xylem properties peculiar to the tension wood are caused by the G-layer, which will be discussed in Chapter 5. In either case, a single wood fiber can be approximated as the multi-layered tube having a very large aspect ratio. Then, in the present paper, we use the multi-layered tubular cylinder having three layers (CML+S1+S2), or four layers (CML+S1+S2+G) as the model of the single wood fiber (**Fig.2-2**). Three-layered tubular cylinder (CML/S1/S2) is a model of the softwood tracheid or the normal hardwood fiber, on the other hand, four layered one (CML/S1/S2/G) is a model of the tension wood gelatinous fiber.

Each layer can be approximated as a "two-phase structure", specifically the unidirectionally reinforcing element of polysaccharide bundle as the framework and the encrusting or embedding substance of lignin-hemicellulose compound as the matrix (MT). The former is mainly composed of highly crystallized cellulose microfibril (CMF), which is oriented in a certain direction to the fiber axis in each layer except the CML. This makes the secondary wall, including the G-layer, mechanically anisotropic. On the other hand, the orientation of the CMF is randomly distributed in the CML, then, we consider it to be mechanically isotropic.

In the case of the softwood secondary wall, oriented but non-crystalline polyose, such as (acetyle-) glucomannan, is often arranged along and around the CMF, forming the polysaccharide framework with the highly crystallized CMF, while non-oriented polyose has been detected in the matrix region of the cell wall (Liang et al. 1960, Fushitani 1973, Salmen 2000). Disoriented polyose, that is mainly xylan, is blended with lignin, forming the isotropic skeleton of the MT substance.

Behavior of each cell wall layer is controlled by the mechanical or physical properties of constituent materials in addition to their volumetric proportions and conjugation mode. It is comparatively easier to correlate the mechanical or physical properties of constituting cell wall layers to the behavior of the whole wood fiber on the basis of theory of polar-anisotropic elasticity (e.g. Lekhnitski 1960). However, it is not so easy task to formulate the behavior of each cell wall layer with a cognition that the cell wall layer should be treated as an assembly of constituent materials. If we succeed in such a task, then, we can formulate the mechanical hierarchy of the wood from each constituent material to the macroscopic xylem (Fig.2-3). It is anticipated that the reinforced matrix theory originally proposed by Barber and Meylan (1964) gives a useful approach to complete the above task.

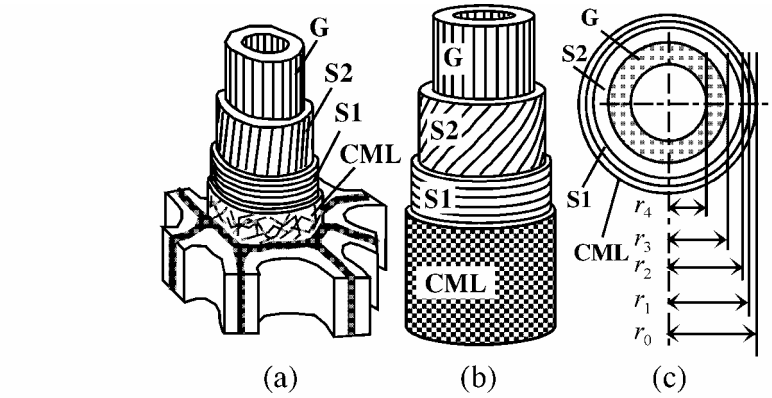

Fig.2-2. A model of the single wood fiber and its multi-layered structure. (a) Galatinous fiber in the tension wood. (b) Multi-layered circular tube model, and (c) its crosscut shape.

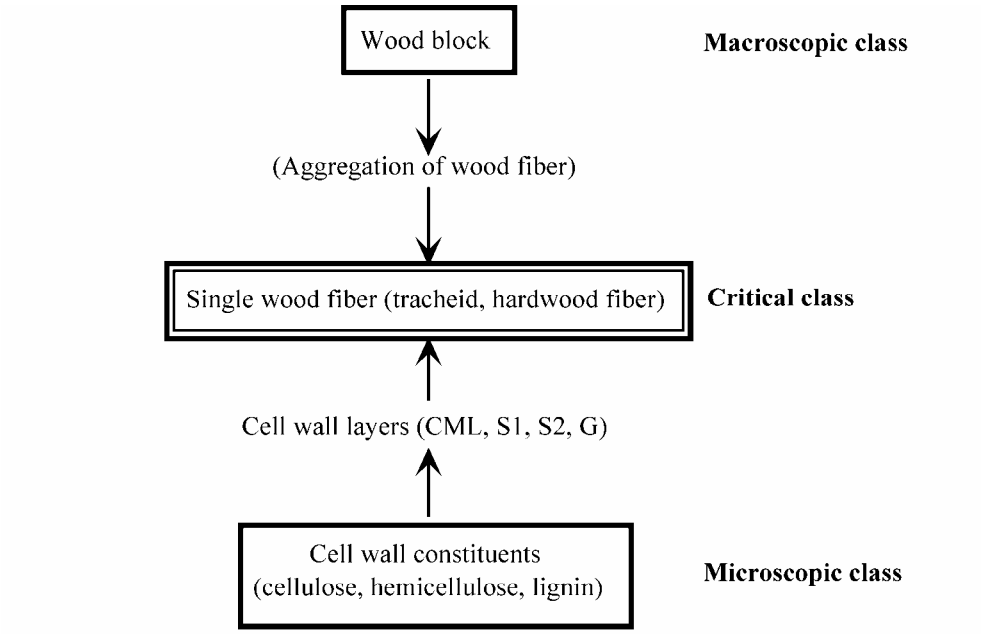

Fig.2-3. Diagramed idea of the "structural hierarchy". Single wood fiber is a critical class that connects the macroscopic class with the microscopic one in the wood.

2-1-3 Method of modeling the two-phase structure by the reinforced-matrix theory

In this study, we define the term “modeling” as a following meaning. First, we elucidate what kind of components constitutes “the wood at each hierarchical level”. Second, we transform morphological or physical properties of the components into observable parameters. Lastly, we combine those parameters into the mathematical formula that describes the behaviors or

properties of the wood at that hierarchical level.

(a) Application of micromechanics

We start our discussion from the mathematical formulation of “the two-phase structure” of the cell wall layer with reference to the micromechanics developed by J. D. Eshelby, T. Mura, T. Mori, K. Tanaka, et al. Every layer is approximated by “the two phase structure” of the crystalline polysaccharide bundle as the reinforcing phase and the lignin-hemicellulose compound as an isotropic matrix phase. The reinforcing phase consists of numerous fibrous crystal, and each crystal can be regarded as an “inclusion” or an “inhomogeneity” immersed in the matrix phase.

Eshelby (1957) supposed a material which contains an ellipsoidal inclusion in the matrix, and develop a mathematical theory to predict the stress field inside and around the inclusion when the material is subjected to a certain external stimulation, e.g., heating, cooling, or induction of an external load. The coefficient of thermal expansion is generally different between the inclusion and the matrix, and the same can be said for the elastic modulus. In those senses, we recently call such the inclusions “inhomogeneities”. Then, a certain dimensional misfit is caused between the inhomogeneity and the matrix, which induces an inhomogeneous stress disturbance inside the material. In order to calculate such stresses disturbance concretely, Eshelby (1957,1959) proposed a convenient method called “the equivalent inclusion method”. He replaced the inhomogeneity by the “equivalent inclusion” that has same elastic modulus as the matrix substance, and same shape as the inhomogeneity. He supposed that an inelastic strain (eigen-strain) is induced in the equivalent inclusion. And, he carried out the stress analysis in the material on the basis of the suitably supposed eigen-strain (see APPENDIX [1] and [2]). Eshelby’s method essentially should be applied to the cases that the inclusion exists at an enough distance from the free boundary of the material, and that the volume of the inclusions is quite smaller than that of the material. If the present inclusion is placed near the free surface of the material, or if the another inclusion exists near the present one, the stress disturbance from those situations would affect the stress field in the present inclusion and the matrix around it. This stress disturbance is called “the background stress” (Mura&Mori 1976, Hal&Klein 2003).

In the case that a background stress exists in the material, Eshelby’s idea can be developed as follows (Mori&Tanaka 1973). If the inclusion is “an equivalent inclusion” having same elastic modulus as the matrix, the background stress is uniformly distributed

inside the material whether the inclusion exists or not. In such a case, we can use the following formula as the stress equilibrium (see APPENDIX [2]):

$$(1-\phi)\sigma^{b} + \phi(\sigma^{F} + \sigma^{b}) = 0 \tag{2-4}$$

where ϕ is the volume fraction of the inclusions in the material, σ^{b} is the field of background stress generated in the equivalent inclusion, and σ^{F} is a stress disturbance induced by the eigen-stress of the equivalent inclusion. It is impossible to know accurate distribution of the background stress in the material. However, it is natural to assume that background stress in a domain containing an inclusion would be identical everywhere in the material. We call this assumption “the mean field approximation”. According to this assumption, we can identify the background stress σ^{b} in eq.(2-4) with the mean stress in the matrix region (as denoted by $\langle\sigma^{M}\rangle$), on the other hand, $\sigma^{F}+\sigma^{b}$ is regarded as the mean stress in the inhomogeneity (as denoted by $\langle\sigma^{F}\rangle$). Then, eq.(2-4) is rewritten as

$$(1-\phi)\ \langle\sigma^{M}\rangle\ +\ \phi\langle\sigma^{F}\rangle\ =\ 0. \tag{2-5}$$

Next, we try to apply Mori and Tanaka’s method (1973) to the case that the material containing the inhomogeneity is subjected to the external load. Also in such a case, eq.(2-5) is basically proper, provided that the field of external load σ^{A} must be superimposed on the mean stresses $\langle\sigma^{M}\rangle$ and $\langle\sigma^{F}\rangle$ in eq.(2-5) as follows:.

$$[\sigma^{M}] = \langle\sigma^{M}\rangle + \sigma^{A}, \quad \text{and} \quad [\sigma^{F}] = \langle\sigma^{F}\rangle + \sigma^{A} \tag{2-6}$$

Therefore, eq.(2-5) is rewritten as the following expression:

$$(1-\phi)\ [\sigma^{M}]\ +\ \phi[\sigma^{F}]\ =\ \sigma^{A}. \tag{2-7}$$

(b) Reinforced-matrix hypothesis

In the present study, an infinitely long rod-like polysaccharide fibril embedded in the matrix substance corresponds to the ellipsoidal inclusion with infinitely large long axis. $[\sigma^{M}]$ in eq.(2-7) is regarded as the mean stress generated in the matrix substance, and $[\sigma^{F}]$ is also mean stress in the single polysaccharide crystalline fibril. We introduce the stresses σ^{m} and σ^{f} as follows:

$$\sigma^{m} = (1-\phi)\,[\sigma^{M}]\,, \qquad \sigma^{f} = \phi\,[\sigma^{F}]\,. \tag{2-8}$$

Then, eq.(2-7) can be rewritten as

$$\sigma^{m} + \sigma^{f} = \sigma^{A}. \tag{2-9}$$

We try to give the following explanation as the physical interpretations of eqs.(2-9) and the tensorial quantities σ^{m} and σ^{f}.

Under lower magnification, the reinforcing element of the polysaccharide framework is

spatially dispersed uniformly in each cell wall layer forming the framework bundle. Similarly, the lignin-hemicellulose compound is diffused in each layer forming the isotropic MT skeleton. Therefore, it is considered that both the framework bundle and the MT skeleton occupy the same domain in the macroscopic limit (Yamamoto 1998, 1999). Thus, σ^m is regarded as the stress in the matrix as the skeleton, and σ^f is the stress in the polysaccharide framework as a bundle. Eq.(2-9) gives the condition that σ^m and σ^f should satisfy. We call this interpretation on the physical meanings of σ^m and σ^f "the reinforced-matrix hypothesis" hereinafter. N.F. Barber and B.A. Meylan intoduced a prototype of this hypothesis in their study on the mechanism of the shrinking anisotropy of the drying wood (Barber&Meylan 1964).

We introduce the elastic constant of the crystalline rope of the polysaccharide framework C^F and that of the matrix substance C^M, which are respectively related to $[\sigma^M]$ and $[\sigma^F]$ in eq.(2-7) as follows:

$$[\sigma^M] = C^M(\varepsilon^M - \alpha^M), \quad [\sigma^F] = C^F(\varepsilon^F - \alpha^F), \tag{2-10}$$

where ε^M and ε^F are strains of the dimensional changes, and α^M and α^F are the eigen-strains occurring in the respective components. Furthermore, we introduce the elastic constants C^m and C^f as follows:

$$C^m = (1-\phi)C^M, \qquad C^f = \phi \cdot C^F \tag{2-11}$$

C^m and C^f can be regarded as the elastic constants of the matrix skeleton and the polysaccharide framework bundle, respectively. Then, from eqs.(2-8), (2-10), and (2-11), the following constitive relations are derived for both phases:

$$\sigma^m = C^m(\varepsilon^M - \alpha^M), \quad \sigma^f = C^f(\varepsilon^F - \alpha^F)\,. \tag{2-12}$$

Thus, we obtain the constitutive relations which describe the elastic behaviors of the matrix skeleton and the framework bundle. By the way, it is natural to consider that ε^M and ε^F become identical at the macroscopic limit if no detachment occurs between the crystalline rope of the polysaccharide framework and the matrix substance. In the present paper, we adopt the following supposition *a priori*, then,

$$\varepsilon^M\ (=\varepsilon^m) = \varepsilon^F\ (=\varepsilon^f) = \varepsilon\,, \tag{2-13}$$

where ε is the strain of the dimensional change which is observed at the level of the layer. Based on this assumption (2-13), eqs.(2-12) can be rewritten as follows:

$$\sigma^m = C^m(\varepsilon - \alpha^M), \quad \sigma^f = C^f(\varepsilon - \alpha^F) \quad .$$

These equations clearly means the constitutive equations of a matrix as a skeleton and the polysaccharide framework as a bundle, respectively. Therefore, we can consider

$$\alpha^M = \alpha^m , \qquad \alpha^F = \alpha^f . \tag{2-13'}$$

We can derive the following equations in place of eqs.(2-12) accordingly:

$$\sigma^m = C^m(\varepsilon - \alpha^m), \quad \sigma^f = C^f(\varepsilon - \alpha^f) \ . \tag{2-12'}$$

Eqs.(2-9) and (2-12') are mathematical expressions of the reinforced-matrix hypothesis originally proposed by Barber and Maylan (1964).

2-2 Mechanics of the single wood fiber having multi-layered structure

How does a wood fiber behave inside the xylem, when a certain change occurs in the physical state of the cell wall? In the present section, on the basis of the reinforced matrix hypothesis which is formulated by eqs.(2-9) and (2-12'), we try to calculate the dimensional change of the isolated single wood fiber which is caused by the physical state change caused in the cell wall. In the present discussion, examples of the physical state change in the cell wall are (1) depositions of the matrix substance and the maturation of the polysaccharide framework during the cell wall formation (see Chapter 3), (2) moisture adsorption during the wood drying or swelling (see Section 4-1), and (3) elastic deformation due to the action of the external force (see Section 4-2).

2-2-1 Wood fiber model and coordinate system

(a) Coordinate system

As shown in Fig.2-4, two kinds of coordinate systems are used in the present analysis. One is the O-*l*tr local Cartesian coordinate system which is set at an arbitrary point (O) in the cell wall, provided that this system must satisfy the general conditions of the cylindrical coordinate system. "*l*" is the coordinate in the direction along the central axis of the cylinder, and "t" is the one in the direction along the tangent, which corresponds to the azimuthal angle in the cylindricall coordinate system. "r" is the one in the radial direction, which is equivalent to the radius from the central axis of the cylinder.

The other one is the O-xyz Cartesian coordinate system which is set at an arbitrary point (O) in the small plane element cut from each layer. The direction of x-axis is arranged in the direction parallel to the axis of the polysaccharide microfibril, and that of y-axis is the normal to the x-axis. z-axis is taken so that its positive direction coincides with r-axis of the O-*l*tr system. We assume that the polysaccharide microfibril in the S2 layer takes "S-helix", and that the O-*l*tr and the O-xyz coordinate systems are both right-handed as displayed in Fig.2-4.

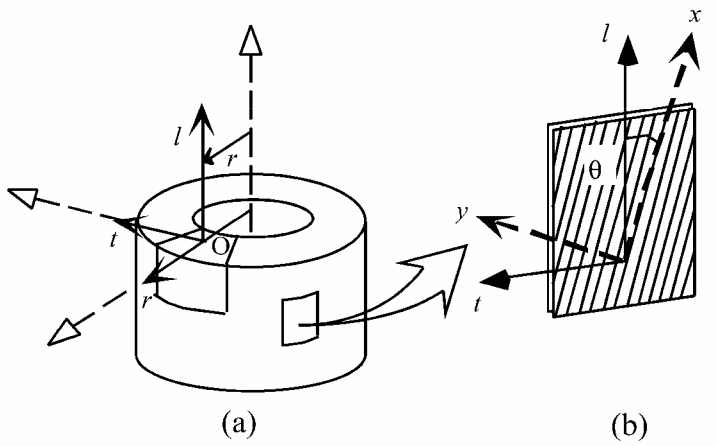

Fig.2-4. Two kinds of coordinate systems are used in the present analysis. **(a)** Local cartesian coordinate system bound to cylindrical coordinates, O- *l*tr . **(b)** Cartesian coordinate system O-*xy* bound to the plane element of the polysaccharide framework bundle.

(b) Constitutive equations

We start our discussion in the present section from eqs.(2-12') and (2-13'). α_{kl}^{m} in eq.(2-12') is a tensor of internal expansion which is caused by a certain biomechanical change. α_{kl}^{m} is observed that in each layer, $\alpha_{kl}^{m} = \varepsilon^{m}\delta_{kl}$, where δ_{kl} is Kronecker's symbol. ε^{m} is a scalar. We must take care not to confuse the present ε^{m} with the same sign used in eq.(2-13). C_{ijkl}^{m} and α_{kl}^{m} are both assumed to be isotropic. The elastic constants of the isotropic MT skeleton (non zero terms) C_{ijkl}^{m} are denoted as follows:

$$\begin{aligned} &C_{llll}^{m} = C_{tttt}^{m} = C_{rrrr}^{m} = \frac{1}{3}(K+2S), \quad C_{lltt}^{m} = C_{ttrr}^{m} = C_{ttll}^{m} = C_{llrr}^{m} \\ &= C_{rrll}^{m} = C_{rrtt}^{m} = \frac{1}{3}(K-S), \quad C_{trtr}^{m} = C_{rlrl}^{m} = C_{ltlt}^{m} = \frac{1}{2}S \end{aligned} \tag{2-14}$$

where $K = 3\lambda + 2\mu$, $S = 2\mu$. λ and μ are Lame's constant.

In Fig. 2-4, a small flat-board element of the framework bundle in the S2 layer is shown, provided that the positive direction of normal axis (z-axis) is coincident with the radial direction (*r*-axis) of the fiber model. In this model, the CMF and other oriented polyose in the S2 layer are assumed to be oriented in a S-helix at an angle of θ, and the one in the S1 layer is assumed to be aligned normally to the fiber axis. The relationship between stress (σ_{ij}^{f}) and strain (ε_{ij}) components induced in the framework bundle of each layer of the secondary wall can be written in eq.(2-12). We again show the constitutive equation of the framework bundle

in the O-xyz orthogonal coordinate system,

$$\sigma_{ab}{}^{f} = C_{abcd}{}^{f}(\varepsilon_{cd} - \alpha_{cd}{}^{f}), \tag{2-15}$$

where $C_{abcd}{}^{f}$ is the elastic constant of the framework bundle in each layer in the 0-xyz coordinate system. $\alpha_{ab}{}^{f}$ is an internal expansive strain originating in a fibril-like structure consisting of the CMF and other oriented polyose, caused by a certain biomechanical change. $\alpha_{ab}{}^{f}$ is expressed as a diagonal tensor whose components are

$$\mathrm{diag}\,(\alpha_{ab}{}^{f}) = \{\varepsilon^{f}, \varepsilon^{f'}, \varepsilon^{f'}\},$$

where ε^{f} and $\varepsilon^{f'}$ are the internal expansive strains induced in the polysaccharide framework in the directions parallel and perpendicular to the cellulose molecular chain, respectively. In the same way as the case of the matrix substance, we must pay attention not to confuse present "ε^{F}" with the same sign used in (2-13).

We supposed that each fibril-like structure of the oriented polysaccharide in the framework bundle is not so strongly connected to each other. Therefore, we can consider that the framework bundle is considerably compliant in its transverse direction, and all shear moduli, Poisson's ratios, and the Young's modulus in the transverse direction are small enough to be neglected. This means that the CMF including other oriented polysaccharide cannot be kept in a bundle shape without a reinforcing agent. The reinforcing agent is considered to be the lignin-hemicellulose isotropic matrix. Then, we may consider the stiffness components $C_{abcd}{}^{f}$ are all nil except $C_{xxxx}{}^{f}$ (=E).

By transforming the coordinate system from 0-xyz into 0-$l$tr system, eq.(2-15) is rewritten into new expression as follows:

$$\sigma_{ij}{}^{f} = C_{ijkl}{}^{f}\,(\varepsilon_{kl} - \alpha_{kl}{}^{f}), \tag{2-16}$$

where $C_{ijkl}{}^{f} = R_{ia}R_{jb}R_{kc}R_{ld}\,C_{abcd}{}^{f*}$, $\alpha_{ij}{}^{f} = R_{ia}R_{jb}\,\alpha_{ab}{}^{f*}$. R_{ij} is a transformation matrix between both coordinate systems. Under the coordinate system O-$l$tr, the non-zero terms of the stiffness components of the framework bundle ($C_{ijkl}{}^{f}$) are expressed as follows:

$$\begin{aligned}
&C_{llll}{}^{f} = c^4E, \quad C_{ll\mathrm{tt}}{}^{f} = C_{\mathrm{tt}ll}{}^{f} = c^2s^2E, \quad C_{lll\mathrm{t}}{}^{f} = C_{\mathrm{t}lll}{}^{f} = -c^3sE,\\
&C_{\mathrm{tttt}}{}^{f} = s^4E, \quad C_{\mathrm{tt}l\mathrm{t}}{}^{f} = C_{l\mathrm{ttt}}{}^{f} = -cs^3E, \quad C_{l\mathrm{t}l\mathrm{t}}{}^{f} = c^2s^2E,\\
&\alpha_{ll}{}^{f} = \varepsilon^{f}c^2 + \varepsilon^{f'}s^2\,, \quad \alpha_{\mathrm{tt}}{}^{f} = \varepsilon^{f}s^2 + \varepsilon^{f'}c^2\,, \quad \alpha_{l\mathrm{t}}{}^{f} = -(\varepsilon^{f} - \varepsilon^{f'})cs\,,
\end{aligned} \tag{2-17}$$

provided that we considerd $C_{ijkl}{}^{f} = C_{jikl}{}^{f} = C_{ijlk}{}^{f}$ and $C_{ijkl}{}^{f} = C_{klij}{}^{f}$, where c = cos φ, s = sin φ, and E is Young's modulus of the framework bundle in the direction along the cellulose molecular chain. E, S, ε^{m}, ε^{f}, ρ (= $r_{\mathrm{out}}/r_{\mathrm{in}}$), and φ take respective values in each layer as assumed in Table 2-1. They are not unknown values to be solved but known constants to be given in advance.

By substituting those derived equations in eq.(2-9), moreover considering the

compatibility of strains for the axisymmetrical deformation without torsion,

$$\varepsilon_r - \varepsilon_t = r\frac{d\varepsilon_t}{dr}, \tag{2-18}$$

we obtain the following constitutive equation for each layer of the secondary wall.

$$\sigma_l = -K\varepsilon^m - E\,c^2\varepsilon^f + \left\{\frac{1}{3}(K+2S) + Ec^4\right\}\varepsilon_l + \left\{\frac{2}{3}(K-S) + E\,c^2s^2\right\}\varepsilon_t + \frac{1}{3}(K-S)r\frac{d\varepsilon_t}{dr},$$

$$\sigma_t = -K\varepsilon^m - E\,s^2\varepsilon^f + \left\{\frac{1}{3}(K-S) + Ec^2s^2\right\}\varepsilon_l + \left\{\frac{2}{3}(2K+S) + E\,s^4\right\}\varepsilon_t + \frac{1}{3}(K-S)r\frac{d\varepsilon_t}{dr},$$

$$\sigma_r = -K\varepsilon^m + \frac{1}{3}(K-S)\varepsilon_l + \frac{1}{3}(2K+S)\varepsilon_t + \frac{1}{3}(K+2S)r\frac{d\varepsilon_t}{dr},$$

$$\tau_{lt} = -E\,cs\left(\varepsilon_l c^2 + \varepsilon_t s^2 - \varepsilon^f\right), \qquad \tau_{tr} = \tau_{rl} = 0, \tag{2-19}$$

where $\sigma_l \equiv \sigma_{ll}$, $\sigma_t \equiv \sigma_{tt}$,$\sigma_r \equiv \sigma_{rr}$, $\varepsilon_l \equiv \varepsilon_{ll}$, $\varepsilon_t \equiv \varepsilon_{tt}$,$\varepsilon_r \equiv \varepsilon_{rr}$. r is a radial distance from the central axis. Among the shear stress components, only σ_{lt} is not null, which is an inevitable consequence from the assumption of the axisymmetrical deformation, i.e. $\gamma_{lt} = 0$.

Table 2-1. List of the parameters in the basic formulae **[A]** and **[B]**.

layer	φ	r_{in}	r_{out}	ρ	S	E	P_{in}	P_{out}	L	ε^m	ε^f
CML	——	r_1	r_0 $(=r_1+h)$	$\rho_0 (= \frac{r_0}{r_1})$	S_0	$E_0(=0)$	P_1	$P_0(=0)$	L_0	0	0
S1	90 deg	r_2	r_1	$\rho_1 (= \frac{r_1}{r_2})$	S_1	E_1	P_2	P_1	L_1	ε_1^m	ε_1^f
S2	θ	r_3	r_2	$\rho_2 (= \frac{r_2}{r_3})$	S_2	E_2	P_3	P_2	L_2	ε_2^m	ε_2^f
G	0 deg	r_4	r_3	$\rho_3 (= \frac{r_3}{r_4})$	S_3	E_3	$P_4(=0)$	P_3	L_3	ε_3^m	ε_3^f

Note. $G = E/S$. $G_1 = E_1/S_1$, $G_2 = E_2/S_2$, $G_3 = E_3/S_3$, $Q = F/E_1$, $(F = S_0 \cdot h/r_1)$. $\rho = r_{out}/r_{in}$.

2-2-2 Deriving the basic equations

(a) Assumptions

The dimensional change of the complex tubular cylinder can be expressed as a set of normal

strains, namely, ε_l in the longitudinal direction, and $\varepsilon_t(r)|_{r=r0}$, $\varepsilon_t(r)|_{r=r1}$, $\varepsilon_t(r)|_{r=r2}$, $\varepsilon_t(r)|_{r=r3}$, and $\varepsilon_t(r)|_{r=r4}$ in the tangential directions at respective radius. As described in our previous report (Yamamoto et al. 2002, Yamamoto 2004), based on Eqs.(2-19), we solve ε_l, $\varepsilon_t(r)|_{r=r0}$, $\varepsilon_t(r)|_{r=r1}$, $\varepsilon_t(r)|_{r=r2}$, $\varepsilon_t(r)|_{r=r3}$, and $\varepsilon_t(r)|_{r=r4}$ under the following conditions (C1), (C2), (C3) and assumptions (A1), (A2), (A3):

(C1) ε_l is constant for all r. This is based on the assumption that the wood fiber model is an infinitely long cylinder in the l-direction. We denote ε_l as ε_L hereinafter.

(C2) $[\sigma_r(r)]_{r=r4} = -P_4$, $[\sigma_r(r)]_{r=r0} = -P_0$. $P_0 = P_4 = 0$. These boundary conditions mean there are no internal and external pressures acting on the wood fiber model.

(C3) The external force (P_L) induced parallel to the wood fiber model satisfies the following equation:

$$P_L = 2\pi L = \int_{\substack{crosscut\\surface}} \sigma_l \mathrm{d}A = \int_{\substack{crosscut\\surface}} \sigma_l r \mathrm{d}r\mathrm{d}\theta = 2\pi \int_{r_4}^{r_0} r\sigma_l(r)\mathrm{d}r. \qquad (2\text{-}20)$$

(C4) The deformation of the wood fiber model is assumed to be symmetric with respect to the central axis. Thus, we can express the fact that torsional deformation of individual fiber is completely restricted by the force of binding fibers inside the wood specimen.

Besides those conditions, the following assumptions (A1) ~ (A3) were added at processing;

(A1) $K >> S$, then S/K is enough small to be negligible in each layer. This hypothesizes that the bulk modulus of the MT skeleton (K) is quite larger than S. This postulates that the Poisson's ratio of the matrix skeleton is almost 0.5 like a kind of elastomers.

(A2) It is considered that E, S, ε^m, ε^f, and ρ (= r_{out}/r_{in}) tend to change their values during a certain bio-physical change, however, those changes can be neglected in the case that biomechanical changes were infinitesimally small.

(A3) $E = 0$ in eq. (7) in the CML. Namely, $E_0 = 0$. This does not mean that there is no oriented polysaccharide framework in the CML, but means that mechanical contribution of the randomly distributed polysaccharide framework in the CML should be isotropic. For convenience, we assume that S_0 means the shear modulus (× 2) of the CML itself. Moreover, $(h/r_1)^2 \sim 0$, $\varepsilon_0^f = 0$ and $\varepsilon_0^m = 0$ in the CML. Those assume that the thickness of the CML is quite smaller than the S1 and the S2 layers.

(b) Basic formula [A]

In this study, stress equilibrium for axisymmetrical deformation was given as follow:

$$\sigma_t - \sigma_r = r\frac{d\sigma_r}{dr} \quad . \tag{2-21}$$

Solving the second and third formula in the eqs.(2-19) for ε_t and $rd\varepsilon_t/dr$, and eliminating the term of σ_t using the equilibrium condition (2-21), we obtain

$$\begin{aligned}
&\left\{2S + Em^4 + u\left(S + 2Em^4\right)\right\}\varepsilon_t \\
&= 3S \cdot \varepsilon^m + (1+2u)E \cdot s^2 \cdot \varepsilon^f - \left\{S + Ec^2s^2 + u\left(-S + 2Ec^2s^2\right)\right\}\varepsilon_L + (1+2u)r\frac{d\sigma_r}{dr} + 3u\sigma_r, \\
&\left\{2S + Em^4 + u\left(S + 2Em^4\right)\right\}r\frac{d\varepsilon_t}{dr} \\
&= 3E \cdot s^4 \cdot \varepsilon^m - (2+u)E \cdot s^2 \cdot \varepsilon^f + \left(2 - 3s^2 + u\right)E \cdot s^2 \cdot \varepsilon_L - (2+u)r\frac{d\sigma_r}{dr} + 3Gus^4\sigma_r
\end{aligned} \tag{2-22}$$

where, $u = S/K$. Moreover, combining them by eliminating the term of ε_t, we obtain a differential equation of r:

$$\begin{aligned}
(1+2u)r^2\frac{d^2\sigma_r}{dr^2} + 3(1+2u)r\frac{d\sigma_r}{dr} - 3Gus^4\sigma_r \\
= 3E \cdot s^4\varepsilon^m - (2+u)E \cdot s^2\varepsilon^f + E \cdot s^2\left(2 - 3s^2 + u\right)\varepsilon_L .
\end{aligned} \tag{2-23}$$

General solution of eq.(2-23) is given as,

$$\begin{aligned}
\sigma_r &= C_1 r^{\alpha-1} + C_2 r^{-\alpha-1} \\
&\quad - \frac{1}{1+2u} \cdot \frac{1}{2\alpha}\left\{3E \cdot s^4\varepsilon^m - (2+u)E \cdot s^2\varepsilon^f + E \cdot s^2\left(2 - 3s^2 + u\right)\varepsilon_L\right\}\left\{\frac{1}{1+\alpha} - \left(\frac{r^{\alpha-1}-1}{\alpha-1}\right)\right\}
\end{aligned} \tag{2-24}$$

where C_1 and C_2 are integral constants, and α is described as follows (see also APPENDIX [3]):

$$\alpha = \sqrt{1 + 3G \cdot s^4\frac{u}{1+2u}} = \sqrt{1 + 3G \cdot s^4\frac{S}{K+2S}} \quad , \tag{2-25}$$

where $G=E/S$. Based on the assumption (A1) , we impose the following conditions:

$$u \to +0 \qquad \text{then} \qquad \alpha \to 1 + 0$$

which yields

$$\lim_{\alpha \to 1+0}\frac{r^{\alpha-1}-1}{\alpha-1} \to \ln r \quad .$$

Then, we can simplify the solution (2-24) as follows:

$$\sigma_r = C_1' + C_2 r^{-2} + \frac{1}{2}\left\{3E\cdot s^4\varepsilon^m - 2E\cdot s^2\varepsilon^f + \left(2-3s^2\right)E\cdot s^2\varepsilon_L\right\}\ln r \quad .$$

Under the boundary conditions $[\sigma_r(r)]_{r=rin} = -P_{in}$ and $[\sigma_r(r)]_{r=rout} = -P_{out}$, we can decide the integral constants C_1' and C_2, then, we obtain the following solution:

$$\sigma_r = -P_{in} - \frac{\rho^2 - r_{out}^2/r^2}{\rho^2-1}\left[P_{out} - P_{in} + \frac{1}{2}\left\{3E\cdot s^4\varepsilon^m - 2E\cdot s^2\varepsilon^f + E\cdot s^2\left(2-3s^2\right)\varepsilon_L\right\}\ln\rho\right]$$
$$+\frac{1}{2}\left\{3E\cdot s^4\varepsilon^m - 2E\cdot s^2\varepsilon^f + E\cdot s^2\left(2-3s^2\right)\varepsilon_L\right\}\ln\frac{r}{r_{in}} \quad . \tag{2-26}$$

Then, we substitute the above solution into the first equation of (2-22), and we obtain the following equation [**Basic formula A**]:

$$\Gamma\cdot\varepsilon_L + \Lambda\cdot\varepsilon_t = X\cdot\varepsilon^m + \Delta\cdot\varepsilon^f - 2\frac{1}{\left(\rho^2-1\right)}\left(\frac{r_{out}^2}{r^2}\right)\frac{P_{out}}{S} + 2\frac{1}{\left(\rho^2-1\right)}\left(\frac{r_{out}^2}{r^2}\right)\frac{P_{in}}{S}\,, \tag{2-27}$$

where

$$\Gamma = 1 + \frac{1}{2}G\cdot s^4 + G\cdot s^2\left(2-3s^2\right)\frac{\ln\rho}{\rho^2-1}\frac{r_{out}^2}{r^2}, \qquad \Lambda = 2 + G\cdot s^4,$$
$$X = 3 + \frac{3}{2}G\cdot s^4 - 3G\cdot s^4\frac{\ln\rho}{\rho^2-1}\frac{r_{out}^2}{r^2}, \qquad \text{and}\Delta = 2G\cdot s^2\frac{\ln\rho}{\rho^2-1}\left(\frac{r_{out}^2}{r^2}\right) \quad .$$

Coefficients, Γ, Λ, X, and Δ are dependent on G (=E/S), φ, r, r_{out}, and ρ, provided that those variables take their respective values in each layer as shown in Table 2-2.

(c) Basic formula [B]

We solve the eqs.(2-19) for ε_L, and integrate it over the crosscut area of each layer. When integrating it, we assume that ε^m and ε^f are independent of r in the respective layer, and ε_l takes a constant value (=ε_L) over the crosscut surface of the cell wall because of condition (C1). As the result, we obtain the following equation [**Basic formula B**]:

$$\Omega\cdot\varepsilon_L = \Phi\cdot\varepsilon^m + \Sigma\cdot\varepsilon^f + \frac{2}{3}\frac{L}{S\cdot r_{in}^2}\frac{\Lambda}{\rho^2-1} + \frac{2}{3}\frac{\rho^2}{\rho^2-1}\frac{P_{out}}{S}\left[\Gamma\right]_{r=r_{out}} - \frac{2}{3}\frac{1}{\rho^2-1}\frac{P_{in}}{S}\left[\Gamma\right]_{r=r_{in}}, \tag{2-28}$$

where

$$\Omega = 1 + \frac{2}{3}G\left(1 - 3s^2 + 3s^4\right) - \frac{1}{3}G^2 \cdot s^4\left(2 - 3s^2\right)^2 \left\{\left(\frac{\rho}{\rho^2 - 1}\ln\rho\right)^2 - \frac{1}{4}\right\},$$

$$\Phi = 1 - G \cdot s^2(c^2 - s^2) + G^2 \cdot s^6\left(2 - 3s^2\right)\left\{\left(\frac{\rho}{\rho^2 - 1}\ln\rho\right)^2 - \frac{1}{4}\right\},$$

$$\Sigma = \frac{1}{3}G\left(2 - 3s^2\right) - \frac{2}{3}G^2 \cdot s^4\left(2 - 3s^2\right)\left\{\left(\frac{\rho}{\rho^2 - 1}\ln\rho\right)^2 - \frac{1}{4}\right\}, \qquad L = \frac{1}{2\pi}\int_{\text{each layer}} \sigma_l \, r dr d\theta.$$

Coefficients, Ω, Φ, and Σ are dependent on G (=E/S), φ, and ρ provided that those coefficients take their respective values in each layer as shown in Table 2-2.

Table 2-2. List of the coefficients in the basic formulae **[A]** and **[B]**.

layer	location	Γ	Λ	X	Δ	Ω	Φ	Σ
CML	at $r = r_0$ at $r = r_1$	Γ_0' (=1) Γ_0 (=1)	Λ_0' (=2) Λ_0 (=2)	X_0' (=3) X_0 (=3)	Δ_0' (=0) Δ_0 (=0)	Ω_0 (=1)	Φ_0 (=1)	Σ_0 (=0)
S1	at $r = r_1$ at $r = r_2$	Γ_1' Γ_1	Λ_1' Λ_1	X_1' X_1	Δ_1' Δ_1	Ω_1	Φ_1	Σ_1
S2	at $r = r_2$ at $r = r_3$	Γ_2' Γ_2	Λ_2' Λ_2	X_2' X_2	Δ_2' Δ_2	Ω_2	Φ_2	Σ_2
G	at $r = r_3$ at $r = r_4$	Γ_3' (=1) Γ_3 (=1)	Λ_3' (=2) Λ_3 (=2)	X_3' (=3) X_3 (=3)	Δ_3' (=0) Δ_3 (=0)	Ω_3	Φ_3 (=1)	Σ_3

(d) Formulae to describe the deforming single G-fiber (four-layered circular tube)

In the G-fiber model as the whole, we obtain twelve equations based on the basic formulae [A] and [B]. Those are as follows:

Basic form.[A] in CML at $r = r_0$ (a0), Basic form.[A] in CML at $r = r_1$ (a0'),

Basic form.[B] in CML (b0),

Basic form.[A] in S1 at $r = r_1$ (a1), Basic form.[A] in S1 at $r = r_2$ (a1'),

Basic form.[B] in S1 (b1),

Basic form.[A] in S2 at $r = r_2$ (a2), Basic form.[A] in S2 at $r = r_3$ (a2'),

Basic form.[B] in S2 (b2),

Basic form.[A] in G at $r = r_3$ (a3), Basic form.[A] in G at $r = r_4$ (a3'),

Basic form.[B] in G (b3).

Those equations constitute simultaneous equations whose unknown valuables are

$$\varepsilon_L,\ \varepsilon_t|_{r=r0},\ \varepsilon_t|_{r=r1},\ \varepsilon_t|_{r=r2},\ \varepsilon_t|_{r=r3},\ \varepsilon_t|_{r=r4}\ ;\quad P_0, P_1, P_2, P_3, P_4\ ;\quad L_0, L_1, L_2, L_3\ .$$

According to the assumption (A3), eq.(a0) and (a0') are degenerated each other, which yields

$$\varepsilon_t|_{r=r0} \approx \varepsilon_t|_{r=r1}\ .$$

Therefore, unknown variables become finally as follows;

$$\varepsilon_L,\ \varepsilon_t|_{r=r1},\ \varepsilon_t|_{r=r2},\ \varepsilon_t|_{r=r3},\ \varepsilon_t|_{r=r4}\ ;\quad P_0, P_1, P_2, P_3, P_4\ ;\quad L_0, L_1, L_2, L_3\ .$$

To solve eqs.(a0'), (a1), -----, (a3'); (b1), ---, (b3) for those unknown variables, we impose the following conditions on the basis of the conditions (C2) and (C3):

$$P_0 = 0 \quad \text{(c1)}, \qquad P_4 = 0 \quad \text{(c2)}, \qquad L = L_0 + L_1 + L_2 + L_3 \quad \text{(c3)}.$$

The unknown variables explicitly required in our study are ε_L, $\varepsilon_t|_{r=r1}$, $\varepsilon_t|_{r=r2}$, $\varepsilon_t|_{r=r3}$, and $\varepsilon_t|_{r=r4}$. Thus, by eliminating the unknown variables P_0, P_1, P_2, P_3, P_4, L_0, L_1, L_2, L_3, and L_4 in the following manner, we degenerated the simultaneous equations (a0'), (a1), -----, (b3), (c1), (c2), and (c3) into the simpler ones of which unknown variables are ε_L, $\varepsilon_t|_{r=r1}$, $\varepsilon_t|_{r=r2}$, $\varepsilon_t|_{r=r3}$, and $\varepsilon_t|_{r=r4}$.

– The first equation –

From eqs.(a0'), (b0), (a1'), (b1), (a2'), (b2),(b3), (c1), (c2), and (c3), we eliminate P_0, P_1, P_2, P_3, P_4, L_0, L_1, L_2, L_3, and L_4. Thus, we obtain the first equation,

$$\begin{aligned} &a_{11}\varepsilon_L + a_{12}\varepsilon_t\big|_{r=r_1} + a_{13}\varepsilon_t\big|_{r=r_2} + a_{14}\varepsilon_t\big|_{r=r_3} + a_{15}\varepsilon_t\big|_{r=r_4} \\ &= b_{11}\varepsilon_1^m + b_{12}\varepsilon_2^m + b_{13}\varepsilon_3^m + c_{11}\varepsilon_1^f + c_{12}\varepsilon_2^f + c_{13}\varepsilon_3^f + d_{11}P_L\ , \end{aligned} \qquad \text{(2-29-1)}$$

where coefficients a_{11}, a_{12}, a_{13}, a_{14}, a_{15} , b_{11}, b_{12}, b_{13}, c_{11}, c_{12}, c_{13}, and d_{11} are respective functions whose concrete forms are composed of θ, ρ_1, ρ_2, ρ_3, Q, G_1, G_2, G_3, M, and N. Detailed shapes of those coefficients are described in the APPENDIX [4]. P_L stands for the external force induced parallel to the wood fiber model, which is related with L_0, L_1, L_2, and L_3 as follows:

$$P_L = 2\pi L = 2\pi(L_0 + L_1 + L_2 + L_3) = \int_{\substack{crosscut\\surface}} \sigma_l\, r dr d\theta = 2\pi \int_{r_4}^{r_0} \sigma_l\, r dr$$

.

ε_L, $\varepsilon_t|_{r=r1}$, $\varepsilon_t|_{r=r2}$, $\varepsilon_t|_{r=r3}$, and $\varepsilon_t|_{r=r4}$ are unknown variables to be solved as solutions of an algebraic equation (2-29-1).

– The second ~ the fifth equation –

To solve the equations for ε_L, $\varepsilon_t|_{r=r1}$, $\varepsilon_t|_{r=r2}$, $\varepsilon_t|_{r=r3}$, and $\varepsilon_t|_{r=r4}$, we must have at least four necessary equations which are constituted by the same unknown variables. Those equations can be derived from the basic formula **[A]** as follows.

(The second equation)

From eqs.(a0'), (a1'), (a2'), (a3), (c1), and (c2), we eliminate P_0, P_1, P_2, P_3, and P_4. Thus, we obtain

$$\begin{aligned} &a_{21}\varepsilon_L + a_{22}\varepsilon_t\big|_{r=r1} + a_{23}\varepsilon_t\big|_{r=r2} + a_{24}\varepsilon_t\big|_{r=r3} + a_{25}\varepsilon_t\big|_{r=r4} \\ &\qquad = b_{21}\varepsilon_1^m + b_{22}\varepsilon_2^m + b_{23}\varepsilon_3^m + c_{21}\varepsilon_1^f + c_{22}\varepsilon_2^f + c_{23}\varepsilon_3^f + d_{21}P_L. \end{aligned} \tag{2-29-2}$$

(The third equation)

From eqs.(a0'), (a1'), (a2), (a3), (c1), and (c2), we eliminate P_0, P_1, P_2, P_3, and P_4. Thus, we obtain

$$\begin{aligned} &a_{31}\varepsilon_L + a_{32}\varepsilon_t\big|_{r=r1} + a_{33}\varepsilon_t\big|_{r=r2} + a_{34}\varepsilon_t\big|_{r=r3} + a_{35}\varepsilon_t\big|_{r=r4} \\ &\qquad = b_{31}\varepsilon_1^m + b_{32}\varepsilon_2^m + b_{33}\varepsilon_3^m + c_{31}\varepsilon_1^f + c_{32}\varepsilon_2^f + c_{33}\varepsilon_3^f + d_{31}P_L. \end{aligned} \tag{2-29-3}$$

(The fourth equation)

From eqs.(a0'), (a1), (a2), (a3), (c1), and (c2), we eliminate P_0, P_1, P_2, P_3, and P_4. Thus, we obtain

$$\begin{aligned} &a_{41}\varepsilon_L + a_{42}\varepsilon_t\big|_{r=r1} + a_{43}\varepsilon_t\big|_{r=r2} + a_{44}\varepsilon_t\big|_{r=r3} + a_{45}\varepsilon_t\big|_{r=r4} \\ &\qquad = b_{41}\varepsilon_1^m + b_{42}\varepsilon_2^m + b_{43}\varepsilon_3^m + c_{41}\varepsilon_1^f + c_{42}\varepsilon_2^f + c_{43}\varepsilon_3^f + d_{41}P_L. \end{aligned} \tag{2-29-4}$$

(The fifth equation)

From eqs.(a0'), (a1'), (a2'), (a3'), (c1), and (c2), we eliminate P_0, P_1, P_2, P_3, and P_4. Thus, we obtain

$$\begin{aligned} a_{51}\varepsilon_{\mathrm{L}} + a_{52}\varepsilon_{\mathrm{t}}\big|_{r=r_1} + a_{53}\varepsilon_{\mathrm{t}}\big|_{r=r_2} + a_{54}\varepsilon_{\mathrm{t}}\big|_{r=r_3} + a_{55}\varepsilon_{\mathrm{t}}\big|_{r=r_4} \\ = b_{51}\varepsilon_1^{\mathrm{m}} + b_{52}\varepsilon_2^{\mathrm{m}} + b_{53}\varepsilon_3^{\mathrm{m}} + c_{51}\varepsilon_1^{\mathrm{f}} + c_{52}\varepsilon_2^{\mathrm{f}} + c_{53}\varepsilon_3^{\mathrm{f}} + d_{51}P_{\mathrm{L}}, \end{aligned} \tag{2-29-5}$$

where coefficients a_{21}, a_{22}, a_{23}, --- , a_{55}, b_{21}, b_{22}, ---, b_{53}, c_{11}, c_{12}, ---, c_{53}, and d_{11}, ---, d_{51} are respective functions of whose concrete forms are described in the APPENDIX [4].

Equations (2-29-1~5) constitute the simultaneous algebraic equations whose unknown variables are ε_{L}, $\varepsilon_{\mathrm{t}}^{r1}$ (= $\varepsilon_{\mathrm{t}}|_{r=r1}$), $\varepsilon_{\mathrm{t}}^{r2}$ (= $\varepsilon_{\mathrm{t}}|_{r=r2}$), $\varepsilon_{\mathrm{t}}^{r3}$ (= $\varepsilon_{\mathrm{t}}|_{r=r3}$), and $\varepsilon_{\mathrm{t}}^{r4}$ (= $\varepsilon_{\mathrm{t}}|_{r=r4}$), on the other hand, the values of $\varepsilon_1^{\mathrm{m}}$, $\varepsilon_2^{\mathrm{m}}$, $\varepsilon_3^{\mathrm{m}}$, $\varepsilon_1^{\mathrm{f}}$, $\varepsilon_2^{\mathrm{f}}$, $\varepsilon_3^{\mathrm{f}}$, and P_{L} should be given as eigen-strains and external load in advance. From those simultaneous equations, the solutions can be derived as following forms:

$$\begin{aligned} \varepsilon_{\mathrm{L}} &= f_{11}(\mathbf{p})\varepsilon_1^{\mathrm{m}} + f_{12}(\mathbf{p})\varepsilon_2^{\mathrm{m}} + f_{13}(\mathbf{p})\varepsilon_3^{\mathrm{m}} + f_{14}(\mathbf{p})\varepsilon_1^{\mathrm{f}} + f_{15}(\mathbf{p})\varepsilon_2^{\mathrm{f}} + f_{16}(\mathbf{p})\varepsilon_3^{\mathrm{f}} + f_{17}(\mathbf{p})P_{\mathrm{L}} \\ \varepsilon_{\mathrm{t}}^{r1} &= f_{21}(\mathbf{p})\varepsilon_1^{\mathrm{m}} + f_{22}(\mathbf{p})\varepsilon_2^{\mathrm{m}} + f_{23}(\mathbf{p})\varepsilon_3^{\mathrm{m}} + f_{24}(\mathbf{p})\varepsilon_1^{\mathrm{f}} + f_{25}(\mathbf{p})\varepsilon_2^{\mathrm{f}} + f_{26}(\mathbf{p})\varepsilon_3^{\mathrm{f}} + f_{27}(\mathbf{p})P_{\mathrm{L}} \\ \varepsilon_{\mathrm{t}}^{r2} &= f_{31}(\mathbf{p})\varepsilon_1^{\mathrm{m}} + f_{32}(\mathbf{p})\varepsilon_2^{\mathrm{m}} + f_{33}(\mathbf{p})\varepsilon_3^{\mathrm{m}} + f_{34}(\mathbf{p})\varepsilon_1^{\mathrm{f}} + f_{35}(\mathbf{p})\varepsilon_2^{\mathrm{f}} + f_{36}(\mathbf{p})\varepsilon_3^{\mathrm{f}} + f_{37}(\mathbf{p})P_{\mathrm{L}} \\ \varepsilon_{\mathrm{t}}^{r3} &= f_{41}(\mathbf{p})\varepsilon_1^{\mathrm{m}} + f_{42}(\mathbf{p})\varepsilon_2^{\mathrm{m}} + f_{43}(\mathbf{p})\varepsilon_3^{\mathrm{m}} + f_{44}(\mathbf{p})\varepsilon_1^{\mathrm{f}} + f_{45}(\mathbf{p})\varepsilon_2^{\mathrm{f}} + f_{46}(\mathbf{p})\varepsilon_3^{\mathrm{f}} + f_{47}(\mathbf{p})P \\ \varepsilon_{\mathrm{t}}^{r4} &= f_{51}(\mathbf{p})\varepsilon_1^{\mathrm{m}} + f_{52}(\mathbf{p})\varepsilon_2^{\mathrm{m}} + f_{53}(\mathbf{p})\varepsilon_3^{\mathrm{m}} + f_{54}(\mathbf{p})\varepsilon_1^{\mathrm{f}} + f_{55}(\mathbf{p})\varepsilon_2^{\mathrm{f}} + f_{56}(\mathbf{p})\varepsilon_3^{\mathrm{f}} + f_{57}(\mathbf{p})P_{\mathrm{L}}, \end{aligned} \tag{2-30}$$

where coefficients f_{11}, f_{12}, ..., f_{57} are functions of $\mathbf{p}$, and $\mathbf{p}$ is a parameter vector whose components are θ, ρ_1, ρ_2, ρ_3, Q, G_1, G_2, G_3, M, and $\tilde{N}$ Among the solutions, ε_{L} stands for the strain of the G-fiber model in the axial direction. According to the condition (C4), the wood fiber model deforms axisymmetrically, then, $\varepsilon_{\mathrm{t}}^{r1}$(=$\varepsilon_{\mathrm{t}}^{r0}$), $\varepsilon_{\mathrm{t}}^{r2}$, $\varepsilon_{\mathrm{t}}^{r3}$, and $\varepsilon_{\mathrm{t}}^{r4}$ are equivalent strains to the diametral deformations at their respective radii. Those strains are induced by a certain biomechanical change in the G-fiber. The thickness of the CML is enough small to be negligible if compared to those of the S1 and S2 layers. Therefore, $\varepsilon_{\mathrm{t}}^{r1}$ can be regarded as the strain of the diameter in the wood fiber model (=ε_{T}).

– Developing the eqs.(2-30) into the differential equations –

According to the assumption (A2), eqs.(2-30) are valid under the duration that the

biomechanical change is infinitesimally small enough to be neglected. This means that ε_L, ε_t^{r1}, ε_t^{r2}, ε_t^{r3}, and ε_t^{r4} in addition to ε_1^m, ε_2^m, ε_3^m, ε_1^f, ε_2^f, ε_3^f, and P_L in eqs.(2-30) should be replaced as differential quantities, i.e. $d\varepsilon_L$, $d\varepsilon_t^{r1,}$ $d\varepsilon_t^{r2}$, $d\varepsilon_t^{r3}$, $d\varepsilon_t^{r4}$, $d\varepsilon_1^m$, $d\varepsilon_2^m$, $d\varepsilon_3^m$, $d\varepsilon_1^f$, $d\varepsilon_2^f$, $d\varepsilon_3^f$, and dP_L. Then, each equation in (2-30) should be rewritten as a simple differential form, moreover, they are divided by dt, and are converted into following differential equations:

$$\begin{aligned}
\dot{\varepsilon}_L &= f_{11}(\mathbf{p})\dot{\varepsilon}_1^m + f_{12}(\mathbf{p})\dot{\varepsilon}_2^m + f_{13}(\mathbf{p})\dot{\varepsilon}_3^m + f_{14}(\mathbf{p})\dot{\varepsilon}_1^f + f_{15}(\mathbf{p})\dot{\varepsilon}_2^f + f_{16}(\mathbf{p})\dot{\varepsilon}_3^f + f_{17}(\mathbf{p})\dot{P}_L \\
\dot{\varepsilon}_t^{r1} &= f_{21}(\mathbf{p})\dot{\varepsilon}_1^m + f_{22}(\mathbf{p})\dot{\varepsilon}_2^m + f_{23}(\mathbf{p})\dot{\varepsilon}_3^m + f_{24}(\mathbf{p})\dot{\varepsilon}_1^f + f_{25}(\mathbf{p})\dot{\varepsilon}_2^f + f_{26}(\mathbf{p})\dot{\varepsilon}_3^f + f_{27}(\mathbf{p})\dot{P}_L \\
\dot{\varepsilon}_t^{r2} &= f_{31}(\mathbf{p})\dot{\varepsilon}_1^m + f_{32}(\mathbf{p})\dot{\varepsilon}_2^m + f_{33}(\mathbf{p})\dot{\varepsilon}_3^m + f_{34}(\mathbf{p})\dot{\varepsilon}_1^f + f_{35}(\mathbf{p})\dot{\varepsilon}_2^f + f_{36}(\mathbf{p})\dot{\varepsilon}_3^f + f_{37}(\mathbf{p})\dot{P}_L \\
\dot{\varepsilon}_t^{r3} &= f_{41}(\mathbf{p})\dot{\varepsilon}_1^m + f_{42}(\mathbf{p})\dot{\varepsilon}_2^m + f_{43}(\mathbf{p})\dot{\varepsilon}_3^m + f_{44}(\mathbf{p})\dot{\varepsilon}_1^f + f_{45}(\mathbf{p})\dot{\varepsilon}_2^f + f_{46}(\mathbf{p})\dot{\varepsilon}_3^f + f_{47}(\mathbf{p})\dot{P}_L, \\
\dot{\varepsilon}_t^{r4} &= f_{51}(\mathbf{p})\dot{\varepsilon}_1^m + f_{52}(\mathbf{p})\dot{\varepsilon}_2^m + f_{53}(\mathbf{p})\dot{\varepsilon}_3^m + f_{54}(\mathbf{p})\dot{\varepsilon}_1^f + f_{55}(\mathbf{p})\dot{\varepsilon}_2^f + f_{56}(\mathbf{p})\dot{\varepsilon}_3^f + f_{57}(\mathbf{p})\dot{P}_L,
\end{aligned} \tag{2-31}$$

provided that a dot on each of ε_L, ε_t^{r1}, ε_t^{r2}, ε_t^{r3}, ε_t^{r4}, ε_1^m, ε_2^m, ε_3^m, ε_1^f, ε_2^f, ε_3^f, and $P_L$stands for the derivative by t. Furthermore, ρ_1, ρ_2, and ρ_3 among the components of **p** should be rewritten into differential quantities, $d\rho_1$, $d\rho_2$, and $d\rho_3$, since they depend on the elapsed time during a certain biomechanical change. Due to the assumption of axisymmetrical deformation, the following relations are required among respective layers:

$$\rho_1 + d\rho_1 = \frac{r_1 + dr_1}{r_2 + dr_2} = \frac{1 + d\varepsilon_t^{r1}}{1 + d\varepsilon_t^{r2}}\rho_1 \ , \quad \rho_2 + d\rho_2 = \frac{r_2 + dr_2}{r_3 + dr_3} = \frac{1 + d\varepsilon_t^{r2}}{1 + d\varepsilon_t^{r3}}\rho_2 \ ,$$

$$\rho_3 + d\rho_3 = \frac{r_3 + dr_3}{r_4 + dr_4} = \frac{1 + d\varepsilon_t^{r3}}{1 + d\varepsilon_t^{r4}}\rho_3 \ .$$

Since $d\rho_3 \cdot d\varepsilon_t^{r4}$, $d\rho_2 \cdot d\varepsilon_t^{r3}$, and $d\rho_1 \cdot d\varepsilon_t^{r2}$ are regarded as higher order infinitesimal quantities, we can obtain the following differential forms:

$$d\rho_1 = (d\varepsilon_t^{r1} - d\varepsilon_t^{r2})\rho_1, \quad d\rho_2 = (d\varepsilon_t^{r2} - d\varepsilon_t^{r3})\rho_2, \quad d\rho_3 = (d\varepsilon_t^{r3} - d\varepsilon_t^{r4})\rho_3.$$

These equations can be rewritten as differential equations of t as follows:

$$\dot{\rho}_1 = (\dot{\varepsilon}_t^{r1} - \dot{\varepsilon}_t^{r2})\rho_1, \quad \rho_2 = (\dot{\varepsilon}_t^{r2} - \dot{\varepsilon}_t^{r3})\rho_2, \quad \dot{\rho}_3 = (\dot{\varepsilon}_t^{r3} - \dot{\varepsilon}_t^{r4})\rho_3. \tag{2-32}$$

Solutions of eqs.(2-32) are included as components of parameter vector **p** in eqs.(2-31). Therefore, eqs. (2-31) and (2-32) constitute a system of simultaneous differential equations whose unknown functions are ε_L, ε_t^{r1}, ε_t^{r2}, ε_t^{r3}, ε_t^{r4}, ρ_1, ρ_2, and ρ_3. On the other hand, ε_1^m, ε_2^m, ε_3^m, ε_1^f, ε_2^f, ε_3^f, and P_L are the functions whose t-dependent shapes should be given in advance.

(e) Solving the simultaneous differential equations (2-31) and (2-32)

We assume that change of the physical state in the cell wall starts at $t = 0$ and ends at $t = Z$. By integrating simultaneous equations (2-31) and (2-32) from $t = 0$ to $t = Z$ under the proper initial condition, we can solve them for ε_L, ε_t^{r1}, ε_t^{r2}, ε_t^{r3}, ε_t^{r4}, ρ_1, ρ_2, and ρ_3. Or, we can express those solutions as functions of t if we stop the integration at t (>0). As the initial conditions at $t = 0$, we assume

$$\varepsilon_L(0) = \varepsilon_t^{r1}(0) = \varepsilon_t^{r2}(0) = \varepsilon_t^{r3}(0) = \varepsilon_t^{r4}(0) = 0, \quad \rho_1(0) = \hat{\rho}_1, \quad \rho_2(0) = \hat{\rho}_2, \quad \rho_3(0) = \hat{\rho}_3 .$$

Then, we divide the integral interval into n small parts, and denote the integrals of eqs.(21) in the i-th small interval ($(i-1)Z/n < t < iZ/n$, i = 1, 2, ..., n) as $\Delta^i\varepsilon_L$, $\Delta^i\varepsilon_t^{r1}$, $\Delta^i\varepsilon_t^{r2}$, $\Delta^i\varepsilon_t^{r3}$, and $\Delta^i\varepsilon_t^{r4}$. For example, $\Delta^i\varepsilon_L$ is calculated as

$$\begin{aligned}\Delta^i\varepsilon_L &\equiv \int_{(i-1)Z/n}^{i\cdot Z/n} \frac{d\varepsilon_L}{dt} dt \\ &= \int_{(i-1)Z/n}^{i\cdot Z/n} \left(f_{11}(\mathbf{p})\dot{\varepsilon}_1^{m} + f_{12}(\mathbf{p})\dot{\varepsilon}_2^{m} + f_{13}(\mathbf{p})\dot{\varepsilon}_3^{m} + f_{14}(\mathbf{p})\dot{\varepsilon}_1^{f} + f_{15}(\mathbf{p})\dot{\varepsilon}_2^{f} + f_{16}(\mathbf{p})\dot{\varepsilon}_3^{f} + f_{17}(\mathbf{p})\dot{P}_L \right) dt .\end{aligned} \tag{2-33}$$

In each small integral interval, the functions $\varepsilon_1^{m}(t)$, $\varepsilon_2^{m}(t)$, $\varepsilon_3^{m}(t)$, $\varepsilon_1^{f}(t)$, $\varepsilon_2^{f}(t)$, $\varepsilon_3^{f}(t)$, and respective components in $\mathbf{p}$, including ρ_1, ρ_2, and ρ_3, must be given in advance. However, ρ_1, ρ_2, and ρ_3 are unknown functions to be solved from the simultaneous differential equations (2-31) and (2-32). The values of ρ_1, ρ_2, and ρ_3 which should be used in the i-th small interval can be estimated as the following process. At first, we integrate eqs.(2-32) in the (i-1)-th small interval. Then, we obtain

$$\int_{(i-2)Z/n}^{(i-1)Z/n} \frac{d\rho_1}{dt} dt \left(\equiv \Delta^{i-1}\rho_1 \right) = \left\{ \int_{(i-2)Z/n}^{(i-1)Z/n} \left(\frac{d\varepsilon_t^{r1}}{dt} - \frac{d\varepsilon_t^{r2}}{dt} \right) \cdot \rho_1(t) dt \right\} \quad , \ \ldots\ldots\ldots\ldots \quad \text{etc.}$$

If n is taken as an enough large number, this equation gives

$$\Delta^{i-1}\rho_1 = (\Delta^{i-1}\varepsilon_t^{r1} - \Delta^{i-1}\varepsilon_t^{r2}) \cdot \rho_1^{i-2} \text{ ---------- etc.}$$

where ρ_1^{i-2} is equal to $\rho_1(t)$ at $t=(i-2)Z/n$. Thus, the value of ρ_1^{i-1}, which is $\rho_1(t)$ in the i-th small interval, is given as

$$\rho_1^{i-1} = \rho_1^{i-2} + \Delta^{i-1}\rho_1 = (1 + \Delta^{i-1}\varepsilon_t^{r1} - \Delta^{i-1}\varepsilon_t^{r2}) \cdot \rho_1^{i-2} \quad \text{---------- etc.} \tag{2-34}$$

By using simultaneous recurrence euations (2-33) and (2-34), we can integrate simultaneous differential eqs.(2-31) and (2-32) numerically.

Thus, the natural strain of the deforming wood fiber model at a certain time t ($=j\cdot Z/n$, j

is positive integer smaller than n) can be derived as follows:

$$\bar{\varepsilon}_{\mathrm{L}}(t) \equiv \lim_{n\to\infty} \sum_{i=1}^{j} \Delta^{\mathrm{i}}\varepsilon_{\mathrm{L}} = \int_{0}^{t} \frac{d\varepsilon_{\mathrm{L}}}{dt} dt, \quad \bar{\varepsilon}_{\mathrm{T}}(t) \equiv \lim_{n\to\infty} \sum_{i=1}^{j} \Delta^{\mathrm{i}}\varepsilon_{\mathrm{t}}^{\eta} = \int_{0}^{t} \frac{d\varepsilon_{\mathrm{t}}^{\eta}}{dt} dt \ . \tag{2-35}$$

Strains $\varepsilon_{\mathrm{L}}^{-}(t)$ and $\varepsilon_{\mathrm{T}}^{-}(t)$ give natural strains of the dimensional changes induced in the wood fiber model. However, the released strain of the growth stress and the swelling due to water sorption are measured as the nominal strains in the deforming wood specimen. Then, we need to solve eqs.(2-33) and (2-34) so as to give anisotropic dimensional changes of the wood fiber model as nominal strains.

The nominal strain of the deforming wood fiber model at a certain time t (= $j \cdot Z/n$) in respective directions can be derived as follows,

$$\alpha(\mathrm{t}) = \lim_{n\to\infty} \left\{ \prod_{i=1}^{j} \left(1 + \Delta^{\mathrm{i}}\varepsilon_{\mathrm{L}}\right) - 1 \right\} \quad , \qquad \beta(\mathrm{t}) = \lim_{n\to\infty} \left\{ \prod_{i=1}^{j} \left(1 + \Delta^{\mathrm{i}}\varepsilon_{\mathrm{t}}^{\eta}\right) - 1 \right\}. \tag{2-36}$$

If the values of $\alpha(Z)$ and $\beta(Z)$ are smaller than 1%, changes of ρ_1, ρ_2, and ρ_3 are small enough to be neglected. In that case, we can obtain the $\alpha(t)$ and $\beta(t)$ from the first and the second formulae of the eqs.(2-31), which simplifies eqs.(2-36) as follows:

$$\alpha(t) = \lim_{n\to\infty} \sum_{i=1}^{j} \Delta^{\mathrm{i}}\varepsilon_{\mathrm{L}} = \int_{0}^{t} \frac{d\varepsilon_{\mathrm{L}}}{dt} dt \quad , \quad \beta(t) = \lim_{n\to\infty} \sum_{i=1}^{j} \Delta^{\mathrm{i}}\varepsilon_{\mathrm{t}}^{\eta} = \int_{0}^{t} \frac{d\varepsilon_{\mathrm{t}}^{\eta}}{dt} dt. \tag{2-37}$$

References in Chapter 2

Barber, N.F., Meylan, B.A.: The anisotropic shrinkage of wood. A theoretical model. *Holzforschung*, **18**, 146-156 (1964).

Eshelby, J. D.: The determnation of the elastic field of an ellipsoidal inclusion, and related problems. *Proc. Roy. Soc.*, **A241**, 376-396 (1957).

Eshelby, J. D.: The elastic field outside an ellipsoidal inclusion. *Proc. Roy. Soc.*, **A252**, 561-569 (1959).

Fushitani, M.: Study of Molecular Orientation in Wood by Fluorescence Method, *Mokuzai Gakkaishi*, **19**, 135-140 (1973) – in Japanese.

Hull, D., Clyne, T.W. (translated in Japanese by Miyairi, Ikegami, Kinbara): " Hukugozairyou nyumon, kaiteiban", Baihukan, Tokyo, 2003. (original title: Hull, D., Clyne, T.W.: "An Introduction to Composite Materials, 2nd Edition", Cambridge University Press, Cambridge, 1996.)

Mori, T., Tanaka, K.: Average stress in matrix and average elastic energy of materials with misfitting inclusions, *Act. Metall.*, **21**, 571-574 (1973).

Mura, T.: "Micromechanics of Defects in Solids," 2nd rev., Kluwer Academic Publishers, Dordrecht, 1987.

Mura, T., Mori, T.:"Micromechanics - Dislocation and inclusions,"Baifukan, 1976.

Lekhnitski, S.G.: "Theory of Elasticity of an Anisotropic Elastic Body," Holden Day, San Francisco, 1960.

Liang, C.Y., Bassett, K.H., McGiness, E.A., Marchessault, R.H.: Infrared Spectra of Crystalline Polysaccharides. VII. Thin Wood Sections, *Tappi*, **43**, 1017-1024 (1960).

Salmen, L.:, Structure - Property Relations for Wood; from the Cell-Wall Polymeric Arrangement to the Macroscopic Behavior, In: Proc. 3rd Plant Biomechanics Conf., Freiburg-Badenweiler, pp. 452-462 (2000).

Yamamoto, H.: Generation mechanism of growth stresses in wood cell walls: Roles of lignin deposition and cellulose microfibril during cell wall maturation, *Wood Sci. Technol.*, **32**, 171-182 (1998).

Yamamoto, H.: A model of anisotropic swelling and shrinking process of wood (part 1). Generalization of Barber's wood fiber model, *Wood Sci. Technol.*, **33**, 311-325 (1999).

Yamamaoto, H., Kojima, Y.: Properties of cell wall constituents in relation to longitudinal elasticity of wood. Part 1. Formulation of the longitudinal elasticity of an isolated wood fiber, *Wood Sci. Technol.*, **36**, 55-74 (2002).

Yamamoto, H.: Role of the gelatinous layer (G-layer) on the origin of the physical properties of the tension wood. *Journal of Wood Science*, **50**, 197-208 (2004).

APPENDIX

[1] Outline for the micromechanics of "the two-phase structure" introduced by Eshelby (1957, 1959).

Equivalent inclusion method (1):

We consider a situation that a composite material covers the domain D, and inhomogeneity occupies a bounded region Ω inside D. Then, D–Ω stands for the matrix substance. Elastic constant in D–Ω is assumed to be C^M, and that in Ω is C^I. Moreover, we assume that heating will cause an eigen-strain (a coefficient of thermal expansion) ε^M in D–Ω, and ε^I in Ω. If thermal expansion occurs without any external load, a misfit of the dimensional change would be induced between both phases. By using the misfit strain ε^T ($\equiv \varepsilon^I - \varepsilon^M$), we can describe stress-strain relation in the inhomogeneity Ω as follows:

$$\sigma = C^I (\varepsilon - \varepsilon^I) = C^I (\varepsilon - \varepsilon^M - \varepsilon^T) , \tag{3-A1}$$

where ε is the compatible strain which is calculated from the observed displacement.

Let the region Ω be not inhomogeneity but an inclusion which has the same elastic constant as the matrix, that is, C^M. In such a case, we could calculate the elastic strain energy of the composite material directly from the strain field (or from the stress field), since the elastic constant would become homogeneous everywhere in the composite material. Thus, it is expected that the stress analysis becomes quite simplified one. On the basis of such an idea, Eshelby (1957, 1957) developed a convenient procedure to predict the mechanical behaviors of the composite material. His theory was called "the equivalent inclusion method" afterward.

He imaginarily replaced the inhomogeneity Ω with "the equivalent inclusion" whose elastic constant is C^M, and introduced the equivalent transformation strain ε^{T*} ($\equiv \varepsilon^{I*} - \varepsilon^M$), where ε^{I*} is the unknown eigen-strain of the equivalent inclusion. He assumed that the strain of the displacement in the equivalent inclusion (ε) takes the same value as that in the inhomogeneity. Then, the stress-strain relationship in the equivalent inclusion becomes as follows:

$$\sigma = C^M (\varepsilon - \varepsilon^{I*}) = C^M (\varepsilon - \varepsilon^M - \varepsilon^{T*}) , \tag{3-A2}$$

Esheby (1957, 1959) pointed out that the stress and the strain in the equivalent inclusion (3-A2) become identical with those in the actual inhomogeneity (3-A1) if the value of ε^{T*} (or ε^{I*}) is properly chosen.

$$C^I (\varepsilon - \varepsilon^M - \varepsilon^T) = C^m (\varepsilon - \varepsilon^M - \varepsilon^{T*}) \tag{3-A3}$$

Moreover, he proved that the strain of the displacement (ε) is related to the value of ε^{T*} by the following formula if the inclusion (inhomogeneity) is ellipsoidal:

$$\varepsilon = S\varepsilon^{T*}, \tag{3-A4}$$

where S is called "Eshelby tensor" that is determined from the shape of the ellipsoidal inhomogeneity and the Poisson's ratio of the matrix substance (Mura& Mori 1976).

Thus, we determine the value of ε^{T*} so as to satisfy the formulas (3-A3) and (3-A4) simultaneously. Afterward, by using the determined value of ε^{T*}, we can handle the composite material as the homogeneous field of the elastic constant.

Equivalent inclusion method (2):

We consider the matrix substance with elastic constant C^M, covering the domain D [model A], and the composite material having an inhomogeneity with elastic constant C^I. We assume this inhomogeneity covers the closed region Ω inside D [model B]. Let us give a load σ^0 to those materials. A uniform stress σ^0 and a uniform strain ε^0 are distributed in model A. On the other hand, in model B, a stress disturbance σ' is superposed on the stress field σ^0 since an inhomogeneity exists. The same situation can be said for the strain field in model B (provided that we consider $\sigma'=C^I\varepsilon'$ in Ω, and $\sigma'=C^M\varepsilon'$ in D–Ω).

We can determine the stress disturbance σ' (or strain disturbance ε') on the basis of "the equivalent inclusion method" (Eshelby 1957). We replace the inhomogeneity Ω with the equivalent inclusion (model C). In model C, we imaginarily induce an eigen-strain ε^* in the equivalent inclusion without giving any external load. And, we calculate the strain of the dimensional change ε and the stress σ which are induced by the eigen-strain in the equivalent inclusion. The stress σ in model C is called "the eigen-stress". The eigen stress σ in model C satisfies as the following formula

$$\sigma = C^M(\varepsilon-\varepsilon^*) \quad \text{in } \Omega, \qquad \sigma = C^M\varepsilon \quad \text{in D–}\Omega. \tag{3-A5}$$

If the inclusion is ellipsoidal, ε and ε* can be related by the following formula:

$$\varepsilon = S\varepsilon^* \quad \text{in } \Omega, \tag{3-A6}$$

where S is Eshelby's tensor of the inhomogeneity. Then, the eigen-stress in the equivalent inclusion Ω is given as

$$\sigma = C^M(S\varepsilon^* - \varepsilon^*) \quad \text{in } \Omega. \tag{3-A7}$$

According to the idea of "the equivalent inclusion method", eigen-strain ε^* in the region Ω of model C should be determined so as to satisfy the following relation:

$$\sigma \text{ [in } \Omega \text{ of model B]} = \sigma \text{ [model A]} + \sigma \text{ [in } \Omega \text{ of model C]},$$

that is to say,

$$C^I(\varepsilon^0+\varepsilon') = C^M\varepsilon^0 + C^M(\varepsilon-\varepsilon^*) , \qquad (3\text{-A8})$$

provided that ε in model C is identified with ε' in model B, which is also identified with $S\varepsilon^*$.

Thus, the problem is attributed to the simultaneous algebraic equation whose unknown values are ε_{11}^*, ε_{12}^*, ε_{13}^*, ε_{22}^*, ε_{23}^*, and ε_{33}^*. Substituting the solution ε^* into eq.(3-A6), we can determine the strain disturbance ε' in model B (= ε in model C). Afterward, we obtain the stress disturbance σ' in model B by the formulas, $\sigma' = C^I\varepsilon'$ (in Ω) or $\sigma' = C^M\varepsilon'$ (in D–Ω).

[2] Homogenization of the stress field in the composite material by the mean field method

We consider a situation that matrix covers the finite domain D, and numerous inhomogeneities are uniformly distributed inside D. We denote the elastic constant of the matrix substance by C^M, and that of the inhomogeneity by C^I. Our problem is to determine the stress field in this composite material. In this problem, we consult "the mean field method" developed by Mori and Tanaka (1973). Outline of "the mean field method" is given in the textbook written by Mura and Mori (1976).

Since the volume of the domain D is finite, some inhomogeneity exists near the free surface of the material. Stress field in such an inhomogeneity is more or less disturbed by the free boundary of the material. To solve the stress field in this composite material, we first consider a special case that only one inhomogeneity exists inside the matrix. On the basis of the equivalent inclusion method, we can determine the stress field in the infinitely large material having one inhomogeneity. We call this stress field "Eshelby's solution", and denote it by σ^∞. Next, we find a correction term (called an image stress) σ^i that makes the stress field null on the free surface of the material, and superpose it on Eshelby's solution σ^∞. Thus, $\sigma = \sigma^\infty+\sigma^i$ is the stress field in the finite body including one inhomogeneity.

Second, we consider a general case that many inhomogeneities are distributed inside the finite body. In this case, Eshelby's solution from one inhomogeneity would be affected not only by the image stress but also by Eshelby's solutions from the other inhomogeneities. We call the sum of the image stress and Eshelby's solutions from the other inhomogeneities "the background stress", and denote it by σ^b. Regardless of in the inhomogeneity or in the matrix, the background stress σ^b is widely distributed in the material.

Let a point x be set inside the material. If the point x exists in any inhomogeneity Ω, the stress σ at the point x can be given as the sum of Eshelby's solution σ^∞ and the background

stress σ^b. If the point x does not belong to any inhomogeneity, the stress at the point x is the background stress σ^b, which is nothing but the stress generated in the matrix substance. In such a sense, we identify the background stress with the stress in the matrix substance, and we sometimes denote σ^b by $\langle\sigma^M\rangle$.

Our next question is to find the relationship between Eshelby's solution σ^∞ and $\langle\sigma^M\rangle$. Before giving an answer to this question, we prove the following lemma:

[Lemma] Volume integral of the internal stress field in the finite body becomes null,

$$\text{i.e.} \quad \int_D \sigma_{ij} dV = 0, \tag{3-A9}$$

provided that $dV=dx_1dx_2dx_3$. And, subscripts i, j mean tensorial suffices.

- - - Proof - - - -

By using Gauss' theorem for divergence and the method of integration by parts, eq.(3-A9) can be deformed as follows:

$$\int_D \sigma_{ij} dV = \int_D \sigma_{ik}\delta_{jk} dV = \int_D \sigma_{ik} \frac{\partial x_j}{\partial x_k} dV = \int_{\partial D} \sigma_{ik} x_j n_k dS - \int_D \sigma_{ik,k} x_j dV,$$

where δ_{ij} is Kronecher's symbol, and ∂D stands for the boundary surface of the domain D, and $\sigma_{ik,k} \equiv (\partial\sigma_{i1}/\partial x_1) + (\partial\sigma_{i2}/\partial x_2) + (\partial\sigma_{i3}/\partial x_3)$. By the way, stress field σ must satisfy $\sigma_{ij}n_j=0$ on ∂D (Cauchy's boundary condition), and $\sigma_{ik,k}=0$ in D (equilibrium condition), then, the last side in the above equation becomes 0. (*q.e.d.*)

If there are *n* inhomogeneties in the composite material, we obtain the following expression from eq.(3-A9):

$$\int_D \sigma_{ij} dV = \int_{n\Omega} \sigma_{ij} dV + \int_{D-n\Omega} \sigma_{ij} dV = 0. \tag{3-A10}$$

The first term in the middle side can be written as $n\Omega(\sigma^\infty + \langle\sigma^M\rangle)$, and the second term can be replaced by $(D-n\Omega)\langle\sigma^m\rangle$. Thus, we obtain

$$\langle\sigma^M\rangle = -\phi\cdot\sigma^\infty, \tag{3-A11}$$

where ϕ is the volume fraction of the inhomogeneities to the composite material. This formula can be expressed as the following equation:

$$(1-\phi)\langle\sigma^M\rangle + \phi(\sigma^\infty + \langle\sigma^M\rangle) = 0. \tag{3-A12}$$

If we denote the mean stress in each inhomogeneity by $\langle\sigma^I\rangle$, it is obvious that $\langle\sigma^I\rangle=\sigma^\infty+\langle\sigma^M\rangle$, then, we can obtain the following formula:

$$(1-\phi)\langle\sigma^M\rangle + \phi\langle\sigma^I\rangle = 0. \tag{3-A13}$$

In Section 2-2, eqs.(3-A12) and (3-A13) are used as eqs.(2-4) and (2-5), respectively.

[3] A note on the solution of the differential equation (2-23)

Differential equation (2-23) is categorized into the nonhomogeneous linear ordinary differential equation of the second order with variable coefficients whose independent variable is r, and the unknown variable to be solved is σ_r. The equation (2-23) is called Euler-Caucy's equation, and its solution and property have been well investigated before now.

We assume $\sigma_r^h = r^m$, and substitute it into the corresponding homogeneous equation of (2-23), then, we can decide the characteristic root m. As the result, we obtain two functions $\varphi_1(r)$ $(= r^{-1+\alpha})$ and $\varphi_2(r)$ $(= r^{-1-\alpha})$ as the bases of solutions of the homogeneous equation. Thus, we obtain the general solution of the corresponding homogeneous equation of (2-23):

$$\sigma_r^h = \tilde{C}_1 \cdot \varphi_1(r) + \tilde{C}_2 \cdot \varphi_2(r)\,, \tag{3-A14}$$

where $C_1\tilde{}$ and $C_2\tilde{}$ are arbitrary constants.

Next, we try to find a particular solution of nonhomogeneous equation (2-23) in the following manner called the method of variation of parameters. We try to determine the functions $C_1(r)$ and $C_2(r)$ in the following expression so that the σ_r^p becomes a particular solution of the nonhomogeneous equation (2-23),

$$\sigma_r^p = C_1(r)\cdot\varphi_1(r) + C_2(r)\cdot\varphi_2(r)\,, \tag{3-A15}$$

provided that $C_1(r)$ and $C_2(r)$ must satisfy the following condition:

$$C_1'(r)\varphi_1(r) + C_2'(r)\varphi_2(r) = 0 \tag{3-A16}$$

By substituting (1) into the differential equation (2-23), and considering the relation (3-A16), we derive the following relation:

$$C_1'(r)\cdot r^2\cdot\varphi_1'(r) + C_2'(r)\cdot r^2\cdot\varphi_2'(r) = A/(1+2u) \tag{3-A17}$$

where the superscript "′" on C_1, C_2, φ_1, and φ_2 means that the first derivative by r is taken for each function. We can regard eqs.(3-A16) and (3-A17) as the simultaneous algebraic equations having $C_1'(r)$ and $C_2'(r)$ as unknown variables, then, we can determine them as follows:

$$C_1'(r) = \frac{A}{2\alpha(1+2u)} r^{-\alpha}, \qquad C_2'(r) = -\frac{A}{2\alpha(1+2u)} r^{\alpha} \quad .$$

We can easily obtain the indefinite integral of $C_1'(r)$ as follows:

$$C_1(r) = \frac{A}{1+2u} \cdot \frac{r^{1-\alpha}}{2\alpha(1-\alpha)} + \bar{k}_1 = \frac{A}{1+2u} \cdot \frac{1}{2\alpha} \cdot \left(\frac{r^{1-\alpha} - 1}{1-\alpha} + \frac{1}{1-\alpha} \right) + \bar{k}_1 \, . \tag{3-A18}$$

We should look after the behavior of the right hand side of the above equation in a case of $\alpha \to 1+0$. In such a case, the first term inside the bracket converges on "ln r". However, the second term obviously diverge to negative infinity. Then, we require the following condition so that $C_1(r)$ takes a certain finite value also in a case of $\alpha \to 1+0$.

$$\bar{k}_1 = -\frac{A}{1+2u} \cdot \frac{1}{2\alpha(1-\alpha)} + k_1 \quad ,$$

where k_1 is an arbitrary constant. Thus, $C_1(r)$ can be rather expressed as the following form:

$$C_1(r) = \frac{A}{1+2u} \cdot \frac{1}{2\alpha} \left(\frac{r^{1-\alpha} - 1}{1-\alpha} \right) + k_1 \quad .$$

C_2'can be easily integrated, then, the indefinite integral becomes

$$C_2(r) = -\frac{A}{1+2u} \cdot \frac{r^{1+\alpha}}{2\alpha(1+\alpha)} + k_2 \quad .$$

Thus, we obtain a particular solution of the nonhomogeneous equation (2-23)

$$\sigma^{\mathrm{p}} = \frac{A}{1+2u} \cdot \frac{1}{2\alpha} \left(\frac{r^{1-\alpha} - 1}{\alpha - 1} \right) - \frac{A}{1+2u} \cdot \frac{1}{2\alpha} \cdot \frac{1}{1+\alpha} + k_1 \cdot r^{-1+\alpha} + k_2 \cdot r^{-1-\alpha} \quad . \tag{3-A19}$$

The sum of the general solution of the corresponding homogeneous equation ($\sigma_{\mathrm{r}}^{\mathrm{h}}$ in eq.(3-A14)) and the particular solution of the nonhomogeneous equation ($\sigma_{\mathrm{r}}^{\mathrm{p}}$ in eq.(3-A19)) gives a general solution of the nonhomogeneous equation (2-23), which becomes

$$\sigma_{\mathrm{r}} = \tilde{C}_1 r^{\alpha-1} + \tilde{C}_2 r^{-\alpha-1}$$
$$- \frac{1}{1+2u} \cdot \frac{1}{2\alpha} \left\{ 3E \cdot s^4 \varepsilon^{\mathrm{m}} - (2+u) E \cdot s^2 \varepsilon^{\mathrm{f}} + E \cdot s^2 \left(2 - 3s^2 + u \right) \varepsilon_{\mathrm{L}} \right\} \left\{ \frac{1}{1+\alpha} - \left(\frac{r^{\alpha-1} - 1}{\alpha - 1} \right) \right\}.$$

[4] Detailed expressions of coefficients a_{11}, a_{12}, ----, a_{55}; b_{11}, b_{12}, ---, b_{53}; c_{11}, c_{12}, ---, c_{53}; d_{11}, d_{21}, ---, d_{51} in eqs.(2-29-1~5).

$$a_{11}=\Omega_2\alpha+A+B+C,\quad a_{12}=D,\quad a_{13}=E,\quad a_{14}=-\frac{1}{6}\frac{\alpha}{\rho_2{}^2}\Lambda_2(\Lambda_2-2\Gamma_2),\quad a_{15}=0,$$

$$b_{11}=H-\frac{\alpha X_1}{6M}(\Lambda_2-2\Gamma_2)\left(\frac{1}{\rho_2{}^2-1}\right)\left(\frac{\rho_1{}^2-1}{\rho_1{}^2}\right),\quad b_{12}=\alpha\cdot\Phi_2-\frac{1}{6}\frac{X_2}{\rho_2{}^2}\alpha(\Lambda_2-2\Gamma_2),$$

$$b_{13}=\frac{1}{2}N\alpha\Lambda_2\left(\frac{1}{\rho_2{}^2-1}\right)\left(\frac{\rho_3{}^2-1}{\rho_3{}^2}\right),\quad c_{11}=I-\frac{\alpha\Delta_1}{6M}(\Lambda_2-2\Gamma_2)\left(\frac{1}{\rho_2{}^2-1}\right)\left(\frac{\rho_1{}^2-1}{\rho_1{}^2}\right),$$

$$c_{12}=\alpha\cdot\Sigma_2-\frac{1}{6}\frac{\Delta_2}{\rho_2{}^2}\alpha(\Lambda_2-2\Gamma_2),\quad c_{13}=\frac{1}{3}N\alpha\Lambda_2\left(\frac{1}{\rho_2{}^2-1}\right)\left(\frac{\rho_3{}^2-1}{\rho_3{}^2}\right)G_3,$$

$$d_{11}=\frac{2}{3}\frac{\Lambda_2}{M}\alpha\left(\frac{\rho_2{}^2}{\rho_2{}^2-1}\right)\frac{1}{S_1r_2^2}\frac{1}{2\pi},$$

$$a_{21}=G_1Q+\frac{1}{2}\left(\frac{\rho_1{}^2-1}{\rho_1{}^2}\right)\Gamma_1+\frac{M}{2}\left(\frac{\rho_2{}^2-1}{\rho_2{}^2}\right)\Gamma_2+\frac{1}{2}MN(\rho_3{}^2-1),\quad a_{22}=2G_1Q,$$

$$a_{23}=\frac{1}{2}\left(\frac{\rho_1{}^2-1}{\rho_1{}^2}\right)\Lambda_1,\quad a_{24}=\frac{M}{2}\left(\frac{\rho_2{}^2-1}{\rho_2{}^2}\right)\Lambda_2+MN(\rho_3{}^2-1),\quad a_{25}=0,$$

$$b_{21}=\frac{1}{2}\left(\frac{\rho_1{}^2-1}{\rho_1{}^2}\right)X_1,\quad b_{22}=\frac{M}{2}\left(\frac{\rho_2{}^2-1}{\rho_2{}^2}\right)X_2,\quad b_{23}=\frac{3}{2}MN(\rho_3{}^2-1),$$

$$c_{21}=\frac{1}{2}\left(\frac{\rho_1{}^2-1}{\rho_1{}^2}\right)\Delta_1,\quad c_{22}=\frac{M}{2}\left(\frac{\rho_2{}^2-1}{\rho_2{}^2}\right)\Delta_2,\quad c_{23}=0,\quad d_{21}=0\ ,$$

$$a_{31}=G_1Q+\frac{1}{2}\left(\frac{\rho_1{}^2-1}{\rho_1{}^2}\right)\Gamma_1+\frac{M}{2}(\rho_2{}^2-1)\Gamma_2{}'+\frac{1}{2}MN(\rho_3{}^2-1),\quad a_{32}=2G_1Q,$$

$$a_{33}=\frac{1}{2}\left(\frac{\rho_1{}^2-1}{\rho_1{}^2}\right)\Lambda_1+\frac{M}{2}(\rho_2{}^2-1)\Lambda_2,\quad a_{34}=MN(\rho_3{}^2-1),\quad a_{35}=0,$$

$$b_{31}=\frac{1}{2}\left(\frac{\rho_1{}^2-1}{\rho_1{}^2}\right)X_1,\quad b_{32}=\frac{M}{2}(\rho_2{}^2-1)X_2{}',\quad b_{33}=\frac{3}{2}MN(\rho_3{}^2-1),$$

$$c_{31}=\frac{1}{2}\left(\frac{\rho_1{}^2-1}{\rho_1{}^2}\right)\Delta_1,\quad c_{32}=\frac{M}{2}(\rho_2{}^2-1)\Delta_2{}',\quad c_{33}=0,\quad d_{31}=0\ ,$$

$$a_{41}=G_1Q+\frac{1}{2}(\rho_1{}^2-1)\Gamma_1{}'+\frac{M}{2}(\rho_2{}^2-1)\Gamma_2{}'+\frac{1}{2}MN(\rho_3{}^2-1),\quad a_{42}=2G_1Q+\frac{1}{2}(\rho_1{}^2-1)\Lambda_1,$$

$$a_{43}=\frac{M}{2}(\rho_2{}^2-1)\Lambda_2,\quad a_{44}=MN(\rho_3{}^2-1),\quad a_{45}=0,$$

$$b_{41}=\frac{1}{2}(\rho_1{}^2-1)X_1{}',\quad b_{42}=\frac{M}{2}(\rho_2{}^2-1)X_2{}',\quad b_{43}=\frac{3}{2}MN(\rho_3{}^2-1),$$

$$c_{41}=\frac{1}{2}\left(\rho_1{}^2-1\right)\Lambda_1{}',\quad c_{42}=\frac{M}{2}\left(\rho_2{}^2-1\right)\Lambda_2{}',\quad c_{43}=0,\quad d_{41}=0\ ,$$

$$a_{51}=G_1Q+\frac{1}{2}\left(\frac{\rho_1{}^2-1}{\rho_1{}^2}\right)\Gamma_1+\frac{M}{2}\left(\frac{\rho_2{}^2-1}{\rho_2{}^2}\right)\Gamma_2+\frac{1}{2}MN\left(\frac{\rho_3{}^2-1}{\rho_3{}^2}\right),\quad a_{52}=2G_1Q\,,$$

$$a_{53}=\frac{1}{2}\left(\frac{\rho_1{}^2-1}{\rho_1{}^2}\right)\Lambda_1\,,\quad a_{54}=\frac{M}{2}\left(\frac{\rho_2{}^2-1}{\rho_2{}^2}\right)\Lambda_2\,,\quad a_{55}=MN\left(\frac{\rho_3{}^2-1}{\rho_3{}^2}\right),$$

$$b_{51}=\frac{1}{2}\left(\frac{\rho_1{}^2-1}{\rho_1{}^2}\right)\mathrm{X}_1\,,\quad b_{52}=\frac{M}{2}\left(\frac{\rho_2{}^2-1}{\rho_2{}^2}\right)\mathrm{X}_2\,,\quad b_{53}=\frac{3}{2}MN\left(\frac{\rho_3{}^2-1}{\rho_3{}^2}\right),$$

$$c_{51}=\frac{1}{2}\left(\frac{\rho_1{}^2-1}{\rho_1{}^2}\right)\Delta_1\,,\quad c_{52}=\frac{M}{2}\left(\frac{\rho_2{}^2-1}{\rho_2{}^2}\right)\Delta_2\,,\quad c_{53}=0,\quad d_{51}=0\ .$$

Provided that detailed shapes of functions *A*, *B*, *C*, *D*, *E*, *H*, *I*, α, and β are as follows:

$$A=\frac{1}{M}\left(\frac{\Gamma_2{}'}{\Gamma_1}\right)\left(\frac{\rho_2{}^2}{\rho_2{}^2-1}\right)\left\{\left(\rho_1{}^2-1\right)\Omega_1+\frac{2}{3}\rho_1{}^2G_1G_0\left(-\Gamma_1{}'+2\Lambda_1\right)\right\}\ ,$$

$$B=\frac{1}{M}\left(\frac{\Gamma_2{}'}{3}\right)\left(\frac{\rho_2{}^2}{\rho_2{}^2-1}\right)\beta\left(2G_1Q+\frac{\rho_1{}^2-1}{\rho_1{}^2}\Gamma_1\right),\alpha=\left(\frac{\Gamma_2{}'}{\Gamma_1}\right)\left(\frac{\Lambda_1}{\Lambda_2}\right),\quad \beta=1-\alpha=1-\left(\frac{\Gamma_2{}'}{\Gamma_1}\right)\left(\frac{\Lambda_1}{\Lambda_2}\right),$$

$$C=-\alpha\left(\Lambda_2-2\Gamma_2\right)\left\{\frac{1}{6}\frac{\Gamma_2}{\rho_2{}^2}+\frac{1}{6}\left(\frac{\Gamma_1}{M}\right)\left(\frac{1}{\rho_2{}^2-1}\right)\left(\frac{\rho_1{}^2-1}{\rho_1{}^2}\right)+\frac{1}{3}\left(\frac{1}{M}\right)\left(\frac{1}{\rho_2{}^2-1}\right)G_1Q\right\}$$
$$+\frac{1}{2}N\cdot\Lambda_2\cdot\alpha\left(\frac{1}{\rho_2{}^2-1}\right)\left(\frac{\rho_3{}^2-1}{\rho_3{}^2}\right)\left(1+\frac{2}{3}G_3\right)\quad ,$$

$$D=\frac{2}{3}\left(\frac{1}{\rho_2{}^2-1}\right)\left(\frac{1}{M}\right)\left\{\rho_2{}^2\Gamma_2{}'\left(2\beta+\frac{\Lambda_1-2\Gamma_1{}'}{\Gamma_1}\rho_1{}^2\right)+\alpha\left(2\Gamma_2-\Lambda_2\right)\right\}G_1Q\ ,$$

$$E=\frac{1}{6}\left(\frac{\Lambda_1}{M}\right)\left(\frac{1}{\rho_2{}^2-1}\right)\left(\frac{\rho_1{}^2-1}{\rho_1{}^2}\right)\left(2\Gamma_2{}'\beta\rho_2{}^2-\alpha\left(\Lambda_2-2\Gamma_2\right)\right),$$

$$H=\left(\frac{\Gamma_2{}'}{M}\right)\left(\frac{\rho_2{}^2}{\rho_2{}^2-1}\right)\left(\frac{\rho_1{}^2-1}{\rho_1{}^2}\right)\left(\frac{\Phi_1}{\Gamma_1}\rho_1{}^2+\frac{1}{3}\beta\cdot\mathrm{X}_1\right),$$

$$I=\left(\frac{\Gamma_2{}'}{M}\right)\left(\frac{\rho_2{}^2}{\rho_2{}^2-1}\right)\left(\frac{\rho_1{}^2-1}{\rho_1{}^2}\right)\left(\frac{\Sigma_1}{\Gamma_1}\rho_1{}^2+\frac{1}{3}\beta\cdot\Delta_1\right).$$

Chapter 3

BIOMECHANICS OF WOOD FORMATION AND TREE GROWTH

3-1 Mechanism of growth stress generation

3-1-1 Background

(a) Measurement of tree growth stresses

Xylem fiber, including gymnosperm tracheid and angiosperm wood fiber, becomes mature after completion of the secondary wall followed by its lignification. During the secondary wall maturation, each xylem fiber tends to deform in its axial and diametral directions. Those dimensional changes are completely restricted by the neighboring tissues inside the actual xylem, which induces a mechanical stress in the cell wall of newly-formed xylem fiber. Consequently, two-dimensional stress distribution is set on the outermost surface of the secondary xylem of the tree stem. This is called the surface growth stress or the growth stress. The surface growth stress provokes a counteractive stress distribution in the older xylem, which is superimposed inside the stem after the repetition of the thickening growth. Thus, a three-dimensional residual stress distribution is formed inside the stem.

We can detect the surface growth stress as follows on the basis of the strain-gauge method. In a standing tree, we remove the phloem and the immature xylem at each measuring position, and exposure the surface of the mature xylem. Thereafter, we paste two strain-gauges in the directions parallel and perpendicular to the grain, respectively, with a quick-dried glue, and connect them to the electric strain meter (see Fig. 3-1). Then, we release two-dimensional surface stress by making grooves of 1 – 2cm in depth around the strain-gauges with a handsaw and a chisel. Soon, we detect the released strains ε_L and ε_T in the longitudinal and tangential directions, respectively. After obtaining the released strains, we take wood blocks from each measuring position, and convert them into the samples for measuring the Young's moduli, E_L and E_T, and the Poisson's ratios, ν_{LT} and ν_{TL}. Thus, we can determine the surface growth stress by using following formulas (Sasaki et al. 1978):

$$\sigma_L = -\frac{E_L}{1-\nu_{TL}\nu_{LT}}\left(\varepsilon_L + \nu_{TL}\varepsilon_T\right), \quad \sigma_T = -\frac{E_T}{1-\nu_{TL}\nu_{LT}}\left(\varepsilon_T + \nu_{LT}\varepsilon_L\right) \quad . \qquad (3\text{-}1)$$

We must put "–" in front of right hand side of each equation since strains ε_L and ε_T are

obtained as the released strains of the residual stress σ_L and σ_T. By the way, $\nu_{TL} \times \nu_{LT}$ is quite smaller than 1, moreover, $\nu_{TL}\varepsilon_T$ is also smaller as compared with ε_L, then, we can simplify the first formula of eqs.(3-1) into the following formula.

$$\sigma_L \cong -E_L \times \varepsilon_L \tag{3-2}$$

In the case that the divergence of E_L among the measuring positions is thought to be negligible, we can use the value of ε_L as an indicator of the longitudinal growth stress σ_L (Archer 1987). From eq.(3-2), it is reasonable to consider that σ_L would be tensile (compressive) if ε_L was negative (positive). However, it is improper to use the value of ε_T as an indicator of σ_T since $\nu_{LT}\varepsilon_L$ is not exactly smaller than ε_T.

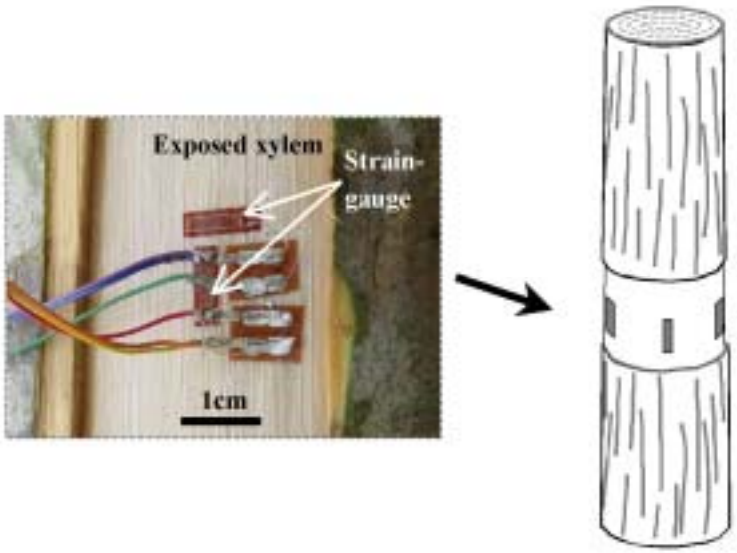

Fig.3-1. Measurement of the released strains of two-dimensional surface growth stress on the outermost surface of the xylem by the strain-gauge method.

(b) Examples of experimental results

Normal wood (NW):

Sasaki et al.(1978) collected many experimental data on the surface growth stress of 15 Japanese domestic trees, including 13 species, on the basis of the strain-gauge method. As the result, they induced a conclusion that σ_L takes the value of 1~10 MPa (3.62 MPa in average), on the other hand, σ_T takes –0.2 ~ –1 MPa (0.38 MPa in average) in a straight trunk. Those

values correspond to the value of –0.02 ~ –0.1 % (–0.042 in average) for ε_L, and the value of 0.04 ~ 0.15% (0.091 % in average) for ε_T.

Compression wood (CW):

In the CW region, the microfibril angle (MFA) in the middle layer of the secondary wall (S2) becomes larger, and the lignin content also becomes higher than in the NW region (Yamamoto et al. 1991, Yamamoto & Okuyama 1993, Sugiyama et al. 1993). From the observation using ultra-violet photomicroscope, some researchers clarified that the increase in the lignin concentration occurs at the secondary wall of the tracheid in the CW region (Fujita et al. 1978, Okuyama et al. 1998).

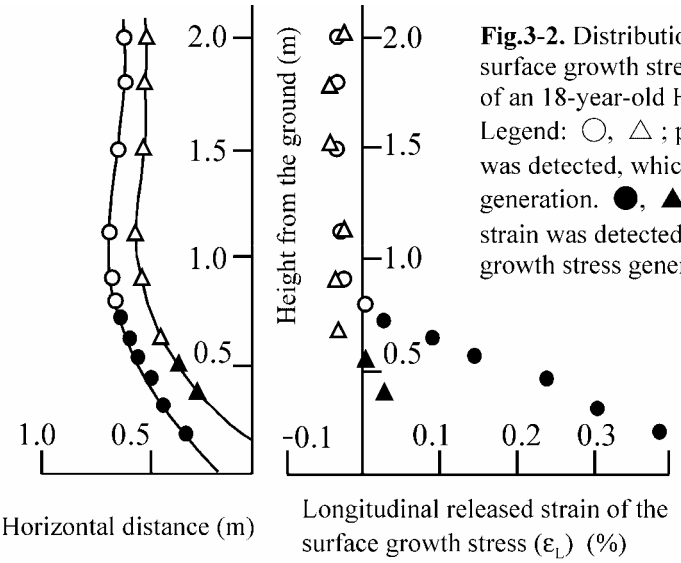

Fig.3-2. Distribution of the longitudinal released strain of the surface growth stress along the height of standing tilted stem of an 18-year-old Hinoki (*Chamaecyparis obtusa*). Legend: ○, △ ; position where a contractive released strain was detected, which was attributable to a tensile growth stress generation. ●, ▲ ; position where an expansive released strain was detected, which was attributable to a compressive growth stress generation.

The longitudinal growth stress is always tensile in the NW region, while it becomes large compressive in the CW region. The compressive growth stress in the longitudinal direction tends to increase with the MFA and the lignin content. Figure 3-2 shows the distribution of the longitudinal released strain of the surface growth stress (ε_L) along the height of the standing stem of an 18-year-old tilted Hinoki (*Chamaecyparis obtuse*) (Yamamoto et al.1991). In this case, the stem was crooked up to the height of 80 cm from the ground, where the values of ε_L were all expansive along the convex side (lower side of the leaning stem). Especially, at the nearest position to the ground, ε_L took the largest value of 0.38 %. In each measuring position along the convex side of the inclined trunk, anatomical properties peculiar to the CW xylem were observed, of which intensity was proportional to

the magnitude of the expansive released strain. In this example, even in the concave side, expansive but small released strains were observed at the positions near the ground, which is attributed to the property of the opposite wood.

Tension wood (TW):

Most arboreal angiosperm produces the gelatinous fiber (G-fiber) in the upper side of the inclined stem or branch. We call the xylem containing the G-fiber "tension wood (TW)". The G-fiber has a gelatinous layer (G-layer) as the innermost layer in its cell wall. The G-layer consists of highly crystallized and less-lignified polysaccharide microfibril, of which orientation is almost parallel to the fiber axis. In the TW region, the longitudinal growth stress becomes very large tensile stresses. Figure 3-3 shows peripheral distributions of the longitudinal released strain of the surface growth stress (ε_L) and the area fraction of the G-layer (*g*) in the outermost annual ring at the beast height of an inclined stem of a 23-year-old Blacklocust (*Robinia pseudoacacia*) (Yamamoto & Okuyama 1994). The azimuth angle 0° corresponds to the uppermost side of the inclined stem. As can be seen from Fig.3-3, the maximum value of the contractive released strain amounts to –0.49% on the uppermost side of the leaning stem, where the area fraction of the G-layer to the total xylem area locally becomes highest. On the other hand, the value of ε_L becomes very small in the opposite wood region, where no G-fiber was formed. It is reported that the area fraction of the G-layer to the total xylem area is proportional to the contractive value of the longitudinal released strain in several angiosperm species (Okuyama et al. 1990, 1994, Yamamoto et al. 1992, Yamamoto et al. in press).

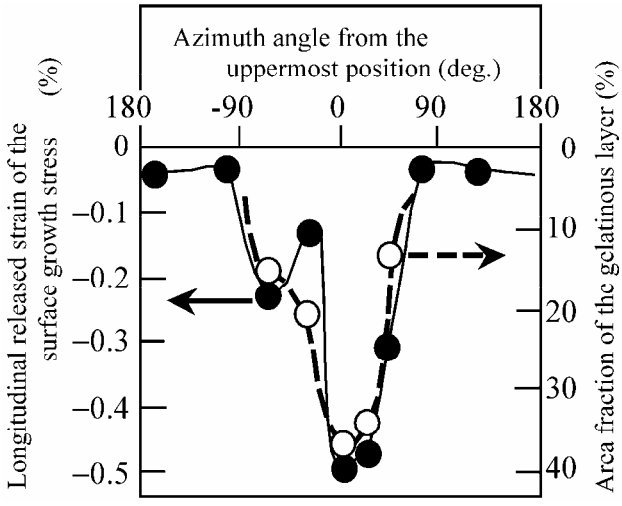

Fig.3-3. Peripheral distributions of the longitudinal released strain of the surface growth stress (●), and the area fraction of the gelatinous layer in the outermost annual ring (○) at the breast height of an inclined stem of a 23-year-old Blacklocust (*Robinia pseudoacacia*).

From those observations, it is rather reasonable to consider that the G-layer produces high tensile stresses in its axial direction, which induces very large tensile stress generation in the TW region. However, more than few researchers believe that the G-layer is mechanically too compliant to bear a large stress generation. They base their argument on the fact that the detached G-layer is often convoluted in the lumen of the transverse section that is sampled from the water swollen block, and it is easily peeled off the lignified layer in the same direction during microtoming. This gives an impression that the G-layer is attached only loosely to the remainder of the cell wall. On the other hand, Okuyama et al.(1990), Yamamoto et al. (1992), and Yamamoto et al.(in press) reported that the Young's modulus of the G-layer in the direction parallel to the fiber axis becomes 1.5−3 times as large as that of the lignified wall. Lately, Clair et al. (in press) clarified that the G-layer in a small wood portion is not peeled off from the lignified wall even after the drying process besides the nearest positions to the crosscut end. Thus, they concluded that detachment of the G-layer often observed in the transverse section would be caused by the extremely high stress concentration from the microtome blade. Those evidences well support an idea that the cellulose microfibril (CMF) in the G-layer produces a high tensile stress in its axial direction.

In the species belonging to the family *Magnoliaceae*, such as *Liriodendron tulipifera*, *Magnolia obovata*, or *Magnolkia kobus*, etc., a large longitudinal tensile stress is generated on the upper side of the leaning stem, where no G-fiber is formed. In such a region, the MFA becomes significantly lower, and the cellulose content becomes quite larger, furthermore, the lignin concentration is more or less smaller than in the regions on the lower side of the leaning stem or the straight stem (Okuyama et al.1990, 1994, Sugiyama et al.1993). From the observation using the ultra-violet photomicroscope, Yoshida et al. (2002) confirmed that the decrease in the lignin concentration in the TW xylem of *Liriodendron tulipifera* occurs in the secondary wall of the wood fiber in the region where a large tensile growth stress is measured. Such xylem properties become more remarkable in the G-layer, i.e. a pure cellulosic component, a high degree of crystallinity, a very small MFA. As mentioned above, it is considered that those characteristics in the G-layer induce the generation of the extremely high tensile growth stress in the TW xylem. In the case of rather primitive angiosperm, e.g. *Magnoliaceae*, a large cellulose content and a low MFA produce the similar effect as the formation of clear G-layer in the highly evolved eudicot species. However, the magnitude of the tensile growth stress in the "TW" region of those primitive species is more or less inferior to that of the eudicot species. For example, Okuyama et al. (1994) reported that the

longitudinal growth stress was 20 MPa at the largest in the TW region of a 51-year-old *Liriodendron tulipifera*, which is equivalent to –0.15 % in the released strain.

(c) Previous theory on the mechanism of the growth stress generation

Lignin swelling hypothesis:

Based on numerous experimental observations, M.R. Jacobs (1938), an Australian scientist, induced a conclusion that the tree growth stress is generated in the secondary xylem during the secondary growth. Thereafter, not a few scientists in this field have proposed various hypotheses to explain the mechanism of the growth stress generation (see, Timell's (1986) review). Up to present, two hypotheses have survived; one is "Cellulose tension hypothesis" and the other is "Lignin swelling hypothesis". The first one was proposed by A.B. Wardrop (1965) who studied the formation of the G-layer and the rightning force in the tilted tree. Thereafter, Wardrop's idea was strongly developed by R.K. Bamber (1978). The second one was proposed by H. Watanabe (1965) and J.D. Boyd (1972) who noticed the compressive stress generation in the CW xylem.

The compellation "swelling" does not necessarily mean that the cell wall matrix swells by the impregnated lignin or other materials. However, some researcher used the expression "the lignin swelling" since the cell wall looks like more or less swollen during its lignification in their observations (Munch 1938, Onaka 1949, Wardrop 1965, Watanabe 1965, Boyd 1972). Among those pioneers' works, Munch (1938) and Onaka (1949) discussed the cause of the rightening movement in the tilted gymnosperm in relation to two-phasic structure of the cell wall (especially, in relation to the MFA in the S2 layer). Their ideas were developed into a more sophisticated theory, "the lignin swelling hypothesis" by H. Watanabe and J.D. Boyd. Wardrop (1964) also pointed out the possibility that the lignification often makes the cell wall swollen, however, he did not develop this fact into the mechanism of the growth stress generation.

Watanabe (1965) and Boyd (1972) applied their "lignin swelling hypothesis" to explain not only the origin of the longitudinal compressive stress in the CW xylem but also the origin of the tensile stress generation in the NW and the TW xylem. Their theory can be summarized as the following:

During the cell wall maturation, the lignin precursors are staffed into the gaps of the polysaccharide framework and the matrix region, that had already been deposited, and

they polymerized immediately. After repeating this process, the amount of the matrix substance increases irreversibly inside the matrix region of which volume is spatially limited. As the result, the matrix tends to swell isotropically, however, free expansion of the matrix skeleton is restricted by the rigid framework of the polysaccharide bundle. Thus, the cell wall tends to expand largely in the direction perpendicular to the cellulose microfibril orientation, which causes the deformation of the wood fiber that is dependent on the MFA in the S2 layer. Free dimensional change of the wood fiber is fully restricted inside the actual stem, thus, anisotropic growth stress is generated in the newly-formed xylem.

Based on this idea, Boyd (1972) made a theoretical calculation on the observed relationship between the longitudinal growth stress and the MFA. In his calculation, he adopted a mechanical model that Barber & Meylan (1964) introduced to explain the anisotropic shrinkage of drying S2 element. His calculation succeeds in qualitatively explaining the fact that the longitudinal compressive stress tends to increase with the MFA and the lignin content in the S2 layer. However, his calculation often underestimates the magnitude of the tensile stress generated in the region of the small MFA. Furthermore, his theory never explain a large tensile growth stress generation in the TW xylem with a very small MFA, since his model always gives compressive stress in the region of very small MFA, which seriously contradicts the experimental fact.

Cellulose tension hypothesis:

The idea on "the cellulose tension hypothesis" was originally proposed by Wardrop (1965) who investigated the relation between the tensile stress generation and the G-layer formation in the TW fiber.(1) Thereafter, R.K. Bamber (1978) developed Wordrop's idea into a new theory which explains the origin of the growth stress not only in the TW region but also in the NW and the CW regions. As an opponent of "the lignin swelling hypothesis", Bamber has strongly propagated this theory, therefore, it is widely believed that he is the most devoted polemist of "the cellulose tension hypothesis". His theory is summarized as the following:

The CMF generates a high tensile stress in the direction parallel to its molecular chains during the cell wall maturation, which is converted into a very large longitudinal tensile growth stress in the TW fiber with a small MFA, and a large longitudinal compressive growth stress in the CW fiber with a large MFA. The lignin deposition does not take part in the growth stress generation, which only contributed to the increase in the

compressive strength of the CW xylem

He presumed that an increase in the CMF crystallinity causes a contractive force in the CMF bundle in the same manner as Wardorop's early idea. His theory can explain the origin of the longitudinal tensile growth stress in the TW and the NW fiber with small MFAs, however, it is more or less meaningless for the compressive stress generation in the CW region. Afterward, he improved his early theory so as to explain the longitudinal compressive stress generation in the CW region without any vagueness, that is, as the following (Bamber 2001):

> In the CW region with a large MFA, the CMF bundle behaves as a helical spring which was formed in a compressed state, then, it exerts a large compressive growth stress in the longitudinal direction.

If he presumes that the CMF behaves as a pre-compressed helicoidal spring, he must explain what is the original force to compress the helical spring of CMF. As for the explanation on the compressive stress generation in the CW xylem, his new idea is no more "the cellulose tension hypothesis", and he implicitly recognize that one should presume an other additional mechanism than "the cellulose tension hypothesis" so as to explain the origin of the growth stress generation over a wide range of the MFA.

B.F. Wilson (1981) had already pointed out that neither of above two theories alone seems adequate to explain the experimental phenomena over a wide range of the MFA. He suggested that integration of those two theories could possibly solve the discrepancy in each theory. On the other hand, progress in the strain-gauge technique enabled us to collect the numerous data on the surface growth stress both in the NW, the TW and the CW regions (Kikata et al.1972, Kikata & Miwa 1977, Sasaki et al. 1978, Okuyama et al. 1981, 1983). This developed Wilson's suggestion into a more sophisticated theory, i.e. "the unified hypothesis" proposed by Okuyama and his associates afterward.(2)

Unified hypothesis:

On the basis of numerous data on the released strains of the growth stress over a wide range of the MFA, Okuyama and his associates clarified that both the value of the released strain and the intensity of the reaction wood anatomy vary monotonously and continuously from the NW region to the CW or the TW regions. This means that the common mechanism should control the magnitude and the sign of the growth stress in the NW, the CW, and the TW regions. Moreover, they revealed that the mechanism of "the lignin swelling hypothesis" becomes actualized in the region with a large MFA, on the other hand, the mechanism of "the

cellulose tension hypothesis" becomes effective in a small MFA region. Then, Okuyama et al.(1986), and Yamamoto and Okuyama (1988) considered that both theories are indispensable for explaining the origin of tree growth stress, and they developed Wilson's (1981) idea into a new theory that can explain the observed relationship between the anisotropic surface growth stress and the MFA in the S2 layer. They call their new theory "the unified hypothesis", which is summarized as the following:

> Just after completion of the CMF framework as a bundle, the irreversible lignin deposition starts in the gaps between the CMF bundles. As the result of it, the matrix skeleton tends to expand isotropically. The CMF bundle in the secondary wall simultaneously tends to contract in its axial direction by a certain biomechanical change caused in the CMF framework. Thus, in a short period Δt, expansive inelastic strain $\Delta\varepsilon^m$ and the contractive one $\Delta\varepsilon^f$ are generated in the matrix skeleton and the CMF bundle, respectively. These two inelastic strains cause the wood fiber to deform isotropically. However, free deformation of each fiber is fully rectricted inside an actual stem. Thus, anisotropic growth stresses, σ_L and σ_T, are generated in the newly-formed xylem. Signs and intensities of σ_L and σ_T are controlled by the MFA and the magnitudes of $\Delta\varepsilon^m$ and $\Delta\varepsilon^f$.

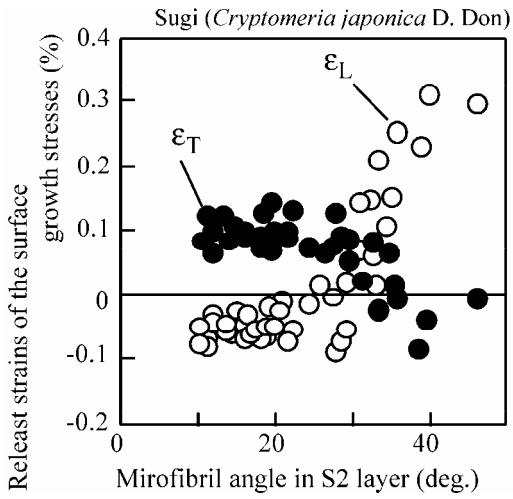

Fig. 3-4. Observed relationships between the released strains, ε_L and ε_T, and the MFAs in the S2 layers of a 9- and a 34-year-old sugi trees (*Cryptomeria japonica*) having tilted stems.

Figure 3-4 shows the observed relationships between the released strains, ε_L and ε_T, and the MFA in the S2 layer of 9- and 34-year-old sugi trees (*Cryptomeria japonica*) having tilted stems (Yamamoto & Okuyama 1988, Yamamoto 1998). As can be seen from the figure, ε_L and ε_T are highly dependent on the MFA in the S2 layer. This result can be naturally understood

on the basis of “the unified hypothesis”.

To make this hypothesis more scientific one, it is indispensable to confirm the mechanical propriety and the biogenetic consistency of “the unified hypothesis” by a quantitative discussions using a continuum mechanics model that imitates fine composite structure of the multi-layered wood fiber and its differentiating process as true as possible. This is the main object in the present section.

3-1-2 Mechanical model of differentiating wood fiber

(a) Parameters used for the modeling

It is considered that the released strain of the surface growth stress is equivalent to “the growth strain” which is defined as the elastic component in the strain of the free dimensional change that a virtually isolated wood fiber would produce during its secondary wall lignification. This is almost true in case of the longitudinal strain, which was already proved in Chapter 2 by the discussion based on the application of the simple mixture law to a homogeneous wood specimen that consists of a large amount of same shaped and same sized wood fibers. In this section, we will simulate the generation process of the growth strain of a single wood fiber.

In the present simulation, we adopt a complex circular cylinder model having three layers, the compound middle lamella (CML), the outer layer of the secondary wall (S1), and its middle layer (S2), for calculating the dimensional change of maturing wood fiber.[(3)] As described in Chapter 2, each layer is composed of the polysaccharide framework as a bundle and the lignin-hemicellulose matrix as a skeleton. The framework bundle consists of cellulose microfibril (CMF) and non-cellulosic polyose which is oriented in the direction along the molecular chain of the cellulose. The matrix skeleton is composed of lignin and non-oriented polyose e.g. xylan. According to “the reinforced-matrix theory”, they occupy the same domain of the cell wall elsewhere in the macroscopic limit.

In each layer of the secondary wall, the CMF is oriented in a certain direction, which is the microfibril angle (MFA), 5° ~ 50° in the S2 layer, and 90° in the S1 layer. In the CML, the CMF is randomly oriented, which makes the CML mechanically isotropic. The S3 is not taken into consideration in the present model since its volume is quite smaller than those in the S1 and the S2.

By using eqs.(2-37) which was derived in Section 2-2, we can calculate the growth

strains ε_L and ε_T. In the present case, eqs.(2-37) is derived from the following differential equations:

$$d\varepsilon_L = f_{11}(\mathbf{p})\, d\varepsilon_1^m + f_{12}(\mathbf{p})\, d\varepsilon_2^m + f_{13}(\mathbf{p})\, d\varepsilon_3^m + f_{14}(\mathbf{p})\, d\varepsilon_1^f + f_{15}(\mathbf{p})\, d\varepsilon_2^f + f_{16}(\mathbf{p})\, d\varepsilon_3^m$$
$$d\varepsilon_T = f_{21}(\mathbf{p})\, d\varepsilon_1^m + f_{22}(\mathbf{p})\, d\varepsilon_2^m + f_{23}(\mathbf{p})\, d\varepsilon_3^m + f_{24}(\mathbf{p})\, d\varepsilon_1^f + f_{25}(\mathbf{p})\, d\varepsilon_2^f + f_{26}(\mathbf{p})\, d\varepsilon_3^m \qquad (3\text{–}3)$$

Divided by a short period dt, eqs.(3-3) become

$$\dot{\varepsilon}_L = f_{11}(\mathbf{p})\dot{\varepsilon}_1^m + f_{12}(\mathbf{p})\dot{\varepsilon}_2^m + f_{13}(\mathbf{p})\dot{\varepsilon}_3^m + f_{14}(\mathbf{p})\dot{\varepsilon}_1^f + f_{15}(\mathbf{p})\dot{\varepsilon}_2^f + f_{13}(\mathbf{p})\dot{\varepsilon}_3^f$$
$$\dot{\varepsilon}_T = f_{21}(\mathbf{p})\dot{\varepsilon}_1^m + f_{22}(\mathbf{p})\dot{\varepsilon}_2^m + f_{23}(\mathbf{p})\dot{\varepsilon}_3^m + f_{24}(\mathbf{p})\dot{\varepsilon}_1^f + f_{25}(\mathbf{p})\dot{\varepsilon}_2^f + f_{23}(\mathbf{p})\dot{\varepsilon}_3^f \qquad (3\text{-}4)$$

where f_{11}, f_{12}, - - - -, f_{26} are functions of **p**, and **p** is a parameter vector whose components are θ, ρ_1, ρ_2, ρ_3, Q, G_1, G_2, G_3, M (=S_2/S_1), N (=S_3/S_2). Several components in **p** depend on elapsed time t, while θ, ρ_1, ρ_2, ρ_3, are independent of t.[(4)] In either case, each component in **p** should be given in advance as a known function of t or a constant.

ε_1^m, ε_2^m, ε_3^m, ε_1^f, ε_2^f, ε_3^f in the right hand side of eqs.(3-3) or (3-4) are functions of t, and these quantities are eigen-strains generated in the frameworks or the matrix substances during the secondary wall maturation. Superscripts “f” and “m” refer to the framework and the matrix, respectively. Subscript in each quantity stands for number of the wall layer (1 for S1, 2 for S2, and 3 for G). Functional shapes of ε_1^m, ε_2^m, ε_3^m, ε_1^f, ε_2^f, and ε_3^f should be given in advance as known functions of t when integrating the differential equations (3-4).

In this section, we discuss the behavior of the softwood tracheid or the hardwood normal wood fiber. Then, we eliminate the terms of ε_3^m and ε_3^f in addition to ρ_3, G_3, and N in eqs.(3-3) and (3-4). The values of θ, ρ_1, ρ_2, and h are determined from the microscopic observation and the image analysis. We can calculate Q (=$S_0 \cdot h/(r_1 \cdot E_1)$), G_1 (=E_1/S_1), and G_2 (=E_2/S_2) after determining the values of S_0, E_1, S_1, E_2, and S_2.

It is considered that the framework bundle in each layer of the secondary wall is a parallel composite of the uni-directionally oriented polysaccharide consisting of the crystalline cellulose and non-crystalline polyose, and the void. Non-crystalline polyose is a mixture of non-crystalline cellulose, (acetyle-)glucomannan, and so forth. Similar idea is applied to the case of the isotropic matrix skeleton which is a blended compound of lignin, xylan, and the void. To determine the values of E_1, S_1, E_2, and S_2, applying the simple mixture law to the polysaccharide framework bundle and the matrix skeleton, we derive the following formulas:

$$E_i = A_i \cdot C_i \cdot E_{cry} + A_i \cdot (1 - C_i) \cdot \psi(\tau) \cdot E_{poly} ,$$

$$S_i = \{1 - A_i + (1 - C_i) \cdot A_i \cdot (1 - \psi(\tau))\} \cdot E_{matr}/(1+\nu_i) \ , \qquad (i = 1, 2) \qquad (3\text{-}5)$$

where A_i and C_i are respectively the weight ratio of the polysaccharide framework and its crystallinity in each layer of the secondary wall. In eqs.(3-5), we introduced a function $\psi(\tau)$ whose independent variable τ is the moisture content normalized by the moisture content at the FSP. We assumed that $\psi(\tau)$ monotonously decreases with increase of τ, and satisfies $\psi(\tau)|_{\tau=0}=1$ and $\psi(\tau)|_{\tau=1}=0$. In our study, we assume the matrix skeleton behaves as an incompressive material like an elastomer, then, we use 0.5 for the value of ν.

The values of E_{cry}, E_{matr}, E_{poly}, and the weight ratio of polysaccharide framework in each layer become important factors when calculating eqs.(3-5). We adopt 134 GPa as the value of E_{cry}, which is not affected by the water adsorption (Sakurada et al. 1962). On the other hand, E_{matr} is highly dependent on the moisture content as proved by Cousins (1976, 1978). In the present simulation, we use 2 GPa for E_{matr} at the humid state, and 4 GPa at the oven-dried state. When we derived eqs.(3-5), we assumed that only dried part among the oriented polyose takes part in constituting the framework bundle, however, humid polyose is integrated into the isotropic matrix skeleton. This is why we assume that $\psi(\tau)$ is monotonously decreasing function of τ in its definition. We used 8 GPa as the axial Young's modulus of dried polyose (E_{poly}) with reference to Cousins's (1976) report.[5]

Values of A_1, C_1, A_2, and C_2 in the completed secondary wall are hypothesized in Table 3-1(a) in addition to the values of A_0 and C_0 in the CML. In this simulation, we will simulate the generation of the growth strain in the late wood tracheid of sugi. Then, being conscious of the anatomical properties of sugi late wood, we hypothesized the values of ρ_1, ρ_2, and h. The values of ρ_1, ρ_2, F, E_1, E_2, S_0, S_1, and S_2 used for the present simulation are calculated as displayed in Table 3-1(b). The value of S_0 can be obtained as described in Footnote.[6]

Table 3-1 (a). Composition of chemical constituents in each layer.*

Layer	Polysaccharide framework (A)		Matrix substance	Crystallinity in the Polysaccharide framework (C)
	Crystalline cellulose ($A \times C$)	Oriented polyose (non-Crystalline ($(1-C) \times A$)		
CML	15 (%)	0	85	0
S1	15	5	80	75
S2	30	10	60	75
S3	-----	-----	-----	-----

* supposed values for sugi (Japanese cedar) late wood.

(b) Values of parameters used for the simulation of the growth stress generation.

Maturation stage &	E_1	E_2	S_1	S_2	F	ρ_1	ρ_2
$t = 0 \sim T_1$	20.1*	40.2*	increase from 0 to 1.13*	0*	0.098*	1.1 #	1.5 #
$t = T_1 \sim T_2$	20.1*	40.2*	1.13*	increase from 0 to 0.933*	0.098*	1.1 #	1.5 #

* units: GPa. # hypothesized for sugi, late wood tracheid. & Lignin deposition starts at t=0, and ends at t=T_1 in the S1 layer, and it starts at t =T_1 and ends at t =T_2 in the S2 layer, then, the wood fiber is completed.

(b) Modeling the maturation process of the secondary wall

By using the autoradiography, Terashima and his associates came to a conclusion that cell wall maturation, that is lignification, proceeds in the three distinct stages preceded by deposition of carbohydrates (e.g. Terashima 1990). In the softwood tracheid, the lignification starts almost concurrently with the formation of the polysaccharide framework of the secondary wall. The first lignification occurs at the cell corner and the intercellular layer. After that, the second slow lignification proceeds at the primary wall and the S1 layer in parallel with the formation of the S2 and the S3 layers. Finally, the third main lignification occurs in the secondary wall just after the carbohydrate framework are deposited in the secondary wall in order of the CMF and other polyose. Some researcher commented that the lignification proceeds centripetally (e.g. Takabe et al.1992).

In the present simulation, we divided the lignification process of the secondary wall into two steps. On the first step, completion of the matrix skeleton in the S1 layer proceeds by

deposition of the matrix substances, preceded by completion of the polysaccharide framework in the S1 and the S2 layers. On the following step, the matrix skeleton in the S2 layer is deposited, and the formation of a xylem cell wall is finished. Matuation of the matrix skeleton, that is, lignification, starts at $t = 0$, and ends at $t = T_1$ in the S1 layer. And, that in the S2 layer starts at $t = T_1$, and ends at $t = T_2$. During the lignification process in each layer, values of the parameters S_i, ε_i^m, and ε_i^f (i = 1, 2) tend to vary their values monotonously with increase of the lignin content, and reach the terminal values at the end of the process. On the other hand, it is considered that the values of E_i (i = 1, 2) are constant during the lignification process in each layer, since the polysaccharide framework has been already completed before the lignification starts. For the similar reason, we suppose the parameters θ, ρ_1, ρ_2, and Q are constant for t. In this process, a virtually isolated wood fiber tends to deform in its axial and diameter directions, which is the growth strain of the newly-differentiated wood fiber. The growth strain is calculated as follows by integrating eqs.(3-4) along the lignification process of the secondary wall ($0 \le t \le T_2$).

$$\begin{aligned}
\varepsilon_L(T_2) - \varepsilon_L(0) &= \int_0^{T_2} \left\{ f_{11}(\mathbf{p})\dot{\varepsilon}_1^m + f_{12}(\mathbf{p})\dot{\varepsilon}_2^m + f_{13}(\mathbf{p})\dot{\varepsilon}_1^f + f_{14}(\mathbf{p})\dot{\varepsilon}_2^f \right\} dt \\
\varepsilon_T(T_2) - \varepsilon_T(0) &= \int_0^{T_2} \left\{ f_{21}(\mathbf{p})\dot{\varepsilon}_1^m + f_{22}(\mathbf{p})\dot{\varepsilon}_2^m + f_{23}(\mathbf{p})\dot{\varepsilon}_1^f + f_{24}(\mathbf{p})\dot{\varepsilon}_2^f \right\} dt
\end{aligned} \tag{3-6}$$

It is natural to assume the initial condition, $\varepsilon_L(0) = 0$. $\varepsilon_T(0) = 0$.

(c) Integral conditions – assumed for time-dependent parameters

From the above-mentioned discussion, we obtained rough images on the functional shapes of time-dependent parameters $S_1(t)$, $\varepsilon_1^m(t)$, $\varepsilon_1^f(t)$, $S_2(t)$, $\varepsilon_2^m(t)$, $\varepsilon_2^f(t)$. They are controlled by the lignin content which varies smoothly and monotonously in each layer, then, we can postulate the following condition on the functional shapes of the parameters $S_1(t)$, $\varepsilon_1^m(t)$, $\varepsilon_1^f(t)$, $S_2(t)$, $\varepsilon_2^m(t)$, $\varepsilon_2^f(t)$:

> [Condition 3-1] The t-dependent parameters $S_i(t)$, $\varepsilon_i^m(t)$, and $\varepsilon_i^f(t)$ (i =1, 2) can be expressed as follows by introducing the functions φ_1 and φ_2 which vary from 0 to 1 in the range of $0 \le t \le T_2$.
>
> $$S_i(t) = k_i \cdot \varphi_1(t), \quad \varepsilon_i^m(t) = m_i \cdot \varphi_i(t), \quad \varepsilon_i^f(t) = n_i \cdot \varphi_i(t)\,. \qquad (i = 1, 2) \tag{3-7}$$

$$\varphi_1(t)=\begin{cases} P(t) & (0 \le t \le T_1) \\ 1 & (T_1 \le t) \end{cases}, \quad \varphi_2(t)=\begin{cases} 0 & (0 \le t \le T_1) \\ Q(t) & (T_1 \le t \le T_2) \\ 1 & (T_2 \le t) \end{cases}, \qquad (3\text{-}8)$$

where k_i, m_i, and n_i are constants, and $P(t)$ and $Q(t)$ are monotonously increasing and differentiable functions which vary from 0 to 1 smoothly in respective domains. //

Condition (3-1) assumes that the functional shapes of $S_1(t)$, $\varepsilon_1^m(t)$, and $\varepsilon_1^f(t)$ become similar one another in $0 \le t \le T_1$, the same holds for $S_2(t)$, $\varepsilon_2^m(t)$, and $\varepsilon_2^f(t)$ in $T_1 \le t \le T_2$. We deduce the following proposition:

[Proposition 3-1] If we assume Condition (3-1), the integration (3-6) does not depend on either the functional shapes of $\varphi_1(t)$ and $\varphi_2(t)$ (or $P(t)$ and $Q(t)$), nor the times T_1 and T_2. It depends on only k_i, m_i, and n_i (i = 1, 2). //

Proof for Proposition (3-1) is described in *Footnote* (7).

3-1-3 Simulated result and discussion

When we integrate eqs.(3-6) under the condition (3-1), we have only to give care to the terminal values of t-dependent parameters $S_1(t)$, $\varepsilon_1^m(t)$, $\varepsilon_1^f(t)$, $S_2(t)$, $\varepsilon_2^m(t)$, $\varepsilon_2^f(t)$, which were introduced as k_1, m_1, n_1, k_2, m_2, and n_2 in this order (see equations (3-7)). The values of k_1 and k_2 are shown in Table 3-1(b) in addition to the values of S_0, which can be determined from the weight ratio of the polysaccharide framework to whole cell wall substance and the degree of crystallinity in each layer. The quantities m_1, m_2, n_1, and n_2 are the terminal values of the internal expansive terms, i.e. eigen strains of the matrix skeletons and the framework bundles which are generated during the secondary wall lignification. From the concept of "the lignin swelling hypothesis", m_1 and m_2 become positive values. On the other hand, from the concept of "the cellulose tension hypothesis", n_1, and n_2 would take negative values.

Here, supposing various values as m_1, m_2, n_1, and n_2, we integrate eqs.(3-6), and compare the simulated result with the experimental one. Thus, we can verify the physical proprieties of both concepts, i.e., "the lignin swelling hypothesis" and "the cellulose tension hypothesis". By the way, as shown in Fig.3-4, the growth strain generated in the

newly-formed xylem is strongly affected by the MFA in the S2 layer. Thus, in the present sub-section, we will try to explain the observed relationship between the released strains of the anisotropic surface growth stress and the MFA of a sugi tree having a crooked stem by integrating eqs.(3-6) under Condition (3-1).

(a) Effect of "the Lignin swelling hypothesis"

We firstly discuss the physical propriety of "the lignin swelling hypothesis". Here, we assume various positive values as m_1 and m_2 on the basis of the concept of the lignin swelling hypothesis. In the present simulation, we suppose m_1 ($= \varepsilon_1^{m}(t)\big|_{t=T1}$) is more or less larger than that of m_2 ($= \varepsilon_2^{m}(t)\big|_{t=T2}$) since the content of the matrix substance (lignin) is higher in the S1 layer than in the S2 layer. On the other hand, we suppose n_1 ($= \varepsilon_1^{f}(t)\big|_{t=T1}$) = n_2 ($= \varepsilon_2^{f}(t)\big|_{t=T2}$) = 0.

Figure 3-5(a) are the calculated results on the relationships between ε_L, ε_T, and θ (MFA in the S2 layer). Dots are the experimental results of sugi trees already shown in Fig.3-4. Calculated ε_L takes positive value over all ranges of the MFA, that is, the wood fiber model tends to expand in the direction of fiber axis for all MFAs. Moreover, as the values of m_1 ($= \varepsilon_1^{m}(t)\big|_{t=T1}$) and m_2 ($= \varepsilon_2^{m}(t)\big|_{t=T2}$) become larger, the curve of ε_L tends to shift upward from **a** to **d** in the figure. Thus, "the lignin swelling hypothesis" can explain the mechanism of the longitudinal compressive stress generation in the CW region with large MFAs, however, it cannot explain the origin of tensile stress generation in the TW or NW region with small MFAs. Furthermore, ε_T becomes considerably larger than the experimental one.

(b) Effect of "the cellulose tension hypothesis"

In this case, we integrate eqs.(3-6) supposing various negative values as n_1 ($= \varepsilon_1^{f}(t)\big|_{t=T1}$) and n_2 ($= \varepsilon_2^{f}(t)\big|_{t=T2}$), on the other hand, we supposed m_1 ($= \varepsilon_1^{m}(t)\big|_{t=T1}$) and m_2 ($= \varepsilon_2^{m}(t)\big|_{t=T2}$) are all nil during the secondary wall lignification. Figure 3-5(b) shows the simulated results calculated on the basis of "the cellulose tension hypothesis". Over a wide range of the MFAs, the wood fiber model tends to contract in its axial direction, and the curve of ε_L tends to shift downward from α to δ as the values of n_1 ($= \varepsilon_1^{f}(t)\big|_{t=T1}$) and n_2 ($= \varepsilon_2^{f}(t)\big|_{t=T2}$) become larger. These can explain the generation of the longitudinal tensile stress in the region of small MFAs, however, it cannot explain the mechanism of the longitudinal compressive stress generation in the CW region with large MFAs. Besides, the calculated value of ε_T becomes negative over all ranges of the MFAs which is seriously contradictory to the observed fact that the tangential

released strain takes almost constant positive values of 0.1%.

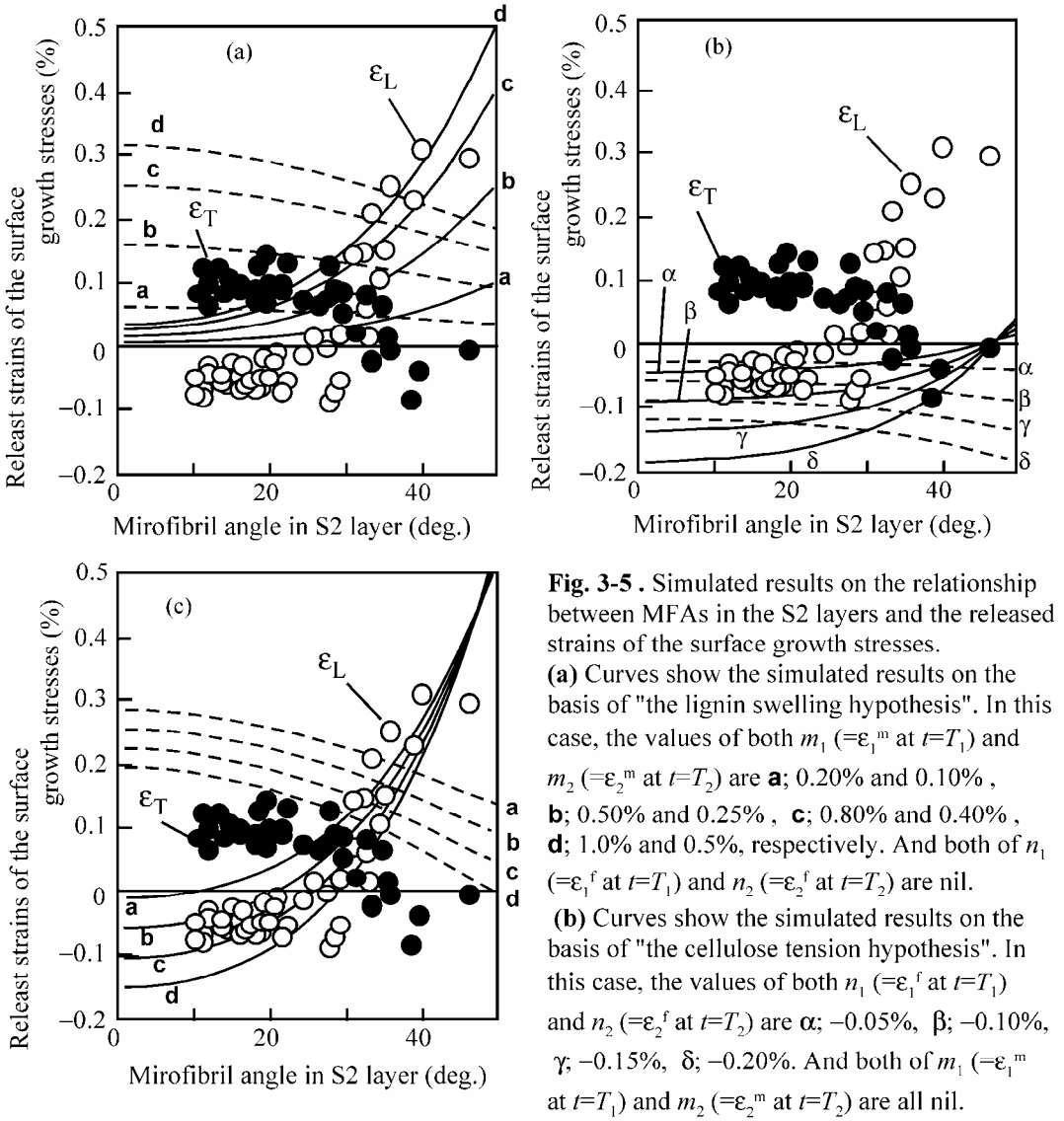

Fig. 3-5 . Simulated results on the relationship between MFAs in the S2 layers and the released strains of the surface growth stresses.
(a) Curves show the simulated results on the basis of "the lignin swelling hypothesis". In this case, the values of both m_1 ($=\varepsilon_1^m$ at $t=T_1$) and m_2 ($=\varepsilon_2^m$ at $t=T_2$) are **a**; 0.20% and 0.10% , **b**; 0.50% and 0.25% , **c**; 0.80% and 0.40% , **d**; 1.0% and 0.5%, respectively. And both of n_1 ($=\varepsilon_1^f$ at $t=T_1$) and n_2 ($=\varepsilon_2^f$ at $t=T_2$) are nil.
(b) Curves show the simulated results on the basis of "the cellulose tension hypothesis". In this case, the values of both n_1 ($=\varepsilon_1^f$ at $t=T_1$) and n_2 ($=\varepsilon_2^f$ at $t=T_2$) are α; –0.05%, β; –0.10%, γ; –0.15%, δ; –0.20%. And both of m_1 ($=\varepsilon_1^m$ at $t=T_1$) and m_2 ($=\varepsilon_2^m$ at $t=T_2$) are all nil.
(c) Curves show the simulated results on the basis of "the unified hypothesis". In this case, the values of both n_1 ($=\varepsilon_1^f$ at $t=T_1$) and n_2 ($=\varepsilon_2^f$ at $t=T_2$) are **a**; –0.05%, **b**; –0.10%, **c**; –0.15%, and **d**; –0.20%. And those of m_1 ($=\varepsilon_1^m$ at $t=T_1$) and m_2 ($=\varepsilon_2^m$ at $t=T_2$) are 1.0% and 0.5%, respectively. The values of other parameters in p are shown in Table 3-1(b). Dots are experimental resuts from two sugi trees (*Cryptomeria japonica*) having tilted stems.

(c) Effect of "the unified hypothesis"

The last simulation concerns the effect of "the unified hypothesis" which takes both hypotheses into consideration. In this simulation, we supposed that m_1 ($= \varepsilon_1^m(t)\big|_{t=T1}$) and m_2 ($= \varepsilon_2^m(t)\big|_{t=T2}$) take positive values of 1.0% and 0.5% respectively, on the other hand, we assumed various negative values for n_1 ($= \varepsilon_1^f(t)\big|_{t=T1}$) and n_2 ($= \varepsilon_2^f(t)\big|_{t=T2}$). According to the

simulation, ε_L takes negative value in the region of less than 30° of MFAs, and ε_L is nearly compatible with the observed one. In the region of more than 30° of MFAs, positive value of ε_L tends to increase with increase in the MFA. Those results well represent the observed data quantitatively as shown in Fig.3-5(c). In a case of $n_1 = n_2 = -0.0015$ (= –0.15%), the curve of ε_L can well represent the experimental tendency. On the other hand, calculated value of ε_T becomes pretty larger expansion than the observed value. It is considered that the residual stress in the transverse direction is easy to decrease due to stress relaxation in comparison with that in the longitudinal direction inside an actual xylem, then, the observed value of released strain in the tangential direction is considered to become slightly smaller than the value calculated by means of elastic analysis.

(d) Discussions

As we have seen, "the unified hypothesis" can explain clearly the observable relations between released strains of the surface growth stresses and the MFAs. This leads us to the following conclusions:

The anisotropic growth stresses in tree xylem are generated in wood cell walls by an interactive effect between the increase in the contractive stress generated in the polysaccharide framework bundle and the increase in the expansive stress generated in the matrix skeleton of the secondary wall by the irreversible deposition of lignin. The CMF orientation in the S2 layer, *i.e.* MFA, is one of the most important factor which control the magnitudes and the signs of the growth stress in the cell wall.

However, we have not yet discovered conclusive evidences to prove that contractive stress is spontaneously generated in the framework bundle. The same may be said of the expansive stress generation in the matrix skeleton. We must explain how the tensile stress originates in the polysaccharide framework bundle, and how the compressive stress is generated in the matrix skeleton during the secondary wall maturation, on the basis of the experimental and theoretical verifications.

3-1-4 Summary and concluding remarks

In Chapter 2, we showed that the wood fiber tends to deform in its axial and the diameter directions by the generation of the eigen-strains in the polysaccharide framework bundle and the lignin-hemicellulose matrix skeleton when a certain biomechanical state change occurs in

the cell wall. In this chapter, we discussed the important roles of those eigen-strains on the generation of the growth stress in the differentiating xylem fiber. Here, we postulated the secondary wall maturation (lignification) as a biomechanical state change occurring in the cell wall.

The simulation using the softwood tracheid model deduced that expansive eigen-strains are generated in the matrix skeleton during the secondary wall lignification, which finally amount to 0.5~1%. At the same time, contractive eigen-strains are generated in the polysaccharide framework bundle, which become –0.15% during the secondary wall lignification. This result strongly supports the unified hypothesis as a possible theory to explain the origin of the surface growth stress.

In the TW region, the G-fiber is often formed, where a very large contractive growth stress is generated in its longitudinal direction. However, the analytical model presented here is not applicable to the G-fiber property. In Chapter 5, we will analyze the origin of the very large growth stress in the TW region by using the G-fiber model which is an improved version of the tracheid model presented here.

Footnote:

(1) Wardrop (1965) observed a phenomenon that the G-layer often tends to shrink in its volume during the cell wall maturation. This observation led him to a conception that the shrinking CMF in the G-layer causes a very large tensile stress in the G-fiber. To explain the origin of the contractive stress of the CMF, he proposed a hypothetical mechanism as the following (Wardrop 1956):

> "If cellulose is initially deposited wholly or partly in this condition (= paracrystalline condition) then it is reasonable to assume that subsequent crystallization would involve a contraction in volume and it is suggested that this phase of crystallization may be the source of the contractile forces generated during differentiation. In general the crystallinity of cellulose seems highest when the lignin content is low and it may be that crystallization is facilitated by the absence of lignin. Such a hypothesis remains to be proved, since it has been shown in this laboratory (= Division of Forest Products, CSIRO, Australia) (unpublished data) that the cellulose of fresh undried

tension wood is highly crystalline although this in itself does not preclude the possibility that contraction takes place as a result of crystallization of the cellulose."

In short, the CMF is deposited in only a partly crystalline state, subsequent crystallization proceeds when lignification starts, and further lignification serves inhibit the endless increase of crystallization of the CMFs. According to his idea, CMF crystalinity becomes very low in the CW xylem having a high content of lignin, while it takes a high value in the TW xylem containing a very low lignin. Those idea was partly verified by himself on the basis of the observation of the X-ray diffraction pattern from the TW, the NW, and the CW xylem, which showed that the intensity of non-crystalline scattering from the TW is clearly lower than that of the NW, and the CW. Moreover, he reported that the computed crystalline size becomes larger by the delignification, which is more prominent in the NW region, while less prominent in the TW region. However, no one has not succeeded in detecting either the significant increase in the CMF crystallinity or generation of the contractive stress in the CMF framework during the cell wall maturation.

(2) The first reference that the terminology "the unified hypothesis" was used is Okuyama's (1993) review article on the tree growth stress, in Japanese, "統一仮説 (*Toh-itsu kasetsu*)". English terminology has been used from Yamamoto et al. (1995).

(3) The wood fiber model, consisting of the CML the S1, and the S2 layers, describes mechanical properties of the CW, and the NW tracheid, the hardwood NW fiber, and the TW fiber in *Magnoliaceae* which belongs to a primitive angiosperm without forming clear G-fiber in the TW xylem. In Chapter 5, we will discuss the mechanical properties of the TW xylem by using the G-fiber model having the CML, the S1, the S2, and the G layers.

(4) Correctly speaking, thickness in each layer tends to vary with the elapsed time during the cell wall maturation, of which behaviors are described as the differential equations (2-32). Eqs.(2-32), having ρ_1, ρ_2, ρ_3 as solutions to be solved, are coupled with eqs.(2-31), having ε_L, ε_T^{r1} ($=\varepsilon_T$), ε_T^{r2}, ε_T^{r3} as unknowns to be solved. If we can assume that ε_L and ε_T would not exceed 1%, we may eliminate the differentials of ρ_1, ρ_2, and ρ_3

as very small quantities. In such a case, coupling between eqs.(2-31) and (2-32) are dissolved into eqs.(3-3) (or (3-4)). For the present, no one has reported that observed values of ε_L and ε_T become larger than 1%, then, the above assumption is enough valid.

(5) Srinivasan (1941) measured the elastic modulus of the electrochemically prepared lignin and molded lignosic preticipate, and obtained 2GPa at the humid state, which is taken equal to the value of E_{matr}. Afterward, Cousins (1976) tried to measure the elastic modulus of the rod of chemically isolated lignin in relation to the moisture dependencies. He concluded that elastic modulus of the molded lignin takes 4~8 GPa at the fully dried state, and it linearly decreases with the moisture content, and it becomes 2~3 GPa at the humid state. Cousin (1978) also reported that elastic modulus of the isolated hemicellulose takes a value of 8 GPa at a low moistute content, and it decreases to 0.01 GPa by moisture saturation. Besides, Ishikawa et al.(1998) estimated the elastic modulus of the amorphous region in the cellulose microfibril of bleached ramie fiber, and she obtained 8~10 GPa at the fully dried state. In the actual cell wall, it is considered that there are covalent and/or hydrogen bonds among hemicellulose, lignin, and amorphous cellulose, and some kind of hemicellulose is oriented along the cellulose microfibril, and the other is isotropically blended with lignin (Liang et al. 1960, Fushitani 1973, Salmen 2000), which prevents a flow of hemicellulose that Cousins (1978) found. If some flow of hemicellulose would occur in the cell wall, the elastic modulus of the matrix substance should become more or less smaller than that of isolated and purified lignin. This is why the elastic modulus of the isolated matrix substance at the humid state given by Srinivasan (1941) was a little smaller than that of isolated lignin.

(6) In the actual compound middle lamella (CML), the CMF is oriented randomly in the matrix skeleton so that the elastic property of the CML is rather isotropic, and the value of S_0 is considered to be slightly larger than the value of S_{matr}. To calculate the value of S_0, we assume that the CML is a quasi-isotropic material which is made of four unidirectional continuous fiber laminae with an equal angle between each adjacent lamina. In this model, we should pay attention that each lamina is not a plate of the framework bundle but the composite consisting of the framework bundle and the matrix skeleton. We denote the elastic constants of each lamina in the direction along the

principal axis as E_L and ν_{LT}, and those in the transverse direction as E_T and ν_{TL}. Those constants can be calculated from the following Uemura and Yamada's formulas (1975) on the basis of the ratio of chemical constituents in the CML and the degree of crystallinity in the polysaccharide framework as assumed in Table 3-1(a).

$$
\begin{aligned}
E_L &= A_f \cdot C_f \cdot E_{cry} + A_f \cdot (1 - C_f) \cdot \psi(\tau) \cdot E_{poly} + \{1 - A_f + A_f \cdot (1 - C_f)(1 - \psi(\tau))\} E_{matr} \\
&= A_f \{C_f + (1 - C_f) \cdot \psi(\tau)\} E_L^{framework} + \{1 - A_f + A_f \cdot (1 - C_f)(1 - \psi(\tau))\} E_{matr} \\
&= V_f \cdot E_L^{framework} + V_m \cdot E_{matr} \quad ,
\end{aligned}
$$

$$
E_T = (1 - k) \frac{E_T^{framework} \cdot E_{matr}}{V_f \cdot E_{matr} + V_m \cdot E_T^{framework}} + k\left[V_f \cdot E_T^{framework} + V_m \cdot E_{matr}\right] \quad ,
$$

$$
G_{LT} = (1 - k) \frac{G_{12}^{framework} \cdot G_{matr}}{V_f \cdot G_{matr} + V_m \cdot G_{12}^{framework}} + k\left\{V_f \cdot G_{12}^{framework} + V_m \cdot G_{matr}\right\} \quad ,
$$

$$
\nu_{LT} = (1 - k)\left(V_f \cdot \nu_{12}^{cry} + V_m \cdot \nu_{matr}\right) + k \frac{\nu_{12}^{cry} \cdot V_f \cdot E_T^{framework} + \nu_{matr} \cdot V_m \cdot E_{matr}}{V_f \cdot E_T^{framework} + V_m \cdot E_{matr}} \quad ,
$$

$$
\nu_{TL} = \nu_{LT}\left(\frac{E_T}{E_L}\right) \quad , \qquad k = 0.4 \cdot V_f - 0.025. \qquad \text{(3-A1)}
$$

where $E_L^{framework}$ and $E_T^{framework}$ are substantial Young's modulae of the polysaccharide as the complex of the cellulose crystal and the polyose in its axial and transverse directions, respectively.

Double shear modulus of a quasi-isotropic sheet consisting of [0°/+45°/–45°/90°] can be given as the following formula:

$$
S_0 = \frac{1}{4}\left(\frac{E_L - 2\nu_T E_L + E_T}{1 - \nu_L \nu_T}\right) + G_{LT} \ . \qquad \text{(3-A1')}
$$

(7) If we substitute (3-7) and (3-8) into eq.(3-6), we obtain the following expression:

$$\begin{aligned}
\varepsilon_{\mathrm{L}}(T_2) &= \int_0^{T_2} \left\{ f_{11}(\mathbf{p})\dot{\varepsilon}_1^{\mathrm{m}} + f_{12}(\mathbf{p})\dot{\varepsilon}_2^{\mathrm{m}} + f_{13}(\mathbf{p})\dot{\varepsilon}_1^{\mathrm{f}} + f_{14}(\mathbf{p})\dot{\varepsilon}_2^{\mathrm{f}} \right\} dt \\
&= \int_0^{T_2} \left[m_1 \cdot f_{11}(\mathbf{p}) \left(\frac{d\varphi_1(t)}{dt} \right) + m_2 \cdot f_{12}(\mathbf{p}) \left(\frac{d\varphi_2(t)}{dt} \right) \right. \\
&\quad \left. + n_1 \cdot f_{13}(\mathbf{p}) \left(\frac{d\varphi_1(t)}{dt} \right) + n_2 \cdot f_{14}(\mathbf{p}) \left(\frac{d\varphi_2(t)}{dt} \right) \right] dt \\
&= \int_0^{T_1} g_1(P(t)) \left(\frac{dP(t)}{dt} \right) dt + \int_{T_1}^{T_2} g_2(Q(t)) \left(\frac{dQ(t)}{dt} \right) dt \quad ,
\end{aligned} \tag{3-A2}$$

$$\begin{aligned}
\varepsilon_{\mathrm{T}}(T_2) &= \int_0^{T_2} \left\{ f_{21}(\mathbf{p})\dot{\varepsilon}_1^{\mathrm{m}} + f_{22}(\mathbf{p})\dot{\varepsilon}_2^{\mathrm{m}} + f_{23}(\mathbf{p})\dot{\varepsilon}_1^{\mathrm{f}} + f_{24}(\mathbf{p})\dot{\varepsilon}_2^{\mathrm{f}} \right\} dt \\
&= \int_0^{T_1} g_3(P(t)) \left(\frac{dP(t)}{dt} \right) dt + \int_{T_1}^{T_2} g_4(Q(t)) \cdot \left(\frac{dQ(t)}{dt} \right) dt \, .
\end{aligned} \tag{3-A2'}$$

where functions g_1 , g_2 , g_3, and g_4 are defined as the following relations:

$$\begin{cases}
g_1(P(t)) = \left(m_1 \cdot f_{11}(\mathbf{p}) + n_1 \cdot f_{13}(\mathbf{p}) \right)\big|_{S_1 = k_1 \cdot P(t),\, S_2 = 0} \quad (0 \le t \le T_1), \\
g_2(Q(t)) = \left(m_2 \cdot f_{12}(\mathbf{p}) + n_2 \cdot f_{14}(\mathbf{p}) \right)\big|_{S_1 = k_1,\, S_2 = k_2 \cdot Q(t)} \quad (T_1 \le t \le T_2), \\
g_3(P(t)) = \left(m_1 \cdot f_{21}(\mathbf{p}) + n_1 \cdot f_{23}(\mathbf{p}) \right)\big|_{S_1 = k_1 \cdot P(t),\, S_2 = 0} \quad (0 \le t \le T_1), \\
g_4(Q(t)) = \left(m_2 \cdot f_{22}(\mathbf{p}) + n_2 \cdot f_{24}(\mathbf{p}) \right)\big|_{S_1 = k_1,\, S_2 = k_2 \cdot Q(t)} \quad (T_1 \le t \le T_2).
\end{cases} \tag{3-A3}$$

provided that we consider here, $\mathbf{p}$ = (θ, ρ_1, ρ_2, h, E_1, E_2, S_0, $S_1(t)$, $S_2(t)$). The quantities k_1, m_1, n_1, k_2, m_2, and n_2 are constants which have no relation with the integration variable t. $P(t)$ and $Q(t)$ vary from 0 to 1 smoothly and monotonously for elapsed time t in respective integration intervals. Therefore, we can rewrite eqs.(3-A2) and (3-A2') as follows under the condition (3-1):

$$\begin{aligned}
\varepsilon_{\mathrm{L}}\left(= \varepsilon_{\mathrm{L}}(t)\big|_{t=T_2} \right) &= \int_0^1 g_1(P)dP + \int_0^1 g_2(Q)dQ \\
\varepsilon_{\mathrm{T}}\left(= \varepsilon_{\mathrm{T}}(t)\big|_{t=T_2} \right) &= \int_0^1 g_3(P)dP + \int_0^1 g_4(Q)dQ
\end{aligned} \tag{3-A4}$$

This result indicates that the integration value in eq.(3-6) does not depend on the concrete

values of T_1 and T_2, furthermore, it is not affected by the functional shapes of t-dependent variables S_1, S_2, ε_1^m, ε_2^m, ε_1^f, and ε_2^f if we assume the condition (3-1).

(q.e.d.)

3-2 Growth stress controls negative gravitropism in woody plant stems

3-2-1 Background

Various tropic behaviors serve to maintain a plant's ideal shape, thus optimizing photosynthetic efficiency and relaxing the bending stress at the base of an inclined stem or branch (Timell 1986; Yoshida et al. 1991, 1992a, 1992b; Fournier et al. 1994; Hangarter 1997).

Shortly after the main axis of a young, growing herbaceous plant is inclined from the vertical by the weight of added tissue, differential growth is induced in the stem, resulting in a renewal of upward growth (Iwami and Masuda 1974; Silk 1984; Mueller et al. 1984; Kohji et al. 1995; Cosgrove 1997). This behavior is called *negative gravitropism*. In the case of woody plant stems, however, differential growth does not occur because of the restrictions imposed by the rigid secondary xylem. Thus, the recovery of the orientation of the inclined stem must be attained by mechanical bending of the thick, rigid secondary xylem (Wardrop 1965; Hejnowicz 1997).

Woody plants generate a two-dimensional stress distribution in the outermost layer of the secondary xylem during the deposition of secondary cell wall components (Boyd 1972; Okuyama et al. 1981; Archer 1987; Hejnowicz 1997). This stress, called *the growth stress*, has an axial tension component of several MPa in the case of a vertically oriented trunk (Sasaki et al. 1978; Archer 1987; Hejnowicz 1997). In an inclined trunk or branch of an angiosperm, tension wood (TW) fiber is often formed in the secondary xylem on the upper side of the inclined stem as mentioned in Section 3-1, where the axial growth stress becomes extremely large (Okuyama et al. 1990, 1994; Yamamoto et al. 1992). In contrast, compression wood (CW) tracheids are formed on the lower side of the inclined trunk or branch of gymnosperms where a large compressive growth stress is generated in the axial direction (Okuyama et al. 1983; Yamamoto et al. 1991). The growth stress in the region opposite to the TW or CW is reduced, resulting in an upright bending moment (recovery moment) in the inclined trunk or branch (Okuyama et al. 1990, 1994; Yamamoto et al. 1991). These behaviors suggest that formation of the TW or CW enables the woody plant stem to exhibit the observed negative-gravitropic responses.

In woody plant shoots, the higher-ordered branches grow thicker with each growing period, and after many years the weight of the xylem becomes huge. It remains unclear whether the growth stresses in the TW or the CW regions could compensate for the bending

moment resulting from the increasing mass of the shoot. Furthermore, some other as yet unknown factor could control the negative-gravitropic behavior in woody plant stems. To investigate these questions, the growth behavior of the woody plant shoot was examined using a structural mechanics model. Pioneer works by Archer and Wilson (1970, 1973, 1982) describing the graviresponse of the woody plant stem were augmented by Castera and Morlier (1991), Fournier et al. (1994), and Fourcaud and Lac (1996) who proposed mathematical models to describe the righting movement of tilted young woody shoots. Some of the models contain parameters whose physical meanings are not clearly defined, or which neglect the action of the growth stress. Fine-tuning the models should result in a more accurate understanding of the mechanism responsible for negative-gravitropic behavior in woody plant shoots.

With the goal of formulating a model to describe the time-dependent change in spatial shape of inclined tree trunks or branches, we proposed that the spatial shape of the inclined growing shoot could be calculated mathematically as the interactive balance between the bending moment due to weight growth of the shoot, the recovery moment caused by the large growth stress generation in the TW or CW regions, and the directional angle of the terminal shoot (Yamamoto et al.2002). Using the model to simulate observable responses permitted evaluation of the contribution of growth stress generation in the TW or CW regions to the degree of gravitropic movement and shoot shape control.

3-2-2 Basic equation

(a) Model and assumption

Modelling the shoot growth:

In the current study, a zigzag elastic cantilever consisting of several straight members is used as a model of the growing woody plant shoot, as shown in Fig.3-6. Each member is rigidly connected in series. It is assumed that no higher-ordered long shoot is formed during the shoot growth. Foliage grows at each node through the higher-ordered short shoot and at the shoot apex.

Shoot growth is achieved by repeating the following growth step: each growth step consists of two processes, the primary growth and the secondary growth, as shown in Fig.3-7. *Primary growth* is considered to be the elongation of the primary tissue at the shoot apex. In

this process, a small elastic cylinder, whose diameter and length are respectively r_0 and Δl, appears at the shoot apex. This newly formed tissue, represented by an additional member, is called *the elongation zone*.

Secondary growth occurs in the stem as primary growth begins. In this process, each member of the stem, with the exception of the elongation zone, increases its radius by Δr. Concurrently, new foliage appears at each node and shoot apex.

During each growth step, the shoot increases in weight, and the growth stress is generated in the newly formed secondary xylem, or *thickening zone*, during cell wall formation. Each member tends to be deflected by the bending moment of the weight increase in the shoot and the recovery moment of growth stress generation. After each growth step, each nodal point moves, and it is renamed the *new node*.

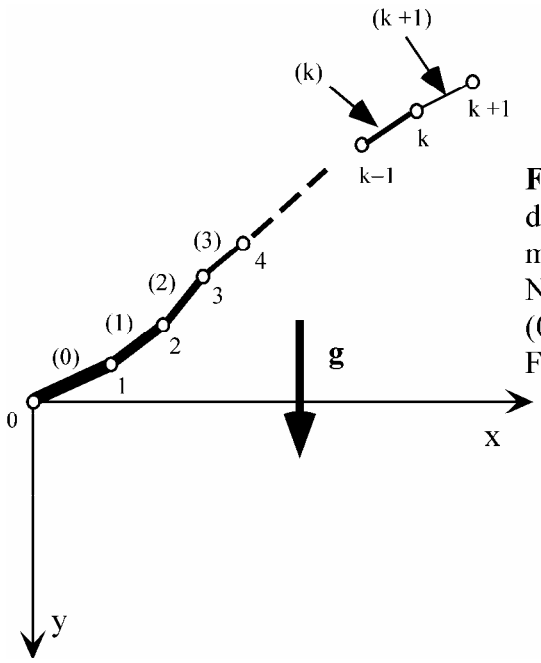

Fig.3-6. A model of growing shoot. White dots means the nodes conecting neighboring members.
Note: 0, 1, - - - , k +1 indicate node numbers.
(0), (1), - - - , (k+1) indicate member numbers.
Foliage was omitted here.

Assumption of structural mechanics:

To analyze shoot growth mechanically, we assumed the following structural and mechanical properties of the growing shoot.

Assumption 1: The angle between two neighboring members is constant during each growth step.

Assumption 2: When growth starts, each member in the stem is considered to be a straight member connecting neighboring nodes.

Assumption 3: The deformation caused by the axial component of the external load acting on each member is often smaller if compared to the one due to the bending component. Thus, axial expansion or contraction due to external loading is considered to be negligible when calculating the deflection of the growing shoot.

Assumption 4: The foliage acts as a concentrated load at each node. However, it does not contribute to the bending or torsional moment of the main axis through the leafstalk or the short shoot.

(b) Structural mechanics of the growing shoot

Initial setting; appearance of the shoot, and the first growth step:

We begin our discussion from an initial setting at the 0th member, that is, an inclined cantilever whose radius and length are respectively r_0 and Δl, as shown in Fig.3-7. The supporting and the free ends are respectively denoted as "the 0th node" and "the 1st node". The directional angle of the 0th member is θ_0, which is measured in a clockwise direction from the x-axis to the radial direction of the 0th member.

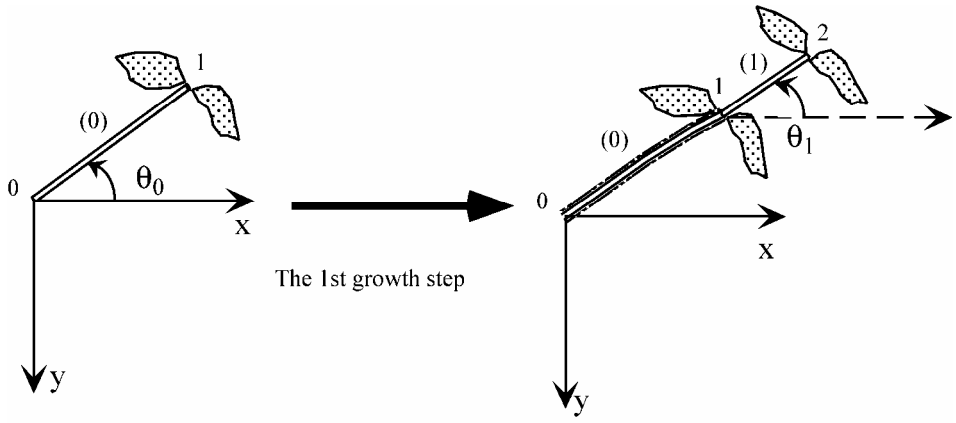

Fig. 3-7. Appearance of the shoot (generation of the 0th member), and the 1st growth step (generation of the 1st member and thickening of the 0th member). Note: 0, 1, and 2 indicate node numbers. (0) and (1) indicate member number.

When the 1st growth step is performed in the 0th member, a new elongation zone appears from the 1st node in the direction of θ_1, whose length and radius are respectively denoted by Δl and r_0. At the same time, the radius in the 0th member increases by Δr, and the new foliage appears at the 1st and 2nd node. The growth stress is generated in the thickening zone, whose peripheral distribution often becomes uneven in the inclined stem.

As the result of the 1st growth step, the 0th member is deflected, and the 1st node is strained to other coordinates. The new coordinates of the 1st and the 2nd nodes after completion of the 1st growth step can be calculated by the beam theory.

Load and moment at each node just after completion of the k-th growth step:

We denote the xy-coordinates of the i-th node just after completion of the (k–1)-th growth step as

$$\left(m_{\mathrm{i}}^{(\mathrm{k}-1)},\, n_{\mathrm{i}}^{(\mathrm{k}-1)}\right)$$

The length of the i-th member ($l_{\mathrm{i}}^{(\mathrm{k}-1)}$) is given by

$$l_{\mathrm{i}}^{(\mathrm{k}-1)} = \sqrt{\left(m_{\mathrm{i+1}}^{(\mathrm{k}-1)} - m_{\mathrm{i}}^{(\mathrm{k}-1)}\right)^2 + \left(n_{\mathrm{i+1}}^{(\mathrm{k}-1)} - n_{\mathrm{i}}^{(\mathrm{k}-1)}\right)^2} \quad , \tag{3-9}$$

where i = 0,1, 2, - - - - - , k–1. For simplification, we often denote $l_{\mathrm{i}}^{(\mathrm{k}-1)}$ as l_{i}, hereinafter.

As the result of the k-th growth step, each member from the 0-th to (k–1)-th, increases in radius by Δr. At the same time, a cylinder, whose diameter and length are respectively r_0 and Δl, appears at the shoot apex. As the result of the weight growth during the k-th growth step, the load acting on the i-th node increases by $\Delta p_{\mathrm{i}}^{(\mathrm{k})}$, which is given as

$$\Delta p_{\mathrm{i}}^{(\mathrm{k})} = \rho\pi\Delta r \sum_{\mathrm{j=i}}^{\mathrm{k}-1} l_{\mathrm{j}}\left(2r_0 + (2\mathrm{k} - 2\mathrm{i} - 1)\Delta r\right) + \rho\pi r_0^2 \Delta l + \sum_{\mathrm{j=i}}^{\mathrm{k}} \Delta h_{\mathrm{j}}^{(\mathrm{k})} + h_{\mathrm{k+1}}^{(\mathrm{k})} \quad , \tag{3-10}$$

where i = 0, 1, 2, - - - - - , k–1. The first term on the right-hand side is the sum of the weight of the newly formed thickening zone in the j-th member, the second term is the weight of the elongation zone, and the third term is the sum of the weights of the newly appeared foliages in the i-th through k-th nodes. The last term is the weight of the new foliage at the shoot apex.

When i=k, $$\Delta p_{\mathrm{k}}^{(\mathrm{k})} = \rho\pi r_0^2 \Delta l + \Delta h_{\mathrm{k}}^{(\mathrm{k})} + h_{\mathrm{k+1}}^{(\mathrm{k})} \quad . \tag{3-11}$$

And, when i=k+1, $$\Delta p_{\mathrm{k+1}}^{(\mathrm{k})} = h_{\mathrm{k+1}}^{(\mathrm{k})} \quad . \tag{3-12}$$

During the k-th growth step, the weight of the i-th member increases by $\Delta\Omega_{\mathrm{i}}^{(\mathrm{k})}$, which is given as

$$\Delta\Omega_{\mathrm{i}}^{(\mathrm{k})} = \rho\pi\Delta r\left\{2r_0 + (2\mathrm{k} - 2\mathrm{i} - 1)\Delta r\right\} l_{\mathrm{i}}^{(\mathrm{k}-1)}. \quad (\mathrm{i} = 0, 1, 2, \text{- - - -}, \mathrm{k}-1)$$

The normal component of the weight increment to the central axis of the i-th member is

$$\Delta\Lambda_i^{(k)} = \Delta\Omega_i^{(k)} \cos\theta_i^{(k-1)} = \rho\pi\Delta r\{2r_0 + (2k - 2i - 1)\Delta r\}\, l_i^{(k-1)} \cos\theta_i^{(k-1)}.$$

Then, the quantity $\Delta\omega_i^{(k)}$ is introduced from $\Delta\Lambda_i^{(k)}$ as follows,

$$\Delta\omega_i^{(k)} = \Delta\Lambda_i^{(k)} / l_i^{(k-1)} = \rho\pi\Delta r\{2r_0 + (2k - 2i - 1)\Delta r\}\cos\theta_i^{(k-1)},$$

$$(\ i = 0, 1, 2, - - - -, k-1) \qquad (3\text{-}13)$$

$$\Delta\omega_k^{(k)} = \rho\pi r_0^2 \cos\theta_k^{(k-1)} \quad (i = k), \qquad (3\text{-}14)$$

where $\theta_i^{(k-1)}$ is the directional angle of the i-th member just before starting the k-th growth step, as measured in a clockwise direction from the x-axis to the radial direction of the i-th member as shown in Fig.3-8. $\theta_i^{(k-1)}$ is calculated automatically from the coordinates of the i-th and the (i+1)-th nodes after completing the (k–1)-th growth step. $\theta_k^{(k-1)}$ is the directional angle of the elongation zone when the k-th growth step starts, which must be given a value in advance. In the case that $\theta_k^{(k-1)} = \theta_C$ (= constant) for any k, the extension zone always appears with a certain directional angle (θ_C). However, if the elongation zone has no specific directional angle, a relation of $\theta_k^{(k-1)} = \theta_{k-1}^{(k-1)}$ should always be established. Similarly, when $l_i^{(k-1)}$, we often denote $\theta_i^{(k-1)}$ as θ_i.

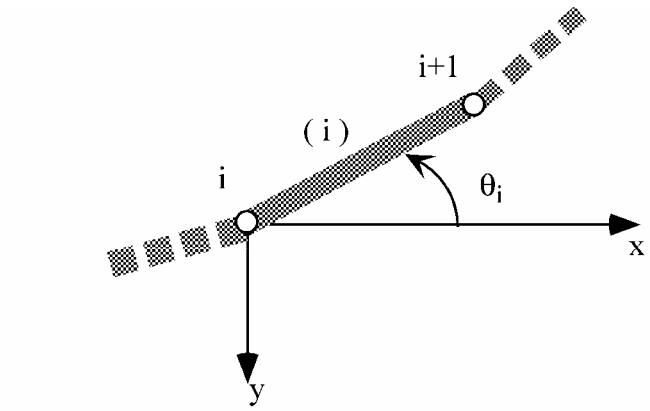

Fig. 3-8. The i-th member and its directional angle θ_i.

As the result of the weight increase during the k-th growth step, the bending moment in the i-th member increases by

$$\Delta M_i^{(k)}(\eta_i) = -\frac{1}{2}\Delta\omega_i^{(k)}(\eta_i - l_i)^2 + \Delta p_{i+1}^{(k)}(\eta_i - l_i)\cos\theta_i + \Delta M_{i+1}^{\circ(k)} + \Delta M_i^{s(k)},$$

$$(\ i = 0, 1, 2,- - -, k) \qquad (3\text{-}15)$$

where η_i is the distance from the i-th node to an arbitrary point in the i-th member. $\Delta M_{i+1}{}^{o(k)}$ is an increment of the nodal moment at the (i+1)-th node, and $\Delta M_i^{s(k)}$ is an internal bending moment which is generated in the i-th member during the k-th growth step. The growth stress is distributed peripherally in the newly formed secondary xylem, which induces the internal bending moment $\Delta M_i^{s(k)}$ in each member. $\Delta M_i^{s(k)}$ is calculated from the peripheral distribution of the growth stress generated in the thickening zone in each member as discussed later.

By assuming $\eta_i = 0$ in eq.(3-15), we obtain the following recurrence equation

$$\Delta M_i^{\circ(k)} = -\frac{1}{2}\Delta\omega_i^{(k)} l_i^2 - \Delta p_{i+1}^{(k)} l_i \cos\theta_i + \Delta M_i^{s(k)} + \Delta M_{i+1}^{\circ(k)}. \quad (i = 0, 1, 2, - - -, k) \quad (3\text{-}16)$$

Considering that $\Delta M_{k+1}{}^{o(k)} = 0$, eq.(3-16) can be solved as

$$\Delta M_i^{\circ(k)} = -\sum_{j=i}^{k}\left(\frac{1}{2}\Delta\omega_j^{(k)} l_j^2 + \Delta p_{j+1}^{(k)} l_j \cos\theta_j - \Delta M_j^{s(k)}\right) . \quad (3\text{-}17)$$

This equation leads to an increment of the nodal moment at the i-th node during the k-th growth step.

Coordinates of each node just after completion of the k-th growth step:

In the i-th member just before starting the k-th growth step, we measured the distance η_i from the i-th node toward the (i+1)-th node along the central axis. A cartesian coordinate system O-$\eta_i\gamma_i$ is introduced, as shown in Fig.3-9. The i-th member is deflected by the weight increase during the k-th growth step. We adopt the differential equation describing the deflection $\gamma_i(\eta_i)$ as

$$\frac{d^2\gamma_i^{(k)}}{d\eta_i^2} = -\frac{\Delta M_i^{(k)}(\eta_i)}{E \cdot I_i^{(k)}}, \quad (3\text{-}18)$$

where $I_i^{(k)}$ is the moment of inertia of the cross section of the i-th member, that is,

$$I_i^{(k)} = \frac{\pi}{4}\{r_0 + (k - i)\Delta r\}^4 \quad .$$

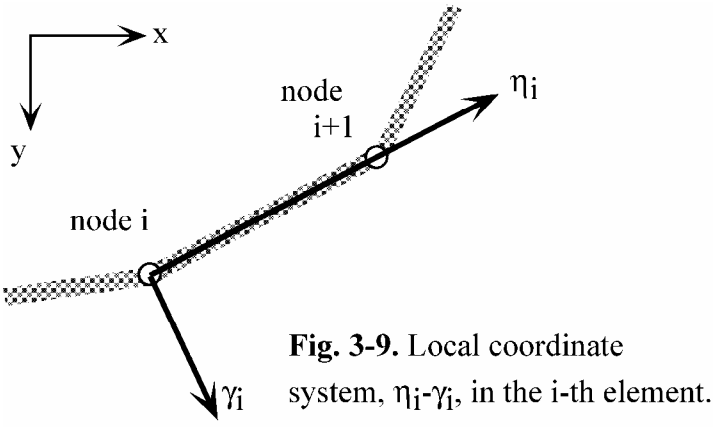

Fig. 3-9. Local coordinate system, η_i-γ_i, in the i-th element.

We introduce the following conditions to solve eq.(3-18):

$$\left.\frac{d\gamma_i^{(k)}}{d\eta_i}\right|_{\eta_i=l_i} = \alpha_i^{(k)}, \qquad \left.\frac{d\gamma_i^{(k)}}{d\eta_i}\right|_{\eta_i=0} = \beta_i^{(k)}, \qquad \left.\gamma_i^{(k)}\right|_{\eta_i=l_i} = C_i^{(k)}, \tag{3-19}$$

where $C_i^{(k)}$ is the displacement of the (i+1)-th node to the direction of γ_i-axis. The coordinates of the (i+1)-th node just after completion of the k-th growth step may be calculated as

$$\left(l_i^{(k-1)}, C_i^{(k)}\right), \tag{3-20}$$

in the O-$\eta_i\gamma_i$ coordinate system. In the O-xy coordinate system, as introduced in Fig.3-6, this point is expressed as

$$\left(m_{i+1}^{(k)}, n_{i+1}^{(k)}\right). \tag{3-21}$$

These two coordinates are related by the following transformation rule:

$$\begin{bmatrix} m_{i+1}^{(k)} \\ n_{i+1}^{(k)} \end{bmatrix} = \begin{bmatrix} \cos\theta_i^{(k-1)} & \sin\theta_i^{(k-1)} \\ -\sin\theta_i^{(k-1)} & \cos\theta_i^{(k-1)} \end{bmatrix} \begin{bmatrix} l_i^{(k-1)} \\ C_i^{(k)} \end{bmatrix} + \begin{bmatrix} m_i^{(k)} \\ m_i^{(k)} \end{bmatrix}. \tag{3-22}$$

This recurrence equation can be solved as follows:

$$\begin{bmatrix} m_i^{(k)} \\ n_i^{(k)} \end{bmatrix} = \sum_{j=0}^{i-1} \begin{bmatrix} \cos\theta_j^{(k-1)} & \sin\theta_j^{(k-1)} \\ -\sin\theta_j^{(k-1)} & \cos\theta_j^{(k-1)} \end{bmatrix} \begin{bmatrix} l_j^{(k-1)} \\ C_j^{(k)} \end{bmatrix} + \begin{bmatrix} m_0^{(k)} \\ m_0^{(k)} \end{bmatrix}, \quad (i = 1,\ 2, - - - , k+1) \tag{3-23}$$

provided that the following condition exists:

$$\begin{bmatrix} m_0^{(k)} \\ n_0^{(k)} \end{bmatrix} = \begin{bmatrix} 0 \\ 0 \end{bmatrix}.$$

Eq.(3-23) gives the xy-coordinates of the i-th node just after completion of the k-th growth step. Ultimately, we must solve for $\alpha_i^{(k)}$ and $C_i^{(k)}$ in eq.(3-19). According to assumption 1, the angle between neighboring members is invariant during each growth step. When assumption 1 is applied to eqs.(3-18,19), the following relationship is obtained:

$$\beta_i^{(k)} = \alpha_{i-1}^{(k)} . \tag{3-24}$$

From eqs.(3-18,19, 24), the following recurrence equation is obtained.

$$\alpha_i^{(k)} - \alpha_{i-1}^{(k)} = \frac{\Delta\omega_i^{(k)} l_i^3}{6EI_i^{(k)}} + \frac{\Delta p_{i+1}^{(k)} l_i^2}{2EI_i^{(k)}} \cos\theta_i - \frac{\Delta M_{i+1}^{\circ(k)}}{EI_i^{(k)}} l_i - \frac{\Delta M_i^{s(k)}}{EI_i^{(k)}} l_i \quad . \tag{3-25}$$

Moreover, the following equation is obtained from eq.(3-18),

$$\alpha_0^{(k)} = \frac{\Delta\omega_0^{(k)}}{6EI_0^{(k)}} l_0^3 + \frac{\Delta p_1^{(k)} \cos\theta_0}{2EI_0^{(k)}} l_0^2 - \frac{\Delta M_1^{\circ(k)}}{EI_0^{(k)}} l_0 - \frac{\Delta M_0^{s(k)}}{EI_0^{(k)}} l_0 ,$$

provided that the condition, $d\gamma_0^{(k)}/d\eta_0 = 0$ at $\eta_0=0$, was used to derive the equation above. Finally, the following solution is obtained from eq.(3-25).

$$\alpha_i^{(k)} = \sum_{j=0}^{i} \left(\frac{\Delta\omega_j^{(k)} l_j^3}{6EI_j^{(k)}} + \frac{\Delta p_{j+1}^{(k)} l_j^2}{2EI_j^{(k)}} \cos\theta_j - \frac{\Delta M_{j+1}^{\circ(k)}}{EI_j^{(k)}} l_j - \frac{\Delta M_j^{s(k)}}{EI_j^{(k)}} l_j \right).$$

(i = 0, 1, 2, - - - - , k) (3-26)

From the solution of eq.(3-18) and the conditions (3-19), we obtain

$$C_i^{(k)} = -\frac{\Delta\omega_i^{(k)} l_i^4}{24EI_i^{(k)}} - \frac{\Delta p_{i+1}^{(k)} l_i^3}{6EI_i^{(k)}} \cos\theta_i + \frac{\Delta M_{i+1}^{\circ(k)}}{2EI_i^{(k)}} l_i^2 + \frac{\Delta M_i^{s(k)}}{2EI_i^{(k)}} l_i^2 + \alpha_i^{(k)} l_i .$$

(i = 0, 1, 2, - - - - , k) (3-27)

For each growth step, we calculate $\Delta p_i^{(k)}$ by using eqs.(3-10,11,12), and calculate $\Delta\omega_i^{(k)}$ by using eqs.(3-13,14), and calculate $\Delta M_i^{o(k)}$ by using eq.(3-17). We calculate $C_i^{(k)}$ by using eqs.(3-25,26). Thus, from eq.(3-23), we obtain the coordinates of the i-th node just after completing the k-th growth step, ($m_i^{(k)}$, $n_i^{(k)}$). Connecting those coordinates from i = 0 to i = k+1, we can obtain the skeleton form of the stem just after completing the k-th growth step.

3-2-3 Determination of parameters

(a) Characteristics of the branches of tree species

Materials:

In the present study, the stem shapes of the branches listed below were simulated. Characteristics of the individual branches were recorded in advance of the simulations. Apparently healthy, smoothly shaped branches were selected, while those having higher-ordered long shoots or color-changed leaves were avoided. Similarly, branches with an arc deviating from the vertical plane were also avoided.

Sampling and measurements were performed in early September, except for a *Prunus spachiana* branch, which had already shed its leaves. Materials tested included:

1. A 4-year-old-, sinusoidally-shaped, weeping branch of *Magnolia kobus* DC
2. A 5-year-old, hyponastic branch of *Juniperus chinensis* L.
3. A 9-year-old, hyponastic branch of *Abies saccharinensis* Fr. Schum.
4. A 1-year-old, epinastic branch of *Prunus spachiana* Kitamura f. spachiana cv. Plenarosea.

The stem shapes of these materials in the vertical plane are shown in Figs.3-12 and 3-13. The trees from which the materials were sampled were growing on the Furo campus of Nagoya University, and were individual specimens.

Items measured:

The living branches were photographed in natural light with a yardstick reference prior to sampling, to provide an accurate tracing of the stem shapes in the vertical plane from the pictures. Immediately after sampling, the branch stems were divided into small bolts of 10~to approx.20 cm in length. For every bolt, the arc length from the shoot apex to the bottom end (s), the diameter at the bottom end (D), the weight of living leaves and short shoots (H), the specific weight of the stem (ρ), and the longitudinal elastic modulus of the stem (E) were measured in the laboratory.

Determination of the values of Δl, Δr, and r_0 :

The D-s relationship of each sample is shown in Fig.3-10 for four material species. Every case can be approximated by the linear regression,

$$D = \xi \cdot s + \zeta \tag{3-28}$$

as follows:

a *M. kobus* branch: $D = 0.00420s + 0.309$ ($r = 0.971$**)

a *J. chinensis* branch: $D = 0.00961s + 0.251$ ($r = 0.967$**)

an *A. saccharinensis* branch: $D = 0.00897s + 0.413$ ($r = 0.975$**)

a *P. spachiana* branch: $D = 0.00852s + 0.226$ ($r = 0.977$**)

(units; cm for D and s)

In the stem model, just after completion of the k-th growth step, the relationship between the diameter at the bottom end of the i-th member (D_i) and the arc length from the shoot apex to the bottom end of the i-th member (s_i) is given by

$$D_i = 2\{r_0 + (k - i)\Delta r\} = 2\{(k - i + 1)\Delta r + r_0 - \Delta r\} \cong 2\left(\frac{\Delta r}{\Delta l}\right)s_i + 2(r_0 - \Delta r) \qquad (3\text{-}29)$$

provided that Δl, r_0, and Δr are assumed to be constant. From the comparison between eqs.(3-28,29), Δr and r_0 must satisfy

$$\Delta r = \frac{1}{2}\xi \cdot \Delta l \ , \quad r_0 = \frac{1}{2}\xi \cdot \Delta l + \frac{\zeta}{2} \ . \qquad (3\text{-}30)$$

Only Δl is unknown in eqs.(3-30). At the current time, there is no way to suppose an arbitrary value for Δl. In this simulation, we supposed Δl = 5 cm, regardless of tree species. Thus, we can calculate the values of Δr and r_0 that should be used for the simulations, as follows:

a *M. kobus* branch : $r_0 = 0.165$ cm, $\Delta r = 0.0105$ cm,

a *J. chinensis* branch: $r_0 = 0.150$ cm, $\Delta r = 0.0241$ cm,

an *A. saccharinensis* branch: $r_0 = 0.229$ cm, $\Delta r = 0.0224$ cm,

a *P. spachiana* branch: $r_0 = 0.134$ cm, $\Delta r = 0.0213$ cm.

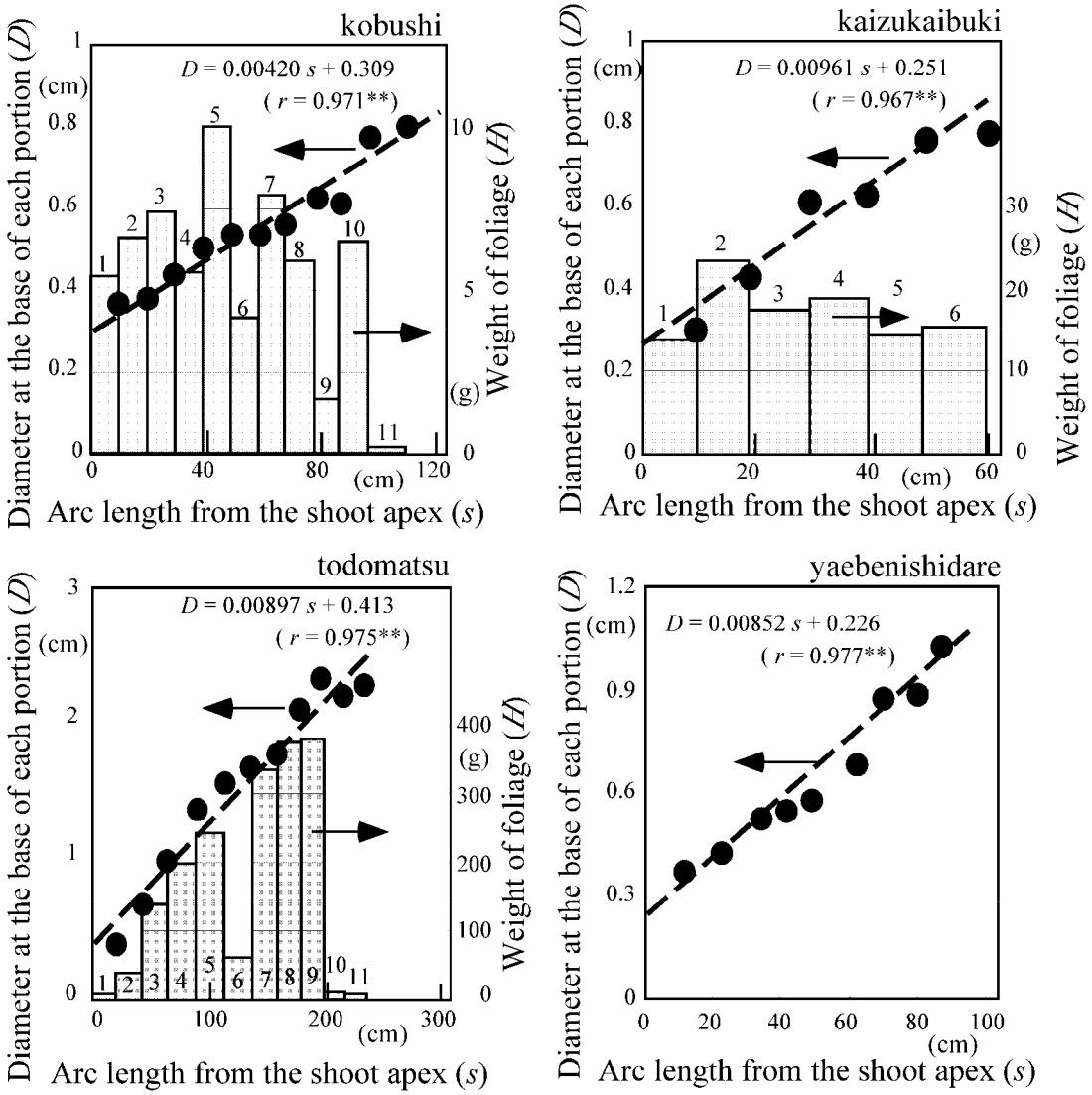

Fig. 3-10. Diameter and foliage distributions along the branch stem.
Note: Numbers in each figure identify the divided bolts in each sampled branch stem.

Determination of the values of $\Delta h_i^{(k)}$, $h_{k+1}^{(k)}$:

In Fig.3-10, the *H*-*s* relationships are shown for three tree species. In the *J. chinensis* branch, the foliage is produced homogeneously in the longitudinal direction. In the *M. kobus* branch, the distribution of the foliage is rather irregular compared to the *J. chinensis* branch, but it can be regarded as homogeneous enough in practice. In the *A. saccharinensis* branch, the amount of foliage appears to increase linearly with increasing *s*, since the higher-ordered branches hanging from the main axis (main branch) grow thicker with increased *s*.

From these observations, it can be said that $h_{k+1}^{(k)}$ takes a constant value for every

species regardless of the value of k, and that $\Delta h_i^{(k)}$ takes a null value for the *J. chinensis* and *M. kobus* branches, but takes a non-zero constant value for the *A. saccharinensis* branch. When simulating the growing process of the branch stem for each species, we gave concrete values to $h_{k+1}^{(k)}$ and $\Delta h_i^{(k)}$ in order to regenerate the observed *H-s* relationships.

It was impossible to measure the weight of the foliage produced by the stem of the *P. spachiana* branch, as it was sampled after defoliation. When foliated, the foliage is distributed homogeneously along the central axis of the stem, similar to that on a *M. kobus* branch. In the case of the *P. spachiana* branch, it is assumed that $h_{k+1}^{(k)}$ takes a constant value, and that $\Delta h_i^{(k)}$ is null for any k.

Preferred angle of the elongation zone:

It is difficult to measure the preferred angle of the elongation zone as well as proving its existence. If a certain value is required for θ_C in order to re-create the shape of the branch stem, it can be considered that such a stem had a preferred angle θ_C. On the contrary, if the relation of $\theta_k^{(k-1)}=\theta_{k-1}^{(k-1)}$ is always required for every k, we can propose that the elongation zone has no specific directional angle during branch growth.

(b) Recovery moment generated in the thickening zone

When simulating branch growth, it is necessary to assign a concrete value to $\Delta M_i^{s(k)}$ in advance. As displayed in Fig.3-11, the γ-ζ Cartesian coordinate system and the *r*-ϕ polar coordinate system are introduced in the cross-section of the i-th member just before starting the k-th growth step. $\Delta M_i^{s(k)}$ is calculated by the following equation,

$$\Delta M_i^{s(k)} = -\int_{\Delta A} \sigma_i^{(k)}(r,\varphi,\theta_i) r^2 \cos\varphi \, dr d\varphi \quad , \tag{3-31}$$

where $\sigma_i^{(k)}$ is the longitudinal growth stress generated in the thickening zone of the i-th member (ΔA) during the k-th growth step, provided that $\sigma_i^{(k)}$ is assumed to be independent of the position (η_i) of the individual member. Of course, θ_i means $\theta_i^{(k-1)}$.

To calculate eq.3-31, we needed to measure the functional shape of $\sigma_i^{(k)}$ as precisely as possible. However, it was practically impossible to measure the peripheral distributions of the growth stresses in the material branches, as their diameters were too thin to facilitate measurement by the usual strain-gauge method (Okuyama et al. 1981, 1983). Consequently, we presumed that the functional shape of $\sigma_i^{(k)}$ would be similar to that previously described and useful for calculating the value of $\Delta M_i^{s(k)}$.

The following assumptions were used to calculate the functional shapes of $\sigma_i^{(k)}$:

i) $\sigma_i^{(k)}$ is generated in the newly-formed secondary xylem during secondary cell wall maturation, and remains in the secondary xylem of the stem.

ii) The reaction wood tissue is formed on the upper or lower side in the inclined stem. $\sigma_i^{(k)}$ shows a peak there, and its magnitude tends to become larger with any increase in the inclination of the stem.

iii) $\sigma_i^{(k)}$ is independent of r, therefore, $\sigma_i^{(k)}$ is a function of φ and θ_i. Then, $\sigma_i^{(k)} = f(\varphi, \theta_i)$.

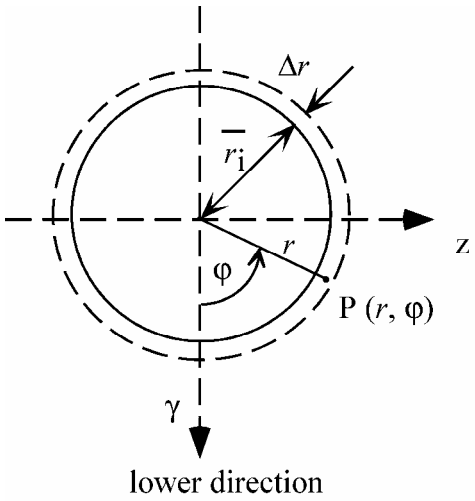

Fig. 3-11. Cross section of the i-th member, and the polar coordinate system, r-φ.

The propriety of assumption i) is based on several publications on the relationship between growth stresses and xylem formation in trees (Archer and Byrnes 1974; Okuyama and Kikata 1975; Fournier et al. 1990). Assumption ii) is based on recent experiments by several researchers (Wilson and Gartner 1996; Yoshida et al. 2000), who investigated the relationships between growth stress, reaction wood tissue formation and stem inclination by using an inclined juvenile trunk or a mature branch. Assumption iii) postulates that the magnitude of growth stress is not affected by the stem diameter and/or the rate of thickening. This assumption has already been verified for a vertically growing trunk (Wahyudi et al. 1999, 2000), but its applicability to inclined stems or branches is unknown.

The following sinusoidal curve is described as $\sigma_i^{(k)}$ [$= f(\varphi, \theta_i)$].

$$\begin{aligned}\sigma_i^{(k)} &= f(\varphi, \theta_i) \\ &= \sigma_0\{1+\sin(\theta_i-\theta_P)\} - \frac{1}{2}(M_1+m_1)\sin(\theta_i-\theta_P) + \frac{1}{2}(M_1-m_1)\sin(\theta_i-\theta_P)\cos\varphi\end{aligned} \tag{3-32}$$

where σ_0 in eq.(3-32) is a constant and θ_P is the preferred angle in the lignified stem. For the time being, it is assumed that θ_P is constant during branch growth, and is independent of the

position on the stem. If it were assumed that $\theta_i = \theta_P - \pi/2$, the longitudinal growth stress would become M_1 on the uppermost side ($\varphi=\pi, -\pi$) of the i-th member, and m_1 on the lowermost side ($\varphi = 0$). Therefore, $M_1 - m_1$ is the maximum difference between the growth stresses of the uppermost and lowermost sides of the branch stem. When Δr is sufficiently small, eq.3-31 can be expressed as follows:

$$\Delta M_i^{s(k)} \cong \bar{r}_i^2 \cdot \Delta r \int_{-\pi/2}^{\pi/2} f(\varphi, \theta_i) \cos\varphi \, d\varphi \,, \tag{3-33}$$

where r_i^- is calculated by

$$\bar{r}_i = r_0 + (k - i - 1)\Delta r . (i = 0, 1, 2, \cdots, k - 1)$$

By substituting eqs.(3-32,33), we obtain the recovery moment $M_i^{s(k)}$ by

$$\Delta M_i^{s(k)} = \frac{1}{2}\bar{r}_i^2 \cdot \pi \cdot \Delta r \cdot (M_i - m_i) \cdot \cos\left(\theta_i - \theta_P + \frac{\pi}{2}\right)$$

$$= -\frac{1}{2}\bar{r}_i^2 \cdot \pi \cdot \Delta r \cdot (M_i - m_i) \cdot \sin(\theta_i - \theta_P) \quad . \tag{3-34}$$

This formula postulates that the recovery moment $\Delta M_i^{s(k)}$, which returns the member from a position of deviation to equilibrium, is generated in each member as in the case of $\theta_i = \theta_P$.

3-2-4 Simulated results

(a) Simulation 1 (Fig.3-12)

In simulation 1, the general roles of $M_1 - m_1$ and θ_C in the generation of the negative gravitropic movement of a woody plant stem were examined to determine whether negative gravitropic movement could be caused by factors other than the generation of a large growth stress.

The conditions described in Table 3-2(a) were used for the simulation. The values applied to E, ρ, Δr, and r_0 were those of a 1-year-old branch of *P. spachiana*, when the value of Δl was assigned as 5 cm. The observed value of θ_0 was 0 degrees in the *P. spachiana* branch stem; however, a value of 30 degrees was used for θ_0 in the simulation. According to the authors' previous studies, almost no reaction wood tissue is formed in the vertical part of a crooked tree trunk, where the peripheral distribution of the longitudinal growth stress becomes evenly distributed (Yamamoto et al. 1991; Okuyama and Yamamoto 1992). In those studies, a value of 90 degrees was used for θ_P. The values of $\Delta h_i^{(k)}$ and $h_{k+1}^{(k)}$ were also

hypothesized.

Table 3-2(a). Conditions for simulation 1.

	Condition 1-A	Condition 1-B	Condition 1-C
E	48×10^3 kgf/cm^2	48×10^3kgf/cm^2	48×10^3kgf/cm^2
ρ	0.82 gf/cm^3	0.82 gf/cm^3	0.82 gf/cm^3
r_0	0.134 cm	0.134 cm	0.134 cm
Δr	0.0213 cm	0.0213 cm	0.0213 cm
Δl	5 cm	5 cm	5 cm
$\Delta h_i^{(k)}$	0 gf	0 gf	0 gf
$h_{k+1}^{(k)}$	3 gf	3 gf	3gf
θ_0	30 deg	30 deg	30 deg
θ_C	---- deg	30 deg	---- deg
θ_P	90 deg	90 deg	90 deg
M_1-m_1	0 kgf/cm^2	0 kgf/cm^2	0, 8, 16, 24 kgf/cm^2
N	10, 40, 80	10, 40, 80	20

Number of the growth step N (Condition 1-A):

Two conditions were assumed: $M_1 - m_1 = 0$; and $\theta_k^{(k-1)} = \theta_{k-1}^{(k-1)}$ at the k-th growth step. The first assumption means that there is no difference in the growth stresses between the uppermost and the lowermost sides of the inclined stem. The second supposes that the elongation zone has no specific directional angle when it appears at the shoot apex.

As the branch stem grew from the early stage ($N = 10$) to the middle ($N = 40$) or late ($N = 80$) stages, the woody stem gradually began to weep downward due to the increased weight of the biomass.

Preferred angle of the elongation zone (Condition 1-B):

To determine the preferred angle of the elongation zone, we assumed that $\theta_k^{(k-1)}=\theta_C$ at the k-th growth step, and that $M_1 - m_1 = 0$. Some researchers think that the inclined woody stem can continue growing upward if the elongation zone has an upward preferred angle (Castera and Morlier 1991). According to our model, the inclined woody stem would grow upward during the early growth stage ($N = 10$) even though $M_1 - m_1 = 0$. As the shoot growth progressed in the model, the new tissue elongated laterally, showing a characteristic sinusoidal shape ($N = 40$,

80); this shape can be observed in the mature branches of maritime pine (*Pinus mariana*), as described by Castera and Morlier (1991), who indicated the importance of the preferred angle in the elongation zone in controlling the shape of the branch stem. With prolonged growth, however, the branch eventually hung downwards.

Growth stress generated in the reaction wood region (Condition 1-C):

To examine growth stress in the reaction wood region, we assigned various values to $M_1 - m_1$, while supposing that the elongation zone had no specific directional angle when it appeared at the shoot apex. When $M_1 - m_1 = 0$, the woody stem did not generate a negative gravitropic movement, and the stem shape became epinastic, as demonstrated by the *P. spachiana* branch. With increasing values for $M_1 - m_1$, the woody stem grew upward, and became hyponastic. The results suggest that it is reasonable to propose that the large growth stress generated in the reaction wood region causes the negative gravitropic movement in an inclined woody stem.

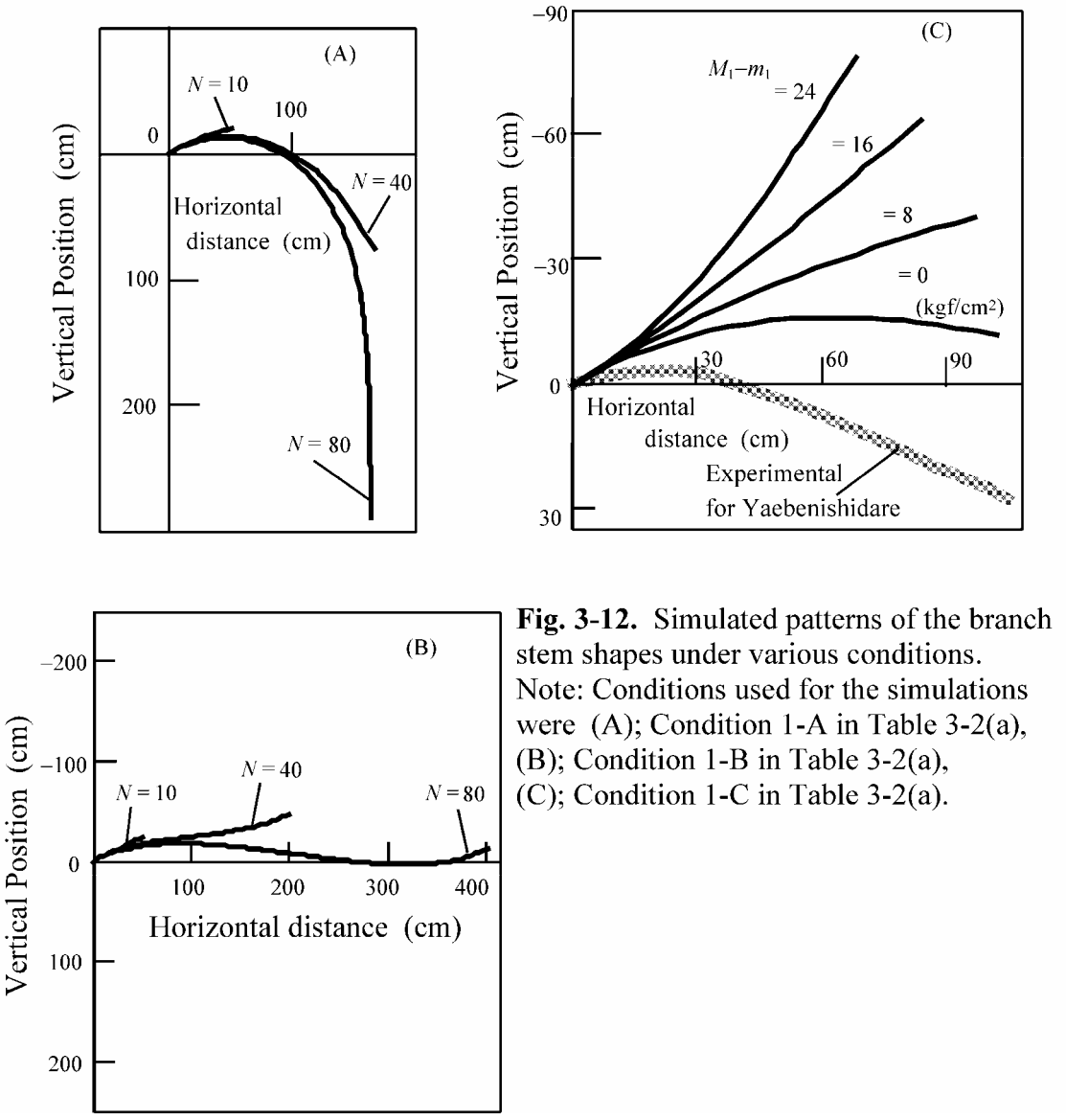

Fig. 3-12. Simulated patterns of the branch stem shapes under various conditions.
Note: Conditions used for the simulations were (A); Condition 1-A in Table 3-2(a), (B); Condition 1-B in Table 3-2(a), (C); Condition 1-C in Table 3-2(a).

(b) Simulation 2 (Fig. 3-13)

Conditions 2-A, 2-B, and 2-C in Table 3-2(b) were extracted, respectively, from a 4-year-old branch of *M. kobus*, a 5-year-old branch of *J. chinensis*, and a 9-year-old branch of *A. saccharinensis*. The values applied to Δr, r_0, $\Delta h_i^{(k)}$, and $h_{k+1}^{(k)}$ were estimated from each branch in order to explain the *D-s* and *H-s* relationships shown in Fig.3-10, when the value of Δl was set at 5 cm. The values applied to E and ρ were those of each branch. As in Simulation 1, θ_P was set at 90 degrees.

Table 3-2(b). Conditions for simulation 2.

	Condition 2-A	Condition 2-B	Condition 2-C
E	6.9×10^3 kgf/cm^2	30×10^3 kgf/cm^2	57×10^3 kgf/cm^2
ρ	0.75 gf/cm^3	0.94 gf/cm^3	0.72 gf/cm^3
r_0	0.165 cm	0.150 cm	0.229 cm
Δr	0.0105 cm	0.0241 cm	0.0224 cm
Δl	5 cm	5 cm	5 cm
$\Delta h_i^{(k)}$	0 gf	0 gf	2.598 gf
$h_{k+1}^{(k)}$	2.76 gf	8.62 gf	2.598 gf
θ_0	0 deg	0 deg	-40 deg
θ_C	0 deg	---- deg	---- deg
θ_P	90 deg	90 deg	90 deg
M_1-m_1	0,12,24,36 kgf/cm^2	0,28,56,84 kgf/cm^2	0,14,28,42 kgf/cm^2
N	21	11	46

A 4-year-old branch of M. kobus (Condition 2-A):

In this simulation, it was assumed that θ_C= 0 deg. This describes an elongation zone at the shoot apex with a horizontal directional angle. The actual material branch, however, hung downward, with a sinusoidal shape. The best-fitting simulation was obtained by assuming M_1-m_1= 12 kgf/cm^2. When larger values were assumed for M_1-m_1, the branch stem tended to rise with the characteristic sinusoidal curve. The result suggests that the growth stress difference (M_1-m_1) was not sufficient to generate the negative gravitropism in the *M. kobus* branch.

A *5-year-old branch of J. chinensis (Condition 2-B):*

In this case, it was assumed that the elongation zone had no preferred angle. The actual *J. chinensis* branch was hyponastic, and was elongated in an obliquely upward fashion. The best-fitting simulation was obtained by assuming M_1-m_1=56 kgf/cm^2. When smaller values ranging from 0 to 28 kgf/cm^2 were assigned to M_1-m_1, the branch stem would not rise above the horizontal axis, and the stem shapes became epinastic.

A 9-year-old branch of A. saccharinensis (Condition 2-C):

Similarly, it was assumed that the elongation zone had no preferred angle. The actual *A.*

saccharinensis branch tended to extend obliquely downward near the base, and it was bent upward near the apex, tracing a circular arc. The actual stem shape was best fitted by assuming M_1-m_1= 28 kgf/cm^2. As with the *J. chinensis* branch, smaller values of 0 to 14 kgf/cm^2 assigned to M_1-m_1 resulted in a branch stem that was incapable of generating negative gravitropism, hung downwards, and became epinastic.

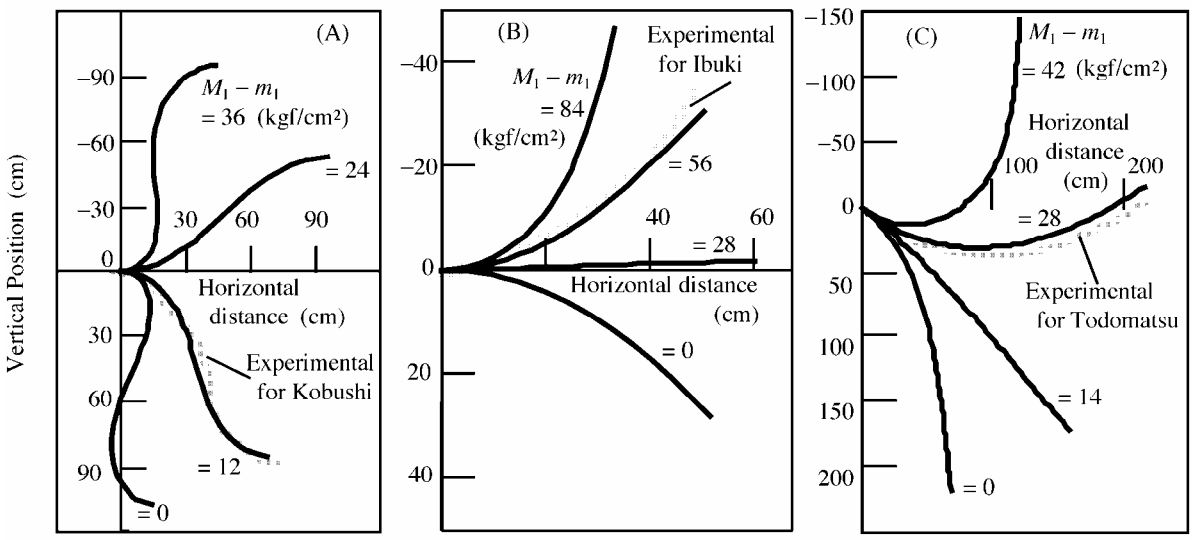

Fig. 3-13. Simulated patterns of the branch stem shapes for tested three species.
Note: Conditions used for the simulations were
(A); Condition 2-A in Table 3-2, (B); Condition 2-B in Table 3-2,
(C); Condition 2-C in Table 3-2.

3-2-5 Discussion

(a) The role of growth stress generation in negative gravitropic movement in woody plant shoots

In this study, we analyzed the growth behavior of woody plant shoots using a structural mechanics model, and compared living samples to simulations of anticipated, time-dependent spatial change in inclined trunk or branch stems. Consequently, our interest became more sharply focused on the preferred angle of the elongation zone and growth stress generation in the reaction wood region.

Simulations 1-(B) and 2-(A) failed to show a positive correlation between the preferred angle of the elongation zone and generation of a negative gravitropism response in woody plant stems. As stem rigidity (*EI*) increased, the degree of weeping was more or less reduced,

yet such a property would not independently cause negative gravitropic movement. When an appropriate value was chosen for $M_l - m_l$, however, the negative gravitropic movement of the inclined woody stem could be simulated quantitatively, as shown in Simulations 1-(C), 2-(B), and 2-(C). These results show that the large growth stress generated in the reaction-wood region positively correlates with the observed negative gravitropic movement of the woody plant shoot. The simulations that best fitted the natural plant materials collected were calculated when $M_l - m_l$=56 kgf/cm^2 for a 5-year-old branch of *J. chinensis* [Simulation 2-(B)], and $M_l - m_l$= 28 kgf/cm^2 for a 9-year-old branch of *A. saccharinensis* [Simulation 2-(C)].

Recently, Okuyama and his associates have offered corrected data on the peripheral distribution of growth stresses in the secondary xylem of an inclined stem. From their results, we calculated the difference between the growth stresses on the uppermost and lowermost sides of each inclined stem as follows:

a) Inclined part of a mature trunk (Okuyama et al. 1983, 1990, 1994).

A very crooked, 31-year-old sugi (*Cryptomeria japonica* D. Don.), 20 cm in diameter at breast height. Growth stress difference: 120 kgf/cm^2.

A slightly inclined, 42-year-old *Acer mono* Sieb. et Zucc., 12 cm in diameter at breast height. Growth stress difference: 186 kgf/cm^2.

Three slightly inclined, 51-year-old Yellow poplars (*Liriodendron tulipifera* L.), 28 - 30 cm in diameter at breast height. Growth stress differences: 167, 206, 362 kgf/cm^2.

b) Basal part of a mature branch (Yoshida et al. 1992b).

A 14-year-old *Chamaecyparis obtusa* Endl., inclination angle 80 degrees to the vertical, 6 cm in diameter at the base. Growth stress difference: 127 - 290 kgf/cm^2.

A eucalyptus (*Eucalyptus grandis* L.) of unknown age, inclination angle 55 degrees to the vertical, 8 cm in diameter at the base. Growth stress difference: 107 - 382 kgf/cm^2.

The predicted values of $M_l - m_l$ for the behaviors of the *J. chinensis* and the *A. saccharinensis* branches seem to be considerably smaller than those measured from the trunks or branches described above. We offer the following explanation:

From Eqs.(3-23,24,25,26), we derive the following equation:

$$\Delta\left(\frac{1}{\rho_i^{s(k)}}\right) \equiv \frac{\Delta M_i^{s(k)}}{E \cdot I_i^{(k)}} \cong -\frac{2}{\bar{r}_i^2 E}\Delta r \cdot \left(M_l - m_l\right) \cdot \sin\left(\theta_i - \theta_P\right) \quad , \tag{3-35}$$

where $\Delta(1/\rho_i^{s(k)})$ is the increment of the curvature induced in the neutral axis of the i-th member

at the k-th growth step by the generated recovery moment $\Delta M_i^{s(k)}$. In order to compensate for weeping due to the increasing weight of the shoot, $\Delta(1/\rho_i^{s(k)})$ must be kept constant or more throughout secondary growth. Likewise, $(M_1-m_1)/r_i^2$ must be kept at least constant or more. Thus, a larger value would be required for M_1-m_1 as thickening progressed, resulting in an increase of r_i. The diameter of each sampled branch stem was smaller than that of a trunk or mature branch. We suspect that a lower value of M_1-m_1 is sufficient to generate the negative gravitropic movement in thin stems.

(b) The role of the specific directional angle (preferred angle) in the elongation zone in determining the spatial shape of a branch stem

The results do not support a positive correlation between the specific directional angle (preferred angle) in the elongation zone and negative gravitropic behavior in woody plant shoots. Nevertheless, by assuming a suitable value for the preferred angle of the elongation zone, Simulation 2-(A) explained the sinusoidal stem shape of a weeping *M. kobus* branch. Moreover, by assuming that the elongation zone of a branch stem had no preferred angle when it appeared at the shoot apex, a quantitative explanation for the hyponastic stem shapes of the *J. chinensis* and the *A. saccharinensis* branches could be made.

The results of Simulations 1-(C) and 2-(B) suggest that the epinastic shapes of woody branch stems are induced by a balance between the weeping due to increased shoot weight and the recovery moment caused by the unevenly distributed growth stress. The presence of a preferred angle may be species- or individual-specific.

(c) Tropic behavior of the elongation zone

The elongation zone in a woody plant shoot is histologically similar to that of a mature herbaceous shoot, and consists of primary tissues; its gravitropic movement is controlled by differential growth on the upper and lower sides of the inclined shoot (Silk 1984; Mueller et al. 1984; Cosgrove 1997), or by asymmetric tissue stresses occurring in the turgid herbaceous stem, as discussed by Hejnowicz and Sievers (1996), and Hejnowicz (1997).

In either case, a particular angle of the elongation zone could be predicted by a distribution of curvature, which is produced by the differential growth pattern distributed over the elongating shoot. When analyzing the kinematics of plant development, we need to distinguish properties associated with spatial regions from those associated with the plant elements which move through the regions during the plant development (see the formulation

by Silk 1984).

Researchers have used terms such as *plagio-gravitropism* or *diagravitropism* to explain the origin of the preferred angle of the axilliary axis (branch stem) in the higher plant-shoot, and some have considered the properties of the behaviors to be intrinsic to such organs (see Timell 1986). Others attribute this behavior to the balance between the forces of negative- and positive-orthogravitropism (Rufelt 1962), or to the balance between negative gravitropism and epinasty (Palmer 1985). Our observations show that the elongation zone of a mature woody branch often grows vertically as it emerges from the dim and crowded crown into the sunlight. Further evidence supporting an important role for the emerging elongation zone comes from the well-documented fact that apical dominance is controlled by the apical tissues, and that their removal stimulates axillary growth. The demonstration of a preferred angle of elongation may well arise from the concerted effects of negative gravitropism, phototropism, and response to plant growth hormones, such as auxins.

3-2-6 Summary and concluding remarks

In this section, beam theory (structural mechanics) was used to describe the negative (plagio-) gravitropic behavior of woody plant stems. Through simulating the observable shapes of various tree branches, the following conclusions were deduced.

1. Growth stress is generated in the secondary xylem of woody plant stems. In reaction wood tissue, growth stress is sufficiently large as to bend the leaning shoot upward against the weeping caused by increasing weight, and thus is responsible for the negative gravitropic movement of the inclined woody stem.
2. The specific directional angle of the shoot apex (preferred angle of the elongation zone) plays an important role in controlling the spatial shape of branch stems that is peculiar to different species, for example, the sinusoidal shapes of the *M. kobus* branch presented in this study and the maritime pine branch studied by Castera and Morlier (1992).

The interactive effect between the large growth stress generated in reaction wood tissue and the preferred angle in the elongation zone controls the time-dependent morphogenesis of the woody plant shoot.

References in Chapter 3

Archer, R.R.: "Growth stresses and strains in trees," Springer-Verlag, Berlin, 1987.

Archer, R.R., Wilson, B.F.: Mechanics of the compression wood response. I. Preliminary analysis, *Plant. Physiol*., **46**, 550-556 (1970).

Archer, R.R., Wilson, B.F.: Mechanics of the compression wood response. II. On the location, action, and distribution of compression wood formation, *Plant Physiol*. **46**, 550-556 (1973).

Archer, R.R., Byrnes, F.E.: On the distribution of growth stresses. Part 1: an anisotropic plane strain theory, *Wood Sci. Technol.*, **8**, 184-196 (1974).

Archer, R.R., Wilson, B.F.: Apical control of branch movements in white pine. Compression wood action, *Wood Sci. Technol.,* **16**, 181-191 (1982).

Bamber, R.K.: The origin of growth stresses, In: Proceedings of the IUFRO Conference, Laguna, Philippines, contributed paper, pp 1-7 (1978).

Bamber, R.K.: A general theory for the origin of growth stresses in reaction wood: How trees stay upright, IAWA J., **22**, 205-212 (2001).

Barber, N.F., Meylan, B.A.: The anisotropic shrinkage of wood. A theoretical model. *Holzforschung*, **18**, 146-156 (1964).

Boyd, J.D.: Tree growth stresses. V. Evidence of an origin in differentiation and lignification, *Wood Sci. Technol.*, **12**, 25-35 (1972).

Castera, P., Morlier, V.: Growth pattern and bending mechanics of branches, *Trees*, **5**, 232-238 (1991).

Clair, B., Thibaut, B., Sugiyama, J.: private communication.

Cosgrove, D.J.: Cellular mechanisms underlying growth asymmetry during stem gravitropism, *Planta*, [Suppl] **203**, 130-135 (1997).

Cousins, W.J.: Elastic modulus of lignin as related to moisture content, *Wood Science and Technology*, **10**, 9-17 (1976).

Cousins, W.J.: Young's modulus of hemicellulose as related to moisture content, *Wood Science and Technology*, **12**, 161-167 (1978)

Fourcaud, TH., Lac, P.: Mechanical analysis of the form and internal stresses of a growing tree by the finite element method, *Proc. Eng. Syst. Design Anal., ASME*, Montpellier, 77, 213-220 (1996).

Fournier, M., Bordonne, P., Guitard, D., Okuyama, T.: Growth stress pattern in tree stems. A model assuming evolution with the tree age of maturation strains, *Wood Sci. Technol.*, **24**, 131-142 (1990).

Fournier, M., Bailleres, H., Chanson, B.: Tree biomechanics: growth, cumulative prestresses, and reorientations,

Biomimetics, **2**, 229-251(1994).

Fujita, M., Saiki, H., Harada, H.: The secondary wall formation in compression wood tracheids: cell wall thickening and lignification, *Mokuzai Gakkaishi*, **24**, 158-163 (1978).

Fushitani, M.: Study of Molecular Orientation in Wood by Fluorescence Method, *Mokuzai Gakkaishi*, **19**, 135-140 (1973).

Hangarter, R.P.: Gravity, light and plant form, *Plant Cell Environ*., **20**, 796-800 (1997).

Hejnowicz, Z.: Graviresponses in herbs and trees: a major role for the redistribution of tissue and growth stresses, *Planta*, [Suppl] **203**, 136-146 (1997).

Hejnowicz, Z., Sievers, A.: Tissue stresses and their graviresponsive changes in stems of *Raynoutria japonica* Houtt., *J. Plant Physiol*., **149**, 91-101 (1996).

Ishikawa, A., Kuga, S., Okano, T.: Determination of parameters in mechanical model for cellulose III fiber, *Polymer*, **39**, 1875-1878 (1998).

Iwami, S., Masuda, Y.: Geotropic response of cucumber hypocotyls, *Plant Cell Physiol*., **5**, 121- 129 (1974).

Jacobs, M. R.: The fiber tension of woody stems, with special reference to the genus Eucalyptus. Commonw. For. Bur. Canberra Bull., **22**, pp39 (1938).

Kohji, J., Yamamoto, R., Masuda, Y.: Gravitropic response in *Eichhornia cressipes* (water hyacinth) I. Process of gravitropic bending in the peduncle, *J. Plant Sci*., **108**, 387-393 (1995).

Kikata, Y.: The effect of lean of on level of growth stress in Pinus densiflora, *Mokuzai Gakkaishi*, **18**, 443-449 (1972).

Kikata, Y., Miwa, K.: A modified hole-drilling technique for determining residual stresses (growth stresses) in the trunk, *J. Soc. Matr. Sci. Jpn.*, **26**, 429-432 (1977). Thin Wood Sections, *Tappi*, **43**, 1017-1024 (1960).

Liang, C.Y., Bassett, K.H., McGiness, E.A., Marchessault, R.H.: Infrared Spectra of Crystalline Polysaccharides. VII. Thin Wood Sections, *Tappi*, **43**, 1017-1024 (1960).

Mueller, W.J., Salisbury, F.B., Blotter, P.T.: Gravitropism in higher plant shoots. II. Dimensional and pressure changes during stem bending, *Plant Physiol*., **76**, 993-999 (1984).

Munch, E.: Statik und Dynamik des Schraubigen Baues der Zellwand besonders des Druck –und Zugholzes, *Flora*, **32**, 357-427 (1938).

Okuyama, T., Kikata, Y.: The residual stresses in wood logs due to growth stresses, *Mokuzai Gakkaishi*, **21**, 335-341 (1975).

Okuyama, T., Sasaki, Y., Kikata, Y., Kawai, N.: The seasonal change in growth stress in the tree trunk, *Mokuzai Gakkaishi*, **27**, 35-355 (1981).

Okuyama, T., Kawai, A., Kikata, Y., Sasaki, Y.: Growth stresses and uneven gravitational stimulus in trees containing reaction wood, *Mokuzai Gakkaishi*, **29**, 190-196 (1983).

Okuyama, T., Kawai, A., Kikata, Y., Yamamoto, H.: The growth stresses in reaction wood. In: Proceedings of the XVIII IUFRO World Congress, Yugoslavia, pp 249-260 (1986).

Okuyama, T., Yamamoto H., Iguchi M., Yoshida, M.: Generation process of growth stresses in cell walls II. Growth stress in tension wood, *Mokuzai Gakkaishi*, **36**, 797-803 (1990).

Okuyama, T., Yamamoto, H.: Residual stresses in living trees, In "Residual stresses-III science and technology, Fujiwara, A., Abe, T., Tanaka, K. (eds)," Elsevier, Amsterdam, 1992, pp 128-133.

Okuyama, T.: Growth stress in trees, *Mokuzai Gakkaishi*, **39**, 747-756 (1993).

Okuyama, T., Yamamoto, H., Yoshida, M., Hattori, Y., Archer, R.R.: Growth stresses in tension wood. Role of microfibrils and lignification, *Annales des Sciences Forestieres*, **51**, 291-300 (1994).

Okuyama, T., Takeda, H., Yamamoto, H., Yoshida, M.: Relation between growth stress and lignin concentration in the cell wall. Ultraviolet microscopic spectral analysis. *Journal of Wood Science*, **44**, 83-89 (1998).

Onaka, F.: Studies on reaction wood, *Bull. Wood Res. Inst. Kyoto Univ.,* **1**, 1-99 (1949).

Palmer, H.: "Epinasty, hyponasty and related topics", In: Pharis, R.P., Reid, D.M. (eds) Encyclopedia of plant physiology, New Series, vol 11: Springer, Berlin Heidelberg New York, pp 139-168, 1985.

Rufelt, H.: "Plagiogeotropism in root". In: Ruhland W (ed) Physiology of movements. Springer, Berlin-Heidelberg-New York, pp 322-343, 1962.

Sakurada, I., Nukushina, Y., Ito, T.: Eperimental Determination of the Elastic Modulus of Crystalline Regions in Oriented Polymers, *J. Polymer Sci.*, **57**, 651-660 (1962).

Salmen, L.:, Structure - Property Relations for Wood; from the Cell-Wall Polymeric Arrangement to the Macroscopic Behavior, In: Proc. 3rd Plant Biomechanics Conf., Freiburg-Badenweiler, pp. 452-462 (2000).

Sasaki, Y., Okuyama, T., Kikata Y.: The evolution process of the growth stress in the tree: the surface stresses on the tree, *Mokuzai Gakkaishi*, **24**, 149-157 (1978).

Silk, W.K.: Quantitative description of development, *Annu. Rev. Plant Physiol.*, **35**, 479-518 (1984).

Srinivasan, P.S.: The elastic and thermal properties of timber, *Quarterly Journal of Indian Institute of Science*, **4**, 222-314 (1941).

Sugiyama, K., Okuyama, T., Yamamoto, H., Yoshida, M.: Generation process of growth Stresses in cell walls. - Ralation between longitudinal released strain and chemical composition, *Wood Science and Technology*, **27**, 257-262 (1993).

Takabe, K., Miyauchi, T., Fukazawa, K.: Cell-wall formation of compression wood in Todo-fir (*Abies sacchariensis*) 1. Deposition of polysaccharides, *IAWA Bulletin*, **13**, 283-296 (1992).

Terashima, N.: A New Mechanism for Formation of a Structurally Ordered Protolignin Macromolecule in the Cell Wall of Tree Xylem, *J. Pulp Paper Sci.*, **16**, J150- J155 (1990).

Timell, T.E.: “Compression wood in gymnosperms,” Springer, Berlin-Heidelberg-New York, 1986.

Uemura, M.: Yamada, N.: Elastic constants of carbon fiber reinforced plastic materials, *J. Soc. Matr. Sci. Jpn.,* **24**, 156-163 (1975).

Wahyudi, I., Okuyama, T., Hadi, Y.S., Yamamoto, H., Yoshida, M., Watanabe, H.: Relationship between growth rate and growth stresses in *Paraserianthes falcataria* grown in Indonesia, *J. Trop. For. Prod*., **6**, 95-105 (2000).

Wahyudi, I., Okuyama, T., Hadi, Y.S., Yamamoto, H., Yoshida, M., Watanabe, H.: Growth stresses and strains in *Acacia mangium*, *For. Prod. J*., **49**, 77-81 (1999).

Wardrop, A.B., Daswell, H.E.: The nature of reaction wood. I. The structure and properties of tension wood fibers, *Australian Journal of Science Research*, **B**, **1**, 3-20 (1948).

Wardrop, A.B.: The nature of reaction wood. V. The distribution and formation of tension wood in some species of Eucalyptus, *Aust. J. Bot*., **4**, 152-166 (1956).

Wardrop, A.B.: The nature of reaction wood. V. The distribution and formation of tension wood in some species of Eucalyptus, Australian Journal of Botany, 4, 152-169 (1964).

Wardrop, A.B.: The formation and function of reaction wood, In “Cellular structure of woody plants, Cote, W.A. Jr. (ed.),” Syracuse Univ. Press, New York, 1965, pp.373-390.

Watanabe, H.: A study of the origin of longitudinal growth stresses in tree stems, In Proc. IUFRO Congr., Melbourne, 1965, pp.17.

Wilson, B.F.: The development of growth strains and stresses in reaction wood, In “Xylem cell development, Barnet, J.R. (ed.),” Castel House, Turnbridge Wells, 1981, pp.275-290.

Wilson, B.F., Gartner, G.L.: Lean in red alder (*Alnus rubra*): growth stress, tension wood, and righting response, *Can. J. For. Res*., **26**, 1951-1956 (1996).Terashima, N.: A new mechanism for formation of a structural ordered protolignin macromolecule in the cell wall of tree xylem. *J. Pulp Paper Sci.*, **16**, J150-J155 (1990).

Yamamoto H, Okuyama, T.: Generation process of growth stresses in cell walls. I. Analysis of the generation process of growth stresses in cell walls, *Mokuzai Gakkaishi*, **34**, 788-793 (1988).

Yamamoto, H., Okuyama, T., Yoshida, M., Sugiyama, K.: Generation process of growth stresses in cell walls. III. Growth stress in compression wood, *Mokuzai Gakkaishi*, **37**, 94-100 (1991).

Yamamoto, H., Okuyama, T., Sugiyama, K., Yoshida, M.: Generation process of growth stresses in cell walls. IV. Action of the cellulose microfibril upon the generation of the tensile stresses, Mokuzai Gakkaishi, **38**, 107-113 (1992).

Yamamoto, H. Okuyama, T.: Determining the intensity of the reaction wood formation by the strain-gaige method. Part 1, Growth stress and anatomy in compression wood, *Mokuzai Kogyo*, **48**, 270-274 (1993).

Yamamoto, H. Okuyama, T.: Determining the intensity of the reaction wood formation by the strain-gaige method. Part 2, Growth stress and anatomy in tension wood, *Mokuzai Kogyo*, **49**, 20-23 (1994).

Yamamoto, H., Okuyama, T., Yoshida, M.: Generation process of growth stresses in cell walls. VI. Analysis of the growth stress generation by using a cell model having three layers (S1, S2, and I+P), *Mokuzai Gakkaishi*, **41**, 1-8 (1995).

Yamamoto, H., Okuyama, T., Yoshida, M.: Growth stress generation and microfibril angle in reaction wood, In "Microfibrils in wood, Butterfield, B. (ed)," International Association of Wood Anatomists, Christchurch, 1998, pp.225-239.

Yamamoto, H., Yoshida, M., Okuyama, T.: Growth stress controls negative gravitropism in woody plant stems, *Planta*, **216**, 280-292 (2002).

Yamamoto, H.: Generation mechanism of growth stresses in wood cell walls: Roles of lignin deposition and cellulose microfibril during cell wall maturation, *Wood Sci. Technol*., **32**, 171-182 (1998).

Yamamoto, H., Abe, K., Arakawa, Y., Okuyama, T., Gril, J.: Role of the gelatinous layer (G-layer) on the origin of the physical properties of the tension wood *Acer sieboldianum., Journal of Wood Science*, in press (DOI 10.1007/s10086-004-0639-x), (received September 2003, accepted April 2004).

Yoshida, M., Okuyama, T., Yamamoto, H.: Tree forms and internal stresses I. Stresses around joints calculated by the finite element method, *Mokuzai Gakkaishi*, **37**, 283-290 (1991).

Yoshida, M., Okuyama, T., Yamamoto, H.: Tree forms and internal stresses II. Stresses around the base of the branch, *Mokuzai Gakkaishi*, **38**, 657-662 (1992a).

Yoshida, M., Okuyama, T., Yamamoto, H.: Tree forms and internal stresses III. Growth stresses of branches, *Mokuzai Gakkaishi*, **38**, 663-668 (1992b).

Yoshida, M., Okuda, T., Okuyama, T.: Tension wood and growth stress induced by artificial inclination in *Liriodendron tulipifera Linn* and *P. spachiana* Kitamura f ascendens Kitamura, *Ann. For. Sci*., **57**, 739-746(2000).

Yoshida, M., Ohta, H., Yamamoto, H., Okuyama, T.: Tensile growth stress and lignin content in the cell walls of yellow poplar, *Liriodendron tulipifera Linn*., *Trees – Structure and Function*, **16**, 457-464 (2002).

Chapter 4

HYGROMECHANICS OF WOOD IN RELATION TO THE COMPOSITE STRUCTURE OF THE CELL WALL

4-1 Swelling and shrinking anisotropy of wood – microscopic mechanism

4-1-1 Background

For better utilization of wood as the members of the building and the furniture materials, or raw materials for the paper, there is a need to understand the origin of its mechanical properties from the viewpoint of its composite structure. Studies on such topics have been conducted mainly from two standpoints. The first considers the macroscopic composite structure of the woody materials as heterogeneous but a continuum body, and the other is based on the fine composite structure of the lingo-cellulosic cell wall.

From the former standpoint, early authors succeeded in formulating the mechanical behavior of wood as an anisotropic body based on the general theory of continuum mechanics (Timoshenko & Goodier1970, Fun 1965, Lekhnitskii 1963). Thereafter, various behaviors of the solid wood and other woody materials were clarified (Guitard 1987, Gibson & Ashby 1988, Bodig & Jayne 1982).

As for the latter standpoint, from 1950's to the 1960's, progress in microscopic techniques enabled wood anatomists to clearly describe the ultimate structure of the wood cell wall. They showed that each cell wall lamella can be approximated by a "two-phase structure," namely, the reinforcing element of cellulose microfibril (CMF) and the matrix (MT) substance of lignin-hemicellulose compound (Mark 1967, Tsoumis 1991). However, an exact image of the fine structure and functions of each cell wall component have yet to be obtained. To better understand the origin of various properties of the woody material, it is indispensable that such wall characteristics should be revealed. Therefore, it is our goal to clarify these features including their role on the evolution of the mechanical and physical properties of the wood.

In this chapter, certain hygro-mechanical properties peculiar to the wood are formulated on the basis of the "latter standpoint," because it is very important to clearly describe the moisture-related properties of the wood and the wood-based materials when we use them

under various environmental conditions. Through those formulations, the fine structure and internal property of each cell wall constituent will be estimated. This includes anisotropic shrinkage due to wood drying, the change of the increase in the longitudinal Young's modulus due to moisture adsorption, and the change of the mechanical properties of the paper after repetition of the recycling process. The basic equation derived in Chapter 2 is used for those analyses. In the section 4-1, we firstly discuss the relationships between anisotropic shrinkage and the microfibril angle in the S2 layer (MFA) (Yamamoto et al. 1999, 2001). In the following section 4-2, we try to clarify the reason why the longitudinal Young's modulus of wood changes its value with moisture adsorption (Yamamoto&Kojima 2002, Yamamoto et al. 2002, Kojima&Yamamoto 2004). In that section, we simultaneously try to give an explanation to the question why the recyclability of the paper differs among material trees but same species.

4-1-2 Mechanical description

(a) Wood fiber model

The model used for analyzing the shrinking wood is a complex circular tube having three layers that was used for simulating the growth stress generation in Chapter 3. It consists of the compound middle lamella (CML), the outermost layer of the secondary wall (S1), and its middle layer (S2). The microfibril angles (MFA) take 90 degrees in the S1 layer, and a value between 0 – 60 degrees in the S2 layers.

When a certain change occurs in the physical state of the cell wall, internal expansive terms, $\varepsilon_1^{\,f}$ and $\varepsilon_2^{\,f}$, are often generated in the polysaccharide framework bundles, and $\varepsilon_1^{\,m}$ and $\varepsilon_2^{\,m}$ are also induced in the matrix skeleton. As the result, the wood fiber tends to deform in its axial and the diameter directions. We denote the strains of the free deformation of the wood fiber by ε_L and ε_T in the longitudinal and the diameter directions, respectively. In this case, ε_L and ε_T must satisfy the following simultaneous differential equations of elapsed time t:

$$
\begin{aligned}
&\dot{\varepsilon}_L = f_{11}(\mathbf{p})\dot{\varepsilon}_1^{\,m} + f_{12}(\mathbf{p})\dot{\varepsilon}_2^{\,m} + f_{14}(\mathbf{p})\dot{\varepsilon}_1^{\,f} + f_{15}(\mathbf{p})\dot{\varepsilon}_2^{\,m}\\
&\dot{\varepsilon}_t^{\,r1}\ (=\varepsilon_T) = f_{21}(\mathbf{p})\dot{\varepsilon}_1^{\,m} + f_{22}(\mathbf{p})\dot{\varepsilon}_2^{\,m} + f_{24}(\mathbf{p})\dot{\varepsilon}_1^{\,f} + f_{25}(\mathbf{p})\dot{\varepsilon}_2^{\,m}\\
&\dot{\varepsilon}_t^{\,r2} = f_{31}(\mathbf{p})\dot{\varepsilon}_1^{\,m} + f_{32}(\mathbf{p})\dot{\varepsilon}_2^{\,m} + f_{34}(\mathbf{p})\dot{\varepsilon}_1^{\,f} + f_{35}(\mathbf{p})\dot{\varepsilon}_2^{\,m}\\
&\dot{\varepsilon}_t^{\,r3} = f_{41}(\mathbf{p})\dot{\varepsilon}_1^{\,m} + f_{42}(\mathbf{p})\dot{\varepsilon}_2^{\,m} + f_{44}(\mathbf{p})\dot{\varepsilon}_1^{\,f} + f_{45}(\mathbf{p})\dot{\varepsilon}_2^{\,m}\\
&\dot{\rho}_1 = (\dot{\varepsilon}_t^{\,r1} - \dot{\varepsilon}_t^{\,r2})\rho_1, \quad \dot{\rho}_2 = (\dot{\varepsilon}_t^{\,r2} - \dot{\varepsilon}_t^{\,r3})\rho_2
\end{aligned}
\qquad (4\text{-}1)
$$

where and **p** is a parameter vector whose components are θ, ρ_1, ρ_2, Q (=$S_0 \cdot h/(r_1 \cdot E_1)$), G_1 (=E_1/S_1), G_2 (=E_2/S_2), and M (=S_2/S_1) (see Section 3-1). In this simulation, we regard the elapsed time t in the same light with the increasing moisture content. And, we integrate the simultaneous equations (4-1) from 0 to t under the initial conditions;

$\varepsilon_L(0) = 0$, $\varepsilon_t^{r1}(0) = 0$, $\varepsilon_t^{r2}(0) = 0$, $\varepsilon_t^{r3}(0) = 0$, $\rho_1(0) = \rho_1^0$, $\rho_2(0) = \rho_2^0$.

Now, we integrate eqs.(4-1) in a small interval of t, that is, $(i-1)\cdot T/N \le t \le i\cdot T/N$, then we obtain

$$\Delta^i\varepsilon_L = \int_{(i-1)\cdot T/N}^{i\cdot T/N} \frac{d}{dt}\varepsilon_L(t)dt \ , \quad \Delta^i\varepsilon_T = \int_{(i-1)\cdot T/N}^{i\cdot T/N} \frac{d}{dt}\varepsilon_T(t)dt \quad , \tag{4-2}$$

where, i =1, 2, - - - , N, and N is a enough large integer. T is the moisture content at the fiber saturation point (FSP). Finally, we calculate the free swellings of the wood fiber model as the nominal strains in its axial and diameter directions, which are given as the following formula (see eqs.(2-36) in Chapter 2) :

$$\alpha(t) = \lim_{n\to\infty}\left\{\prod_{i=1}^{j}\left(1+\Delta^i\varepsilon_L\right)-1\right\}, \quad \beta(t) = \lim_{n\to\infty}\left\{\prod_{i=1}^{j}\left(1+\Delta^i\varepsilon_t^{r1}\right)-1\right\} \tag{4-3}$$

where $\alpha(t)$ and $\beta(t)$ are the predicted values of the swelling strains of a single wood fiber model in the longitudinal and the diameter directions, respectively, when the moisture content (t) increases from 0 to t (= i/N). If the hysteresis in the dimensional change between the swelling and the shrinking processes are supposed to be small enough to be neglected, we can use the following formulae to predict the shrinking strains $\alpha'(t)$ and $\beta'(t)$:

$$\alpha'(t) = \frac{\alpha(T)-\alpha(t)}{\alpha(T)+1}, \quad \beta'(t) = \frac{\beta(T)-\beta(t)}{\beta(T)+1}. \tag{4-4}$$

As to deriving above equations, we should refer eqs.(2-31) ~ (2-36) in Chapter 2.

(b) Qualitative properties of *t*-dependent variables

To integrate eq. (4-1), proper functional shapes had to be given to the several t-dependent variables in advance, *i.e.* ε_1^f, ε_2^f, ε_1^m, ε_2^m, E_1, E_2, S_1, and S_2. Thickness ratios, ρ_1 and ρ_2, were also functions of t, however, those were given as the unknown functions, which should be solved in the basic equations (4-1). The MFA in the S2 is also an important factor controlling shrinkage of the wood (Meylan 1968, 1972, Cave 1972, Barrett et.al.1972, Koponen

et.al.1989, Watanabe et.al.1996), however, it can be considered to be almost independent of the moisture content.

It is difficult to determine the functional shapes of each *t*-dependent variable experimentally. We have no way except to presume them based on previous information given by various researchers. It is well recognized that both the Young's modulus and the shear modulus of the solid wood tend to decrease monotonously as the moisture content increases below the fiber saturation point (Carrington1922, Kollmann et.al.1960, 1968). Cousins (1976, 1978) attributed this phenomenon to the moisture-dependent properties of the matrix substances, such as the lignin and the hemicellulose. He measured the relationships between the relative humidity and the elastic moduli of the molded lignin and the hemicellulose which were chemically isolated from the wood cell wall, obtaining an evidence that the elastic moduli of these substances decrease monotonously with the increase of the relative humidity (see Footnote (5) in Section 3-1, Chapter 3). With reference to those investigations, it was assumed that the variables E_1, E_2, S_1, and S_2 decrease monotonously with the increase of t below the fiber saturation point T, and become constant above T.

It is well known that the hygroexpansion of wood occurs below the fiber saturation point except for a certain abnormal case, such as the collapse. To explain this phenomenon, it may be quite natural to assume that ε_1^f, ε_2^f, ε_1^m, and ε_2^m are monotonously increasing functions in the moisture content region below T. In the present wood fiber model, the swelling potential of the polysaccharide framework bundle in the direction perpendicular to the cellulose molecular axis has no effect upon the swelling behavior of the framework bundle due to the property of the stiffness tensor of the polysaccharide framework bundle (see Section 2-2, Chapter 2).

Those *t*-dependent variables were transformed into the functions which do not explicitly depend upon T by transforming the parameter t into τ ($=t/T$). The parameter τ ($=t/T$) is arbitrarily called *the normalized moisture content of wood*.

(c) The values of the *t*-dependent variables at τ=0 and τ=1

The values of S_0, E_1, S_1, E_2, and S_2:

The values of θ, ρ_1, ρ_2, and h are determined from the microscopic observation and the image analysis. We calculate Q ($=S_0 \cdot h/(r_1 \cdot E_1)$), G_1 ($=E_1/S_1$), and G_2 ($=E_2/S_2$) after determining the

values of S_0, E_1, S_1, E_2, and S_2. The values of E_1, S_1, E_2, and S_2 can be determined from eqs.(3-5) derived in Section 3-1. We show them again as follows:

$$E_i = A_i \cdot C_i \cdot E_{cry} + A_i \cdot (1 - C_i) \cdot \psi(\tau) \cdot E_{poly} ,$$

$$S_i = \{1 - A_i + (1 - C_i) \cdot A_i \cdot (1 - \psi(\tau))\} \cdot E_{matr} / (1 + \nu_i) , \qquad (i = 1, 2) \qquad (4\text{-}5)$$

where A_i and C_i are respectively the weight ratio of the polysaccharide framework and its crystallinity in each layer, which are hypothesized in Table 4-1. $\psi(\tau)$ is a monotonously decreasing function of τ which satisfies $\psi(\tau)|_{\tau=0}=1$ and $\psi(\tau)|_{\tau=1}=0$. Quantity ν_i is Poisson's ratio of the matrix skeleton in each layer. In our study, we use 0.5 as the value of ν_i.

We assume that E_{cry} takes a constant value of 134 GPa regardless of the moisture content (Sakurada et al. 1960, Nishino et al 1998), since the crystalline cellulose does not absorb water molecule. With reference to Cousins (1976, 1978), we assume that E_{matr} is a function of τ and it takes a value of 2 GPa at the humid state (*i.e.* $\tau=1$), and it tends to increase monotonously as the moisture content decreases, and it takes 4 GPa at $\tau=0$. As described in Section 3-1, we consider that only dried part among the oriented polyose takes part in constituting the framework bundle, on the other hand, humid polyose is integrated into the isotropic matrix skeleton. Then, we assume that $\psi(\tau)$ satisfies $\psi(\tau)|_{\tau=0}=1$ and $\psi(\tau)|_{\tau=1}=0$. As the value of the axial Young's modulus of dried polyose (E_{poly}), we use 8 GPa (see Footnote (5) in Section 3-1).

To estimate the value of F ($= S_0 \cdot h/r_1$), we need to calculate the value of S_0, which can be obtained as described in Footnote (6) in Section 3-1. The CML is reinforced by the rigid crystalline CMFs whose orientations are randomly distributed, therefore, the change of the stiffness of the matrix skeleton in the CML has almost no effect upon the value of S_0. Moreover, the change of h induced by the water adsorption is quite smaller than the value of r_1. Then, we assumed that F is not affected by the moisture content τ.

Thus, we can determine the values of F, E_1, E_2, S_0, S_1, and S_2 at $\tau=0$ and $\tau=1$, which are displayed in Table 4-3.

Table 4-1. Composition for chemical constituents in each layer.

Layer	Polysaccharide framework (*A*)		Matrix substance	Crystallinity in the Polysaccharide framework (*C*)
	Crystalline cellulose ($A\times C$)	Oriented polyose (non-Crystalline ($(1-C)\times A$)		
CML	15 (%)	0	85	0
S1	15	5	80	75
S2	30	10	60	75
S3	- - - - -	- - - - -	- - - - -	- - - - -

The values of ρ_1, ρ_2, *and h* :

The values of ρ_1, ρ_2, and *h* at τ=0 can be determined from the oven-dried density of the wood specimen by using eqs.(4-9). Determined values of ρ_1^0 ($=\rho_1(\tau)|_{\tau=0}$), ρ_2^0 ($=\rho_2(\tau)|_{\tau=0}$), and $h/r_1|_{\tau=0}$ are displayed in Table 4-3.

The values of ε_1^m, ε_2^m, ε_1^f, *and* ε_2^f *at* τ*=0 and* τ*=1* :

According to the definition of the swelling ability of every cell wall component, we can consider that the values of ε_1^m, ε_2^m, ε_1^f, and ε_2^f at τ=0 are all nil, however, we do not know the values of ε_1^m, ε_2^m, ε_1^f, and ε_2^f at τ=1. We calculated the eqs.(4-6~8) by supposing various values as $\varepsilon_1^m(\tau)$, $\varepsilon_2^m(\tau)$, $\varepsilon_1^f(\tau)$, and $\varepsilon_2^f(\tau)$ at τ=1, and compared the simulated results with experimental ones.

(d) Formula for describing the shrinking process of the wood fiber model

The integral term in eqs. (4-2) and (4-3) is rewritten by using the normalized moisture content τ ($\equiv t/T$). For example, the longitudinal component becomes

$$\Delta^i\varepsilon_L = \int_{(i-1)\cdot T/N}^{i\cdot T/N} \frac{d}{dt}\varepsilon_L(t)dt = \int_{(i-1)\cdot 1/N}^{i\cdot 1/N} \frac{d\tau}{dt}\frac{d}{d\tau}\varepsilon_L(\tau)Td\tau = \left[\bar{\varepsilon}_L(\tau)\right]_{(i-1)\cdot 1/N}^{i\cdot 1/N} , \qquad (4\text{-}6)$$

provide that $\bar{\varepsilon}_L(\tau) \equiv \varepsilon_L(t)\big|_{t=T\cdot\tau}$. Thus, the following formulae are obtained:

$$\alpha(\tau) = \lim_{n\to\infty}\left\{\prod_{i=1}^{j}\left(1+\Delta^i\varepsilon_L\right)-1\right\}, \quad \beta(\tau) = \lim_{n\to\infty}\left\{\prod_{i=1}^{j}\left(1+\Delta^i\varepsilon_t^{\eta}\right)-1\right\} . \qquad (4\text{-}7)$$

$\alpha(\tau)$ and $\beta(\tau)$ are the predicted values of swelling strains of the wood fiber model in the longitudinal and the diametral directions, respectively, when the normalized moisture content increases from 0 to τ (= i/*N*).

When calculating the shrinking process of the wood fiber model $\alpha'(\tau)$ and $\beta'(\tau)$, one can deduce following relations, which are essentially equivalent to eq. (4-4):

$$\alpha'(\tau) = \frac{\alpha(1) - \alpha(\tau)}{\alpha(1) + 1}, \quad \beta'(\tau) = \frac{\beta(1) - \beta(\tau)}{\beta(1) + 1} \tag{4-8}$$

where $\alpha(1)$ and $\beta(1)$ mean $\alpha(\tau)|_{\tau=1}$ and $\beta(\tau)|_{\tau=1}$, respectively. $\alpha'(\tau)|_{\tau=0}$ ($\equiv\alpha'(0)$) and $\beta'(\tau)|_{\tau=0}$ ($\equiv \beta'(0)$) mean the oven-dried shrinkages in the longitudinal and the transverse directions, respectively.

4-1-3 Experimental procedure

(a) Specimen

It is indispensable for this discussion to compare the predicted results derived from the eqs. (4-7) or (4-8) with the experimental data obtained from a single wood fiber. However, it is almost impossible to isolate a wood fiber without any damage, since all fibers are strongly bound each other strongly through the compound middle lamella inside the actual xylem. Therefore, it is difficult to measure the shrinking behavior of the intact wood fiber.

Softwood species have a simple structure consisting almost only of tracheids. Thus, thin and small rectangular flat-sawn specimen from the earlywood or latewood region were taken, which may be homogeneous enough in the radial direction. Moreover, it is considered that the shrinking behavior of the thin specimen is approximately equal to that of the single wood fiber.

In the present study, a 14-year-old sugi (*Cryptomeria japonica* D.Don) with a leaning stem was used. A rectangular block was taken from the sapwood region, and was saturated with hot water. Thereafter, by using a sliding microtome and a thin-plate circular saw, a flat-sawn specimen was prepared from the earlywood region. The size of the specimen for measuring the longitudinal shrinkage was 50×10×2-5mm in the longitudinal, the tangential and the radial directions, respectively. In case of the measurement of the tangential shrinkage, the size of the specimen was 10×20×2-5mm in the respective directions.

(b) Measurement of the shrinking process

The specimen was dried step by step inside a small desiccator with saturated solutions of different kinds of salts. The weight (w) and length (l) of the specimen were recorded at each equilibrium condition. An electric scale of 0.1mg reading accuracy was utilized. A comparator with a dial-gauge of 0.001mm reading accuracy was used for the measurement of the length. Fresh water, saturated solutions of $NH_4H_2PO_4$, KCl, NaCl, NH_4NO_3, K_2CO_3, $CaCl_2$6aq, CH_3COOK, and powders of NaOH, P_2O_5 were used in turn for regulating the relative humidity inside the desiccator. After being dried with the P_2O_5 powder, the specimen was dried for 24 hours inside a high temperature oven (105˚C), thereafter, the oven-dried weight (w_0) and the oven-dried length (l_0) were measured. The moisture content of the specimen, t, at every drying step, was calculated by the following formula,

$$t = \frac{w - w_0}{w_0} \times 100 \quad (\%)$$

and the shrinkage of the specimen at every moisture content, $\alpha'(t)$, was calculated by the following formula.

$$\alpha'(t) = \frac{l_g - l(t)}{l_g} \times 100 \quad (\%)$$

where l_g is the length of the specimen in the green condition.

(c) Oven-dried density and average microfibril angle

After measuring the weight and the length of the oven-dried specimen, a small fraction was removed from the central part of the specimen, and the oven-dried density and the average microfibril angle were measured. The oven-dried density was used for determining the values of ρ_1 and ρ_2 at the oven-dried state.

The oven-dried density of the small fraction, m_0, was measured by the mercury impregnating method, thereafter, several flat-sawn sections of 0.1-0.2mm in thickness were prepared from the small fraction by using a sliding microtome, and the microfibril angle in every section was determined by using the improved Cave's method (Cave 1966, Meylan 1967, Yamamoto et.al. 1993b), and the arithmetic average was used as the microfibril angle for the specimen.

(d) Initial values of ρ_1, ρ_2, and h

The moisture dependencies of the values of ρ_1 and ρ_2 were given as eqs. (2-32) in Chapter 2. Therefore, the initial values at $\tau = 0$ have to be selected for them. The initial values, ρ_1^0 ($=\rho_1(\tau)|_{\tau=0}$) and ρ_2^0 ($=\rho_2(\tau)|_{\tau=0}$), are dependent not only on the species, but also on the individual tree, and the location within an annual ring (Saiki 1970). The small early wood specimen used for the measurement of the shrinking process can be regarded as a homogeneous aggregate of many tracheids, therefore we can use the isolated wood fiber model as an equivalent model of the wood specimen. Based on these assumptions, we estimated the values of ρ_1^0, ρ_2^0 and h^0 by introducing the following formulae.

$$\rho_2^0\left(=\rho_2|_{\tau=0}\right)=\sqrt{\frac{1.5}{1.5-m_0}\cdot\frac{V\cdot T}{V+T+V\cdot T}+\frac{V+T}{V+T+V\cdot T}}\ ,$$
$$\rho_1^0\left(=\rho_1|_{\tau=0}\right)=\sqrt{\frac{(1+V)(\rho_2^0)^2-1}{(\rho_2^0)^2\cdot V}}\ ,\quad h^0/r_1|_{\tau=0}=\sqrt{\frac{\left(1+(\rho_1^0)^2\cdot T\right)(\rho_2^0)^2-1}{(\rho_1^0)^2\cdot(\rho_2^0)^2\cdot T}}-1\ , \tag{4-9}$$

where, m_0 is the density of the oven-dried specimen, V is the volume ratio of the S2 layer to the S1 layer, and T is that of the S2 layer to CML layer in the oven-dried conditions, respectively. With reference to the studies made by various researchers, Koponen (1989) proposed a value of the volume ratio of each lamella to the whole cell wall in a typical softwood tracheid as displayed in Table 4-2. The oven-dried density of the early wood specimen of the sugi used in the present study was 0.4 on an average, therefore by substituting m_0=0.4 in eqs.(4-9), we obtain,

$$\rho_1^0=1.015,\quad \rho_2^0=1.122,\ h^0=0.025\cdot r_1|_{\tau=0}$$

Table 4-2. Volume ratios of layers to the whole cell wall of typical early wood tracheid. (Koponen 1989)

CML	17.5(%)
S1	10.0
S2	67.5
S3	5.0
	100.0

Thus, we can decide all values of the parameters, which are required for calculating the eqs. (4-7) and (4-8), as displayed in Table 4-3.

Table 4-3. Values of the τ (normalized moisture content) dependent variables used in the simulation.

	S_1	S_2	E_1	E_2	F	ρ_1	ρ_1	ε_1^f	ε_2^f	ε_1^m	ε_2^m
τ=0	2.09	1.57	20.5	41.0	0.098	1.015	1.122	0	0	0	0
τ=1	1.11	0.915	20.1	40.2	0.098	>1.015	>1.122	*	*	*	*

Note. (1) $\rho_1(\tau)$ and $\rho_2(\tau)$ must satisfy the eqs.(2-32) in Chapter 2. In fact, we can suppose h/u_2 is constant for τ.

(2) Functional shapes and terminal values of $\varepsilon_1^f(\tau)$, $\varepsilon_2^f(\tau)$, $\varepsilon_1^m(\tau)$, and $\varepsilon_2^m(\tau)$ remain unknown for the time being.

(3) Units of the values of E_1, E_2, S_1, S_2 , and S_0 are GPa.

4-1-4 Result and discussion

(a) Experimental results

Dependency of the shrinking anisotropy upon the MFA:

Fig.4-1 shows the experimental relationships between the oven-dried shrinkages and the MFAs. In this figure, the data from a 32 year-old *Pinus jeffreyi* reported by Meylan (1972) are displayed besides our results obtained from a 14-year-old sugi. In the region of the MFA below 30 degrees, the transverse shrinkage reaches 7~9 %, on the other hand, the longitudinal one is less than 1%. However, in the region of the MFA over 30 degrees, the longitudinal shrinkage becomes larger with the increase of the MFA, and the transverse one decreases abruptly as the MFA increases. Consequently, the transverse shrinkage of *Pinus jeffreyi* sometimes becomes smaller than the longitudinal one in the region of the extremely large MFA, where the longitudinal shrinkage reaches more than 6 %, and that of the sugi sometimes exceeds 3%. Thus, the shrinking anisotropy of the wood is highly dependent upon the MFA.

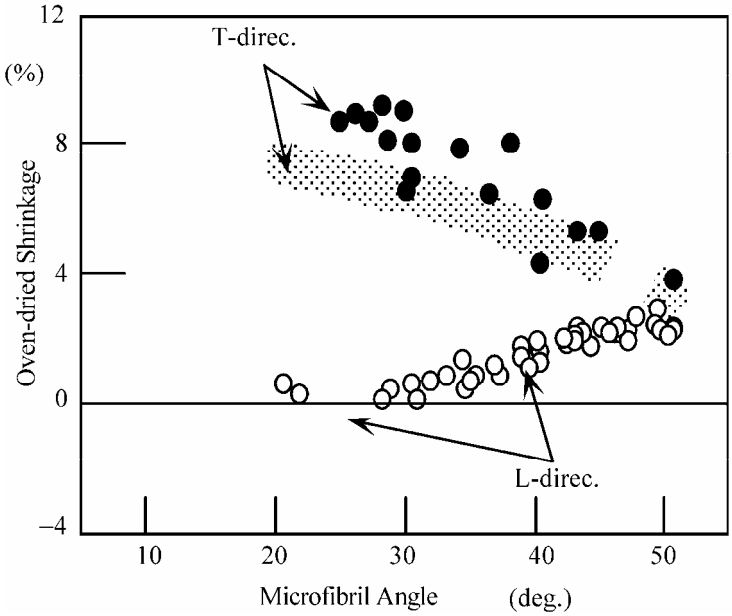

Fig.4-1. Relationship between anisotropic shrinkage (from green to oven-dried) and the microfibril angle.
Legends;
, : *Pinus jeffreyii* (Meylan 1968).
, : Sugi (in the present study).

Shrinking process during water desorption:

Dots in Fig.4-2 (a) show the longitudinal shrinking processes of four different specimens of sugi, whose MFAs in the S2 layers are 31, 38, 41, and 48 degrees, respectively. Each specimen started to shrink around a moisture content of almost 30%. The shrinkage curve tends to shift upwards in the figure as the MFA increases. Each shrinkage curve can be approximated by a straight line in the region of the moisture content between 5 and 20%, however, its gradients seem to reduce in the region of the moisture content smaller than 5% and larger than 20%. Thus, it may be rather natural to consider that each shrinkage curve is not so much linear as sigmoidal as pointed out by Sadoh et.al. (1967), Meylan (1972), and Abe and Yamamoto (in contribution), provided that those three investigations reported that the gradient in the longitudinal shrinking processes became rather higher in the region of the moisture content smaller than 10%.

Fig.4-2(b) shows the tangential shrinking processes of three different specimens of sugi, whose MFAs are 27, 45, and 50 degrees, respectively. In the same way as in the case of the longitudinal shrinking process, each specimen started to shrink around a moisture content of almost 30%, and the shape of the curve of the tangential shrinkage becomes not so much linear as sigmoidal. The curve of tangential shrinkage tends to shift downward in the figure as the MFA increases in contrast with the longitudinal case.

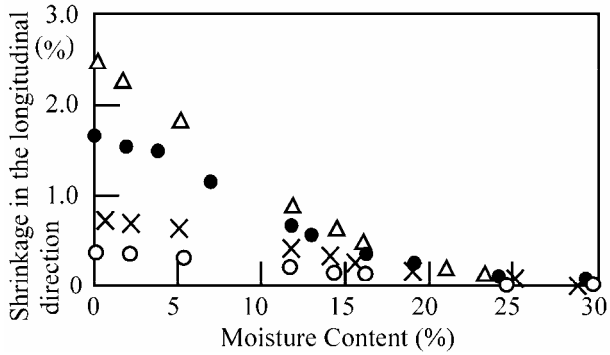

Fig.4-2(a). Longitudinal shrinking processes from a 14-year-old sugi wood specimen.
Legends: Microfibril angles in the S2 layers are ○ ; 31 deg., × ; 38 deg., ● ; 41 deg., △ ; 48 deg.

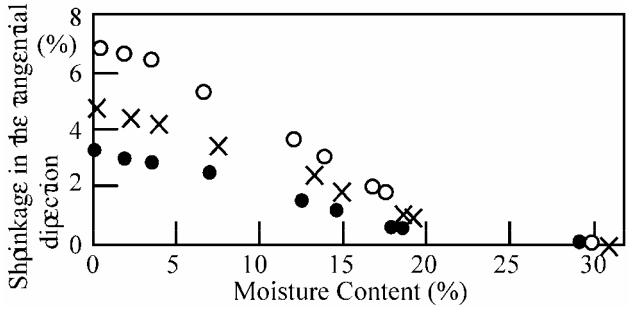

Fig.4-2(b). Tangential shrinking processes from a 14-year-old sugi wood specimen.
Legends: Microfibril angles in the S2 layers are ○; 27 deg. × ; 45 deg. ● ; 50 deg.

(b) Simulated results

Conditions for the simulation:

For calculating eqs.(4-7) and (4-8), we need to give proper functional shapes to τ-dependent variables, *e.g.* ε_1^{m}, ε_2^{m}, ε_1^{f}, ε_2^{f}, E_1, E_2, S_1, and S_2 in advance. Then, we tentatively supposed following sinusoidal curves as the functional shapes of $\varepsilon_1^{m}(\tau)$, $\varepsilon_2^{m}(\tau)$, $\varepsilon_1^{f}(\tau)$, $\varepsilon_2^{f}(\tau)$, $E_{matr}(\tau)$, and $\psi(\tau)$ with reference to the above-mentioned discussions on the shrinking process of the wood specimen of sugi.

$$\begin{aligned}
&\varepsilon_1^{m}(\tau) = \frac{1}{2}\varepsilon_1^{m}(1)\left(1-\cos\pi\tau\right), \quad \varepsilon_2^{m}(\tau) = \frac{1}{2}\varepsilon_2^{m}(1)\left(1-\cos\pi\tau\right),\\
&\varepsilon_1^{f}(\tau) = \frac{1}{2}\varepsilon_1^{f}(1)\left(1-\cos\pi\tau\right), \quad \varepsilon_2^{m}(\tau) = \frac{1}{2}\varepsilon_2^{f}(1)\left(1-\cos\pi\tau\right),\\
&E_{matr}(\tau) = \frac{E_{matr}(0)-E_{matr}(1)}{2}\cos\pi\tau + \frac{E_{matr}(0)+E_{matr}(1)}{2},\\
&\psi(\tau) = \frac{1}{2}\cos\pi\tau + \frac{1}{2}
\end{aligned} \tag{4-10}$$

where, $\varepsilon_1^{m}(1) \equiv \varepsilon_1^{m}(\tau)|_{\tau=1}$, $\varepsilon_2^{m}(1) \equiv \varepsilon_2^{m}(\tau)|_{\tau=1}$, $\varepsilon_1^{f}(1) \equiv \varepsilon_1^{f}(\tau)|_{\tau=1}$, $\varepsilon_2^{f}(1) \equiv \varepsilon_2^{f}(\tau)|_{\tau=1}$, $E_{matr}(0) \equiv E_{matr}(0)|_{\tau=0}$, $E_{matr}(1) \equiv E_{matr}(\tau)|_{\tau=1}$. Functional patterns of $E_1(\tau)$, $E_2(\tau)$, $S_1(\tau)$, and $S_2(\tau)$ can be

estimated from $E_{matr}(\tau)$ and $\psi(\tau)$ through calculating eqs.(4-5), however $\varepsilon_1^m(1)$, $\varepsilon_2^m(1)$, $\varepsilon_1^f(1)$, and $\varepsilon_2^f(1)$ are still unknown values. Then, we set the following two cases as the values of $\varepsilon_1^m(1)$, $\varepsilon_2^m(1)$, $\varepsilon_1^f(1)$, and $\varepsilon_2^f(1)$.

[*CASE 1*] The polysaccharide framework bundle would not swell in any direction during water sorption, namely, $\varepsilon_1^f(1) = \varepsilon_2^f(1) = 0\%$. However, the matrix skeleton tends to swell isotropically by water sorption. Then, we set the cases of (a) $\varepsilon_1^m(1) = \varepsilon_2^m(1) = 0.1$ (10%), (b) $\varepsilon_1^m(1) = \varepsilon_2^m(1) = 0.15$ (15%), and (c) $\varepsilon_1^m(1) = \varepsilon_2^m(1) = 0.2$ (20%).

[*CASE 2*] Not only the matrix skeleton but also the polysaccharide framework bundle tend to swell in the direction along the cellulose molecular chain during water sorption. In this case, 0.15 (15%) were adopted as the values of $\varepsilon_1(1)$ and $\varepsilon_2(1)$, and the following three values were assumed for $\varepsilon_1^f(1)$ and $\varepsilon_2^f(1)$, namely, (α) $\varepsilon_1^f(1) = \varepsilon_2^f(1) = 0\%$, ($\beta$) $\varepsilon_1^f(1) = \varepsilon_2^f(1) = 0.005$ (0.5%), and (γ) $\varepsilon_1^f(1) = \varepsilon_2^f(1) = 0.01$ (1%).

Dependency of the shrinking anisotropy upon the MFA:

The curves in Fig. 4-3(a) stand for the simulated results on the relationships between the MFAs and the anisotropic oven-dried shrinkages. "*CASE 1*" was employed as the conditions for calculating eqs.(4-7) and (4-8). In the cases of $\varepsilon_1^m(1)=\varepsilon_2^m(1)=10\sim20\%$, the experimental results can be well simulated over a wide range of the MFA. According to the simulated results, it is obvious that the value of $\beta'(\tau)|_{\tau=0}$ ($\equiv \beta'(0)$) is largely affected by the swelling potentials of the matrix skeletons, namely $\varepsilon_1^m(1)$ and $\varepsilon_2^m(1)$, especially in the region of comparatively small MFA. On the other hand, the value of $\alpha'(\tau)|_{\tau=0}$ ($\equiv\alpha'(0)$) is highly affected by the swelling potentials of the matrix skeletons in the region of the large MFA. The best fitting curves can be obtained in the case of $\varepsilon_1^m(1)=\varepsilon_2^m(1)=15\%$, however the simulation tends to overestimate the longitudinal shrinkage of the specimen especially in the region of the MFA larger than 40 degrees. The same is true for the transverse shrinkage in the region of the large MFA.

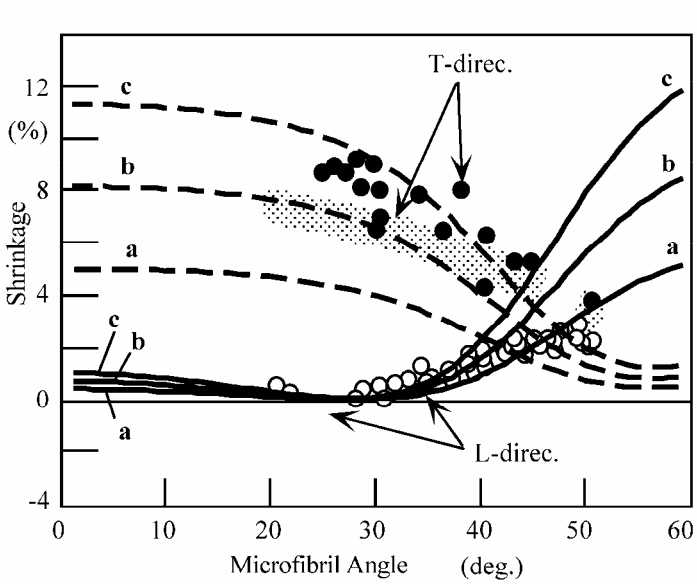

Fig.4-3(a). Simulated result of the relationship between anisotropic shrinkage (from green to oven-dried) and the microfibril angles when only the matrix skeleton tends to shrink during water desorption.
Note: 1) The swelling potential of the polysaccharide framework bundle is supposed to be null.
2) The conditions of the parameters are displayed in Table 4-3.
Legends: 1) The swelling potential of the matrix skeletons (ε_1^m and ε_2^m) at $\tau = 1$ is supposed to be
a; 10 % **b**; 15 % **c**; 20 %.
2) Experimental tendencies of wood specimen.
, ; *Pinus jeffreyii* (Meylan 1968).
○ , ● ; Sugi.

Fig. 4-3(b) shows the simulated results derived from CASE 2. The value of $\beta'(0)$ is unaffected by the swelling potentials of the polysaccharide framework bundle, namely the values of $\varepsilon_1^f(1)$ and $\varepsilon_2^f(1)$, except in the region of extremely large MFA. On the other hand, the value of $\alpha'(0)$ varies sensitively with increase in the swelling potentials of the polysaccharide framework especially in the region of comparatively small MFA. Judging from the simulated results, the best fitting can be obtained in the cases of $\varepsilon_1^m(1)=\varepsilon_2^m(1)=15\%$, and $\varepsilon_1^f(1)=\varepsilon_2^f(1)=0 \sim 0.5\%$. It is rather natural to consider that the polysaccharide framework bundle would not swell in the cellulose chain directions during the water sorption, since it consists of the highly crystallized cellulose as supposed in the wood fiber model.

In Chapter 5, we will report that the longitudinal oven-dried shrinkage of the gelatinous layer becomes several times larger than that of the lignified layer in the gelatinous fiber. From those investigations, we know that the gelatinous layer tends to shrink largely in its axial direction during the water desorption despite the fact that it consists of highly crystallized cellulose microfibril. This sounds rather contradictory to our present speculation that the crystalline framework of polysaccharide bundle almost never shrinks by water desorption. Regarding this phenomena, as reported by Okuyama et.al.(1990) and Yamamoto et.al.(1992), there are interesting facts that the Young's modulus of the gelatinous layer in green condition takes a value of 40-50GPa, which is about two or three times as large as that of the lignified layer, however, it is considerably smaller than that of the cellulose crystals. This means that the

gelatinous layer is composed not only of pure cellulose crystal but also of matrix substances, such as hemicellulose or amorphous cellulose. Thus, if we assume that the CMF as a crystal framework would not shrink due to the water desorption, one could say that "the matrix region" in the gelatinous layer has a considerably large shrinking ability which causes a high shrinkage in the gelatinous layer during water desorption.

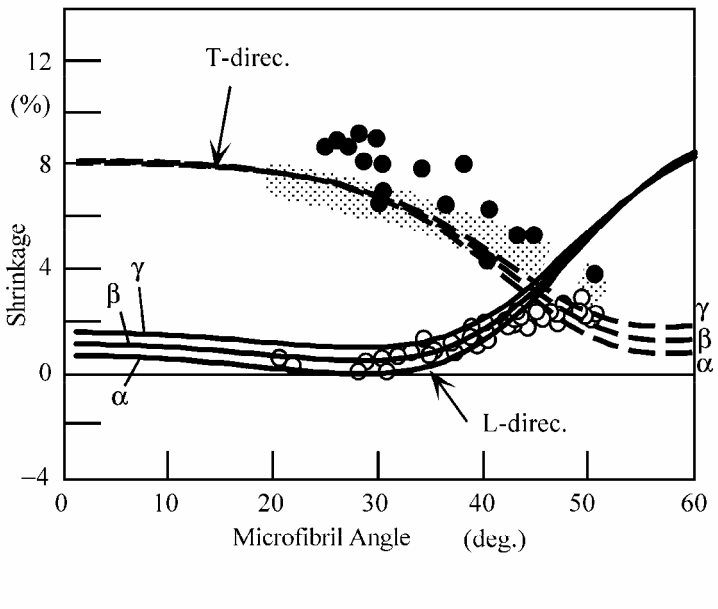

Fig.4-3(b). Simulated result on the relationship between anisotropic shrinkage (from green to oven-dried) and microfibril angle when both polysaccharide framework bundles and the matrix skeleton tend to shrink due to the water desorption.
Note. 1) The swelling potentials of the matrix skeletons (ε_1^m and ε_2^m) at τ =1 are supposed to be 15%.
2) The conditions of the parameters are displayed in the Table 4-2.
Legends. 1) Swelling potentials of the cellulose microfibril (ε_1^f and ε_2^f) at τ =1 are supposed to be ,
α : 0 % β : 0.5 % γ : 1.0 %
2) ○ , ● : Experimental data from a 14-year-old sugi.

Shrinking process during water desorption:

From the above discussions, the values of $\varepsilon_1^f(1)$ and $\varepsilon_2^f(1)$ are considered to be almost nil. And, we tried to simulate the shrinking process of the wood fiber model on the basis of "*CASE 1* - condition (b)". Curves in Fig. 4-4(a) show the simulated results of the longitudinal shrinking process. The dots in the figure stand for the experimental results of the small wood specimens as already shown in Fig. 4-1(a). In the case of comparatively small MFA region (**a** and **b**), the experimental tendency of the wood specimens can be simulated under the condition $\varepsilon_1^m(1) = \varepsilon_2^m(1)$ = 15%. In the case of MFA =41 degrees, the value of the oven-dried shrinkage can be derived from using this condition, however, the shape of the shrinkage curve cannot be simulated by the given condition. In this case, the simulation tends to over-estimate the experimental tendency except in the region of the moisture content below 5 %. It is considered that this discrepancy arises from the supposition that the τ-dependent variables are expressed by the sinusoidal curves as defined in eqs.(4-10). Of course, it cannot be considered that all the

τ-dependent variables should be approximated by eqs.(4-10), however it can be said, at least, that some of those variables vary non-linearly with the moisture content change, therefore, the sugi wood specimen tends to shrink sinusoidally by the water desorption. In the case of extremely large MFA (= 48 degrees), a serious discrepancy occurs between the predicted value and the experimental one if the same condition, namely $\varepsilon_1^m(1) = \varepsilon_2^m(1) = 15\%$, are used for the simulation. In such a large MFA region, it is considered that both the magnitude and the shape of each τ-dependent variable are more or less different from those in other MFA region.

Curves in Fig. 4-4(b) show the calculated values of the transverse shrinking process. In the same way as in the longitudinal cases, the experimental tendency of the wood specimens can be simulated under the condition $\varepsilon_1^m(1) = \varepsilon_2^m(1) = 15\%$ especially in the case of comparatively small MFA region (27 degrees), however in the case of extremely large MFA (= 45 and 50 degrees), serious discrepancy occurs between the predicted value and the experimental one. As discussed in the longitudinal cases, it may be considered that the value and the behavior of each τ-dependent variable in the region of extremely large MFA is somehow different from that in the region of ordinary MFA.

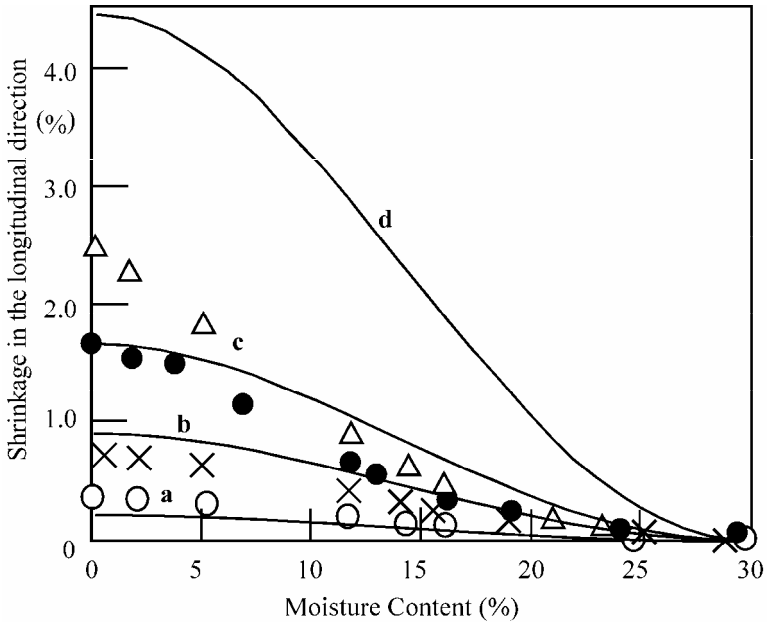

Fig.4-4(a). Longitudinal shrinking process of wood.
Note: The values of the swelling potentials of the matrix skeleton and the polysaccharide framework bundle at τ =1 are supposed to be 15% and 0%, respectively.
Legends. 1) Microfibril angles in the S2 layers are
a , ○; 31 deg. **b** , ×; 38 deg.
c , ●; 41 deg. **d** , △; 48 deg.
2) Curves are Simulated results.

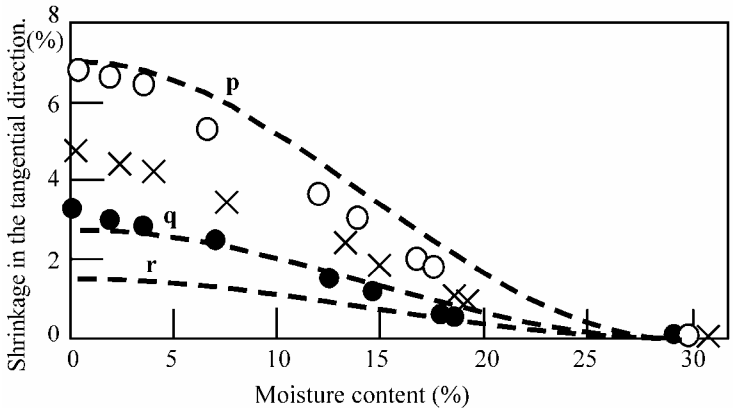

Fig.4-4(b). Tangential shrinking process of wood.
Note: The values of the swelling potentials of the matrix skeleton and the polysaccharide framework bundle at τ =1 are supposed to be 15% and 0%, respectively.
Legends. 1) Microfibril angles in the S2 layers are
p , ○ ; 27 deg. **q** , × ; 45 deg.
r , ● ; 50 deg.
2) Curves are simulated results.

Moisture content at the fiber saturation point (FSP):

It is considered that the values of $\varepsilon_1^m(1)$, $\varepsilon_2^m(1)$, $\varepsilon_1^f(1)$, and $\varepsilon_2^f(1)$ have some relation with the moisture content at τ=1, namely, the fiber saturating point (FSP). To verify this idea, we try to derive the moisture content of wood at τ=1 from the values of $\varepsilon_1^m(1)$, $\varepsilon_2^m(1)$, $\varepsilon_1^f(1)$, and $\varepsilon_2^f(1)$. We denote the volume of the matrix skeleton in the secondary wall at τ=0 as V_0 and the volumetric change of the matrix skeleton attendant upon the water sorption as ΔV, provided that the dimensional change of the matrix skeleton would not be restricted by surroundings. Supposing $\varepsilon_1^f(1) = \varepsilon_2^f(1) = 0$ and $\varepsilon_1^m(1) = \varepsilon_2^m(1) = \varepsilon$, we obtain $\Delta V=((1+\varepsilon)^3-1)V_0$. If the volumetric increase of the matrix skeleton related to the water sorption is equal to the volume of absorbed bound water, the weight of the water in the element at the FSP becomes $\rho\Delta V$, where ρ is the density of the absorbed water. On the other hand, if we consider that the volume of the secondary wall substance in oven-dried condition is equivalent to that of the matrix skeleton, the oven-dried weight of the secondary wall substance is $w_0=\rho_0 V_0$, where ρ_0 is the oven-dried density of the secondary wall substance. Therefore, the moisture content of the secondary wall at the FSP, t_{FSP}, can be obtained as $\rho\Delta V/w_0$, thus, we obtain $t_{FSP} = \rho((1+\varepsilon)^3-1)V_0 /(\rho_0 V_0)= ((1+\varepsilon)^3-1)\ \rho/\ \rho_0$. Generally speaking, the value of ρ_0 is considered to be about 1.5g/cm^3 regardless of the species and age of the tree. If we assume ρ=1g/cm^3 and ε = 15%, we obtain t_{FSP} =35 (%), which is close to the experimental values of the moisture content at the FSP. From this result, it is quite reasonable to consider $\varepsilon_1^m(1) = \varepsilon_2^m(1)$ = 15% and $\varepsilon_1^f(1) = \varepsilon_2^f(1) = 0$ if we simulate the shrinking/swelling process of the single wood fiber by using eqs.(4-7) and (4-8).

4-1-5 Summary and concluding remarks

In this section, we aimed to make clear the origin of the shrinking anisotropy of softwoods or hardwoods without gelatinous layers, as well as to give a first step for elucidating the interaction between moisture and the cell wall components. A multi-layered circular cylinder, having the CML, the S1, and the S2 layers, was used as an analytical model of the ligno-cellulosic (wood) fiber, and we successfully simulated the shrinking process of a single wood fiber, and compared the results with the experimental ones. The following results and conclusions were obtained.

1. The relationship between the oven-dried shrinkage and the MFA can be predicted quantitatively by using the wood fiber model, if the magnitudes and the functional shapes of the τ-dependent variables in the wood fiber model are suitably selected. The most fitting simulation can be obtained by supposing $\varepsilon_1^m(1)$ $(=\varepsilon_1^m(\tau)|_{\tau=1})$ = $\varepsilon_2^m(1)$ $(=\varepsilon_2^m(\tau)|_{\tau=1})$ = 15% and $\varepsilon_1^f(1)$ $(=\varepsilon_1^f(\tau)|_{\tau=1})$ = $\varepsilon_2^f(1)$ $(=\varepsilon_2^f(\tau)|_{\tau=1})$ = 0 ~ 0.5%. The same is true for the simulation of the shrinking processes during the water desorption.

2. The moisture content at the fiber saturation point was estimated from the values of $\varepsilon_1^m(1)$, $\varepsilon_2^m(1)$, $\varepsilon_1^f(1)$ and $\varepsilon_2^f(1)$. If the values of $\varepsilon_1^m(1)$ and $\varepsilon_2^m(1)$ are assumed to be 15%, and those of $\varepsilon_1^f(1)$ and $\varepsilon_2^f(1)$ are assumed to be 0%, the moisture content at the fiber saturation point is calculated to be 35 (%), which is close to the experimental value.

Those indicate that the hygroexpansion of the wood cell wall is controlled by the mechanism of the reinforced matrix hypothesis.

From these results, we can conclude that the matrix substance as a skeleton in the secondary wall of the softwood tracheid tends to swell isotropically up to 15% by the water sorption, however, the CMF as a crystalline framework of polysaccharide bundle almost would not swell by the water sorption.

4-2 Origin of hygroelasticity of wood – microscopic mechanism

4-2-1 Background

In Chapter 2, perceiving Barber's (1968) circular cylinder model consisting of the S2 layer which is a developed version of Barber and Meylan's (1964) original one, we generalized it into the new one having a multi-layered cell wall consisting of the CML, S1, S2, and G layers. And, we formulated the dimensional change of the single wood fiber model that is caused by a certain physical state change occurring in the cell wall. By using the newly-derived formulas, we simulated the dynamics of the growth stress generation in the softwood fiber (in Section 3-1, Chapter 3), and the anisotropic drying shrinkage of the softwood fiber due to moisture desorption (in Section 4-1, present chapter).

In this section, we formulate elastic deformation of the single softwood fiber caused by the action of the axial traction, and we discuss the contribution of each constituent material to the elastic properties of the clear wood specimen through simulating the relationships between the moisture content (t), the microfibril angle in the S2 layer (MFA) and the longitudinal Young's modulus (E_L). The formula that predicts the dimensional change of elastically deformed wood fiber has various parameters which represent mechanical or physical properties of the constituent materials, however, some of them are impossible to be measured by the observation despite that their physical meanings are clearly defined. Values of those parameters can be optimized through the comparison between the simulated results and the observed phenomena, which enables us to estimate the microscopic structure and internal properties of each cell wall constituent as it exists in the cell wall layer. Deep understanding of the microscopic information on each cell wall constituent tends to develop a new technology or destination when we use the forest resources as the raw materials for timber or paper.

4-2-2 Formulas describing the longitudinal Young's modulus and the Poisson's ratio of the wood fiber model

(a) Behaviors of the softwood fiber model

The simultaneous equations (2-29-1~5) derived in Chapter 2 can be used for the present analysis. In the present chapter, we assume the steady moisture condition, therefore, $d\varepsilon_1^m$, $d\varepsilon_2^m$, $d\varepsilon_3^m$, $d\varepsilon_1^f$, $d\varepsilon_2^f$, and $d\varepsilon_3^f$ must be all nil, and S_1, S_2, and S_3 in $\mathbf{p}$ should take constant

values. Thus, we can simplify eqs.(2-29), and the following equation were derived from them:

$$E_L = (1/\pi r_0^2)(dP_L/d\varepsilon_L) = 1/(\pi r_0^2 f_{17}(\mathbf{p})) , \qquad \nu_{LT} = -(d\varepsilon_t^{r1}/d\varepsilon_L) = -f_{27}(\mathbf{p})/f_{17}(\mathbf{p}) . \qquad (4\text{-}11)$$

In the present analysis, we formulate the elastic deformation of the single softwood fiber model, which consists of the CML, the S1, and the S2 layers. The value of ρ_3 must be null. Average moisture content t is an implicit parameter in eqs.(4-11). Here, we will examine the effect of the moisture content on the value of E_L and ν_{LT}.

(b) Determining the values of the parameters in the equations

When calculating the values of E_L and ν_{LT} by using formulas (4-11), we need to give proper values to the parameters, E_1, E_2, S_0, S_1, S_2, ρ_1, ρ_2, h/r_1, and θ in advance.

When we determine the values of E_1, E_2, S_0, S_1, and S_2, the axial Young's modulus of the cellulose crystal (E_{cry}), that of the dried oriented polyose in the framework bundle (E_{poly}), and the isotropic Young's modulus of the MT substance (E_{matr}) become important factors in addition to the weight ratio of the framework polysaccharide to the matrix substance in each cell wall layer (A) and its crystallinity (C). In the same manner as in the previous sections, we assume E_{cry}=134 GPa, E_{poly}=8GPa, $E_{matr}|_{t=FSP}$=2GPa, and $E_{matr}|_{t=0}$=4GPa. We adopt eqs.(4-10) as t-dependent shapes of $E_{matr}(t)$ and $\psi(t)$. Moreover, we assume the values of A and C in each layer as shown in Table 4-3. Based on those assumptions, we determine the values and t-dependent patterns of $E_1(t)$, $E_2(t)$, $S_1(t)$, and $S_2(t)$ by using eqs.(4-5). The value of S_0 is determined from eq.(3A-1').

The values of the parameters ρ_1, ρ_2, and h can be estimated by the formulas on the relationships between the oven-dried density of the specimen and the volume ratio of each layer to the whole cell wall (see eqs.(4-9)). Parameters ρ_1, ρ_2, and h depend on the moisture content, however, their changes due to the moisture adsorption are so small. In the present analysis, we assume $\rho_1(\tau)\approx\rho_1^0$, $\rho_2(\tau)\approx\rho_2^0$, and $h\approx h^0$.

4-2-3 Case studies

(a) Moisture content dependency of the longitudinal Young's modulus

The longitudinal Young's modulus of the wood (E_L) often decreases as the moisture content increases up to the FSP, and becomes constant above the FSP (Kollmann and Krech 1960). Many researchers have reported that E_L tends to decrease to 60 - 70% of the initial value from the oven-dried state to FSP.

It is generally believed that the reduction of the elastic modulus of the wood due to the increase of the moisture content is caused mainly by the hygro-softning of the matrix substance which is an isotropic mixture of lignin, hemicellulose, and amorphous domain of the polysaccharide framework bundle. In this section, we try to verify this explanation on the basis of the mechanical analysis using eq.(4-11).

E_L in eq.(4-11) are controlled by various parameters, and some of them depend on the moisture content (τ) as mentioned before. In the present simulation, the author examines the effect of the moisture content in the cell wall upon the value of E_L, and then adopt 2 GPa and 4 GPa as the standard values for E_{matr} at FSP and the oven-dried state, respectively. Moreover, as the value of E_{matr} at the oven-dried condition, various values besides 4 GPa are assumed, and thus the relationship between E_L and the moisture content is calculated. In this section, we analyze the experimental result on the moisture dependency of the longitudinal Young's modulus of clear wood specimen of black spruce revealed by Kollmann and Krech (1960). The weight ratio of the polysaccharide framework to whole substance in each layer and its crystallinity are supposed in Table 4-4.

Table 4-4. Weight ratio of the polysaccharide framework to whole substance in each layer of the secondary wall (*A*), and the relative crystallinity of the framework (*C*).*

	Polysaccharide framework (*A*)	Oriented Polyose in the framework	Crystallinity of the framework (*C*)
CML	15 (%)	0 (%)	100 (%)
S1	26	6	76.9
S2	52	12	76.9
S3	- - - - -		- - - - -

* supposed values for spruce (*Picea sp.*) mature wood.

Table 4-5. Values of the parameters used for the simulation.

Moisture condition	E_1	E_2	S_1	S_2	F	ρ_1	ρ_2
Oven-dried	##	##	##	##	0.122	#	#
Fiber saturation point	26.8 *	53.6 *	1.04 *	0.784 *	0.122 *		

* units: GPa, ## estimated from eq.(4-5) and Table 4-4. # spruce, early wood tracheid, estimated from oven-dried wood density and eqs. (4-9).

Table 4-5 shows the values of the parameters E_1, E_2, S_1, S_2, F ($=S_0 \cdot h/(E_1 \cdot r_1)$), ρ_1, and ρ_2 which

are used in the simulation.

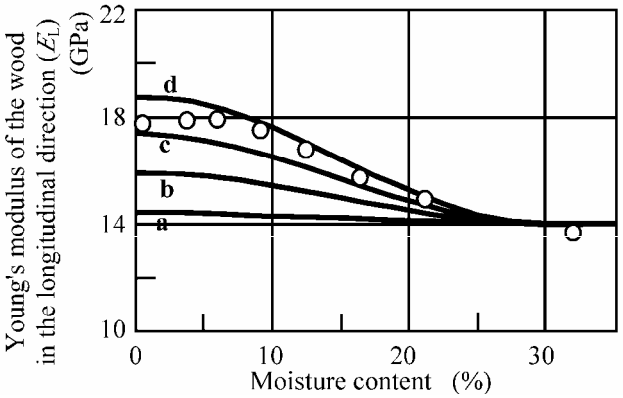

Fig.4-5. Moisture content dependency of the longitudinal Young's modulus of the wood (E_L). Dots are experimental results obtained from a clear wood specimen of white spruce (density 0.48g/cm³, Kollmann & Krech (1960)). Curves are simulated results under the conditions listed in Tables 4-4 and 4-5. In this simulation, the value of E_{matr} increases monotonously from 2GPa at FSP to **a**; 4, **b**; 12, **c**; 20, **d**; 28 GPa at the oven-dried state. MFA in the S2 is supposed to be 10 GPa.

The simulated results are shown in Fig.4-5. Dots represent experimental data of spruce specimens whose density is 0.48g/cm^3 (Kollmann and Krech 1960). Moreover, the MFA in the S2 layer of the experimental specimen had been left unknown. However, considering the specimen used in Fig.4-5 is composed of sufficiently matured tracheids, 10 degrees as the MFA may be assumed when calculating eq.(4-11). In order to obtain a reasonable simulation, we need to assume 24~28 GPa as the value of E_{matr} at the oven-dried state. This is quite larger as compared to the standard value of 4GPa, furthermore, it is in excess of the value of E_{poly} which is the elastic modulus of the dried polyose. According to the present calculation, the content of non-crystalline oriented polyose in the framework has a quite small effect on the relationship between the moisture content and E_L. Accepting both Cousins' (1976, 1978) experiments and the reinforced-matrix hypothesis, one cannot help regarding this result as an unreasonable crux. As the origin of such crux, the following possibilities (1), (2), and (3) are referred to:

(1) Inside the actual wood cell wall, E_{matr} takes on a value of 2 GPa at FSP, however, it takes several times as large a value as that of isolated MT substance at the oven-dried condition.

(2) Inside the actual wood cell wall, E_{matr} takes on several times as large a value as that of isolated MT substance not only at the oven-dried condition but also within a large range of moisture content. However, if the properties of the compound middle lamella (CML) become very compliant with water sorption, then shear or slipping deformations will be caused between adjoining fibers by the tensile load. Thus, E_L becomes considerably small with increasing moisture content.

(3) Inside the actual wood cell wall, E_{matr} takes on values of 2 GPa at FSP, and 4 GPa at oven-dried condition. On the other hand, the polysaccharide framework as a bundle becomes more stiff as the moisture content decreases.

At present, it is not sure which possibility holds, however, an experiment can be proposed so as to verify the possibility (1). If this possibility would be the right one, the reduction of the E_L due to water sorption should become more remarkable in specimens with large MFA than in the one with small MFA. Therefore, it is planned to examine the possibility (1) through an experiment using samples prepared from normal wood and compression wood. However, Kojima and Yamamoto (2004) recently showed that this reduction becomes less distinct as the MFA increases by using specimens of sugi early wood specimen having different MFAs. If the result reported by Kojima and Yamamoto (2004) would hold in general, the possibility (1) is rather disputable for explaining the moisture content dependency of E_L.

It is quite difficult to admit possibility (2) because of the following reasons: First, the wood can be regarded as a continuous parallel fiber lamina consisting of numerous tracheid, thus, it is expected that the contribution of the elastic modulus in the CML to E_L becomes quite small according to the simple rule of mixture (Mallick 1988). Second, if shear or slipping deformations would occur in the CML between adjoining fiber at high moisture content, we expect that many tracheids would have pulled out from one another along the CML when the specimen was broken in tension. On the basis of the scanning electron microscopic observation, Saiki (1976) revealed that separation of the tracheid frequently seems to occur along the CML in the late wood zone, on the other hand, failure in the early wood zone takes the form of brittle tension with separation occurring across the cell walls. Moreover, several researcher, including Saiki (1976), have demonstrated that what appeared to be a pull-out failure in the CML was actually a failure in the outer region of the secondary wall even in the case of high moisture content (e.g. Mark 1967).

As to the possibility (3), the author can propose possible two ideas as follows. One is that the stiffness of the crystal part in the cellulose microfibril becomes higher with the decrease of moisture content. This may sound more or less strange since the pure crystal part would not react with the water molecule. The other is that the content of the cellulose crystal in the polysaccharide framework tends to increase with the reduction in the moisture content. As to this idea, it is required to review the mechanical contribution of the noncrystalline oriented polyose in the framework bundle to the cell wall elasticity. Then, to discuss this idea while still accepting 4GPa as the standard value of E_{matr} at the oven-dried state, the following

hypothesis is assumed on the mechanical property of the polysaccharide framework bundle:

> From a mechanical point of view, there is an intermediate domain between rigid crystal and completely disordered amorphous domains in the wood CMF in the polysaccharide framework bundle, and that such a domain fluctuates between crystal-like and amorphous-like states in accordance with the moisture adsorption. The crystal-like state, which is mechanically close to the complete crystal domain, tends to increase with water desorption. Therefore, the axial Young's modulus of the oriented polysaccharide framework as a bundle tends to increase as the moisture content decreases. Transformation from amorphous-like to crystal-like states is more or less reversible. This is a main reason why the longitudinal Young's modulus of wood becomes higher with drying.

Based on this idea,[(1), (2)] the moisture dependency of the E_L was simulated. Results are shown in Fig.4-6. A reasonable simulation is obtained assuming that the oriented polyose in the polysaccharide framework (as assumed in Table 4-4) is regarded as the unstable domain in the wood CMF, thus, it is expected that the content of the unstable domain in the secondary wall reaches about one-third as much as the content of the stable crystal domain. This result is also effective for simulating the behaviors of specimens with the densities other than 0.48 g/cm^3 (see Fig.4-7). In those cases, it is assumed that non-cellulosic oriented polyose, *e.g.* acetyle-glucomannan, and stable amorphous cellulose in the framework bundle should be regarded as the matrix substance, for convenience.

On the basis of above discussion, we propose an imaginative model of the fine structure of the wood cell wall as shown in Fig.4-8 (see also Yamamoto 2000). It is imagined that deposition of the matrix substances, especially the cellulose-affinitive polyose, *e.g.* acetyle-glucomannan, induces the stable amorphous domains here and there on the surface of the CMF, and the unstable domain as an intermediate state is formed around each stable amorphous domain in the CMF.[(3)]

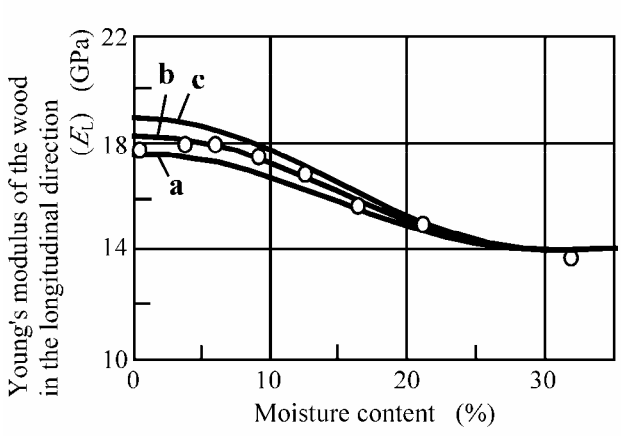

Fig.4-6. Moisture content dependency of the longitudinal Young's modulus of the wood (E_L). Dots are experimental results obtained from a clear wood specimen of white spruce (density 0.48g/cm^3, Kollmann & Krech (1960)). Curves are simulated results.
Note: (1) In this simulation, it is supposed that the CMF contains unstable cellulose which changes from compliant amorphous-like states to rigid crystal-like states in accordance with the moisture desorption. For convenience, we regarded the oriented polyose assumed in Table 4-4 as the unstable cellulose domain. Therefore, non-cellulosic oriented polyose are integrated into the matrix substance in this simulation.
(2) We assumed the value of E_{matr} increases monotonously from 2GPa at FSP to 4GPa at oven-dried state. (3) The weight ratio of the stable crystal in the CMF to whole substance in each layer of the secondary wall is assumed to be 40% (S2) and 20% (S1) (see Table 4-4). (4) In this simulation, we assume that the ratio of unstable cellulose in the CMF to whole substance in each layer of the secondary wall is: **a**; 10% (S2), 5% (S1), **b**; 12% (S2), 6% (S1), **c**; 14% (S2), 7% (S1). MFA in the S2 layer is assumed to be 10 degrees.

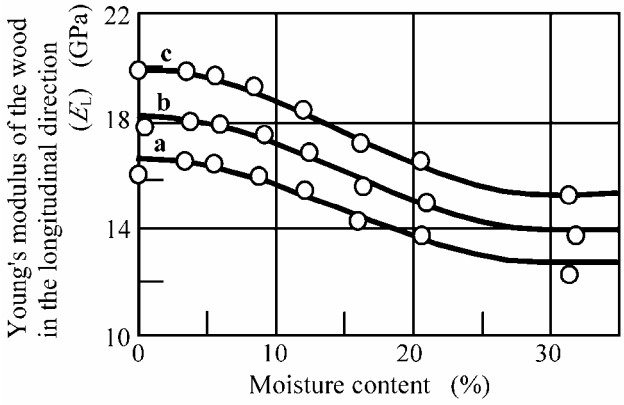

Fig.4-7. Moisture content dependency of the longitudinal Young's modulus of the wood (E_L). Dots are experimental results obtained from clear wood specimens of white spruce (density **a**; 0.44, **b**; 0.48, **c**; 0.52g/cm^3, Kollmann & Krech (1960)). Curves are simulated results.
Note: (1) It is supposed that the polysaccharide framework contains unstable cellulose domain which changes from compliant amorphous-like states to rigid crystal-like states in accordance with moisture desorption. For convenience, we regarded the oriented polyose assumed in Table 4-4 as the unstable cellulose domain. Therefore, non-cellulosic oriented polyose are integrated into the matrix substance in this simulation.
(2) We assumed the value of E_{matr} increases monotonously from 2GPa at FSP to 4 GPa at the oven-dried state. (3) The weight ratio of the stable crystal in the CMF to whole substance in each layer of the secondary wall is assumed to be 40% (S2) and 20% (S1) (see Table 4-4). (4) In this simulation, the ratio of unstable domain in the CMF to whole substance in each layer of the secondary wall is 12% (S2) and 6% (S1). MFA in the S2 layer is assumed to be 10 degrees.

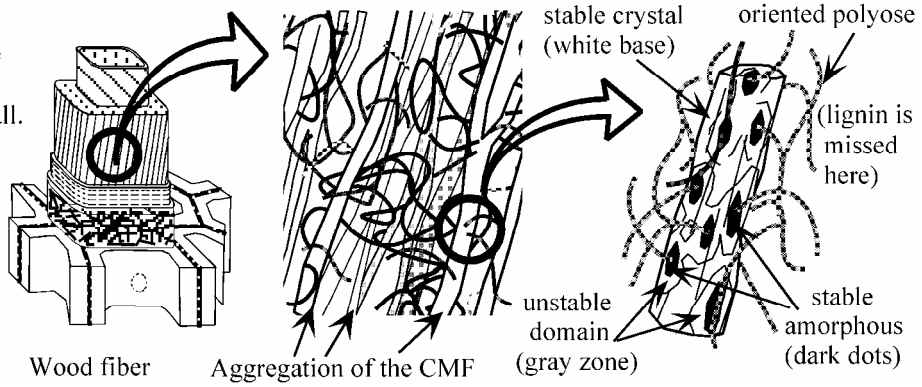

Fig.4-8. An imaginative model of the fine structure of the wood cell wall.

(b) MFA dependency of the longitudinal Young's modulus

Many researchers have reported that the longitudinal Young's modulus of the clear coniferous wood specimen tends to decrease as the MFA in the S2 layer increases (Cave 1968, Sobue and Asano 1976). Their conclusions were confirmed also by the experiment using an isolated softwood fiber (Page et.al. 1977). Furthermore, many authors have tried to explain its origin by using the theoretical models having unidirectionally reinforced cell walls (Norimoto et.al. 1967, Cave 1968, 1972, 1978, Sobue and Asano 1976, Salmen 1982, Salmen and De Ruva 1985, Koponen 1991). Then, based upon the wood fiber model introduced in the present study, it is tried to simulate the MFA-dependency of the substantial Young's moduli of the wood in the longitudinal direction (E_L^W), which is defined as follows:

$$E_L^W = E_L \frac{\rho^W}{\rho_0} \quad ,$$

where ρ^W is the density of the cell wall, and ρ_0 is the density of the wood in the oven-dried condition. When using the formulae (4-2) and (4-3), the weight ratio of the polysaccharide framework (A) and its crystallinity (C) in each layer is assumed as shown in Table 4-6.

Table 4-6. Weight ratio of the polysaccharide framework to the whole substance in each layer (A), and its crystallinity (C).

	(Case 1)		(Case 2)		(Case 3)		(Case 4)	
	A	*C*	*A*	*C*	*A*	*C*	*A*	*C*
CML	15	100	15	100	15	100	15	100
S1	30	40	30	60	30	80	30	100
S2	60	40	60	60	60	80	60	100
S3	---	---	---	---	---	---	---	---

Simulated results were plotted with the observed ones in Fig.4-9. The observed ones were obtained at the air-dried condition (20-25˚C, 50-65% RH), and the simulated results were given under the supposition that the moisture content is 12%. And, it was assumed that unstable cellulose in the crystal-like state, if there were, is integrated into the crystal part of the polysaccharide framework, for convenience. Fig.4-9 demonstrates that the observed result can be quantitatively simulated when the ratio of the polysaccharide framework and its crystallinity in each layer are chosen adequately, which suggests that the elastic properties of the wood can be formulated on the basis of the reinforced-matrix model.

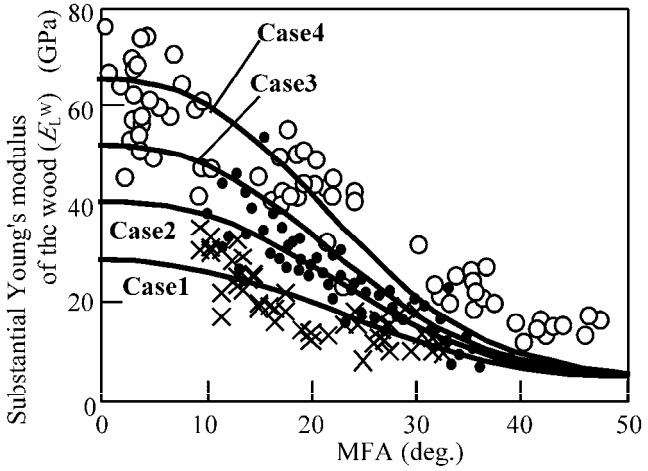

Fig.4-9. Relationship between substantial Young's modulus of the wood (E_L^W) and the microfibril angle in the S2 layer (MFA).
○ ; An isolated holocellulose fiber of *Spruce sp.* (Page et al. 1977).
● ; A thin specimen of *Pinus radiata* (Cave 1978).
× ; A thin specimen of sugi (*Cryptomeria japonica* (Sobue & Asano 1976)).
All specimen were measured under the air-dried conditions. Curves are simulated results. It is supposed that the oven-dried density of the wood is 0.48 g/cm³.

Conditions for the simulation: (1) Weight ratio of the polysaccharide framework to the whole substance in each layer and its crystallinity are assumed as shown in Table 4-6. (2) E_{matr} tends to increase monotonously from 2GPa at FSP to 4GPa at oven-dried state. (3) Average moisture content of the cell wall is assumed to be 12% in this simulation. (4) It is assumed that unstable cellulose in the crystal-like state, if there were, are integrated into the crystal part in the polysaccharide framework in this simulation.

From Fig.4-9, it becomes obvious that the relationship between the MFA and E_L^W is dependent upon tree species. Regarding the dependency of the relationship between MFA and E_L^W on species origin, the following possibilities (1), (2), and (3) can be referred to:

(1) The content of the polysaccharide framework and its crystallinity is different among species, or between the mature wood and juvenile wood in the same trunk. This is a problem concerning the biosynthesis of the secondary xylem.

(2) Crystallinity of the polysaccharide framework tends to vary with time, which changes the ratio of the cellulose crystal to non-crystalline components. This presents a problem regarding the time-dependent properties of the material mechanics after lumbering.

(3) Drying and heating processes give an irreversible change to the cohesion state of each cell wall component as pointed out by Furuta et.al. (1998). In such cases, the value of E_{matr} is different from the original value.

At present, the proprieties of the above-mentioned possibilities (1), (2), and (3) cannot be examined, since we have no information on the sampling positions and ages of the materials used for the experiment in Fig.4-9. Thus, a proper experiment needs to be planed in order to make clear which possibility among (1), (2), and (3) is the most reasonable.

(c) Role of the S1 layer on the Poisson's ratio of the wood fiber model

In authors' previous papers, by using a three layered wood fiber model, it was pointed out that

the S1 layer plays an important part in the growth stress generation and the transverse dimensional stability (Yamamoto et.al. 1995, 2001). However, regarding the influence of the S1 layer on the mechanical properties of the wood, many problems have remained unsolved. Thus in the present paper, the contributions of the S1 layer to the longitudinal Young's modulus E_L and the Poisson's ratio ν_{LT} are discussed.

As an indicator of the thickness of the S1 layer, the author adopts the thickness ratio of the S1 layer to the S2 layer , which is defined as

$$\lambda = (r_1 - r_2)/(r_2 - r_3) = \rho_2(\rho_1 - 1)/(\rho_2 - 1) .$$

Then, supposing the various values of λ, the longitudinal Young's modulus and the Poisson's ratio of the wood fiber model whose oven-dried density is 0.48 g/cm^3 were calculated. It is assumed that the moisture content is 12 %, and the MFA in the S2 layer is 10 deg. Simulated results are shown in Fig.4-10. According to the simulation, the longitudinal Young's modulus E_L becomes almost constant regardless of the value of λ. On the other hand, the longitudinal Poisson's ratio ν_{LT} becomes abruptly larger with decrease of λ, and with increase of the weight ratio of the cellulose crystal to the MT substance.

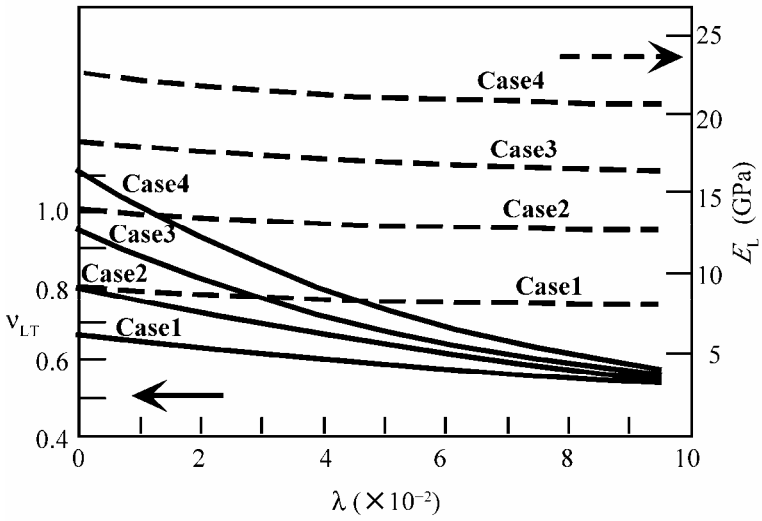

Fig.4-10. Effect of relative thickness of the S1 layer on the longitudinal Young's modulus (E_L) and Poisson's ratio (ν_{LT}). – Simulated results are obtained from eqs.(4-11).
Note: (1) λ is defined as;
$\lambda = (r_1 - r_2)/(r_2 - r_3) = \rho_2(\rho_1 - 1)/(\rho_2 - 1)$.
(2) Standard value of λ is 0.0952.
(3) In this simulation, conditions for parameters are all identical with those of Fig.4-9 except the micro-fibril angle in the S2 layer (MFA). In this case, the MFA is supposed to be 10 deg.

According to the formulae described in our previous section, the values of ρ_1 and ρ_2 in the typical early softwood whose oven-dried density is 0.48 are estimated as 1.015 and 1.187 respectively, hence, the most reasonable value of λ is calculated as 0.0952. When λ is equal to 0.0952, ν_{LT} tends to converge on 0.5 - 0.6 regardless of the weight ratio of the cellulose crystal to the MT substance. Such values closely coincide with the Poisson's ratio of the actual normal wood.

It may be a little hasty to deduce the conclusion obtained from a single fiber model to the macroscopic wood, however, it seems quite reasonable to consider that the longitudinal Poisson's ratio of the wood is highly affected and controlled by the S1 layer.

(d) Recyclable properties of the paper and the fine structure of the wood cell wall

Deterioration of the global environment due to increasing atmospheric carbon dioxide has been a serious problem since 20th century. Many scientists consider that biological mitigation, *e.g.* protection and conservation of the forest environment, becomes one of the most effective solutions to stop the increase of the atmospheric carbon dioxide. On the other hand, excessive exploitation had irreversibly deteriorated the natural forest in many tropical countries. Some scientists recommend the afforestation of the man-made forest of the fast-growing species in order to recover the collapsed green environment in the tropical countries. They consider that the fast-growing species having a very high growth rate can quickly mitigate increasing atmospheric carbon dioxide. If the plantation activity of those species could be supported from the economical viewpoint, it would be realized and become diuturnal one.

Another way to stop the increase of atmospheric carbon dioxide is to develop the technique to prolong the lifetime of the forest products. For example, Ona et al. (2004) notices the necessity of recycle use of the paper resources. Then, they tried to make clear the recyclable properties of the paper by retracing the properties of raw material.

The fibers in the dried paper sheet are glued each other by the force of hydrogen bond. However, once the dry paper is immersed in the water, the cell wall swells again, then, the paper is disjointed into the fibers in the water. After several repetitions of the drying and wetting process, deterioration of each fiber wall gradually progresses, coincidently, the strength of the recycled paper becomes lower. Okayama et al. (2004) found that the tensile index of the paper manufactured from *Acacia spp*. rapidly decreases with the repetitions of the recycle treatment, however, the zerospan tensile index of the paper, which is an indicator of the strength of individual fiber, does not decrease with the repetitions of the recycle treatment. From this result, they considered that a decrease in the strength of the recycled paper is attributable not to the decrease in the tensile strength of the fiber but to the decrease in the coherence between the fibers in the sheet, and they hypothesized that such a decrease in the cohesion between fibers is induced by the “cornification” of the fiber wall. They explained that cornification gradually progresses in the fiber wall after several repetitions of the drying and wetting process. As the result, the swelling ability of the fiber wall decreases with the

number of recycle use, thus, the ability of the hydrogen bond in the fiber wall remarkably decreases. This is a reason why the tensile index of the paper sheet tends to decrease with the number of recycle use.

Ona et al. (2004) reported that the recyclable index of the papers manufactured from 9.5-year-old plantation trees of *Eucalyptus globulus* are scattered unevenly in spite that the strengths of the virgin papers become uniform. Moreover, they found that the recyclable index of the paper showed a high positive correlation with the percentage of hemicellulose (specifically, oriented polyose), on the other hand, a high negative correlation with the cellulose percentage in the raw material. Those results suggest that the oriented polyose in the fiber wall plays a certain part in inhibiting the progress of the cornification in the fiber wall, that is to say, further crystallization of the cellulose microfibril due to the repetitions of the recycle treatment.

It is considered that their discoveries are highly related to the author's prediction on the fine structure of the wood cell wall. It is expected that an irreversible crystallization occurs in the unstable domain of the CMF with the repetition of the drying and wetting process, which is a major cause of the cornification of the fiber wall in the recycled paper.

4-2-4 Summary and concluding remarks

In this section, on the basis of the reinforced-matrix hypothesis, the elastic deformation of the isolated wood fiber was formulated. Thereafter, some case studies on the elastic behaviors of the wood were analyzed by using the newly-derived formulas. As a result, following conclusions were obtained:

1. On the origin of the moisture dependent change of the longitudinal Young's modulus of the clear wood specimen –

There is an intermediate domain between rigid crystal and completely disordered amorphous domains in the CMF in the polysaccharide framework bundle, and that such a domain fluctuates between crystal-like rigid state and amorphous-like compliant state in accordance with the moisture adsorption. This is a main reason why the longitudinal Young's modulus of wood becomes higher with drying.

2. On the origin of the species dependency of the Young's modulus of the cell wall in the direction along the fiber axis –

We derived following three possibilities as the reason to explain the origin of the species

dependency of the relationship between the MFA and E_L^W:

i) Content of the polysaccharide framework and its crystallinity is different among species, or between the mature wood and juvenile one in the same trunk.

ii) Crystallinity of the polysaccharide framework tends to vary with time, which changes the ratio of the cellulose crystal to non-crystalline substance as the time goes on.

iii) Drying and heating processes give an irreversible change to the cohesion state of each cell wall component in the tested specimens. In such a case, the value of E_{matr} would be different from the original one.

3. On the role of the S1 layer in the longitudinal Young's modulus E_L and the Poisson's ratio ν_{LT} –

The S1 layer almost does not affect the value of E_L, however, the thickness ratio of the S1 to the S2 layer highly affects the value of. ν_{LT}. When λ (=$(r_1-r_2)/(r_2-r_3)$) takes the realistic value, ν_{LT} tends to converge on 0.5 - 0.6 regardless of the weight ratio of the cellulose crystal to the MT substance. Such values closely coincide with the Poisson's ratios of the actual normal wood. On the other hand, ν_{LT} becomes unreasonably larger when $\lambda$is assumed to be nearly 0. Thus, the S1 layer takes an important role in determining the longitudinal Poisson's ratio of the wood fiber.

4. Recyclable properties of the paper and the fine structure of the wood cell wall –

Decrease in the strength of the recycled paper is attributable not to the decrease in the tensile strength of the fiber but to the decrease in the coherence between the fibers in the paper sheet, which is induced by the cornification of the fiber wall. It is expected that an irreversible crystallization occurs in the unstable domain of the CMF with the repetition of the drying and wetting process, which is a major cause of the cornification of the fiber wall in the recycled paper.

Footnote

(1) Salmen (1982) pointed out possibility that a hygro-plasticization occurs in the disordered non-crystalline regions of the polysaccharide framework of the wood pulp fiber, and successfully explained the drastic reduction of the elastic modulus of the wood pulp fiber

and the paper when the are immersed in water. At the same time, by using the laminate plane model of the cell wall, and he showed that the observed reduction of E_L in the wood fiber due to moisture adsorption can be predicted by the softening of the hemicellulose (Salmen & De Ruvo 1985). Then, he deduced that no noticeable hygroplasticization due to water impregnation takes place in the CMF of the wood cell wall. Thus, he considered that hygroplasticization of the hemicellulose causes the drastic reduction of the elastic moduli of the wood pulp fiber and the paper when they absorb much moisture.

(2) If one consider the possibility (3) is proper, it may be regarded that the conclusion deduced from Section 4-1 in this chapter was more or less meaningless, since the simulations in Section 4-1 was carried out based on the wood fiber model which produces no unstable domain in its framework bundle. As a trial, taking the above-mentioned hypothesis (*i.e.* possibility (3)) into consideration, the author calculated the relationship between the MFA and the oven-dried shrinkage. However, there was almost no difference in deduced conclusions between before and after considering the effect of unstable domain in the framework bundle.

(3) Recently, Tokoh et al. (1998) observed that the cellulose microfibrils of *Acetobacter xylinum* formed in medium containing acetyle-glucomannan are loosely arranged in contrast to the stiff ribbon-like fibrils formed in the control medium. They further noticed that with the glucomannan, drop-like structures of hemicellulose are developed around the base of the microfibrils. It was therefore concluded that the deposition of the matrix substance, that is, cellulose-affinitive polyose, into the CMF aggregates would not only induce the stability of bundle shape but also assist in the formation of the heterogeneous configuration in the polysaccharide bundle.

References in Chapter 4

Barber, N.F.: A theoretical model of shrinking wood, *Holzforschung*, **22**, 97-103 (1968).

Barber, N.F., Meylan, B.A.: The anisotropic shrinkage of wood. A theoretical model. *Holzforschung*, **18**, 146-156 (1964).

Barrett, J.D., Schniewind, A.P., Taylor, R.L.: Theoretical shrinkage model for wood cell walls. *Wood Science*, **4**, 178-192 (1972).

Bodig, J., Jayne, B.A.: "Mechanics of wood and wood composites". Van Nostrand Reinhold Com., New York, 1982.

Carrington. H.: The elastic constants of spruce as affected by moisture constant, *Aeron. J.*, **26**, 462 (1922).

Cave, I.D.: Theory of X-ray measurement of microfibril angle, *For. Prod. J.*, **16**, 37-42 (1966).

Cave, I.D.: Anisotropic elasticity of the plant cell wall, *Wood Sci. Technol*., **6**, 284-292 (1968).

Cave, I.D.: A theory of shrinkage of wood, *Wood Sci. Technol*., **6**, 284-292(1972).

Cave, I.D.: Modelling moisture-related mechanical properties of wood. part II. Computation of properties of a model of wood and comparison with experimental data, *Wood Sci. Technol*., **12**, 127-139 (1978).

Cousins, W.J.: Elastic modulus of lignin as related to moisture content, *Wood Sci. Technol*., **10**, 9-7 (1976).

Cousins, W.J.: Young's modulus of hemicellulose as related to moisture content, *Wood Sci. Technol*. **12**, 161-167 (1978).

Fung, Y.C.: "Foundation of Solid Mechanics," Prentice-Hall, Englewood Cliffs, New Jersey, 1965.

Furuta ,Y., Norimoto, M., Yano, H.: Thermal-softning properties of water-swollen wood V. The effect of drying and heating histories, *Mokuzai Gakkaishi*, **44**, 82-88 (1998).

Gibson, L.J., Ashby, M.F.: "Cellular Solids. Structure and Properties," Pergamon Press, Oxford, 1988.

Guitard, D.: "Mecanique du Materiau Bois et Composites," Cepadues-Editions, Toulouse, 1987.

Kojima, Y., Yamamaoto, H.: Properties of cell wall constituents in relation to longitudinal elasticity of wood. Part 2. Origin of the moisture dependency of the longitudinal elasticity of wood, *Wood Sci. Technol.*, **37**, 427-434 (2004).

Kollmann, F., Krech, H.: Dynamic measurement of Damping Capacity and elastic properties of wood. *Holz als Roh- und Werkstoff* **18**: 41-54 (1960).

Kollmann, F.F.F., Cote, W.A. Jr.: "Principles of wood science and technology. I Solid wood", Springer-Verlag, Berlin, pp. 292-419, 1968.

Koponen, S., Toratti, T., Kanerva, P.: Modelling longitudinal elastic and shrinkage properties of wood, *Wood Sci. Technol*., **23**, 55-63 (1989).

Koponen, S., Toratti, T., Kanerva, P.: Modelling elastic and shrinkage properties of wood based on cell structure,

Wood Sci. Technol., **25**, 25-32 (1991).

Lekhnitski, S.G.: "Theory of Elasticity of an Anisotropic Elastic Body," Holden Day, San Francisco, 1960.

Mallick, P.K.: "Fiber-reinforced composites. Materials, manufacturings, and design", Marcell Deckker Inc., New York, pp.73-128, 1988.

Mark, R.E.: "Cell wall mechanics of tracheids", Yale Univ. Press, New York, 1967.

Meylan, B.A.: Measurement of microfibril angle by the X-ray diffraction, *For. Prod. J*., **17**, 51-58 (1967).

Meylan, B.A.: Cause of high longitudinal shrinkage of wood, *For. Prod. J.* **18**, 75-78 (1968).

Meylan, B.A.: The influence of microfibril angle on the longitudinal shrinkage-moisture content relationship, *Wood Sci. Technol*., **6**, 293-301 (1972).

Nishino, T., Takano, K., Nakamae, K.: Elastic modulus of the crystalline regions of cellulose polymorphs, *J. Polym. Sci., Part B, Polym. Phys. Ed*., **33**, 1647-1651 (1995).

Norimoto, M., Yamada, T.: The effect of moisture content on modulus of rigidity and dielectric properties of wood, *Wood Research*, **41**, 36-46 (1967).

Okayama, T., Kibatani, Y., Nakayama, K., Kojima, Y., Ona, T.: Fiber properties and papermaking potential of recycled Acacia pulp, In "Improvement of forest resources for recycled forest products, Ona, T. (ed.)," Springer-Verlag Tokyo, Tokyo, 2004, pp.52-59.

Okuyama ,T., Yamamoto, H., Iguchi, M., Yoshida, M.: Generation process of growth stresses in cell walls (II). Growth stresses in tension wood, *Mokuzai Gakkaishi*, **36**, 797-803 (1990).

Ona, T., Kawana, J., Kibatani, Y., Ishikura, Y., Kojima, Y., Okayama, T.: Toward the construction of an efficient link between forest recycling and paper recycling using trees with high performance for paper recycling, "Improvement of forest resources for recycled forest products, Ona, T. (ed.)," Springer-Verlag Tokyo, Tokyo, 2004, pp.29-32.

Page, D.H., El-Hosseiny, F., Winkler, K., Lancaster, A.P.S.: Elastic modulus of single wood pulp fibers, *Tappi*, **60**, 114-117 (1977).

Sadoh, T., Christensen, G.N.: Longitudinal shrinkage of wood I. Longitudinal shrinkage of thin sections, *Wood Sci. Technol*., **1**, 26-44 (1967).

Saiki, H.: Proportion of component layer in tracheid wall of early wood and late wood of some conifers, *Mokuzai Gakkaishi*, **16**, 244-249 (1970).

Saiki, H.: Fractography of wood, *J. Soc. Mater. Sci. Japan*, **22**, 894-902 (1976).

Sakurada, I., Nukushina, A., Ito, T.: Experimental determination of the elastic modulus of crystalline regions in oriented polymers, *J. Polymer Sci.*, **57**, 651-660 (1962).

Salmen, L.: "Temperature and water induced softening behavior of wood fiber based materials", Ph.D. Thesis, KTH, Stockholm, pp.1-53,1982.

Salmen, L., De Ruva, A.: A model for the prediction of fiber elasticity, *Wood and Fiber Science*, **17**, 336-350 (1985).

Sobue, N., Asano, I.: Studies on the fine structure and mechanical properties of wood, *Mokuzai Gakkaishi*, **22**, 211-216 (1976).

Timoshenko, S.P., Goodier, J.N.: "Theory of Elasticity, 3rd edition", McGraw-Hill Kogakusha, Tokyo, 1970.

Tokoh, T., Takabe, K., Fujita, M., Saiki, H.: Cellulose synthesized by Acetobacter xylinum in the presence of Acetyle glucomannan, *Cellulose*, **5**, 249-261 (1998).

Tsoumis, G.: "Science and technology of wood, structure, properties, utilization," Van Nostrand Reinhold, New York, 1991.

Watanabe, U., Norimoto, M.: Shrinkage and elasticity of normal and compression wood in conifers, *Mokuzai Gakkaishi*, **42**, 651-658 (1996).

Yamamoto, H.: A model of anisotropic swelling and shrinking process of wood. Part 1. Generalization of Barber's wood fiber model, *Wood Sci. Technol*, **33**, 311-325 (1999).

Yamamoto, H.: An imagination on the structure of the wood cellulose is stirred by investigating the physical properties of the wood. *Cellulose Communication*, **7**, 9-15 (2000).

Yamamoto, H., Okuyama, T., Sugiyama, K., Yoshida, M.: Generation process of growth stresses in cell walls. IV. Action of the cellulose microfibrils upon the generation of the tensile growth, *Mokuzai Gakkaishi*, **38**, 107-113 (1992).

Yamamoto, H., Okuyama, T., Yoshida, M.: Generation process of growth stresses in cell walls. VI. Analysis of the growth stress generation by using a cell model having three layers (S1, S2, and I+P), *Mokuzai Gakkaishi*, **41**, 1-8 (1995).

Yamamoto, H., Okuyama, T., Sugiyama, K., Yoshida, M.: Generation process of growth stresses in cell walls IV. Action of the cellulose microfibril upon the generation of the tensile stresses, *Mokuzai Gakkaishi*, **38**, 107-113 (1992).

Yamamoto, H., Okuyama, T., Yoshida ,M.: Method of determining the mean microfibril angle of wood over wide range by the improved Cave's method, *Mokuzai Gakkaishi*, **39**, 375-381 (1993b).

Yamamoto, H., Sassus, F., Ninomiya, M., Gril, J.: A model of anisotropic swelling and shrinking process of wood. Part 2. A simulation of shrinking wood, *Wood Sci. Technol*., **35**, 167-181 (2001).

Yamamaoto, H., Kojima, Y.: Properties of cell wall constituents in relation to longitudinal elasticity of wood. Part 1. Formulation of the longitudinal elasticity of an isolated wood fiber, *Wood Sci. Technol.*, **36**, 55-74 (2002).

Yamamoto, H. ; Kojima, Y. ; Okuyama, T. ; Avasolo, W. P. ; Gril, J.: Origin of the biomechanical properties of wood related to the fine structure of the multi-layered cell wall, *Transaction of the ASME Journal of*

Biomechanical Engineering, **124**, 432-440 (2002).

Chapter 5

BIOMECHANICS OF TENSION WOOD PROPERTIES

5-1 Background - Dispute on the role of gelatinous layer in generation of the tension wood properties

Tension wood (TW) often shows characteristic behaviors differently from the normal wood (NW). A high tensile growth stress is generated in the differentiating xylem in the TW region, which often becomes ten times as large as that in the NW region (Okuyama et al. 1990, 1994). The longitudinal Young's modulus of the TW becomes significantly higher than that of the NW (Okuyama et al. 1990, Yamamoto et al. 1992). Moreover, the axial shrinkage of the TW tends to exceed more than 1% during water desorption, while the one in the NW becomes only 0.1~ 0.5% (Yamamoto et al. 1992, Yamamoto & Okuyama 1994). Therefore, formation of the TW in the log or the lumber often causes serious processing defects when the forest products are used for the timber or the raw material for furniture.

The TW often contains a large amount of abnormal fiber that is called gelatinous fiber (G-fiber) since it contains a gelatinous layer (G-layer) as the innermost layer of the secondary wall. Some authors attribute abnormal properties of the TW xylem to the intrinsic properties of the G-fiber (Okuyama et al.1990, 1994, Yamamoto et al. 1992, Clair et al. 2003). On the other hand, not a few researchers believe that the G-layer is mechanically too compliant to bear a large stress generation. They base their argument on the facts that the G-layer is often convoluted in the lumen of the transverse section which is sampled from the water swollen block, and it can be easily peeled off from the lignified layer in the same direction during microtoming. This gives the impression that it is attached only loosely to the remainder of the secondary wall (Kollman & Cote 1984). From those observations, they consider that the various characteristics of the TW should be attributed not to the "compliant G-layer" but to relatively thicker S1 layer (Boyd 1977), and/or to relatively thinner S2 layer whose microfibril angle (MFA) is expected to be more or less different from the one in the NW fiber (Norberg & Meier 1966, Scurfield 1973).

It is impossible to adjudge which possibility holds until we succeed in measuring

directly the mechanical and physical properties of the G-layer and the lignified layer by isolating them each other. However, it is still difficult to obtain the G-layer cylinder without inflicting any damage. No matter how a G-layer cylinder is obtained, it is almost impossible to provide an accurate measurement because the G-layer cylinder is too small to be analyzed by a conventional mechanical testing machine.

By the way, there is no specific difference on the anatomical and chemical aspects in the lignified layer between in the NW and in the TW fibers as pointed by Okuyama et al (1990). It may be quite natural to consider that the lignified layer in the G-fiber would be essentially same as that in the NW fiber, thus, the author expects that the G-layer is attributable to the origin of characteristic behaviors peculiar to the TW. In any case, to verify such an expectation, it is required to observe the behaviors or physical properties of the G-layer by isolating it directly from the lignified secondary wall, which is still impossible as mentioned above.

Simulation using a wood fiber model is one of the most convenient approaches to estimate the internal properties and fine structures of each constituent material as it exists in wood cell wall (Yamamoto et al. 2002, Yamamoto & Kojima 2002). In Chapter 2, we formulated mechanical behaviors of the wood fiber model, consisting of the compound middle lamella (CML), the outer layer of the secondary wall (S1), its middle layer (S2), and the innermost gelatinous layer (G), and derived a basic formula to simulate the deformation process of an isolated wood fiber when a certain biomechanical change occurs, such as cell wall maturation, the water adsorption, and the external load induction (Yamamoto 2004). The basic formula contains several parameters which are derived from the composite structure of the cell wall layer. When we simulate the observed phenomena by using this formula, we need to optimize those parameters so as to give a reasonable result. We consider that optimized values of those parameters should reflect intrinsic information on the internal properties and fine structure of cell wall constituents.

Objective in the present chapter is to clarify the role of the G-layer on the origin of characteristic behaviors of the TW xylem. Then, several TW properties from a 70 year-old Kohauchiwakaede (*Acer sieboldianum* Miq.) will be analyzed by using the analytical formula given in Chapter 2.

5-2 Experiment

5-2-1 Material and method

A 70-year-old kohauchiwakaede (*Acer sieboldianum* Miq.), grown on a steep slope at a private mountain in hikodani-river (彦谷), Kiyomi-cho, Gifu prefecture, Japan, 14 cm in DBH, having a leaning stem, was used for the experiment At breast height, ten measuring points were set peripherally on the xylem surface of the leaning stem. At each point, the released strain of the longitudinal growth stress on the xylem surface (ε_L^X) was measured using the ordinary strain-gauge method in early April 1988. Thereafter, rectangular portions, 70×10×5 mm and 50×10×5 mm in the longitudinal (L), tangential (T), and radial (R) directions, respectively, were sampled away from the upper or lower positions at each measuring point of the released strain. Then, respective portions were used to obtain the tensile Young's modulus under the green condition (E_L^X) and the longitudinal shrinkage (α_L^X) from green to the oven-dried condition (Yamamoto et al. 1992).

After that, a transverse section, 10μm in thickness, was cut from each measuring point of the released strain by a sliding microtome, and the section was stained by safranin and ferric hematoxylin. The section was then mounted on a slide glass with the jelly-like compound of gelatin, glycerin, and water. By using a light microscope connected to an image processor, microscopic images at large and small magnification were photographed within the outermost annual ring of the mounted section. From the images at small magnification, the area composition of domain of each tissue, e.g. vessel element (*V*), ray tissue (*R*), and wood fiber (*F*), was computed. From the images at large magnification, the area ratios of the lignified layer (*s*), the G-layer (*g*), and the cell lumen in the domain of the wood fiber were determined. Frequency of the G-fiber per unit area (N_g) in the domain of the wood fiber and that of the normal wood fiber (N-fiber) (N_n) were also counted.

Flat-sliced samples, 5×5×0.015 mm in L, T, and R respective directions, were cut from the outermost annual rings of both the NW xylem and the highly developed TW xylem. Sampled specimens from the TW xylem were quickly dried with ethanol, and were ultra-sonicated in water to remove the G-layers from the lignified layer (Norberg & Meier 1966). Thereafter, the microfibril angles in the middle layer of the secondary wall (MFA) were measured by the iodine-staining method (Saiki et al.1989).

5-2-2 Observed Results

Obtained results are overviewed in Table 5-1, which was already reported in our previous paper (Yamamoto et al. 1992). From Table 5-1, it can be clearly understood that the TW xylem shows quite distinctive properties when compared with the NW xylem. It is considered that either of the G-layer formation or the relatively small MFA in the S2 layer of the G-fiber would cause the distinctive xylem properties in the TW. However, it is still unknown which possibility is more concerned with the origin of the TW properties, or whether there is something other factor that causes the TW properties. In the present chapter, we attempt to answer this question through simulating the mechanical behaviors of the G-fiber on the basis of the formula derived in Chapter 2.

Table 5-1. Observed data from an inclined stem of a 70-year-old Kohauchiwakaede (*Acer sieboldiunum* Miq.).

Measuring positions	1	2	3	4	5	6	7	8	9	10
[Area composition of domain of each tissue (%) - measured at the small maginification]										
Vessel [V]	7.2	6.2	7.3	7.7	8.8	8.0	9.0	7.9	5.1	9.9
Ray [R]	13.0	17.8	12.8	12.6	12.3	17.6	14.7	12.3	16.6	10.8
Fiber [F]	79.8	76.0	79.9	79.7	78.9	74.4	76.3	79.8	78.3	79.3
[Area ratios of the wall in the wood fiber domain (%) - measured at the large maginification]										
G-layer [g]	8.77	16.4	7.88	10.20	0.507	1.61	0	0	0	0
Lignified layer [s]	70.2	60.5	63.2	62.5	69.1	63.8	60.6	62.0	67.9	65.9
[Frequency of the fiber cell in the wood fiber domain (/ 0.01 mm^2)]										
Total wood fiber [f]	99	107	98	102	85	95	120	84	86	82
(G-fiber [N_g])	(51)	(73)	(34)	(44)	(3)	(11)	(0)	(0)	(0)	(0)
Relative frequency of G-fiber [ϕ]	0.51	0.68	0.35	0.43	0.04	0.12	0	0	0	0
[Physical properties]										
Released strain [ε_L^X] (%)	–0.218	–0.204	–0.094	–0.190	–0.024	–0.038	–0.003	–0.039	0.004	–0.020
Oven-dried shrinkage [α_L^X] (%)	1.16	1.10	0.48	0.93	0.24	0.52	0.51	0.50	0.22	0.018
Green Young's modulus [E_L^X] (GPa)	10.78	9.21	8.42	11.07	8.92	6.57	7.15	6.37	5.59	7.35

[Microfibril angle in the S2 layer (deg.)]	**Tension wood region**	**Normal wood region**
Number of the measured fiber	32	32
Average [θ] (deg)	23.1	27.2
Standard deviation (deg)	(2.18)	(3.38)

5-3 Simulation

5-3-1 G-fiber model

A schematic model of the typical G-fiber, consisting of the compound middle lamella (CML), the S1 and S2 layers, and the G-layer, are shown in Fig.5-1.

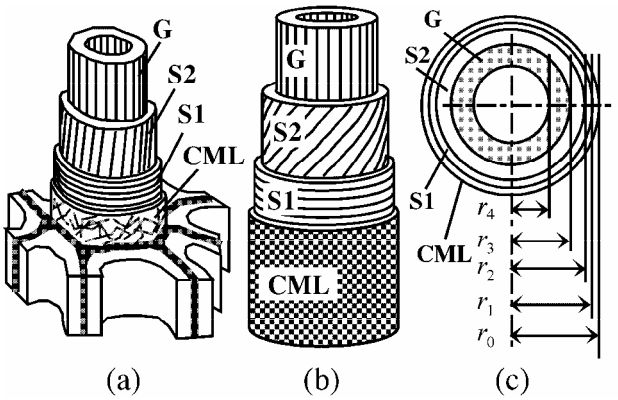

Fig.5-1. Multi-layered structure of the gelatinous fiber.
(a); Microscopic structure,
(b); A mechanical model,
(c); Crosscut surface of the mechanical model.
Each consists of compound middle lamella (CML), the outermost layer of the secondary wall (S1), its middle layer (S2), and gelatinous layer (G).

(a) Parameters in the basic formula

In this paper, we focus on three biomechanical processes in the TW xylem: (1) cell wall maturation, (2) elastic deformation due to action of an axial traction under a steady moisture condition, and (3) moisture adsorption. The G-fiber tends to shrink or expand in its longitudinal or transverse directions when the biomechanical processes occur. We denote the strains of the dimensional changes of the single G-fiber in the longitudinal and the diametral directions by ε_L and ε_T, respectively, which were simulated by the formula derived in Chaper 2. Correctly speaking, it is not a model for the behaviors of an isolated fiber, because the boundary condition imposed in the present formulation considers the shear restraint imposed by neighboring fibers (see eq.(2-19)). A basic formula to calculate ε_L and ε_T contains several parameters, which can be categorized into the anatomical structure, the mechanical properties, and the internal expansive strains of the constituent materials (see Nomenclatures).

(b) Basic equations to calculate the dimensional changes of the single G-fiber

The basic equations that gives ε_L and ε_T were derived as follows (see eq.(2-31) in Chapter 2):

$$\begin{aligned}\dot{\varepsilon}_L &= f_{11}(\mathbf{p})\dot{\varepsilon}_1^m + f_{12}(\mathbf{p})\dot{\varepsilon}_2^m + f_{13}(\mathbf{p})\dot{\varepsilon}_3^m + f_{14}(\mathbf{p})\dot{\varepsilon}_1^f + f_{15}(\mathbf{p})\dot{\varepsilon}_2^f + f_{16}(\mathbf{p})\dot{\varepsilon}_3^f + f_{17}(\mathbf{p})\dot{P}_L\ ,\\ \dot{\varepsilon}_T\left(=\dot{\varepsilon}_t\big|_{r=r1}\right) &= f_{21}(\mathbf{p})\dot{\varepsilon}_1^m + f_{22}(\mathbf{p})\dot{\varepsilon}_2^m + f_{23}(\mathbf{p})\dot{\varepsilon}_3^m + f_{24}(\mathbf{p})\dot{\varepsilon}_1^f + f_{25}(\mathbf{p})\dot{\varepsilon}_2^f \\ &\quad + f_{26}(\mathbf{p})\dot{\varepsilon}_3^f + f_{27}(\mathbf{p})\dot{P}_L\quad .\end{aligned} \tag{5-1}$$

where a dot over a character represents the derivative by an elapsed time t. Coefficients f_{11}, f_{12}, - - - , f_{27} are functions of **p**, and **p** is a parameter vector whose components are ρ_0, ρ_1, ρ_2, ρ_3, θ, E_1, E_2 , E_3, S_0, S_1, S_2, and S_3. Some parameters depend on t during the cell wall maturation, or the moisture adsorption. P_L represents an axial traction that acts on both ends of the G-fiber. We can calculate the dimensional change of the single wood fiber by integrating the differential eqs. (5-1) along the physical state change of the cell wall.

(c) Time -dependent or moisture-dependent behaviors of parameters

Maturation process of the cell wall:

The amorphous constituent, such as xylan and lignin, are irreversibly accumulated among the gaps of the polysaccharide bundle after the completion of the polysaccharide framework of the cellulose microfibril (CMF) and other non-cellulosic but oriented polyose. In this process, the amorphous constituent hardens into the matrix skeleton. Thus, S_1, S_2, and S_3 tend to increase monotonously from very small values to their final values. Moreover, the amount of the substance increases irreversibly inside the matrix skeleton whose volume is spatially limited. As the inevitable consequence, internal strains ε_1^m, ε_2^m, ε_3^m are induced in the S1 and S2 layers, and the G-layer, respectively.

In the same way as in Chapter 3, it is considered that time-dependent changes in E_1, E_2, and E_3 are somewhat smaller than in S_1, S_2, and S_3 since the polysaccharide framework had been already completed before the matrix substance began to deposit. However, we should not ignore the possibility that aging effects, such as an increase in the crystallinity of the CMF, would generate internal strains ε_1^f, ε_2^f, ε_3^f in the polysaccharide framework bundle (Yamanoto & Okuyama 1988, Yamamoto et al.1992, 1995, Yamamoto 1998). In such a case, we need to assume a certain value for each of them.

Drying process in the cell wall:

Because the completed xylem (*i.e.* green wood) contains much water, drying is required before converting the wood into natural resources for building or for producing furniture timber. In this process, the water molecule is discharged from the absorption site in the matrix skeleton, after which the matrix skeleton tends to shrink and harden. This means that S_1, S_2, S_3, ε_1^m, ε_2^m, and ε_3^m tend to change their values monotonously in accordance with the moisture desorption. At the same time, a certain physicochemical change may occur in the bundle of

the polysaccharide framework. However, it is natural to consider that changes of E_1, E_2, E_3 and values of ε_1^f, ε_2^f, and ε_3^f are somewhat smaller than those of S_1, S_2, S_3, ε_1^m, ε_2^m, and ε_3^m because the crystal domain, which is a main component of the polysaccharide framework, almost does not participate in the adsorption of the water molecule.

(d) Determination of the values to be assumed for parameters in eqs.(5-1)

Anatomical factors ρ_0, ρ_1, ρ_2, ρ_3, *and* θ:

In the present chapter, to determine the values of ρ_0, ρ_1, ρ_2, and ρ_3, the following formulas was derived (see APPENDIX [1]). It is required to know the ratio of the area of each layer to the total crosscut area of a single wood fiber when we use formulas (5-2).

$$\rho_0\rho_1\rho_2 = \frac{1}{\sqrt{1-s}}, \rho_0 = 1 + \frac{h}{r_1}, \quad \rho_2 = \frac{1}{\rho_1(1+h/r_1)\sqrt{1-s}},$$
$$\rho_3 = \sqrt{\frac{1-s}{(1-s) - f \cdot g/N_g}} (\text{for } N_g \neq 0), \quad \text{or} \quad \rho_3 = 1 (\text{for } N_g = 0), \tag{5-2}$$

where s and g represent the area ratios of the lignified layer (= CML+S1+S2) and the G layer in the domain of the wood fiber, respectively. f and N_g represent the numbers of the wood fiber and the G-fiber per unit area in the domain of the wood fiber. These are experimentally determined values. To determine the values of ρ_0, ρ_1, ρ_2 by using the eqs.(5-2), we need to give at least two of them. In the present calculation, and with reference to the authors' previous studies (Yamamoto et al. 2001, 2002), we hypothesized 0.025 as the value of h/r_1, and 1.1 as the value of ρ_1. Thereafter, for each measuring point of the released strain, we calculated the values of ρ_2 and ρ_3 by using eqs.(5-2). The estimated values of ρ_2 and ρ_3 are displayed in Table 5-2.

Table 5-2. Values of the parameters ρ_2 and ρ_3 which are estimated from eqs.(5-2).

Measuring positions	1	2	3	4	5	6	7	8	9	10	Mean
ρ_2	1.625	1.411	1.462	1.448	1.596	1.474	1.413	1.439	1.558	1.519	1.494 [1)]
ρ_3	1.527	1.598	1.616	1.645	1.367	1.274	1.000 [2)]	1.000 [2)]	1.000 [2)]	1.000 [2)]	1.505 [3)]

1) Not significant for difference among the positions (by the test of the goodness of fit).
2) No G-fiber was formed at the positions 7, 8, 9, and 10.
3) Mean value among the 6 positions where the G-fiber is formed.

θ is one of the anatomical factors in **p**. In the present simulation, we used the measured values of the MFA in the S2 layer of the N- and the G-fibers, which are displayed in Table 5-1.

Mechanical factors E_1, E_2, E_3, S_1, S_2, S_3, S_0 :

The S1 and S2 layers, and the G-layer can be regarded as the parallel composites of the framework bundle of polysaccharide and the matrix skeleton. It follows that the simple mixture law can be applied to calculate the values of E_1, E_2, E_3, S_1, S_2, and S_3 as follows (see eqs.(3-5) in Section 3-1):

$$E_i = A_i \cdot C_i \cdot E_{cry} + A_i \cdot (1 - C_i) \cdot \psi(\tau) \cdot E_{poly} ,$$
$$S_i = \{1 - A_i + (1 - C_i) \cdot A_i \cdot (1 - \psi(\tau))\} \cdot E_{matr} / (1 + \nu) , \qquad (i = 1, 2, 3) \qquad (5\text{-}3)$$

where ν is Poisson ratio, which is hypothesized to be 0.5 in the same way as in the previous chapters (Yamamoto 1998, 1999, Yamamoto et al. 2001), C_1, C_2, and C_3 are crystallinity indices of the polysaccharide framework in the S1 and S2 layers, and the G-layer, respectively. A_1, A_2, and A_3 are weight ratios of the polysaccharide framework in the respective layers. $\psi(\tau)$ is a monotonously decreasing function of τ, which was introduced in eqs.(3-5) in Section 3-1. It satisfies $\psi(\tau)|_{\tau=0}=1$ and $\psi(\tau)|_{\tau=1}=0$. However, in the present chapter, we tentatively assume $\psi(\tau) = 0$ for all τ for convenience. The values of A_1, A_2, and A_3 are assumed in Table 5-3.

E_{matr} is Young's modulus of the molded matrix substance, which clearly depends on the elapsed time during the cell wall maturation (or moisture content during the moisture adsorption). With reference to Cousins' experiments (Cousins 1976, 1978), it is assumed that E_{matr}= 2 GPa in the green condition, and E_{matr}= 4~6 GPa in the dried condition. On the other hand, it is considered that the Young's modulus of the cellulose crystal along the direction parallel to the molecular chain (E_{cry}) is not affected by moisture adsorption. With reference to Nishino et al's study (Nishino 1996), we assume E_{cry} = 134 GPa regardless of the moisture content.

Then, we assumed the values and *t*-dependent patterns of E_1, E_2, E_3, S_1, S_2, S_3 as displayed in Table 5-3 on the basis of the above-mentioned discussions and the subsidiary conditions described after, provided that the non-crystalline region in the framework bundle was regarded as being integrated into the matrix substance from the mechanical point of view. The value of S_0 was calculated by the method described in Footnote (6) in Section 3-1.

Internal expansive terms ε_1^f, ε_2^f, ε_3^f, ε_1^m, ε_2^m, ε_3^m:

Neither of the values nor *t*-dependent patterns can be experimentally measured for ε_1^f, ε_2^f, ε_3^f, ε_1^m, ε_2^m, ε_3^m. However, we can optimize their values and *t*-dependent patterns so as to obtain a reasonable simulation.

Table 5-3. Values of parameters used for the simulation.
(a) Chemical composition in each layer.

Layer	Polysaccharide framework	Matrix substance	Crystallinity of the framework
CML	15 (%)	85 (%)	100 (%)
S1	26	74	C_1
S2	52	48	C_2
G	90	10	C_3

(b) Time-dependent changes of the mechanical properties of constituents.

Time [#]	E_{cry}	E_{matr} [1)] (in S1)	E_{matr} [1)] (in S2)	E_{matr} [1)] (in G)	S_0 [1)]
$t = 0 \sim T_1$ [2)]	134	increase from 0 to 2	0	0	4
$t = T_1 \sim T_2$ [2)]	134	2	increase from 0 to 2	0	4
$t = T_2 \sim T_3$ [2)]	134	2	2	increase from 0 to 2	4
$t = T_3 \sim T_4$ [3)]	134	increase from 2 to 4	increase from 2 to 4	increase from 2 to 4	4

(c) Geometrical properties of the layers.

Time [#]	ρ_0	ρ_1	ρ_2	ρ_3 [4)]	θ [5), 6)]
$t = 0 \sim T_1$ [2)]	1.025	1.1	1.494	1.0 or 1.505	27.2 or 23.1
$t = T_1 \sim T_2$ [2)]	1.025	1.1	1.494	1.0 or 1.505	27.2 or 23.1
$t = T_2 \sim T_3$ [2)]	1.025	1.1	1.494	1.0 or 1.505	27.2 or 23.1
$t = T_3 \sim T_4$ [3)]	1.025	1.1	1.494	1.0 or 1.505	27.2 or 23.1

1) Unit: GPa.
2) Maturation process after the formation of the polysaccharide framework in the S1, the S2, and the G-layers.
3) Drying process from the FSP ($t = T_3$) to the oven-dried state ($t = T_4$). $\tau = (T_4 - t)/(T_4 - T_3)$.
4) $\rho_3 = 1.0$ in the N-fiber. $\rho_3 = 1.505$ in the G-fiber. 5) Unit: degree.
6) $\theta = 27.2$ in the N-fiber. $\theta = 23.1$ in the G-fiber.
Assumed with reference to Subsidiary condition 1.

5-4 Results

5-4-1 Young's modulus of the green G-layer

(a) Experimental results

Matured secondary xylem of kohauchiwakaede consists of four domains of tissues, *i.e.* the wood fiber, the vessel element, the ray parenchyma, and the axial parenchyma. It is considered that those tissues are arranged in a row in the direction parallel to the axis of wood fiber, and the following formula can be used for calculating the longitudinal Young's modulus of the TW xylem (E_L^X) by the simple law of mixture.

$$E_L^X = \frac{1}{F+V+R+P}\left(F \cdot E_L^F + V \cdot E_L^V + R \cdot E_L^R + P \cdot E_L^P\right), \qquad (5\text{-}4)$$

where E_L^F, E_L^V, E_L^R, and E_L^P are Young's moduli of the wood fiber, vessel element, ray parenchyma, and axial parenchyma, respectively, under the green condition, and $F+V+R+P=1$. Considering $E_L^V/E_L^F \ll 1$, $E_L^R/E_L^F \ll 1$, and $E_L^P/E_L^F \ll 1$, we conclude $E_L^F = E_L^X/F$. In the case of Kohauchiwakaede, the amount of the axial parenchyma is somewhat less than that of the other tissues, and its morphological features are similar to the wood fiber cell apart from the fact that the wall thickness of the axial parenchyma is smaller than that of the wood fiber. In this study, for the simplification, we did not distinguish the axial parenchyma from the wood fiber when we determined the values of F, V, R, and P.

According to the observations, there was no significant difference among the measuring points on the periphery for the morphological properties of the G-fiber, *e.g.* the thickness of the lignified layer, that of the G-layer, and their morphological appearance. The same can be said in the case of the N-fiber. Then, by applying the simple mixture law to the fiber domain that is regarded as a parallel composite of the G-fiber and the N-fiber, we derive the following formula:

$$E_L^F = \phi \cdot E_L^g + (1-\phi)E_L^n = \left(E_L^g - E_L^n\right)\phi + E_L^n, \quad \text{where } \phi = N_g / f, N_g + N_n = f \quad . \qquad (5\text{-}5)$$

E_L^g and E_L^n are the axial Young's modulus of the green G-fiber and that of the green N-fiber, respectively, and ϕ is the relative frequency of the G-fiber in the fiber domain. On the other hand, we obtained the relationship between ϕ and E_L^F ($= E_L^X/F$) in Table 5-1, which was approximated by the following linear regression:

$$E_L^F = 7.74\,\phi + 8.50 \quad (r = 0.857^{**}) . \tag{5-6}$$

Then, comparing eqs.(5-5) and (5-6) directly, we obtain

$$E_L^g = 16.24 \text{ [GPa]} , \quad E_L^n = 8.50 \text{ [GPa]} , \tag{5-7}$$

provided that we do not use the data obtained from measuring point 5 when deriving eq. (5-6). This is because the observed value of the longitudinal Young's modulus at measuring point 5 was larger regardless of having very small amount of G-fiber formation, and therefore the estimated value of E_L^g becomes abnormally large at position 5 in comparison with that at the other positions. It is reasonable to assume that some error occurred in measuring the elastic modulus of the specimen at point 5.

(b) Simulation using the wood fiber model

In this simulation, we assumed the condition of the steady moisture state (green condition, *i.e.* the state at $t = T_3$ in Table 5-3). Then, every component in **p** must be constant, and both $d\varepsilon_i^m$ and $d\varepsilon_i^f$ (i = 1, 2, 3) should all be nil. Then, from eqs.(5-1), we obtain the following formula to calculate the longitudinal Young's modulus of the wood fiber (E_L):

$$E_L = \{1/(\pi r_0^2)\} dP_L/d\varepsilon_L = \{1/(\pi r_0^2)\}/f_{17}(\mathbf{p}) . \tag{5-8}$$

The values assumed in Table 5-3 were used for the simulation using eq.(5-8). Firstly, we optimized the values of C_1 and C_2 in eqs.(5-3) so as to give the experimentally determined value of E_L^n (= 8.50GPa). In this simulation, we assumed that the degree of crystallinity in the framework bundle of the oriented polysaccharide was identical between in the S1 and the S2 for convenience, because there is no reason for considering that properties of the CMF are different in the S1 and in the S2 layers. Thereafter, we applied the optimized values of C_1 and C_2 to the simulation of E_L in the green G-fiber, and optimized the value of C_3 to obtain the experimentally determined value of E_L^g (= 16.24GPa). Finally, the optimized values of C_1, C_2, and C_3 became:

$$C_1 (= C_2) = 0.494, \quad C_3 = 0.221. \tag{5-9}$$

From this result, we calculated the longitudinal Young's modulus of the lignified layer in the N-fiber (E_N^n), that of the lignified layer in the G-fiber (E_N^g), and that of the G-layer (E_G^g) as follows:

$$\begin{aligned} &\text{In the N-fiber :} \quad E_N^n = 13.13 \text{ [GPa]} \\ &\text{In the G-fiber :} \quad E_N^g = 16.28 \text{ [GPa]} , \quad E_G^g = 28.27 \text{ [GPa]} . \end{aligned} \tag{5-10}$$

5-4-2 Growth strain in the G-layer

(a) Experimental Results

The wood fiber, vessel element, ray parenchyma, and axial parenchyma in the differenciating xylem tend to deform during their secondary wall maturation. Thus, the growth strain is generated in the maturing xylem. The infinitesimal increase in the longitudinal growth strain of the xylem at the macroscopic level (ε_L^X) can be expressed by the following formula by the simple mixture law:

$$d\varepsilon_L^X = \frac{F \cdot E_L^F \cdot d\varepsilon_L^F + V \cdot E_L^V \cdot d\varepsilon_L^V + R \cdot E_L^R \cdot d\varepsilon_L^R + P \cdot E_L^P \cdot d\varepsilon_L^P}{F \cdot E_L^F + V \cdot E_L^V + R \cdot E_L^R + P \cdot E_L^P}, \qquad (5\text{-}11)$$

where $d\varepsilon_L^F$, $d\varepsilon_L^V$, $d\varepsilon_L^R$, and $d\varepsilon_L^P$ are infinitesimal increses of the longitudinal growth strain in the respective tissues. Assuming $E_L^V/E_L^F \ll 1$, $E_L^R/E_L^F \ll 1$, $E_L^P/E_L^F \ll 1$, and $F+V+R+P=1$, we obtain

$$d\varepsilon_L^X \cong d\varepsilon_L^F .$$

Moreover, we obtain the following formula:

$$d\varepsilon_L^X (\cong d\varepsilon_L^F) = \frac{\phi \cdot E_L^g \cdot d\varepsilon_L^g + (1-\phi) \cdot E_L^n \cdot d\varepsilon_L^n}{\phi \cdot E_L^g + (1-\phi) \cdot E_L^n} = \frac{\left(E_L^g \cdot d\varepsilon_L^g - E_L^n \cdot d\varepsilon_L^n\right) \cdot \phi + E_L^n \cdot d\varepsilon_L^n}{\left(E_L^g - E_L^n\right) \cdot \phi + E_L^n}, \quad (5\text{-}12)$$

where $d\varepsilon_L^g$ and $d\varepsilon_L^n$ are respective increments in the longitudinal growth strain of the G-fiber and that of the N-fiber, respectively. By integrating the eq.(5-12) along the cell wall maturation, we can obtain the growth strain of the newly-formed xylem (ε_L^X).

In order to integrate the eq.(5-12), we also need to know the changes of E_L^g and E_L^n during the process of secondary wall maturation. It is considered that deposition of the matrix constituents have almost no effect on the increases of E_L^g and E_L^n because the stiffness of the matrix substance is somewhat smaller than that of the framework bundle. Therefore, it is natural to consider that increases in E_L^g and E_L^n are caused by a certain qualitative change of the CMF, such as further crystallization of cellulose (Wardrop 1965). Unfortunately, it is still quite difficult to know the time-dependent change of the CMF crystallinity in the cell wall. In the present study, for convenience, we assumed that the crystallinity in each layer is almost unchanged during cell wall maturation. We then hypothesized that the E_L^g and E_L^n becomes constant through the cell wall maturation.

Growth stress generation is a biomechanical process during the maturation (lignification) of the secondary wall (Wardrop 1965, Boyd 1972, Archer 1987, Yamamoto 1998). Thus, we integrate eq.(5-12) along the cell wall maturation in the G-fiber. As the result, we obtain the following formula:

$$\varepsilon_L^X (\cong \varepsilon_L^F) = \frac{\phi \cdot E_L^g \cdot \varepsilon_L^g + (1-\phi) \cdot E_L^n \cdot \varepsilon_L^n}{\phi \cdot E_L^g + (1-\phi) \cdot E_L^n} = \frac{\left(E_L^g \cdot \varepsilon_L^g - E_L^n \cdot \varepsilon_L^n\right) \cdot \phi + E_L^n \cdot \varepsilon_L^n}{\left(E_L^g - E_L^n\right) \cdot \phi + E_L^n} \qquad (5\text{-}13)$$

where $\varepsilon_L^g = \int_{\text{Maturation process}} d\varepsilon_L^g$, $\varepsilon_L^n = \int_{\text{Maturation process}} d\varepsilon_L^n$.

Results from eq.(5-7) were used as the values of $E_L{}^g$ and $E_L{}^n$ in this formula. The observed relationship between ϕ and $\varepsilon_L{}^X$ ($=\varepsilon_L{}^F$), which was shown in Table 5-1, was approximated by the following curvilinear regression:

$$\varepsilon_L^F = -0.5554 + \frac{0.6003}{\phi + 1.098} . \quad (r = 0.956^{***}) \qquad (5\text{-}14)$$

By comparing the eqs.(5-13) and (5-14) directly, we obtained the growth strains of G-fiber ($\varepsilon_L{}^g$) and the N-fiber ($\varepsilon_L{}^n$) as follows:

$$\varepsilon_L{}^g = -0.2693 \ [\%] , \qquad \varepsilon_L{}^n = -0.0087 \ [\%] . \qquad (5\text{-}15)$$

(b) Simulation based on the G-fiber model

We integrated the basic formula of eq.(5-1) during the G-fiber wall maturation under the assumption of dP_L=0. As initial conditions, we adopted $\varepsilon_L(t)|_{t=0}$=0, $\varepsilon_T(t)|_{t=0}$=0. Results from eq.(5-9) were used as the values of C_1, C_2, and C_3. Values of the parameters assumed in Table 5-3 were also used for the calculation. We then optimized the increments and t-dependent patterns of $\varepsilon_1{}^f$, $\varepsilon_2{}^f$, $\varepsilon_3{}^f$, $\varepsilon_1{}^m$, $\varepsilon_2{}^m$, and $\varepsilon_3{}^m$ to obtain the results in eq.(5-15). However, before integrating eqs.(5-1), we need to know how the maturation of the G-fiber wall proceeds.

Some scientists clarified the lignification process in the secondary wall of the softwood tracheid and the hardwood normal-fiber (Terashima 1990, Donaldson 1992). On the other hand, maturation of the G-fiber has remained unclear. Recently, based on the technique of immuno-TEM observation, Kim et al. discovered that the activity of the peroxidase is localized in the secondary wall rather after the completion of the G-layer (Kim et al. 2002). This suggests that lignification proceeds in the secondary wall after the formation of the thick

G-layer. With reference to those investigations, we assumed the following conditions regarding the maturation of the G-fiber.

Subsidiary Condition 1: Lignification in the S1 layer starts at $t = 0$ after the formation of the frameworks of the cellulose and the other oriented polysaccharide in the secondary wall and the G-layer, and ends at $t = T_1$. This is the first integration interval. Lignification in the S2 layer starts at $t = T_1$, and ends at $t = T_2$. This is the second integration interval. In the G-layer, deposition of a certain matrix substance should proceed, however, no lignification occurs. In this study, as the third integration interval, the deposition of the matrix substance in the G-layer starts at $t = T_2$ and ends at $t = T_3$. Then the G-fiber maturation is completed at $t = T_3$. S_1, S_2, and S_3 tend to increase monotonously and smoothly from very small values to their final values in their respective integration intervals.

We integrate eqs.(5-1) as follows:

$$\varepsilon_L\left(= \int_{t=0}^{t=T_3} \left(\frac{d\varepsilon_L}{dt} \right) dt \right) = \underset{\substack{\text{The first}\\ \text{integration}\\ \text{interval}}}{\int} \left(\frac{d\varepsilon_L}{dt} \right) dt + \underset{\substack{\text{The second}\\ \text{integration}\\ \text{interval}}}{\int} \left(\frac{d\varepsilon_L}{dt} \right) dt + \underset{\substack{\text{The third}\\ \text{integration}\\ \text{interval}}}{\int} \left(\frac{d\varepsilon_L}{dt} \right) dt \qquad (5\text{-}1')$$

We need to impose certain subsidiary conditions on values and t-dependent patterns of ε_1^f, ε_2^f, ε_3^f, ε_1^m, ε_2^m, and ε_3^m to simulate the observed values of ε_L^n and ε_L^g. In the case of the softwood latewood tracheid, the observed relationship between the longitudinal growth strain and the MFA can be simulated by supposing [increment in ε_1^m] = 1%, [increment in ε_2^m] = 0.5%, and [increment in ε_1^f] = [increment in ε_2^f] = –0.15% (Yamamoto 1998). Where, [increment in ε_1^f], etc., are defined as follows:

$$\left[\text{increment in } \varepsilon_1^f\right] \equiv \int_{t=0}^{t=T_3} \left(\frac{d\varepsilon_1^f}{dt} \right) dt \ , \quad etc.$$

With reference to this result, we assumed the following subsidiary conditions.

Subsidiary Condition 2: ε_1^m and ε_2^m take positive values. Each of them increases monotonously and smoothly from 0 to a certain value (= *increment*) as lignification

proceeds in each integration interval (Yamamoto 1998). It is natural to consider that increments in ε_1^m and ε_2^m depend on the lignin content in the respective layers. This is based on *the lignin swelling hypothesis* (Boyd 1972). However, we assume $\varepsilon_3^m = 0$, because no lignification occurs in the G-layer. On the other hand, ε_1^f and ε_2^f take negative values. Each of them tends to change monotonously and smoothly from 0 to a certain value (= *increment*) with the maturation in each integration interval. This postulates *the cellulose tension hypothesis*, which considers that the CMF framework tends to contract in the direction parallel to the cellulose molecular chain with the aging of the CMF (Wardrop 1965, Bamber 1978).

Firstly, we simulated the generation of the growth strain in the N-fiber by integrating eq.(5-1') under the above subsidiary conditions, and optimized the increments in ε_1^f and ε_2^f so as to obtain the observed value of ε_L^n (= –0.0087%). Thereafter, we tried to simulate the generation of the growth strain of the G-fiber (ε_L^g = –0.2693%) and optimized the increment ε_3^f. In this simulation, we assumed the following subsidiary condition in addition to the above two conditions:

Subsidiary Condition 3: According to the observations using the light microscope or ultraviolet microscope, there is no specific difference in the morphological appearance of the secondary wall between the N-fiber and the G-fiber (Yoshida et al. 2002). From this fact, we assumed that *t*-dependent patterns and increments in each of ε_1^m, ε_2^m, ε_1^f and ε_2^f take identical values between in the N-fiber and in the G-fiber.

S_1, ε_1^f, and ε_1^m are all expressed as monotonously increasing (or decreasing) functions of t in the first integration interval. S_2, ε_2^f, and ε_2^m are also monotonously increasing (or decreasing) functions of t in the second integration interval. The same can be said for S_3, ε_3^f, and ε_3^m in the third integral interval. Each of these monotonously increasing (decreasing) functions can be transformed into function that do not contain explicitely T_1, T_2, and T_3 by transforming the integral variable t into γ (= t/T_1; $0<t<T_1$), ξ (= $(t-T_1)/(T_2-T_1)$; $T_1<t<T_2$), and κ (= $(t-T_2)/(T_3-T_2)$; $T_2<t<T_3$). Moreover, we know these variable transformations alter corresponding integration intervals in eq.(5-1') into an identical one that is from 0 to 1. Thus, the concrete value of eq.(5-1') does not depend on T_1, T_2, and T_3. Furthermore, we should

note that integration of eq.(5-1') is not affected by the functional shapes of *t*-dependent variables if each variable changes its value very smoothly in each integration interval. This is quite reasonable because we consider the *t*-dependent changes of those variables gradually proceed with the maturation of the matrix skeleton in the respective layers (see APPENDIX [2]).

Thus, we can optimize the value of the increment in ε_3^f as displayed in Table 5-5 which became quite larger than those in ε_1^f and ε_2^f as shown in Tables 5-4.

Table 5-4. Combination on the increments in ε_1^m, ε_2^m, ε_1^f, ε_2^f which optimize the observed value of ε_L^n. (Units : %)

ε_1^m (at $t = T_1$) [1)]	1	0.8	0.6	0.4	0.2	0	−0.2	−0.4
ε_2^m (at $t = T_2$) [1)]	0.5	0.4	0.3	0.2	0.1	0	−0.1	−0.2
ε_1^f (at $t = T_1$) [2)] ($= \varepsilon_2^f$ at $t = T_2$)	−0.178	−0.145	−0.112	−0.078	−0.045	−0.012	0.021	0.055
ε_T^n (at $t = T_2$) [3)]	0.170	0.135	0.099	0.063	0.028	-0.0078	−0.043	−0.079

1) Assumed arbitrarily under Subsidiary Conditions 1 and 2.
2) Calculated from each pair of ε_1^m and ε_2^m so as to give the observed value of ε_L^n.
3) Calculated from each combination of ε_1^m, ε_2^m, ε_1^f, ε_2^f.

Table 5-5. Estimated value of the increment in ε_3^f which gives the observed value of ε_L^g. (Units : %)

ε_1^m (at $t = T_1$) #	1	0.8	0.6	0.4	0.2	0	−0.2	−0.4
ε_2^m (at $t = T_2$) #	0.5	0.4	0.3	0.2	0.1	0	−0.1	−0.2
ε_1^f (at $t = T_1$) ## ($= \varepsilon_2^f$ at $t = T_2$)	−0.178	−0.145	−0.112	−0.078	−0.045	−0.012	0.021	0.055
ε_3^f (at $t = T_3$) ###	−0.721	−0.737	−0.754	−0.770	−0.786	−0.802	−0.818	−0.834
ε_T^g (at $t = T_3$) ####	0.333	0.298	0.263	0.228	0.193	0.158	0.123	0.088

\# Assumed arbitrarily under Subsidiary Conditions 1, 2, and 3.
\## Calculated for each pair of ε_1^m and ε_2^m so as to obtain the observed value of ε_L^n.
\### Calculated for each combination of ε_1^m, ε_2^m, ε_1^f, ε_2^f so as to obtain the observed value of ε_L^g.
\#### Calculated for each combination of ε_1^m, ε_2^m, ε_1^f, ε_2^f, and ε_3^f.

5-4-3 Drying shrinkage of the G-layer

(a) Experimental results

We can describe the shrinking process of the wood as a function of the moisture content τ that is normalized by the moisture content at the fiber saturation point (FSP). We denote the

longitudinal shrinking process of the wood as $\alpha_L{}^X(\tau)$. According to the definition, the longitudinal shrinkage $\alpha_L{}^X(\tau)$ must satisfy the following boundary condition, $\alpha_L{}^X(\tau)|_{\tau=1}=0$. $\alpha_L{}^X(\tau)|_{\tau=0}$ (= $\alpha_L{}^X$) means the oven-dried shrinkage of the wood. An infinitesimal increase of the moisture content ($d\tau$) causes an infinitesimal change in the shrinkage of the wood ($d\alpha_L{}^X$), which is described in the following formula:

$$d\alpha_L^X = \frac{F\cdot\overline{E}_L^F\cdot d\alpha_L^F + V\cdot\overline{E}_L^V\cdot d\alpha_L^V + R\cdot\overline{E}_L^R\cdot d\alpha_L^R + P\cdot\overline{E}_L^P\cdot d\alpha_L^P}{F\cdot\overline{E}_L^F + V\cdot\overline{E}_L^V + R\cdot\overline{E}_L^R + P\cdot\overline{E}_L^P}, \qquad (5\text{-}16)$$

where $d\alpha_L{}^F$, $d\alpha_L{}^V$, $d\alpha_L{}^R$, and $d\alpha_L{}^P$ stand for infinitesimal changes of the longitudinal shrinkage in respective tissues. $\overline{E}_L^F$, $\overline{E}_L^V$, $\overline{E}_L^R$, and $\overline{E}_L^P$ are respective Young's moduli at the moisture content τ. Assuming $\overline{E}_L^V/\overline{E}_L^F << 1$, $\overline{E}_L^R/\overline{E}_L^F << 1$, $\overline{E}_L^P/\overline{E}_L^F << 1$, and $F+V+R+P=1$, we obtain

$$d\alpha_L^X \cong d\alpha_L^F .$$

We apply the simple mixture law to the fiber domain consisting of the N-fiber and G-fiber in parallel, then, we obtain the following formula:

$$d\alpha_L^F(\cong d\alpha_L^X) = \frac{\phi\cdot\overline{E}_L^g\cdot d\alpha_L^g + (1-\phi)\cdot\overline{E}_L^n\cdot d\alpha_L^n}{\phi\cdot\overline{E}_L^g + (1-\phi)\cdot\overline{E}_L^n} = \frac{\left(\overline{E}_L^g\cdot d\alpha_L^g - \overline{E}_L^n\cdot d\alpha_L^n\right)\cdot\phi + \overline{E}_L^n\cdot d\alpha_L^n}{\left(\overline{E}_L^g - \overline{E}_L^n\right)\cdot\phi + \overline{E}_L^n},$$

(5-17)

where $d\alpha_L{}^g$ and $d\alpha_L{}^n$ are infinitesimal changes in the shrinkage of the G-fiber and that of the N-fiber, respectively, and $\overline{E}_L^g$ and $\overline{E}_L^n$ are axial Young's moduli of G-fibers and N-fiber, respectively.

We obtain an oven-dried shrinkage of the wood fiber domain $\alpha_L{}^F$ ($=\alpha_L{}^X(\tau)|_{\tau=0}$) by integrating eq.(5-17) from an arbitrary τ to FSP (τ =1) and extrapolating $\tau \rightarrow 0$, provided that we need to know the *t*-dependent patterns of $\overline{E}_L^g$ and $\overline{E}_L^n$ in advance. Then, we tentatively expressed $\overline{E}_L^g$ and $\overline{E}_L^n$ as follows:

$$\overline{E}_L^n = E_L^n\cdot\xi(\tau), \quad \overline{E}_L^g = E_L^g\cdot\zeta(\tau), \qquad (5\text{-}18)$$

where $\xi(\tau)$ and $\zeta(\tau)$ are monotonously decreasing functions for τ, and they satisfy$\xi(\tau)|_{\tau=1}$ =1, and $\zeta(\tau)|_{\tau=1}$ =1. $E_L{}^n$ and $E_L{}^g$ are constants, which stand for the axial Young's moduli of the green N-fiber and the green G-fiber, respectively. For simplification, we assumed $\xi(\tau) = \zeta(\tau)$ for all τ, which means the decreasing pattern of the longitudinal Young's modulus in the G-fiber is similar to that in the N-fiber. Then, eq.(5-15) becomes

$$d\alpha_L^F (\cong d\alpha_L^X) = \frac{\left(E_L^g \cdot d\alpha_L^g - E_L^n \cdot d\alpha_L^n\right)\cdot \phi + E_L^n \cdot d\alpha_L^n}{\left(E_L^g - E_L^n\right)\cdot \phi + E_L^n} \,. \tag{5-19}$$

Under these assumptions, we substituted the results from (5-7) to $E_L{}^g$ and $E_L{}^n$ in eq.(5-19). As the initial conditions, $\alpha_L{}^g(\tau)|_{\tau=1} = \alpha_L{}^n(\tau)|_{\tau=1} = 0$, were required. Thus, eq.(5-19) can be integrated over the moisture content (from an arbitrary τ to $\tau=1$). We obtain the oven-dried shrinkage of the wood fiber domain $\alpha_L{}^F$ ($=\alpha_L{}^F(\tau)|_{\tau=0}$) as the following formula.

$$\alpha_L^X (\cong \alpha_L^F) = \frac{\left(E_L^g \cdot \alpha_L^g - E_L^n \cdot \alpha_L^n\right)\cdot \phi + E_L^n \cdot \alpha_L^n}{\left(E_L^g - E_L^n\right)\cdot \phi + E_L^n} \,. \tag{5-20}$$

The observed relationship between ϕ and $\alpha_L{}^F$, which is shown in Table 5-1, was approximated by the following curvilinear regression:

$$\alpha_L^F = -2.429 + \frac{2.363}{\phi + 1.098} \,. \quad (r = 0.867^{***}) \tag{5-21}$$

Then, comparing eqs.(5-20) and (5-21) directly, we obtain the oven-dried shrinkage of the N-fiber ($\alpha_L{}^n$) and the G-fiber ($\alpha_L{}^g$) as follows:

$$\alpha_L{}^n = 0.2771\ [\%] \,, \qquad \alpha_T{}^g = 1.3026\ [\%] \,. \tag{5-22}$$

(b) Simulation based on the G-fiber model

Free dimensional change of the single wood fiber due to moisture adsorption was simulated on the basis of the conditions assumed in Table 5-3. Thus, dP_L should be null in eqs.(5-1). For convenience, we calculated the swelling deformation of the wood fiber model $\varepsilon_L(\tau)$ by integrating eqs.(5-1) from $\tau=0$ to $\tau=1$. The relationship between swelling ε_L ($=\varepsilon_L(\tau)|_{\tau=1}$) and oven-dried shrinkage α_L ($=\alpha_L(\tau)|_{\tau=0}$) are related to each other by the following formulas:

$$\alpha_L = \frac{\varepsilon_L}{\varepsilon_L + 1} \,, \quad \varepsilon_L = \frac{\alpha_L}{1 - \alpha_L} \,. \tag{5-23}$$

The integral interval for calculating ε_L ($=\varepsilon_L(\tau)|_{\tau=1}$) is from the oven-dried state ($t=T_4$; $\tau=0$) to the fiber saturation point ($t=T_3$; $\tau=1$). It is regarded that increasing moisture content τ is equivalent to the reciprocal elapsed time t. The results from (5-9) were used as the values of C_1, C_2, and C_3 in this simulation. Then, we optimized the increments in $\varepsilon_1{}^m$, $\varepsilon_2{}^m$, $\varepsilon_3{}^m$, $\varepsilon_1{}^f$, $\varepsilon_2{}^f$, and $\varepsilon_3{}^f$ to obtain the observed values of $\alpha_L{}^n$ and $\alpha_L{}^g$.

Swelling of the softwood tracheid cell wall is mainly caused by swelling of the matrix substance, *e.g.* hemicellulose, lignin, and noncrystalline cellulose (see Section 4-1, Chapter 4)

(Yamamoto et al. 2001, Barber & Meylan 1964, Barrett et al. 1972, Cave 1972, Koponen et al. 1989). Therefore, it is quite reasonable to postulate that ε_1^m, ε_2^m, and ε_3^m take positive values with the increase of the moisture content, and increase monotonously from 0 to the final values, that is to say, increments.

Firstly, we simulated the swelling of the N-fiber (ε_L^n = 0.2779%). In doing so, we optimized the values of increments in ε_1^m, ε_2^m, ε_1^f, and ε_2^f to give the observed value of the oven-dried shrinkage α_L^n (= 0.2771%). In the present simulation, we assumed that $\varepsilon_1^m = \varepsilon_2^m = \varepsilon_3^m$, and $\varepsilon_1^f = \varepsilon_2^f$ for convenience.

Optimized values of the increments in ε_1^m, ε_2^m, ε_1^f, and ε_2^f were obtained by the simulation as displayed in Table 5-6. In our previous report, we succeeded in simulating the observed relationships between the longitudinal and the tangential swellings, and the MFA in the clear wood specimen of sugi (*Cryptomeria japonica*) by supposing that $\varepsilon_1^m = \varepsilon_2^m$ = 12 ~ 15%, and $\varepsilon_1^f = \varepsilon_2^f$ = 0~1% (Yamamoto et al. 2001). In the present simulation, optimized ε_1^f and ε_2^f became very small but negative, which means that the polysaccharide framework bundles in the S1 and the S2 layers tend to contract in the direction parallel to the cellulose molecular chains in spite of increasing moisture content in the cell wall. It is impossible for the author to provide any comment on such strange results at this stage. However, their absolute values were vary small compared with the increment in ε_1^m and ε_2^m.

We also simulated the oven-dried shrinkage of the G-fiber (α_L^g = 1.3026%), and optimized the value of the increment in ε_3^f. In this simulation it is assumed that increment in each of ε_1^m, ε_2^m, ε_1^f, and ε_2^f takes an identical value between in the N-fiber and in the G-fiber (see *Subsidiary Condition 3*). For convenience, we assumed that $\varepsilon_1^m = \varepsilon_2^m = \varepsilon_3^m$ in this simulation. Thereafter, we optimized the value of the increment in ε_3^f to obtain the observed value of α_L^g. Results are displayed in Table 5-7. The optimized value of the increment in ε_3^f became a large positive value which is quite different from those in ε_1^f and ε_2^f.

Table 5-6. Combinations of the increments of ε_1^m, ε_2^m, ε_1^f, ε_2^f which optimize the observed value of α_L^n. (Units: %)

ε_1^m (= ε_2^m) at $t = T_4$ [1) 2)]	15	12	9	6	3	0	−3	−6
ε_1^f (= ε_2^f) at $t = T_4$ [2) 3)]	−3.345	−2.605	−1.865	−1.126	−0.386	0.353	1.094	1.833
α_T^n [4) 5)]	9.017	7.361	5.643	3.861	2.010	0.086	−1.915	−3.997

1) Assumed arbitrarily.
2) Positive sign means that each cell wall constituent swells during water sorption.
3) Calculated from each pair of ε_1^m and ε_2^m so as to optimize the observed value of α_L^n.
4) Calculated from each combination of ε_1^m, ε_2^m, ε_1^f, ε_2^f.
5) Positive sign means that the wood fiber shrinks in diameter from the FSP to the oven-dried state.

Table 5-7. Estimated value of the increment in ε_3^f which gives the observed value of α_L^g. (Units : %)

ε_1^m (= ε_2^m) at $t = T_4$ [#,*]	15	12	9	6	3	0	−3	−6
ε_1^f (=ε_2^f =ε_3^f) at $t = T_4$ [##,*]	−3.345	−2.605	−1.865	−1.126	−0.386	0.353	1.094	1.833
ε_3^f (at $t = T_4$) [###,*]	5.078	4.782	4.486	4.190	3.897	3.603	3.304	3.010
α_T^g [####,**]	13.66	11.14	8.461	5.616	2.588	−0.641	−4.089	−7.784

\# Assumed arbitrarily.
Calculated from each pair of ε_1^m and ε_2^m so as to optimize the observed value of α_L^n.
Calculated from each combination of ε_1^m, ε_2^m, ε_3^m, ε_1^f, ε_2^f so as to obtain the observed value of α_L^g.
Calculated from each combination of ε_1^m, ε_2^m, ε_3^m, ε_1^f, ε_2^f, and ε_3^f.
* Positive sign means that each cell wall constituent swells during water sorption.
** Positive sign means that the wood fiber shrinks in diameter from the FSP to the oven-dried state.

5-5 Discussion and concluding remarks

5-5-1 Young's modulus of the green G-layer (E_G^g)

According to the results from (5-7), (5-9), and (5-10), the predicted Young's modulus of the green G-layer (E_G^g) became 2.15 times as large as that of the lignified layer in N-fiber (E_N^n), and 1.74 times as large as the one in the G-fiber (E_N^g). In any case, we can say that the longitudinal Young's modulus of the G-layer becomes larger than that of the lignified layer in the G-fiber and N-fiber. The predicted value of the Young's modulus of the lignified layer in the G-fiber (E_N^g) became slightly larger than the one in the N-fiber (E_N^n). This is because we calculated the value of E_N^g in due consideration of an experimental fact that the MFA of the S2 layer in the G-fiber was a little smaller than in the N-fiber. This may be one of the factors to increase the Young's modulus of the TW xylem.

It is well known that the TW becomes very stiffer in the longitudinal direction as it dries. The increase of the Young's modulus of the TW xylem due to drying is highly correlated with the percentage of the G-fiber in the fiber domain (*e.g.* Clair et al. 2003). This suggests that the G-layer becomes abruptly rigid as the water molecule is released. However, the validity of this suggestion remains to be confirmed.

Strangely, the predicted value of the relative crystallinity in the framework bundle of the oriented polysaccharide in the G-layer was somewhat smaller than that in the secondary wall (see results from (5-9)). According to the formula (5-3), the Young's modulus of the G-layer is highly dependent on the ratio of the cellulosic component. In the present simulation, we assumed it to be 90% in the G-layer, which may be a little larger than the true value in the green G-layer. It is likely that the G-layer contains a substantial amount of non-crystalline polyose, *e.g.* hemicellulose. As another possibility, we note the fact that the green G-layer is highly swollen by the water, which causes an apparent decrease in the relative crystallinity of the cellulose in the green G-layer. Hitherto, we have referred to the classical data of Norberg and Meier (1966) on the chemical and physical properties of the G-layer in aspen. However, we need to critically verify their conclusion for various species.

5-5-2 Growth strain in the G-layer (ε_3^f)

Simulated value of ε_3^f is more negative than that in the lignified layer (ε_1^f and ε_2^f). This indicates that a large contractive internal strain originates in the polysaccharide framework of the G-layer in the direction of the cellulose molecular chain, which causes a high longitudinal tensile growth stress in the TW xylem.

5-5-3 Shrinkage and swelling of the G-layer due to moisture adsorption

Many authors have considered that the polysaccharide framework does not swell or shrink by the action of moisture adsorption. However, the present simulation shows that the value of ε_3^f, which is the swelling ability of the polysaccharide framework in the G-layer, becomes a large positive value. Conversely, the polysaccharide framework in the G-layer tends to shrink in the direction parallel to the cellulose molecular chain during the moisture desorption. This means that the high longitudinal drying shrinkage in the TW xylem is induced by the drying shrinkage of the G-layer in its axial direction. Recently, Clair and Thibaut (2001) observed by scanning electron microscopy that the dried G-layer tends to be depressed from surrounding

lignified layer in a crosscut surface of the TW of *Populus sp*., which supports the predicted results in the present simulation.

References in Chapter 5

Archer, R.R.: "Growth stresses and strains in trees," Springer-Verlag, Berlin, 1987.

Bamber, R.K.: The Origin of Growth Stresses. A Rebutal, *IAWA Bull.*, **8**, 80-84 (1987).

Barber, N.F., Meylan, B.A.: The anisotropic shrinkage of wood. A theoretical model, *Holzforschung*, **18**, 146-156 (1964).

Barrett, J.D., Schniewind, A.P., Taylor, R.L.: Theoretical shrinkage model for wood cell walls, *Wood Sci.*, **4**, 178-192 (1972).

Boyd, J.D.: Tree growth stresses. V. Evidence of an origin in differentiation and lignification, *Wood Sci. Technol.*, **12**, 25-35 (1972).

Boyd, J.D.: Relationship between fiber morphology and shrinkage of wood, *Wood. Sic. Technol.*, **11**, 3-22 (1977).

Cave, I.D.: A theory of shrinkage of wood, *Wood Sci. Technol.*, **2**, 268-278 (1972).

Clair, B., Thibaut, B.: Shrinkage of the gelatinous layer of poplar and beech tension wood, *IAWA J.*, **22**, 121-131 (2001).

Clair, B., Ruelle, J., Thibaut, B.: Relationship between growth stress, mechanical-physical properties and proportion of fibre with gelatinous layer in chestnut (*Castanea sativa* Mill.), *Holzforschung*, **57**, 189-195 (2003).

Cousins, W.J.: Elastic modulus of lignin as related to moisture content, *Wood Science and Technology*, **10**, 9-17 (1976).

Cousins, W.J.: Young's modulus of hemicellulose as related to moisture content, *Wood Science and Technology*, **12**, 161-167 (1978).

Donaldson, L.A.: Lignin distribution during latewood formation in Pinus radiata D.Don. *IAWA Bull.*, **13**, 381-387 (1992).

Kim, Y.S., Wi, S.G., Grunwald, C., Schmitt, U.: Immuno Electron Microscopic Localization of Peroxidases in the Differentiating Xylem of Populus spp., *Holzforschung,* **56**, 355-359 (2002).

Kollmann, F.F.P., Cote, Jr W.A.: "Principles of Wood Science and Technology. Volume I: Solid Wood", Springer Verlag, Berlin, 1984.

Koponen, S., Toratti, T., Kanerva, P.: Modelling longitudinal elastic and shrinkage properties of wood, *Wood Sci. Technol.*, **23**, 55-63 (1989).

Nishino, T., Takano, K., Nakamae, K.: Elastic modulus of the crystalline regions of cellulose polymorphs. *J. Polym. Sci.*, Part B **33**, 1647-1651 (1995).

Norberg. H., Meyer, H.: Physical and chemical properties of the gelatinous layer in tension wood fibres of aspen

(*Populus tremula* L.), *Holzforschung,* **6**, 174-178 (1966).

Okuyama, T., Yamamoto, H., Iguchi, M., Yoshida, M.: Generation process of growth stresses in cell walls. II. Growth stress in tension wood, *Mokuzai Gakkaishi*, **36**, 797-803 (1990).

Okuyama, T., Yamamoto, H., Yoshida, M., Hattori, Y., Archer, R.R.: Growth stresses in tension wood. Role of microfibrils and lignification, *Ann. Sci. For.*, **51**, 291-300 (1994).

Scurfield, G.: Reaction wood. Its structure and function, *Science*, **179**, 647-655 (1973).

Saiki, H., Xu, Y., Fujita, M.: The Fibrillar Orientation and Microscopic Measurement of the Fibril Angles in Young Tracheid Walls of Sugi (*Cryptomeria japonica*), *Mokuzai Gakkaishi*, **3**, 786-792 (1989).

Terashima, N.: A New Mechanism for Formation of a Structurally Ordered Protolignin Macromolecule in the Cell Wall of Tree Xylem, *J. Pulp Paper Sci.*, **16**, J150- J155 (1990).

Wardrop, A.B.: The formation and function of reaction wood, In "Cellular structure of woody plants, Cote, W.A. Jr. (ed.)," Syracuse Univ. Press, New York, 1965, pp.373-390.

Yamamoto H, Okuyama, T.: Generation process of growth stresses in cell walls. I. Analysis of the generation process of growth stresses in cell walls, *Mokuzai Gakkaishi*, **34**, 788-793 (1988).

Yamamoto, H., Okuyama, T., Sugiyama, K., Yoshida, M.: Generation process of growth stresses in cell walls. IV. Action of the cellulose microfibrils upon the generation of the tensile stresses, *Mokuzai Gakkaishi*, **38**, 107-113 (1992).

Yamamoto, H. Okuyama, T.: Determining the intensity of the reaction wood formation by the strain-gaige method. Part 2, Growth stress and anatomy in tension wood, *Mokuzai Kogyo*, **49**, 20-23 (1994).

Yamamoto, H., Okuyama, T., Yoshida, M.: Generation process of growth stresses in cell walls. VI. Analysis of the growth stress generation by using a cell model having three layers (S1, S2, and I+P), *Mokuzai Gakkaishi*, **41**, 1-8 (1995).

Yamamoto, H.: Generation mechanism of growth stresses in wood cell walls: Roles of lignin deposition and cellulose microfibril during cell wall maturation, *Wood Sci. Technol.*, **32**, 171-182 (1998).

Yamamoto, H.: A model of the anisotropic swelling and shrinking process of wood. Part 1. Generalization of Barber's wood fiber model, *Wood Sci. Technol.*, **33**, 311-325 (1999).

Yamamoto, H., Sassus, F., Ninomiya, M., Gril, J.: A model of the anisotropic swelling and shrinking process of wood. Part 2. A simulation of shrinking wood, *Wood Sci. Technol.*, **35**, 167-181 (2001).

Yamamoto, H., Kojima, Y., Okuyama, T., Abasolo, W.P., Gril, J.: Origin of the Biomechanical properties of wood related to the fine structure of the multi-layered cell wall. *J. Biomech. Eng. Trans. ASME,* **124**, 432-440 (2002).

Yamamaoto, H., Kojima, Y.: Properties of cell wall constituents in relation to longitudinal elasticity of wood.

Part 1. Formulation of the longitudinal elasticity of an isolated wood fiber, *Wood Sci. Technol.*, **36**, 55-74 (2002).

Yamamoto, H.: Role of the gelatinous layer on the origin of the physical properties of the tension wood. *J. Wood Sci.*, **50**, 197-208 (2004).

Yoshida, M., Ohta, H., Okuyama, T.: Tensile growth stress and lignin distribution in the cell walls of black locust (*Robinia pseudoacacia*), *J. Wood Sci*., **48**, 99-105 (2002).

APPENDIX [1] Deriving eqs. (5-2)

We denote the number of the G-fiber in the wood fiber domain with an area of *A* as *G* and that of the N-fiber as *N*, provided that $G + N = X$. We set the following assumption.

(*Assumption A*) The thickness of the lignified layer in the G-fiber is identical to that of the N-fiber regardless of the measuring position.

This assumption is not so inappropriate to the wood fiber domain in the real xylem because the observed values of *s* and *X*/*A* (= *f*) become almost unchanged regardless of measuring positions as seen from Table 5-1. Moreover, we set the following assumptions.

(*Assumption B*) The diameter of the G-fiber is similar as that of the N-fiber.
(*Assumption C*) Cellular arrangement in the crosscut surface of the xylem takes a tessellation structure consisting of a polygonal cell.

Then, we can connect the area ratio of the lignified layer [*s*], and that of the gelatinous layer [*g*] to ρ_0, ρ_1, ρ_2, and ρ_3 under the assumptions *(A)*, *(B)*, and *(C)*.

It may be a little hasty to apply calculated values of ρ_0, ρ_1, ρ_2, and ρ_3 to the simulation using eqs.(5-1) because the crosscut shape of the G-fiber model used in the present simulation is closely circular. However, we know that the hexagon is the most closely allied to the circle in shape among the polygons that constitute the tessellation arrangement. Then, we set the following assumption

(*Assumption D*) Crosscut shape of the wood fiber in the cellular arrangement is a hexagon with an area of $\left(3\sqrt{3}/2\right)r_0^2$ as displayed in Fig.5-2.

We denote the thickness of the lignified layer as $\left(\sqrt{3}/2\right)(r_0 - r_3)$, and that of the G-layer as $\left(\sqrt{3}/2\right)(r_3 - r_4)$. Distances from the central point of the hexagon to the lignified and gelatinous layers are denoted as $\left(\sqrt{3}/2\right)r_3$ and $\left(\sqrt{3}/2\right)r_4$, respectively. *s* can be given as the following formula:

$$s = \frac{3}{2}\sqrt{3}\left(r_0^2 - r_3^2\right)X/A = 1 - \frac{3}{2}\sqrt{3}\cdot r_3^2 \cdot f \ . \qquad \text{(5-A1)}$$

In a similar manner, *g* is given as the following formula:

$$g = \frac{3}{2}\sqrt{3}\left(r_3^2 - r_4^2\right)G/A = (1-s)\frac{G}{X} - \frac{3}{2}\sqrt{3}\cdot r_4^2 \cdot \frac{G}{A}. \qquad \text{(5-A2)}$$

X/*A*, *G*/*A*, *s*, and *g* can be determined experimentally as displayed in Table 5-1. From eqs.(5-A1) and (5-A2), we can obtain r_3 and r_4 as follows:

$$r_3 = \frac{1}{3}\sqrt{2\sqrt{3}(1-s)\frac{A}{X}}, \quad r_4 = \frac{1}{3}\sqrt{2\sqrt{3}\left((1-s)\frac{A}{X} - g\frac{A}{G}\right)}(G \neq 0). \qquad \text{(5-A3)}$$

If we denote r_0/r_1, r_1/r_2, r_2/r_3, r_3/r_4 as ρ_0, ρ_1, ρ_2, ρ_3 respectively, we obtain the following equation:

$$\rho_0\rho_1\rho_2 = \frac{1}{\sqrt{1-s}}, \quad \rho_3 = \sqrt{\frac{(1-s)}{(1-s) - g\cdot f/N_g}} \ (\text{for } N_g \neq 0), \quad \rho_3 = 1 (\text{for } N_g = 0), \qquad \text{(5-A4)}$$

where $f = X/A$, and $N_g = G/A$.

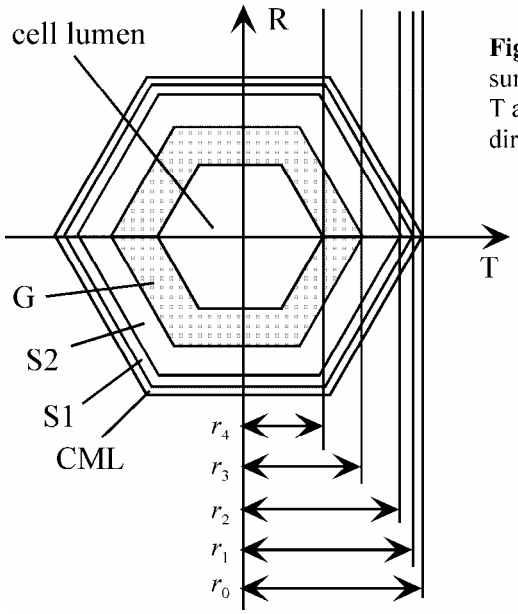

Fig.5-2. A model of the wood fiber whose crosscut surface is hexagonal-shaped for calculating eqs.(5-2). T and R stand for the tangential and the radial directions, respectively.

APPENDIX [2] Integration (5-1') is not affected by the functional shapes of *t*-dependent variables, S_1, S_2, S_3, ε_1^m, ε_2^m, ε_3^m, ε_1^f, ε_2^f, and ε_3^f. (See also Footnote (7) in Chapter 3, section 3-1)

We introduce functions φ_1, φ_2, and φ_3 which vary from 0 to 1 in the range of $0 \le t \le T_3$ as

follows:

$$\varphi_1(t)=\begin{cases} P(t) & (0\le t\le T_1) \\ 1 & (T_1\le t) \end{cases},\quad \varphi_2(t)=\begin{cases} 0 & (0\le t\le T_1) \\ Q(t) & (T_1\le t\le T_2) \\ 1 & (T_2\le t) \end{cases},\quad \varphi_3(t)=\begin{cases} 0 & (0\le t\le T_2) \\ R(t) & (T_2\le t\le T_3) \\ 1 & (T_3\le t) \end{cases},$$

(5-B1)

where P(t), Q(t), and R(t) are monotonously increasing and differentiable functions, which vary from 0 to 1 smoothly in respective domains. With reference to *Subsidiary Conditions 1* and *2*, we assume the following condition as the functional shapes of *t*-dependent variables $S_i(t)$, $\varepsilon_i^{m}(t)$, and $\varepsilon_i^{f}(t)$ (i =1, 2, 3):

$$S_i(t)=k_i\cdot\varphi_1(t),\quad \varepsilon_i^{m}(t)=m_i\cdot\varphi_i(t),\quad \varepsilon_i^{f}(t)=n_i\cdot\varphi_i(t).\qquad (i=1,2,3)\qquad (5\text{-B2})$$

where k_i, m_i, and n_i are constants. It is reasonable to assume this condition if these *t*-dependent variables change the values smoothly during the maturation of the matrix skeleton in their respective integration intervals. Then, by substituting eq.(5-B2) into eq.(5-1'), we obtain the following expression:

$$\begin{aligned}\varepsilon_L(t)\big|_{t=T_3} &= \int_0^{T_3}\left\{f_{11}(\mathbf{p})\dot{\varepsilon}_1^{m}+f_{12}(\mathbf{p})\dot{\varepsilon}_2^{m}+f_{13}(\mathbf{p})\dot{\varepsilon}_3^{m}+f_{14}(\mathbf{p})\dot{\varepsilon}_1^{f}+f_{15}(\mathbf{p})\dot{\varepsilon}_2^{f}+f_{16}(\mathbf{p})\dot{\varepsilon}_3^{f}\right\}dt \\ &= \int_0^{T_1} h_1(P(t))\left(\frac{dP(t)}{dt}\right)dt+\int_{T_1}^{T_2} h_2(Q(t))\left(\frac{dQ(t)}{dt}\right)dt+\int_{T_2}^{T_3} h_3(R(t))\left(\frac{dR(t)}{dt}\right)dt \\ &= \int_0^{T_1} h_1(P(t))\,dP(t)+\int_{T_1}^{T_2} h_2(Q(t))\,dQ(t)+\int_{T_2}^{T_3} h_3(R(t))\,dR(t),\end{aligned}$$

(5-B3)

where

$$\begin{cases} h_1(P(t))=m_1\cdot f_{11}(\mathbf{p})\big|_{S_1=k_1\cdot P(t),\ S_2=0,\ S_3=0} \\ \qquad\qquad +n_1 f_{12}(\mathbf{p})\big|_{S_1=k_1\cdot P(t),S_2=0,S_3=0}\ (0\le t\le T_1) \\ h_2(Q(t))=m_2\cdot f_{13}(\mathbf{p})\big|_{S_1=k_1,\ S_2=k_2\cdot Q(t),\ S_3=0} \\ \qquad\qquad +n_2 f_{14}(\mathbf{p})\big|_{S_1=k_1,\ S_2=k_2\cdot Q(t),\ S_3=0}\ (T_1\le t\le T_2) \\ h_3(R(t))=m_3\cdot f_{13}(\mathbf{p})\big|_{S_1=k_1,\ S_2=k_2,\ S_3=k_3\cdot R(t)} \\ \qquad\qquad +n_3 f_{16}(\mathbf{p})\big|_{S_1=k_1,\ S_2=k_2,\ S_3=k_3\cdot R(t)}\ (T_2\le t\le T_3), \end{cases}$$

provided that we consider here, $\mathbf{p}$ = (θ, ρ_1, ρ_2, ρ_3, h, E_1, E_2, E_3, S_0, $S_1(t)$, $S_2(t)$, $S_3(t)$). By the way, $P(t)$, $Q(t)$, and $R(t)$ change their respective values from 0 to 1 monotonously and continuously for elapsed time *t*, then, we can rewrite eq.(5-B3) as the following expression:

$$\varepsilon_{\mathrm{L}}\left(=\varepsilon_{\mathrm{L}}(t)\big|_{t=T_3}=\varepsilon_{\mathrm{L}}(\mathbf{p}(t))\big|_{t=T_3}\right)=\int_0^1 h_1(P)\,dP+\int_0^1 h_2(Q)\,dQ+\int_0^1 h_3(R)\,dR\ . \qquad \text{(5-B4)}$$

This result indicates that the integration value in eq.(5-B4) does not depend on the concrete values of T_1, T_2 and T_3. Furthermore, it is not affected by the functional shapes of *t*-dependent variables S_1, S_2, S_3, $\varepsilon_1^{\mathrm{m}}$, $\varepsilon_2^{\mathrm{m}}$, $\varepsilon_3^{\mathrm{m}}$, $\varepsilon_1^{\mathrm{f}}$, $\varepsilon_2^{\mathrm{f}}$, and $\varepsilon_3^{\mathrm{f}}$ if we assume the condition described by eq.(5-B2).

APPENDIX [3] Trial to reduce the growth stress and residual stress in logs.

In this chapter, the author focused his interests on the characteristic properties of tension wood from the viewpoint of wood engineering, since many of plantation species in tropical or sub-tropical countries are hardwood species where the tension wood formation is more or less unavoidable. For better utilization of those resources as the timber materials, how to diminish the tension wood formation and how to avoid the processing defects due to high tensile growth stress are very important problem. As well known by many scientists and engineers, the occurrence of heart splitting during logging or lumber crooking during sawing have been very serious problem when we use forest products as timber materials. Many scientists attribute origins of those defects to release of elastic energy from the residual stress gradient at logging and lumbering. Those phenomena reduce the yield of the forest products, therefore, residual stress is considered as an obstacle to wood processing. It is well recognized that the larger becomes the growth stress the higher is the residual stress gradient; hence, in order to solve the problems caused by the growth stress (or residual stress), it is necessary to improve genetic and silvicultural techniques by breeding trees with low growth stress and to develop the operation that reduces the residual stress inside logs.

Several techniques have been proposed to reduce the residual stress in logs. The girdling and the direct heating techniques are both practical trial, and not a few scientists agree their effectiveness on reducing the residual stress especially in the commercial species. Besides those physical treatments, an effective method using a chemical solution was tried by Rigesa Ltd, Santa Catarina, Brazil. They use “Chopper” as the chemical to reduce the residual stress inside standing stem. “Chopper” is a kind of hormone drug that is commercially used for inhibiting sprouting out from harvested stumps of planted Eucalyptus trees. They inject a small amount of “Chopper” solution (5ml) to the sapwood of standing trees, and leaving it for one month or more, they cut the treated trees. They noticed that “Chopper treatment” is

effective not only for stopping the occurrence of sprout from stumps of harvested trees, but also for increasing the yield of timber. Then, author of the present dissertation tried to check the effectiveness of “Chopper treatment” on reducing the surface growth stress of planted 10-year-old *Eucalyptus dunnii*. Chopper injection (5ml) was carried out in mid August 2003 in the plantation of Rigesa Ltd, and treated trees of were harvested in mid September 2003. in Santa Catarina, Brazil. In addition to treated trees, non-treated trees were also harvested from the same plantation. After harvesting, each first log, 2 m in length, was soon transferred to the laboratory of Federal University of Parana, Curitiba. At the breast height, four points were set peripherally, and the strain-gauges were put on the surface of exposed xylem. Soon after, the longitudinal release strain were measured by stress-release method. Moreover, the severity of heart splitting at the upper end of the first log was photographed.

Figure 5-3 shows end split of the harvested log. We notice that “Chopper treatment” is more or less effective to reduce the occurrence of end split.

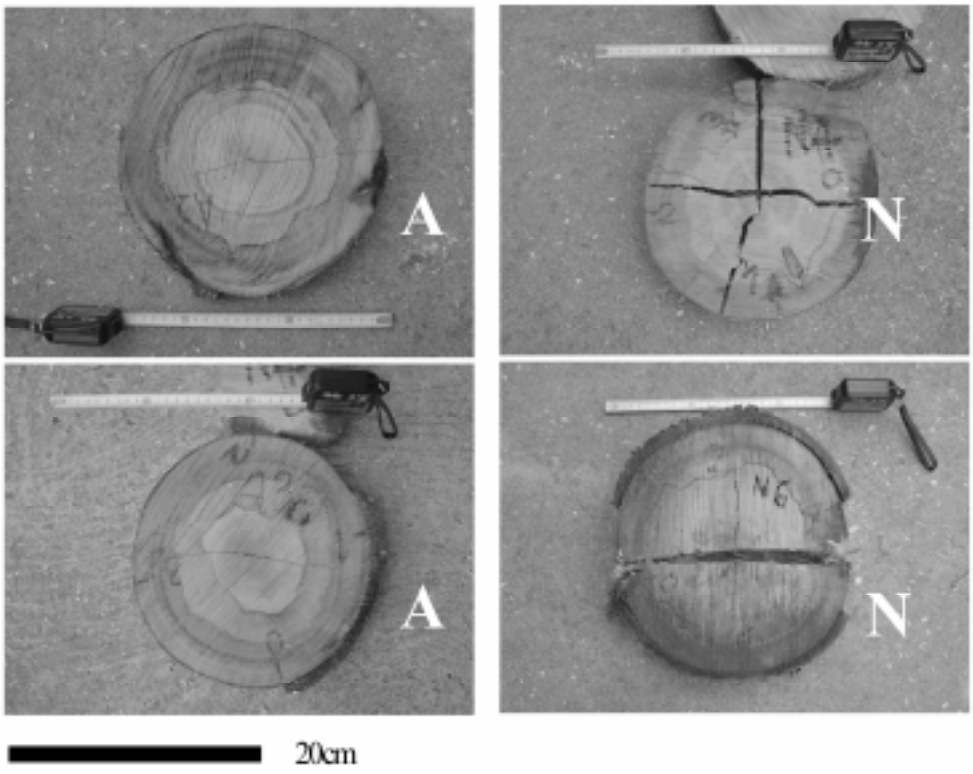

Fig. 5-3. Endsplit of the harvested log, and the effect of Chopper treatment on reducing the occurrence of endsplit. A: Trees treated by Chopper injection for 1 month. N: Trees without treatment.

Table 5A-1 shows the difference of the longitudinal released strain of the surface growth stress between “Chopper treated” and non-treated trees, and Table 5A-2 is the released strain averaged in each log. Those results clearly show the effectiveness of “Chopper treatment” on reducing the growth stress of planted *Eucalyptus dunnii*.

Table A5-1. Effect of Chopper treatment on reducing the surface growth stresses of planted *Eucalyptus dunnii*.

(a) Released strains of surface growth stresses in Chopper treated tress (for 1 month)

Strain gauge number	log number A1	A2	A3	A4	A5	A6	A7	A8	Average
0	**	-795	-773	-753	-859	-1577	-552	**	
2	**	-639	-865	-725	-961	-754	-720	**	
4	**	-691	-731	-1137	-703	-671	-547	**	
6	**	-768	-543	-445	-668	-721	-575	**	
Average in a log	**	-723	-728	-765	-797	-930	-598	**	-757.2

(unit: 10^{-6})

(b) Released strains of surface growth stresses in non-treated tress (for 1 month)

Strain gauge number	log number N1	N2	N3	N4	N5	N6	N7	N8	Average
0	**	-1284	**	-1396	-619	-1369	-1038	-1045	
2	**	-689	**	-1514	-983	-424	-1086	-952	
4	**	-1415	**	-1380	-863	-760	-1446	-893	
6	**	-1514	**	-1142	-945	-415	-790	-945	
Average in a log	**	-1225	**	-1358	-852	-742	-1090	-959	-1037.8

(unit: 10^{-6})

Table A5-2. Effect of Chopper treatment on reducing the surface growth stresses of planted *Eucalyptus dunnii* - Averaged values in each tested log .

Chopper treated logs			Non-treated logs		
log number	A2	-723.2	log number	N2	-1225.5
	A3	-728		N4	-1358
	A4	-765		N5	-852.5
	A5	-797.7		N6	-742
	A6	-930.7		N7	-1090
	A7	-598.5		N8	-958.7
Average		-757.2			-1037.8

(unit: 10^{-6})

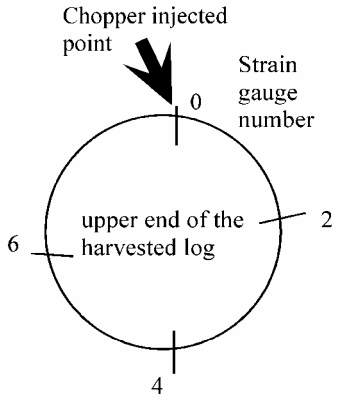

Chapter 6

SUMMARY AND GENERAL CONCLUSION

Fossil fuels and metal resources have been almost exhausted while modern society based on the consumer economy becomes overripe after the Industrial Revolution. Moreover, irreversible destruction of the forest environment has been progressing especially in the tropical countries, and the atmospheric carbon dioxide is still increasing with mass consumption of the fossil fuel. Our urgent countermeasure is to find substitutes for the fossil and metal resources, and to mitigate the increasing atmospheric carbon dioxide as soon as possible. Under those situations, many people believe that “increase of the forest environment” and “utilization of the forest biomass” can solve the above-mentioned crises (Hosokawa et al. 2002). However, many of forest environment disappeared by the overexploitation since the Industrial Revolution, which provokes serious undersupply of the traditional species in the world timber market. Even if we would take a policy to protect the natural forest, it may take several hundred years or more to recover the fallen forest environment as it were!

Some researchers then consider that the expeditious afforestation of the tropical fast-growing species can save the global crises that humankind is now confronted. In this case, what is important is to transform those resources into the commercial-valued products especially as timbers for the construction and the furniture by developing the appropriate techniques, which gives an economical necessity to the silvicultural activity in those species. However, many of resources obtained from those forests are lesser-known or lesser-used species, therefore, we have very little information on the material properties of those species in comparison with that of the traditional species. Before everything else, we need to clarify the material property in each lesser-used species as well as to establish a fundamental theory that makes us possible to develop advanced techniques to utilize the forest biomass as commercial-valued materials. The present study was carried out mainly from the latter standpoint. One of the best ways is to find a general principle that describes the generation mechanism of material properties of various wood species in relation to its higher-ordered structure.

In this dissertation, the author tried to find a general theory to describe the material properties of wood in relation to its hierarchical structure covering from the microscopic

constituents to the macroscopic wood, focusing on the following four topics that will be practically important when we use the forest products as the industrial materials.

[1] *The first topic* is concerned with the general theory of the elastic behavior of the single wood fiber having multi-layered cell wall (=a homogenized model of the clear wood specimen). In this topic, with reference to the theory of micromechanics, mechanical properties of the single wood fiber is mathematically formulated. First, the reinforced-matrix hypothesis was mathematically formulated base on “the mean field theory (Mori and Tanaka 1973)”, and its physical meanings were clearly defined. Second, the reinforced-matrix theory was applied to formulating the dimensional change of the single wood fiber which is caused by a certain physical state change induced in the cell wall.

[2] *The second topic* is the biomechanical problems concerned in the growth stresses and strains in trees. This includes (1) the generation mechanism of the abnormal growth stress in the reaction wood xylem, and (2) its role in controlling the negative-gravitropic behavior and the pattern formation of the growing tree shoot.

In (1), generation process of the growth strain in the softwood tracheid was simulated by the formula derived in *the first topic*. As the result, the simulation deduced that expansive eigen-strain is generated in the matrix skeleton of each layer of the secondary wall during the lignification, which finally amounts to 0.5~1%. At the same time, contractive eigen-strain is generated in the polysaccharide framework bundle in each layer, which becomes –0.15% during the secondary wall lignification. The magnitudes and signs of the longitudinal growth strains are controlled by the microfibril angle in the middle layer of the secondary wall. This result strongly supports the unified hypothesis as a possible theory to explain the origin of the surface growth stress.

In (2), time-dependent evolution of the spatial shape of a growing shoot was simulated on the basis of the structural mechanics. In this simulation, beam theory (structural mechanics) was used to describe the negative (or plagio-) gravitropic behavior of woody plant stems, and the interaction between bending moment due to increasing self-weight and recovery moment resulting from asymmetric growth stress was examined, and a hypothesis that describes the relationship was tested based on the structural mechanics “beam theory”. Simulations of

observed tree branch morphology of *M. kobus* DC., *J. chinensis* L., *A. saccharinensis* Fr. Schum., and *P. spachiana* Kitamura f. spachiana cv. Plenarosea showed that (i) the growth stress generated in the reaction wood is sufficient to counteract the gravitropic response to increasing self-weight, and (ii) the specific directional angle of the shoot apex or preferred angle of the elongation zone plays an important role in controlling the spatial shape of the branch stem that is peculiar to plant species with large growth stress generated in the reaction wood tissue.

[3] *The third topic* is concerned with the biomechanics of sawn wood. The simulation using the formula derived in the first topic plays an important role also in this topic. Aim of this topic is to understand the hygro-mechanical behaviors peculiar to the sawn wood in relation to its hierarchical structure. Especially in this paper, we focus on (1) the hygroexpansive behavior, and (2) the moisture-dependent elasticity of softwood.

In (1), to elucidate the origin of the shrinking anisotropy of wood during the drying process, as well as to begin to gain an understanding of the interaction between the moisture and the cell wall components, the shrinking process of a single wood fiber regarding water desorption was simulated by using an analytical wood fiber model which was developed in *the first topic*. Resulting data were compared with the experimental ones. The following conclusions were obtained: (i) The matrix substance, as a skeleton in the secondary wall, tends to shrink isotropically up to about 15 %. However, the polysaccharide microfibril, as a rigid framework of the cell wall, almost did not shrink at all due to the water desorption (less than 1%). As the result, wood shrinks anisotropically during a drying process. (ii) The microfibril angle in the S2 layer is one of the most important factors related to the degree of shrinking anisotropy of the wood while drying.

In (2), the elastic deformation of the isolated wood fiber and its moisture dependency were analyzed by using the formula derived in *the first topic*. As the result, following conclusions were derived: (i) An intermediate domain, which is contained between rigid crystal and completely disordered amorphous domains in the wood CMF, fluctuates from an amorphous-like compliant state to a crystal-like rigid state in accordance with the moisture desorption. This is a main reason why the longitudinal Young's modulus of wood becomes higher with drying.

(ii) There are three possible hypotheses to explain the species dependency of the longitudinal Young's modulus of the wood cell wall. The first is that the content of the polysaccharide framework and its crystallinity are inherently different among species. The second is that the crystallinity of the polysaccharide framework tends to change with elapsed time. And, the last is that an irreversible change is caused in the cohesion state of each cell wall component by the drying and heating processes.
(iii) Decrease in the strength of the recycled paper is induced by the cornification of the fiber wall. It is expected that an irreversible crystallization tends to proceed in the unstable domain of the CMF after the repetition of the drying and wetting process, which is a major cause of the cornification of the fiber wall in the recycled paper.

[4] *The last fourth topic* is on the biomechanics of the tension wood properties. To discuss the role of the gelatinous layer (G-layer) on the origins of the physical properties peculiar to the tension wood fiber (TW fiber), the tension wood (TW) properties of a 70 year-old *Acer sieboldianum* Miq were analyzed on the basis of the simulation using the G-fiber model which was formulated in *the first topic*. The roles of the G-layer on the origins of (1) a high large tensile growth stress, (2) a large longitudinal Young's modulus, and (3) a high longitudinal drying shrinkage in the tension wood xylem were discussed. The results conclude that the G-layer generates a high tensile stress in the longitudinal direction during the xylem maturation; the longitudinal Young's modulus of the green G-layer becomes significantly higher than that of the lignified layer; furthermore, the G-layer tends to shrink extraordinarily higher than that of the lignified layer during the moisture desorption.

References in Chapter 6

Hosokawa, R.T., Yamamoto, H., Rochadelli, R., Klock, U., Reicher, F., Bochicchio, R.: Reforestation: the dynamics of safe, efficient CO_2 storages, *Nagoya University Forest Science*, **21**, 9-18 (2002).

Mori, T., Tanaka, K.: Average stress in matrix and average elastic energy of materials with misfitting inclusions, *Act. Metall.*, **21**, 571-574 (1973).

List of Publications concerning this dissertation

1. Yamamoto, H.
Generation mechanism of growth stresses in wood cell walls: Roles of lignin deposition and cellulose microfibril during cell wall maturation. **Wood Science and Technology**, Vol. 32, 171-182 (1998).

2. Yamamoto, H.
A model of anisotropic swelling and shrinking process of wood (part 1). Generalization of Barber's wood fiber model. **Wood Science and Technology**, Vol.33, 311-325 (1999).

3. Yamamoto, H. ; Sassus, F.; Ninomiya, M.; Gril, J.
A model of anisotropic swelling and shrinking process of wood (part 2). Simulation of the shrinking wood. **Wood Science and Technology**, Vol.35, 167-181 (2001).

4. Yamamoto, H. ; Kojima, Y.
Properties of the cell wall constituents in relation to the longitudinal elasticity of wood
(Part 1). Formulation of the longitudinal elasticity of an isolated wood fiber. **Wood Science and Technology**, Vol.36, 55-74 (2002).

5. Yamamoto, H. ; Kojima, Y. ; Okuyama, T. ; Avasolo, W. P. ; Gril, J.
Origin of the biomechanical properties of wood related to the fine structure of the multi-layered cell wall. **Transaction of the ASME Journal of Biomechanical Engineering**, Vol.124, 432-440 (2002).

6. Yamamoto, H. ; Yoshida, M. ; Okuyama, T.
Growth stress controls negative gravitropism in woody plant stems. **Planta**, Vol.216, 280-292 (2002).

7. Yamamoto, H.
Role of the gelatinous layer on the origin of the physical properties of the tension wood. **Journal of Wood Science**, Vol.50, 197-208 (2004).

8. Yamamoto, H.; Abe, K.; Arakawa, Y.; Okuyama, T.; Gril, J.
Role of the gelatinous layer (G-layer) on the origin of the physical properties of the tension wood of *Acer sieboldianum*. **Journal of Wood Science**, Vol.51 (2005), in press.

9. Yamamoto, H.; Kojima, Y.; Okuyama, T.; Ona T.; Okayama, T.
An essay on the fine structure of the wood cell wall related to the physical properties of the recycled paper. **In Improvement of forest resources for recycled forest products, T. Ona (ed.), Springer-Verlag,** Tokyo, pp.139-143 (2004).

Memorandum

Memorandum